2019

In-Silico Design and Synthesis of Selective Estrogen Receptor Modulators Targeting Ovarian Cancer

John Apraku
South Dakota State University

IN-SILICO DESIGN AND SYNTHESIS OF SELECTIVE ESTROGEN RECEPTOR MODULATORS TARGETING OVARIAN CANCER

BY

JOHN APRAKU

A dissertation submitted in partial fulfillment of the requirement for the

Doctor of Philosophy

Major in Chemistry

South Dakota State University

2019

IN-SILICO DESIGN AND SYNTHESIS OF SELECTIVE ESTROGEN RECEPTOR MODULATORS TARGETING OVARIAN CANCER

JOHN APRAKU

This dissertation is approved as a credible and independent investigation by a candidate for Doctor of Philosophy in Chemistry degree and is acceptable for meeting the dissertation requirements for this degree. Acceptance of this does not imply that the conclusions reached by the candidate are necessarily the conclusions of the major department.

Fathi T. Halaweish, Ph.D. Date
Dissertation Advisor

Douglas Raynie, Ph.D.
Head, Department of Chemistry Date
and Biochemistry

Dean, Graduate School Date

This manuscript is dedicated to God Almighty for his protection and guidance throughout my education and my entire life. I bless him and give glory to his name: the alpha and omega God you deserve praise and adoration.

To my mother and my late fathers, I am most grateful for your timely support. Without you, I would not be where I am today.

My advisor Dr. Halaweish for his mentorship in my life, I will forever be grateful to you. I could not do it without you.

To my sweetheart, I would not be here without your help and support. I say may God almighty bless you and accomplish your heart desires.

To all my friends, who supported me in diverse ways, I say many thanks to you.

ACKNOWLEDGMENTS

I want to express my thanks and appreciations to my advisor, friends, and family for their support through my entire education. I acknowledge my advisor, Professor Fathi Halaweish for a warm atmosphere, safe and conducive environment he created for me during my studies. His advice, suggestions, and directions had positively influenced my life. I appreciate this Sir. I would also like to thank my collaborators especially Dr. Subhash C. Chauhan at the department of pharmaceutical sciences, University of Tennessee Health Science Centre, Memphis, Tennessee for their support on my biological studies. Special appreciation goes to Dr. Douglas Raynie and the Department of Chemistry and Biochemistry for providing the necessary support during my program. My appreciations to my graduate committee members Dr. Cheng, Zhang, Dr. Iram and Dr. Scott Pedersen for their help and constructive criticisms. Finally, many thanks to my lab mates, Felix, Abusalem, Khaled, Saad and Sara I say thank you for helping me even in times of psychological hardships.

CONTENTS

ABBREVIATIONS

ADME	Absorption, Distribution, Metabolism and Excretion
AUB	Abnormal uterine bleeding
BMD	Bone mineral density
CASH	Cancer and Steroid Hormone studies
CDK	Cyclin-dependent kinase inhibitor protein
CDRI	Central Drug Research Institute
EGFR	Epidermal Growth Factors
ERK	Extracellular Signal-Related Kinase
FDA	Food and Drug Administration
GSK3B	Glycogen synthase kinase 3 beta
HTS	High Throughput Screening
LC	Lead Compound
MEK	MAPK/ERK kinase
MTT	3-(4,5-dimethylthiazol-2-yl)-2,5-diphenyltetrazolium bromide
NMR	Nuclear Magnetic resonance
ORM	Ormeloxifene

OSE	Ovarian surface epithelium
PBAC	Pictorial blood loss assessment chart
RBA	Relative binding affinity
SAR	Structure-Activity Relationship
SERM	Selective estrogen receptor modulator
STAT	Signal Transducer and Activator of Transcription
VAS	Visual analog scale

LIST OF FIGURES

LIST OF TABLES

LIST OF SCHEMES

ABSTRACT

IN-SILICO DESIGN AND SYNTHESIS OF SELECTIVE ESTROGEN RECEPTOR MODULATORS TARGETING OVARIAN CANCER

JOHN APRAKU

2019

The established records of the safety of Ormeloxifene along with its favorable bioavailability and ability to inhibit rapid cell proliferation in the endometrium during embryonic implantation has made it one of the best drug candidates for controlling undesirable rapid cell growth such as endometriosis and cancerous tumor conditions. Recent studies have confirmed the effectiveness of Ormeloxifene to suppress and inhibit epithelial-mesenchymal transition process as evidenced by repression of N-cadherin, slug, snail, vimentin, MMPs, β-catenin/TCF-4 transcriptional activity and induce the expression of pGSK3b. Recently conducted studies have revealed the dynamic binding of ormeloxifene with β-catenin, **GSK3b, CDK4,** and other downstream **EGFR**. In this communication, a novel Ormeloxifene analogs with inhibitory activities towards epidermal growth factor receptor (**EGFR**) is used to develop a potential drug candidate for the treatment of ovarian cancer. Molecular modeling results revealed that the introduction of electron withdrawing group at the para position of aromatic at C-3 such as JA-16 increased binding affinity in **GSK3B** binding pocket relative to Ormeloxifene. Substitution of

trifluoromethylated moiety on the phenoxy position and incorporation of pyrrolidine side chains at C-7 of the benzopyran framework such as **JA-15, JA-16, JA-17,** and **JA-18** improved the inhibitory activity of the compound in the crystal structure of **CDK2** as compared to Ormeloxifene. A total of 25 analogs have been synthesized and biologically evaluated. Cell proliferation inhibitory assay revealed the ability of **JA-15, ORM-Br,** and **JA-28** to inhibit ovarian cancer cell line (**A2780**) with IC_{50} of 9µM, 11.2µM, and 17.6µM respectively. Cell cycle analysis performed by flow cytometry revealed that **JA-15** arrest A2780 cells in the $G_0 – G_1$ phase. **JA-15** showed an increase in the fraction of cells in the G_0-G_1 phase with 61.98% compared to the control with 53.42%**.** However, **JA-28** exhibited an increase in the fractions of cells in the G_2-M phase with 8.74% relative to 3.52% for control. This result indicates that **JA-15** has the potential to chemotherapeutic effects because it arrests (A2780) ovarian cell cycle in G0-G_1 phase. To explore the impact of **ORM** analogs on other cancer cell lines, **ORM-Br** was tested on cervical cancer cell lines (**CaSki and SiHa**). Western blot analysis conducted to establish the effect of **ORM-Br** on β-catenin degradation after using translational inhibitor (cycloheximide) showed a significant decrease in protein levels of β-catenin in CaSki and SiHa cells relative to cycloheximide treatment**.** The clonogenic assay revealed that **ORM-Br** suppresses the clonogenic potential of CaSki and SiHa cell lines.

On the other hand, **ORM-Br** inhibits the migration of cervical cancer cells as predicted by agarose bead assay**.** Boyden chamber and xCELLigence assay revealed that **Br-ORM** inhibits the invasion of cervical cancer (CaSki and SiHa) cells. There was a decrease in the expression of nuclear β-catenin in the cytoplasm of cervical cancer cell lines when subjected to western blot analysis to detect the protein levels of β-catenin**.** Cell lysates and

western blot analysis conducted for EMT markers and MMPs analysis showed the ability of **ORM-Br** to inhibit the EMT associated markers in both CaSki and SiHa cell lines. The knowledge of varying inhibitory activity of **JA-15, JA-28,** and **ORM-Br** on multiple pathways is a possible lead towards the discovery of potential anticancer agent; we propose that ormeloxifene framework can be altered to generate possible drug candidates, which can affect multiple targets following multi-faceted drug strategies to combat ovarian cancer.

Chapter 1

1 Introduction and Background

1.1 Drug Discovery and Development

Before any drug discovery program initiates, there is a disease or clinical conditions with no suitable medication available[1]. Initial research has to be done to generate a hypothesis that will result in a biological or therapeutic effect of the disease state. Understanding the mechanistic pathway of the disease has led to a dramatic improvement in human health, as a result of modern medicine[2]. Diseases and conditions that were thought to be incurable are now treated with highly potent medications. However, drug discovery is a long process that involves many commitments. It is estimated that about 100,000 drug candidate compounds are expected to be screened as wells as numerous clinical trials before a single market drug is produced. On the other hand, the cost associated with developing a single drug is estimated to be over 1.75 billion dollars[3] (**Fig 1.1**).

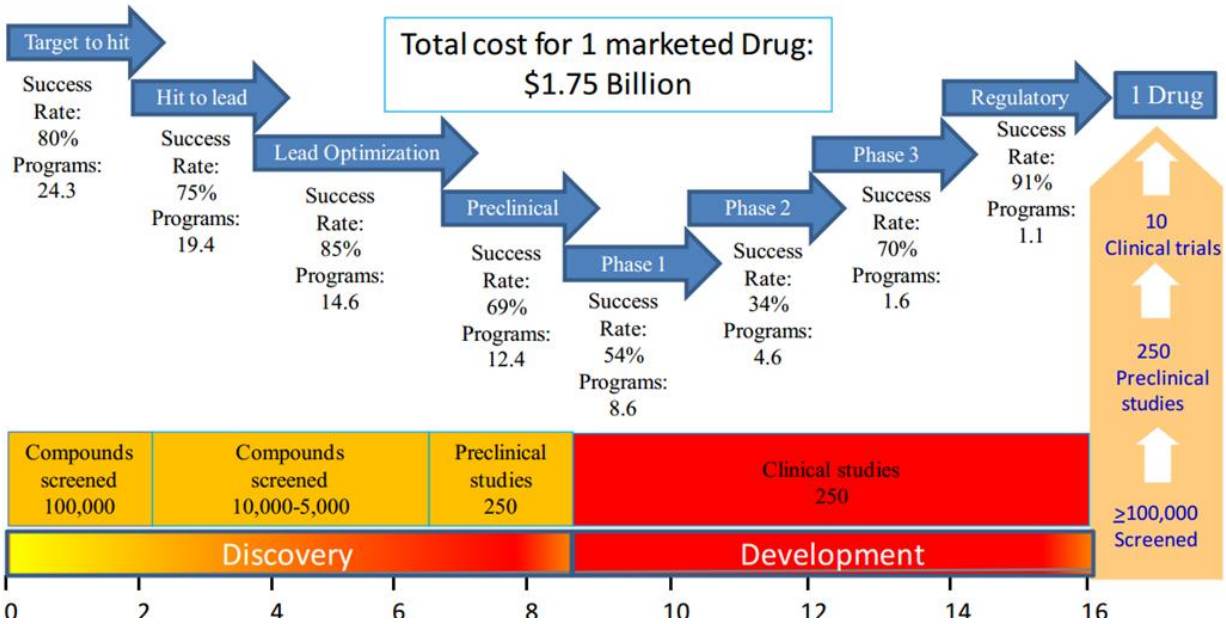

Figure 1.1. An analysis of the various stages of drug discovery and development process.

The complex processes of drug discovery and development have different steps, tasks, and functions. The process can broadly be divided into two major stages. Drug discovery which is the first stage involves chemoinformatics, molecular modeling, and chemical synthesis, toxicity screening, and clinical studies[4]. This stage can further be categorized into three distinct phases namely: target discovery, lead discovery and lead optimization. Each of these stages is designed to establish a scientific link between the biological target and the human diseased model intended. The molecular target validation and progression is accomplished through the use of molecular probes, designed to identify a series of compounds that would alter and modify the activity of the biological target of interest[4]. Once the structurally related compounds with their desired biological activities are identified, the lead optimization begins, where many analogs within the lead compound are

screened to identify compounds that may progress to the drug development stage. The lead optimization (HTS) compounds are then subjected to in vivo studies in various animal models and eventually clinical studies to identify their efficacy[5].

Once a single compound is identified, the second primary stage in drug development begins, where the compound progress through various studies for its approval by various regulatory bodies[6](**Fig 1.2).**

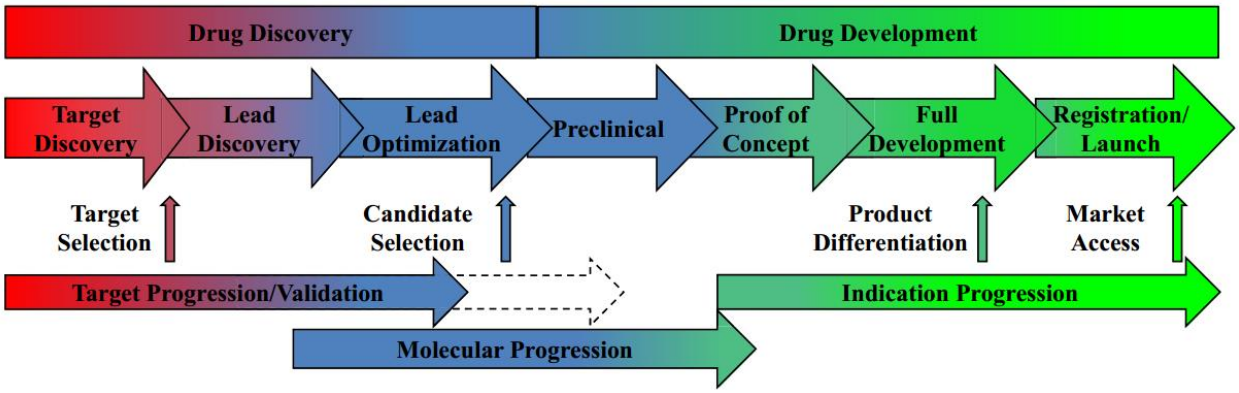

Figure 1.2. The drug discovery and development process.

There is no doubt that the discovery of a new drug has a positive impact on medicine, but it is more challenging, time-consuming and is associated with higher cost.

1.2 Natural products in drug discovery

Before the existence of modern medicine natural products were the only source of medication use by our ancestors to treat wounds and diseases[7]. Even up to date, some tribes in Africa *(Akan*) chew herbs to relieve pains, wraps herbs on wounds for quick healing, as an eye drops to treat various eye diseases and sometimes remove the speck from the eye.

Plants, in particular, have played an essential role in traditional medicine system. The Egyptian medical **papyrus** which dates from 1500 BC documents over 700 drugs that mostly originated from plants. There was other evidence of the use of approximately 1000 plant-derived substances in Mesopotamia around 2600 BC of which many are still being used today for the treatment of various ailments[8].

Over the centuries, the Chinese Materia Medica (1100 BC,Wu Shi Er Bing Fang, containing 52 prescriptions), Shennong Herbal (100 BC, contains about 365 drugs) , the Tang Herbal (659 AD; 850 drugs) and the Indian Ayurvedic system dates from about 1000 BC (Charaka; Sushruta and Samhitas with 341 and 516 drugs respectively) are some of the evidence of the extensive use of natural products as drugs[9].

Natural products and their derivatives have been a most active and productive source of ingredient in medicines. They have contributed to the development of many drugs for various indications and represent a unique and abundant source of therapeutic agents and lead structures for new drug discovery.

According to ***Alan L Harvey, (2007),*** up until 1996, about 80% of medicinal products were either directly derived from naturally occurring compounds or were inspired by a natural product and recent analysis have confirmed that between 1981 and 2002, 28 percent of 868 new chemical entities were natural products or derived from natural products and another 24 percent created around a pharmacophore from natural products[10]. On the other hand, in 2004, about 70 natural product-related compounds were in clinical trials, and more recent analysis confirms the continuing importance of natural products for drug discovery[11]. Based on the recent US prescription data, about 50% most prescribed drugs had a natural

product either as drug or as a progenitor in the synthesis or design of the chemical agent[12]**(Fig. 1.3).**

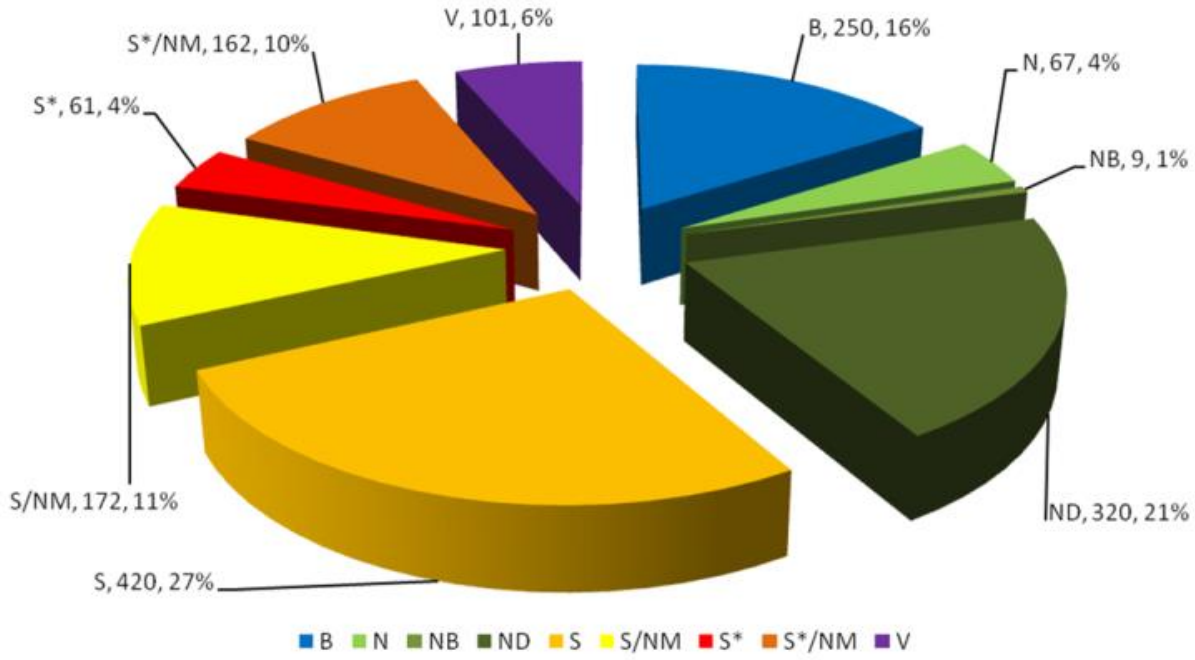

Figure 1.3 All newly approved drugs 1981−2014; n = 15627

B = Biological macromolecule, 1997, **N** = Unaltered natural product, 1997, **NB** = Botanical drug (defined mixture), 2012, **ND** = Natural product derivative, 1997, **S** = Synthetic drug, 1997, **S*** = Synthetic drug (NP pharmacophore), 1997, **V** = Vaccine, 2003, **S /NM** = Mimic of natural product, 2003.

Despite the challenges and challenging synthetic routes of drugs from natural products, technical advancements achieved in the field has helped in the screening and evaluation of natural products and has resulted in the improvement of therapeutic efficacy. Also,

modifications of active natural products skeletons have led to the discovery of several novel agents[13]. One of these novel agents is Centchroman (ormeloxifene) a selective estrogen receptor modulator (SERM), with the ability to suppress cancer cells has become an attractive target for the development of future drugs.

1.2.1 Centchroman (Ormeloxifene)

Ormeloxifene is a nonsteroidal selective estrogen receptor modulator, a class of medications which acts on estrogen receptors, was developed by the Central Drug Research Institute (CDRI), Lucknow, (India)[14]. It was introduced 20 years ago as a safe and effective oral contraceptive because it is free of the side effects associated with estrogen and progestin-based oral contraceptives. It provides an opportunity for effective and efficient reversal of fertility once discontinued by the patient. The contraceptive action of ormeloxifene mainly depends on its ability to suppress embryonic implantation in the uterine wall[15]. It is marketed in India and some other countries under the trade names saheli, central, savista, Novex, and Novex DS. Ormeloxifene is used as a weekly contraceptive which is taken twice per week (30 mg dose) for the first twelve weeks and once every week after that. Studies have shown that the standard 60 mg weekly dose can reduce pregnancy rate by 38% with about 1-2% failure rate [16]. Ormeloxifene with the trade name Savista is used to treat dysfunctional uterine bleeding due to its anti-proliferation effect on the uterus

which causes endometrial atrophy leading to decrease in uterine bleeding[17]. Recent reports have shown the effectiveness of ormeloxifene in various cancer cell lines and its therapeutic effects in other clinical conditions such as dermatitis, uterine fibroid, osteoporosis, restenosis, and endometriosis[18]. Other uses of ormeloxifene are for treatment of conditions such as active liver disease, recant history of jaundice and mastalgia[19]

1.2.1.1 Physical properties of Centchroman (ormeloxifene

Ormeloxifene(1-(2-(4-(3,4-dihydro-7-methoxy-2,2-dimethyl-3-phenyl-2H-chromen-4 yl)phenoxy)ethyl)pyrrolidine) is a white crystalline solid with molecular weight 457 g/mol and has a melting point of 165 -166°C. It is soluble in organic solvents such as Ethyl acetate, dichloromethane, chloroform, acetone, methanol, and ethanol, but sparingly soluble in water, HCl, NaOH, and isobutanol[16]. It is a very stable compound under normal conditions and can retain its physical characteristics and biological activities for over three years when stored in aluminum strips or glass container at room temperature. Previous studies have shown that the racemic mixtures of Ormeloxifene can be resolved into D- and L- enantiomers with L-isomer showing more receptor binding potency and about two-fold higher anti-implantation activity in rat than D and DL- ormeloxifine[20] **(Fig 1.4)**

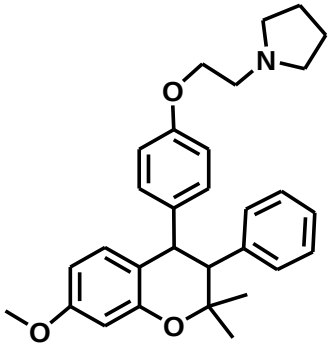

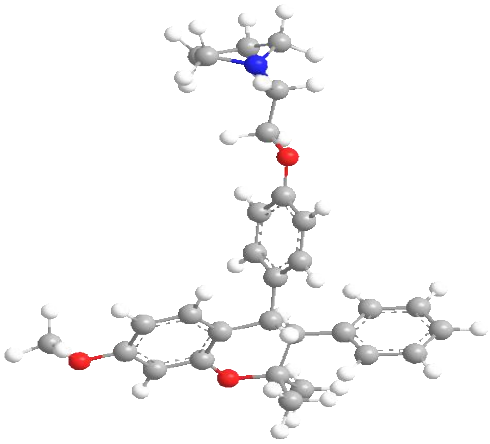

Figure 1.4 Centchroman (Ormeloxifene). 3D Structure of Ormeloxifene

1.2.1.2 Chemistry of Centchroman (ormeloxifene)

Centchroman is antiestrogens of triarylethylene class such as tamoxifen and nafoxidine. They show dual behaviors due to the presence of two molecular components in their structural framework. Their estrogenic nature is accounted for by a trans-stilbene-like core that stimulates diethylstilbestrol, hexestrol, or estradiol and their antiestrogenic property are as a result of the presence of ώ-tert-aminoalkoxy) phenyl residue that interferes with the initiation of estrogenic activity[21]. The stereostructure of centchroman –DL has two notable conformational structural features and are marketed as racemic mixtures with the L-enantiomer being the more potent of the two. Recent structural analysis has predicted that the more active L-ormeloxifene has 3R,4R configuration whiles the less active D-enantiomer has a configuration of 3S,4S (**fig 1.5**)[22]. It has two chain substituents at C-3, and C-4 position that is twisted out of a plane from the chroman system and also have

distinct chair cyclohexane –like wrinkle at C-2, C-3 and C-4 atoms of chroman system. These aryl rings are twisted at 71.5° for C-3 ring and 98.7° for C-4 ring and are more extensive than that of other nonsteroidal estrogens like tamoxifen and nafoxidine[23]. The dihedral twist in ormeloxifene can be attributed to the presence of the two aryl substituents attached to the tetrahedral centers which are in contrast to the tamoxifen and nafoxidine and can form arene double bond conjugation which can enforce ring double bond planarity[20].

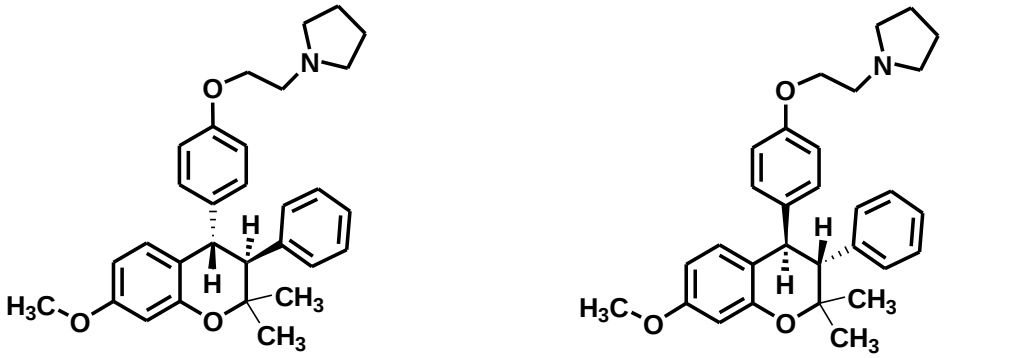

Figure 1.5 Enantiomers of l-, and d- Centchroman.

1.2.1.3 Total synthesis of ormeloxifene

Ormeloxifene (1-(2-(4-(3,4-dihydro-7-methoxy-2,2-dimethyl-3-phenyl-2H-chromen-4 yl)phenoxy)ethyl)pyrrolidine hydrochloride) was first synthesized by Grignard reaction of cis-3-phenyl-4-p-acetoxyphenyl-7-methoxy-3,4-dihydrocoumarin **(a)** and

methylmagnesium iodide with THF as a solvent to produce 2-(3-hydroxy-1-(4-hydroxyphenyl)-3-methyl-2-phenylbutyl)-5-methoxyphenol **(b)**. Cyclisation of (**b**) with polyphosphoric acid at a temperature of 75 - 80°C produced 4-(3,4-dihydro-7-methoxy-2,2-dimethyl-3-phenyl-2H-chromen-4-yl)phenol **(c).** Condensation of 1-(2-chloroethyl) pyrrolidine with potassium carbonate (K_2CO_3) in acetone at 60 °C yielded 1-(2-(4-((3R,4R)-3,4-dihydro-7-methoxy-2,2-dimethyl-3-phenyl-2H-chromen-4-yl)phenoxy)ethyl)pyrrolidine **(d)**. Further isomerization of **(d)** with n-butyl lithium in dimethyl sulfoxide (DMSO) afforded centchroman **(e)**[24] **(Scheme 1.1)**. There has been another alternative and improved synthesis of centchroman over the past years which will be elaborated in the next chapter.

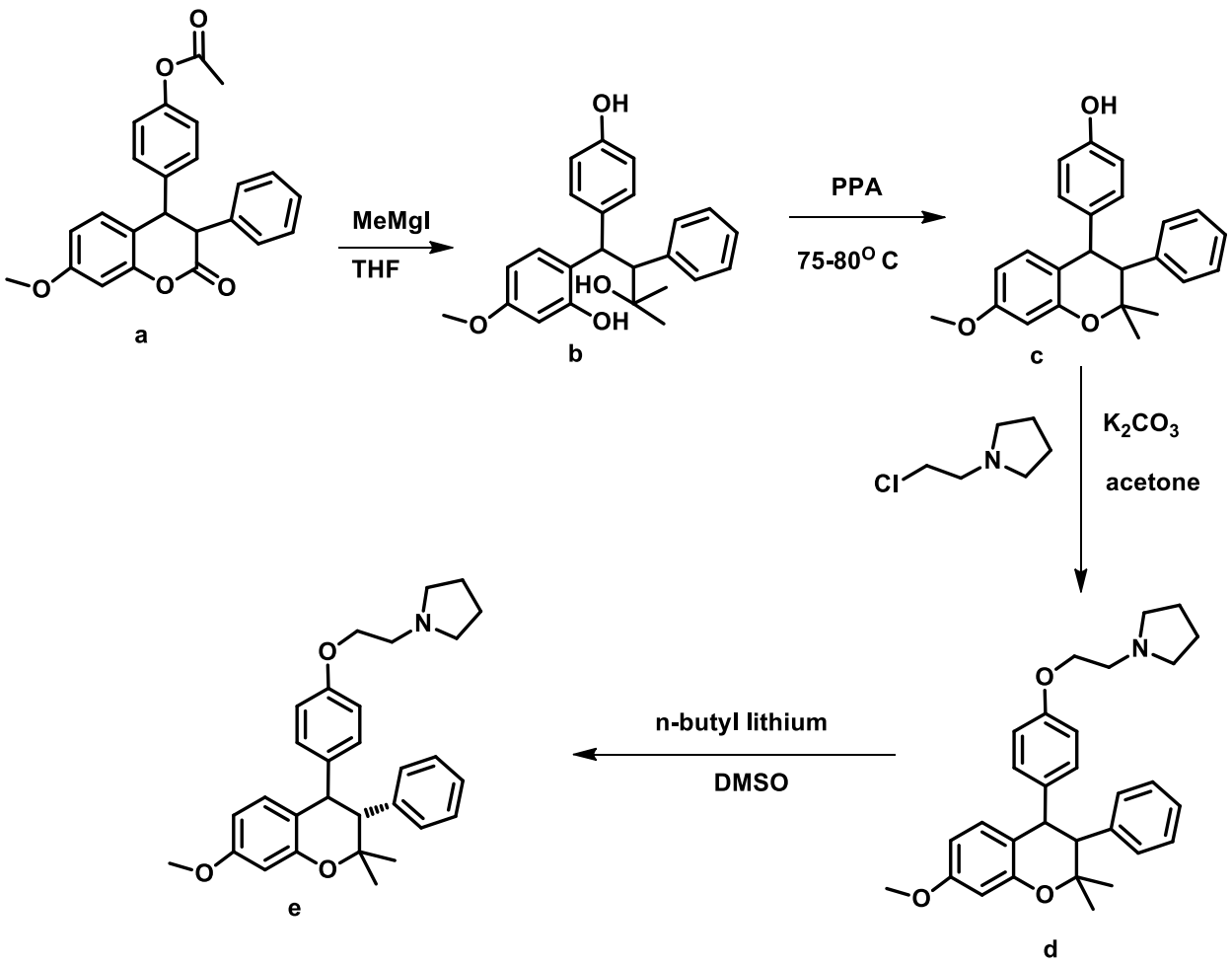

Scheme 1.1 Total synthesis of centchroman.

1.2.1.4 Resolution of dl-centchroman.

D-Centchroman can be resolved by reacting *dl*-centchroman with (+)-O, O′-Di-p-toluoyl-D-tartaric acid ((2S, 3S)-2,3-bis((4-methylbenzoyl)oxy)succinic) acid in dry methanol. The mixture is then stirred for 2 hours at room temperature, the solvent is then evaporated under reduced pressure and the residue crystallized from methanol to afford d-3,4- trans -2,2-Dimethyl-3-phenyl-4-[p -(pyrrolidinioethoxy)phenyl][25]-7-methoxychroman Di-p-toluoyl-d-tartrate a colorless crystalline solid. The *d*-salt is further extracted with aqueous

NaOH (10%) and the organic layer washed with water, dried with anhydrous Na_2SO_4 and concentrated to give *d*-Centchroman. On the other hand *l*-Centchroman is resolved by adding *dl*-centchroman and (−)-O, O′-Di-p-toluoyl-L-tartaric acid ((2R,3R)-2,3-bis((4-methylbenzoyl)oxy)succinic acid) under similar conditions described above to afford the 1-3,4-trans-2,2-Dimethyl-3-phenyl-4-[p-(pyrrolidinioethoxy)benzyl]-7-methoxychromanDi-p-toluoyl-I-tartrate. The L-salt is then extracted with NaOH, and the organic layer was washed with water, dried over anhydrous Na_2SO_4, and concentrated to give *l*- centchroman[22].

1.2.1.5 Pharmacokinetics and bioavailability of Centchroman.

Centchroman (ormeloxifene) is a lipophilic drug and possesses both pharmacodynamics and pharmacokinetic properties. [26] This drug shows low binding affinity to plasma albumen with Kd value of 13.90×10^{-6} which is an evidence of its low binding affinity to albumin and has no interaction with steroids such as cortisol, testosterone, progesterone, and estradiol[27]. It is clear that centchroman does not compete with steroids to a specific binding site and also shows no competition with nonsteroidal agonistics such as diethylstilbestrol nor steroidal antagonistic like tamoxifen[28]. Studies have demonstrated that the liver metabolized centchroman and is quickly excreted from the body through faces[29]. It has also been proved that perfused organs like spleen, liver, and lungs can retain more of this drug as compared to the less perfused organs such as muscles and pancreas. 7- Desmethylated ormeloxifene, the active metabolite (**Scheme 1.2**) of centchroman is formed in a matter of an hour after a patient has taken the drug and peaks within 24 hours[30]. A higher

concentration of this drug as well as its metabolites can be detected in the spleen, liver, lungs, adipose tissues as well as the uterus after administration[31]. It is factual that centchroman and its metabolites accumulate higher in tissues than the plasma and its concentration in tissue or plasma is higher compared to its major metabolite[30]. In human, the overall half-life of ormeloxifene and its primary metabolites with either single dose administration of 30 mg or 60 mg was detected to be around 168 hours whereas that of rats and lower mammals was about 26 hours for 12.5 mg/kg of centchroman[32]. Studies have shown that rats and lower mammals metabolize centchroman faster than humans. The maximum serum concentration (Cmax) of centchroman depends on the dose used, for instance, 30 mg dose has a Cmax of about 55.53 ± 15.43 ng/ml while 60 mg dose has Cmax of 122.57 ± 6.25 ng/ml[32]. Also, the Cmax for 30 mg dose (twice a week for 12 weeks) in breast cancer patients is 54.98 ± 14.19 ng/ml and 60 mg dose for a month or a year is 135 ± 15.5 ng/ml. The Cmax of Centchroman and its half-life are quite similar in both nursing and non–lactating mothers and it is estimated, about 2.5% of the drug is excreted in milk but this is less likely to have any physiological effect on a breastfeeding child. No significant differences were observed in an amount of drug accumulated or time taken for maximum accumulation when multiple repeating doses were administered to adult female volunteers[33]. In rats, a low dosage of centchroman does not affect the hypothalamus-pituitary-ovarian response, but the opposite occurs at much higher dose[34]. The above data is proof that ormeloxifene is a favorable and safe drug candidate for various health problems.

1.2.1.6 Structural activity relationship of centchroman

Anti-implantation, estrogen agnostic, antagonistic and in vitro relative binding affinity (RBA) for rat uterine cytosol endoplasmic reticulum (ER) of DL-centchroman has shown that when the methoxy group at position C-7 is replaced with a phenolic group improves receptor binding affinity[35]. Therefore, a free OH group at the C-7 position is essential for dynamic binding to the estrogen receptor (ER). 7-desmethyl centchroman reported by Merck group is also estrogenic[24] and has been found to prevent implantation in rats at 0.1 mg/kg dose between 1-5 days schedule[36]. Out of the seven metabolites identified in centchroman, after its incubation with rat homogenate, 7-desmethyl centchroman was found to constitute only about 2.5%. When the piperidine moiety, a characteristic of more potent antiestrogens was introduced in the aminoalkoxy side chain, its anti-implantation activity did not improve.

Meanwhile, there was a reduction in relative binding affinity but higher than the methylated moiety[35]. However, the cis – isoforms show negligible binding affinity[35]. The receptor binding affinity, estrogen antagonistic and anti-implantation activities of centchroman is as a result of the pyrrolidinoethoxy side chain at p-4-phenyl position[37]. The removal of the pyrrolidinoethoxy side chain decreases relative binding affinity about tenfold as well as losing its anti-implantation activity[38]. Studies have shown that replacing the pyrrolidine residue with diethyl or dimethyl-amino moiety causes a significant decrease in the relative binding affinity of the compound as a result of the involvement of hydrocarbon component which appears to be in hydrophobic interaction with the receptor[38]. Transposition of pyrrolidinoethoxy moiety to the ortho position on the 4-phenyl ring leads to the total decrease relative binding activity or complete loss of receptor activity of centchroman[22],[39].

Replacement of 3-nbutylamino-2-hydroxypropyloxy moiety with tertbutyl-aminoethoxy increased the anti-implantation activity of centchroman, 3,4-diaryl coumarins, and chromans to 2.5 – 5 fold[40]. The stereochemistry of C-3 and C-4 and substitution at C-2 position offer useful information of stereochemical requirement that influences the optimal receptor fit of centchroman[39]. The relative binding affinity of Centchroman is almost 10-times greater in C-2 unsubstituted 3,4-trans-chroman and four times greater than 2,3-trans-2- methylchroman[39]. A complete loss of receptor affinity was observed when the keto-group was introduced at the C-2 position in 3,4-diarylchromenes[38]. Contribution of these methyl groups to receptor affinity shows the presence of corresponding hydrophobic pocket on receptor fit, though with limited bulk tolerance as evidenced by higher diminished receptor affinity of 3,4-trans-2,2-diethylchroman and decrease in anti-implantation activity by a factor of 20, but its corresponding cis-isomer and its p-4-phenyl hydroxy analogs possess no estrogen and anti-implantation activities[16].

Stepwise increase in relative binding activity was observed when α- and β- methyl groups were introduced at the C-2 of both cis and trans-3,4-chroman. However, the introduction of an additional methyl group resulted in a considerable decrease in receptor binding affinity[39] and may be as a result of the altered stereochemical relationship between the C-4 benzene residue and the two methyl moieties of centchroman (**Scheme 1.2).**

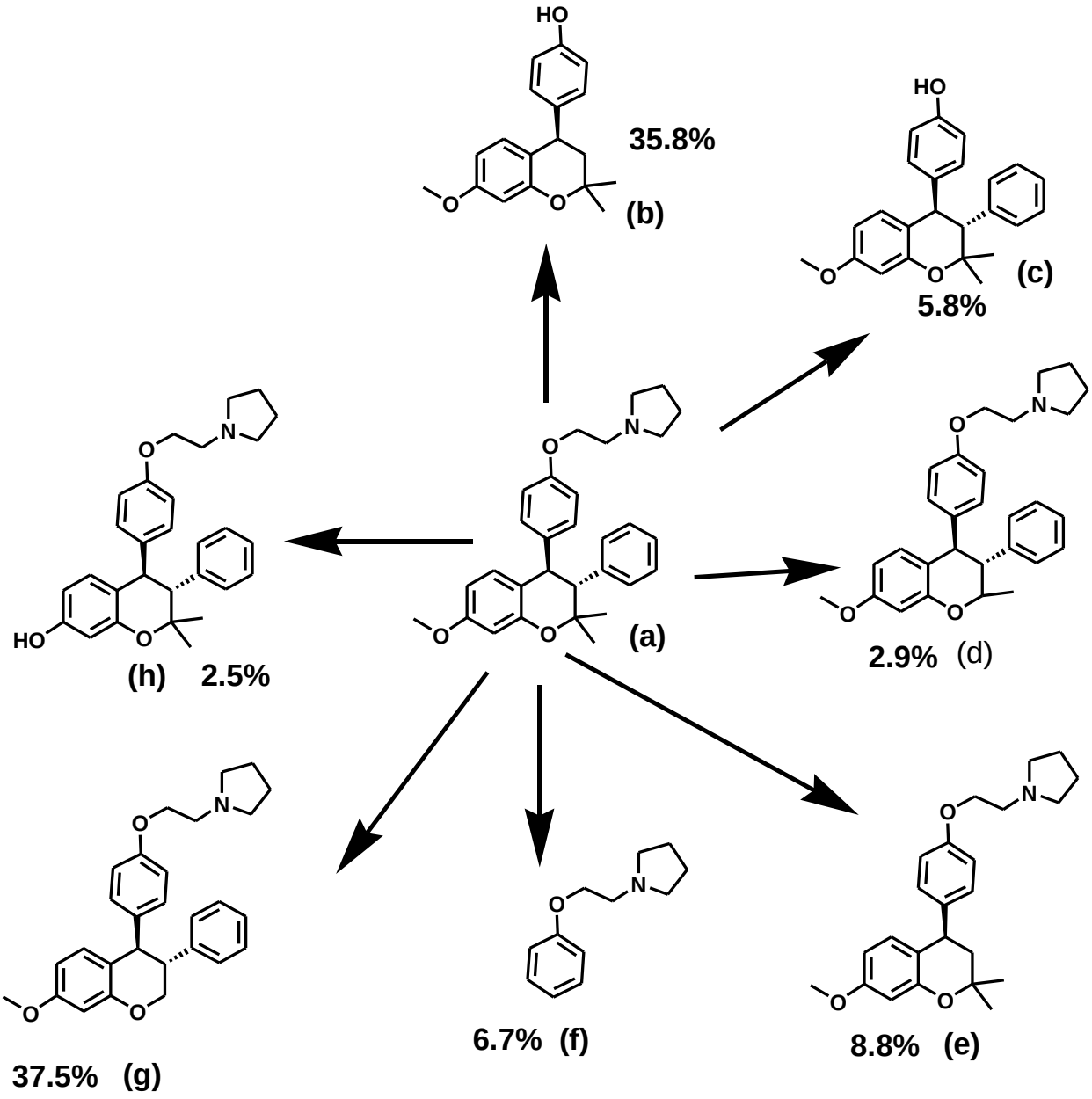

Scheme 1.2 Major metabolites of centchroman isolated from rat liver homogenate after 6 hours incubation.

1.2.1.7 Centchroman (ormeloxifene) and hormone-related disorders

1.2.1.7.1 Abnormal uterine bleeding (AUB)

Menorrhagia affects about 33% of women at some stage in their life, and its management has been a challenging task and available drugs prescribed for this disorder lack consensus for medical treatment[41]. Menorrhagia occurs as a result of uterine abnormalities or large fibroid and is sometimes associated with systemic disorders. This condition is sometimes called dysfunctional uterine bleeding if the cause of the heavy bleeding is not known[41]. There have been several medical options such as anti-inflammatory drugs, combine estrogen and progesterone, Danazol and cyclical combined oral contraceptive pills for the treatment of this condition but comes with a high cost and adverse effects[42].

Centchroman is an estrogen antagonistic on uterine and breast tissues, and its effects are stimulated on bone, vagina, cardiovascular and the central nervous system. It has been revealed that it has no uterine stimulation; it maintains a better function of the brain, lower cholesterol level and has no increased risk of breast cancer and prevents bone loss[43]. The effect of centchroman on the management of menorrhagia and endometriosis was observed when administered as a contraceptive.

In recent studies, one hundred women participated in a clinical study; 60 mg of ormeloxifene was given to each woman twice a week for three months followed by once a week administration for one month. Patients were monitored for six months. Menstrual blood loss was observed by a pictorial blood loss assessment chart (PBAC) score as well as visual analog scale (VAS)[44]. The results showed a significant reduction in median PBAC score ranging from 252 to 102.8 in patients treated with Ormeloxifene and the presence of blood clot reduced from 64 to 12%. On the other hand, the incidence of dysmenorrhea

drastically suppressed from 22 to 8% and the mean endometrial thickness was decreased from 9.7 to 6.7 mm[45]. However, there was an increase in PBAC score to 112.7% when treatment was stopped after six months but lower than the pretreatment level. There was a significant reduction from 64 to 12% in patients with initial passage of clot and massive improvement of patients with mild or severe dysmenorrhea (22 to 12%)[17]. The fact that ormeloxifene is a safe and effective therapeutic option for the management of Menorrhagia cannot be disputed because of its higher potency and minimal side effects.

1.2.1.7.2 Bone loss (Osteoporosis)

According to world health organization (WHO), Osteoporosis is a condition where the patient spinal bone mineral density (BMD) is less than 2.5 standard deviations below the mean of young, average adult of the same gender[46]. It is a condition of increased concern in adults where the bone has been lost to the extent that it is unable to function very well to support its regular activities and this may result in the risk of spontaneous or mild trauma fractures. This condition is highly observed in postmenopausal women with about 75% lifetime risk[47]. There has been an unmet medical need as a result of yearly increased in the number of aged people due to continual increased in life expectancy worldwide. The FDA has recently approved many drugs including selective estrogen receptor modulator, Evista, that can be used to suppress further bone loss in postmenopausal women, but they are not so useful in replacing a significant amount of lost bones[48]. To treat or prevent osteoporosis there has been considerable development of animal models and analytical methods for osteoporosis research.

It has recently been reported that L-centchroman (Levormeloxifene) is capable of preventing bone loss as well as lowering cholesterol level in the rat model and suppress uterine stimulation relative to 17 β estradiol[49] ‘[50]. Studies have also shown that L-centchroman was able to reduce serum cholesterol and biochemical markers of bone turnover in postmenopausal women during clinical trials[51]. On the other hand, Ormeloxifene has demonstrated its antiosteoporotic activity as evidenced by concentration-dependent inhibitor in PTH –induced resorption of ^{45}Ca from pre-labeled chick and rat fetal limb bones with better effect tamoxifen or CDRI-85/287 [52].

1.2.1.7.3 Male infertility

Administration of 30 mg per day of centchroman in oligospermic men for six weeks showed a dramatic increase in sperm count in three individuals with the history of infertility. However, there was a decrease in sperm count in one of the patient, while 4 of the patients were identified to have lower plasma testosterone with no effect on seminal parameters, however, increased in acidic phosphatase and GPC were observed in two of the patients [53]. Increasing dose of centchroman from 30 to 60 and 120 mg a day (twice a week) for six weeks resulted in a significant decreased in sperm count in one of the patients during phase II and III of treatment, but the percentage of nonmotile and abnormal spermatozoa in all the patients escalated. No plasma testosterone or seminal acid phosphatase, Salic acid, GPC or fructose effect was observed in any of the patients[53]. The epididymal motility and vassal spermatozoa pattern nor testicular histology were not affected after up to 10 mg/kg of centchroman was administered throughout the spermatogenic cycle in rats. No adverse effect was observed on the testicular tissue in cholesterol-clamped rabbits after three weeks of administration of L-centchroman[54].

1.2.1.7.3.1 Regulatory safety studies of centchroman

1.2.1.7.3.2 Pharmacological effects

Three months of toxicity studies of centchroman in rats and rhesus monkeys were found to be non-toxic. The compound showed no adverse impact on humans during preclinical trial up to a dose of 120 mg per day[55]. Centchroman has a lower ulcerogenic index (0.8) compared to phenylbutazone (1.7) and is less likely to cause gastric irritation. Its intraperitoneal and oral LD_{50} is higher compared to phenylbutazone and does not in any way produce leucopoenia and eosinopenia as seen in phenylbutazone. Its anti-inflammation and anti-implantation effect is exerted directly on inflamed tissues and does not mediate its weak estrogenic agnostic activity or via pituitary- adrenal axis[56]. Using 30 mg weekly dose of centchroman in women for one year did not cause any hyperaggregability of platelets.[57] The antiaggregatory effects of centchroman are as a result of platelet cyclooxygenase inhibition, and it is an evidence of thromboxane–B2 synthesis as well as inhibition of in malonaldehyde[57,56]. No significant effect on thyroid weight, ^{134}I-uptake, and conversion ratio or excretion rate of 24-hour urinary 17-OH ketosteroids was observed when upon five consecutive administration of centchroman to female rhesus monkeys[58]. When the dose of centchroman was increased to 30, 60 and 120 mg/day for six weeks in normospermic men, it resulted in decreased in urinary 17 –OH ketosteroids in all cases. [53]

1.2.1.7.3.3 Toxicological effect

Centchroman has shown an excellent therapeutic index, upon 12 months administration in rats and rhesus monkey, with no evidence of biochemical, hematological or histopathological toxicity. [59] No evidence of congenital abnormalities of fetuses, anomalies

or aborting was reported during six weeks of oral administration to rabbits and mice[60]. DL-centchroman and its enantiomers possess no mutagenicity, genotoxicity and with a reduced toxic effect on known mutagens and no carcinogenic effects have been observed following life-term administration to rats[61]. Ormeloxifene has a few side effects which include Delayed menstruation, Nausea, Vomiting, headache and Weight gain[62]. Also, women with the desire of becoming pregnant must discontinue taking the drug. However, Ormeloxifene should not be taken by patients with any of the following problems such as polycystic ovarian disease, cervical hyperplasia, the recent history of jaundice or hepatic impairment, severe allergic state, TB, renal impairment[63].

1.2.1.7.3.4 Drug-drug interactions

Oral administration of tetracycline and other non-steroidal anti-inflammation drugs like ibuprofen produces no effect on efficacy or terminal half-life of centchroman, but there was a significant increase in maximum serum concentration, (C_{max}) from 22 to 30 ng/ml and decrease t_{max} from 12 to four hours in rats [64,16]. Similar effects were observed when lactic acid bacillus spores were included in the regimen, C_{max} increased to 47% and $AUC_{0-\infty}$ of 34% of centchroman with a drastic reduction in t_{max}[18]. There is, therefore, no known drug-drug interaction with centchroman, devoid of side effects and safe for prolonged use.

1.2.2 Centchroman as an anti-cancer agent

The established records of the safety of Ormeloxifene along with its favorable bioavailability and ability to inhibit rapid cell proliferation in the endometrium during embryonic implantation has made it a potential drug candidate for controlling undesirable rapid cell growth such as endometriosis and cancerous tumor conditions[65]. Previous studies have confirmed the effectiveness of Ormeloxifene in preventing and suppressing various

cancer cell lines due to its potent estrogen agonist and antagonists functions of the reproductive tissues as well as non-reproductive tissues[66,67] (**Fig.1.6**). Investigations have revealed that Ormeloxifene induced apoptosis, inhibits Akt/mTOR, signal transducers and activators of transcription protein 3 (STAT3) signaling. It can also alter proteins associated with cell cycle regulations and DNA damage and inhibits colony forming efficiency of Head and neck squamous cell carcinoma (HNSCC) cells[68]

1.2.3 Ormeloxifene as an anti-breast cancer agent

Ormeloxifene is known to suppress breast cancer cell migration and invasion in vitro and breast cancer metastasis in vivo. In another development, it has been shown that Ormeloxifene induces G0/G1 phase cell cycle arrest and cellular apoptosis in human breast cancer MDA-MB-231 and MCF-7 cells with IC_{50} of 10µM and 20µM respectively[69]. On the other hand, the migratory and invasion capacity human breast cancer MDA-MB-231 and mouse mammary cancer 4T1 cells were inhibited upon treatment with ormeloxifene. A lower dose of ormeloxifene (< 5M) on breast cancer cells was able to suppress migration and invasion of cells while higher dose inhibited cell proliferation and induced apoptosis which is evidence that suppression of migration and invasion is independent on cell growth or apotosis[70]. Combination of ormeloxifene with other sensitizing agents such as resveratrol and curcumin has also proven to be effective. Combination of these agents relatively lowers the concentration of ormeloxifene induced apoptosis in breast cancer cells[71].

1.2.4 Ormeloxifene as anti-head and neck cancer agent

According to the world health organization, the 6th most common cancer in the world is Head and Neck squamous cell carcinoma (HNSCC) with approximately fifty thousand new cases diagnosed in the United States alone in 2012[72]. The role of the ER in HNSCC is very controversial. While some previous reports have revealed little to no expression of ER in HNSCC because of the controversial role of ER in HNSCC[73]. Recent investigations have shown a significant role for ER in enhancing migration and proliferation of cell in HNSCC[74]. Ormeloxifene has been known to exert its cytotoxicity via ER-dependent and ER-independent pathways in cancer cells, and its potential utilization for HNSCC treatment has been investigated[68]. Dual inhibition of ormeloxifene on Akt and mTOR could be a significant therapeutic breakthrough as these signaling pathways are massively activated in HNSCC which explains how Akt/mTOR inhibitor effectiveness to overcome the effects of feedback loops better than a single inhibitor that selectively targets mTOR[75,76]. It is worth noting that ormeloxifene inhibits multiple HNSCC cell line growth by inducing apoptosis through caspase 3 activation. Treatment with ormeloxifene inhibits phosphorylation of Akt which leads to attenuate downstream Akt signaling thereby suppressing Akt/mTOR, STAT3 signaling and enhanced p21 and p27 protein expressions associated with cell cycle progression[77]. These promising in vitro results have shown ormeloxifene to be a potential drug candidate for the treatment of HNSCC and warrants for further clinical studied.

1.2.5 Ormeloxifene as an anti-prostate cancer agent

The second most common leading cause of cancer death in male is prostate cancer[72]. ER is found in both the stroma and epithelium of the prostate. Studies have revealed estrogen as the genesis of prostate cancer. Rising estrogen and decreasing androgen levels in aged males triggers prostate cancer, and this is where SERM comes in as a potential treatment of prostate cancer where it selectively inhibits ER. There have been several reports where tamoxifen, and in combination with other anticancer agents have been used to suppress the proliferation of prostate cancer cells[78,79]. Other SERM such as raloxifene has been reported to inhibit prostate cancer cell growth expressing in different levels of ERα and ERβ and has efficiently induced apoptosis and inhibited proliferation of prostate cancer cells by modulating multiple signaling pathways [80]. The use of ormeloxifene as a prostate cancer agent has however not been reported, but the initial report has predicted the effectiveness of ormeloxifene to arrest androgen-dependent and independent androgen growth of prostate cancer cell growth[26].

1.2.6 Ormeloxifene and Chronic Myeloid Leukemia

Recent studies have revealed that Ormeloxifene induces apoptosis in several leukemia cells in a dose-dependent manner especially in K562. 2-DE-gel electrophoresis of K562 cells, 57% of the cells induced apoptosis when treated with ormeloxifene while 30% of proteins belong to cell cycle pathways. Activation of the extracellular signal-regulated kinase (ERKs) and further cytochrome C release, leading to mitochondria-mediated caspase-3 activation are evidence of ormeloxifene-induced apoptosis[81]. Moreover, Ormeloxifene suppresses the proliferation of K562 cells by blocking them in the G0/G1 phase and suppressing c-myc promoters via ormeloxifene induced MBP-1 and upregulation of p21

expression[81]. The ability of ormeloxifene to induce apoptosis in K562 cell via phosphorylation or ERK and block them in G0/G1 through reciprocal regulation of p21 and c-myc has been demonstrated[81].

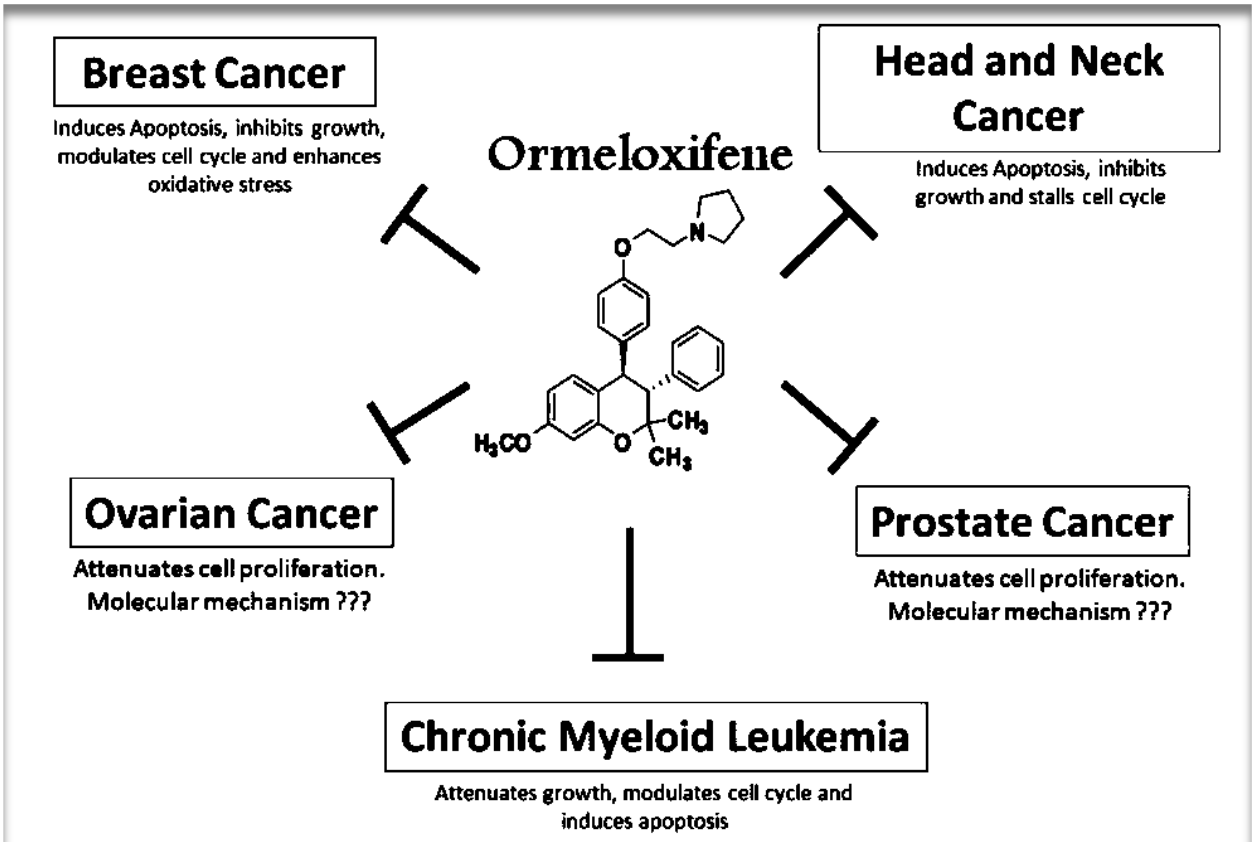

Figure 1.6 Ormeloxifene efficiently attenuates the growth of multiple types of cancer cells Adapted from (Kumar G et al., 2013).

1.3 Ovarian Cancer

Ovarian cancer remains the leading clinical challenge in gynecological oncology. It is among the leading cause of death (approximately 140,000 per year) worldwide and estimated to be diagnosed in over 220,000 women every year [82]. Ovarian cancer is the second most frequent malignancy after cancers of the uterine corpus in the United States with 20,880 estimated cases each year. About 13,850 women die from ovarian cancer annually representing the most common cause of death among women with gynecological malignancies[83]. The lifetime incidence for ovarian cancer is approximately 1.39% (1 in 72) and about 1.04% death risk from ovarian cancer for women living in the united states. The higher mortality rate of ovarian cancer is attributed to its late stage of diagnosis as approximately 75% of patients present with evidence of metastasis spreads beyond the ovaries[84]. The median survival rate is as between 24 to 60 month depending on the magnitude of residual disease following initial surgery(**Fig 1.7**)[85].

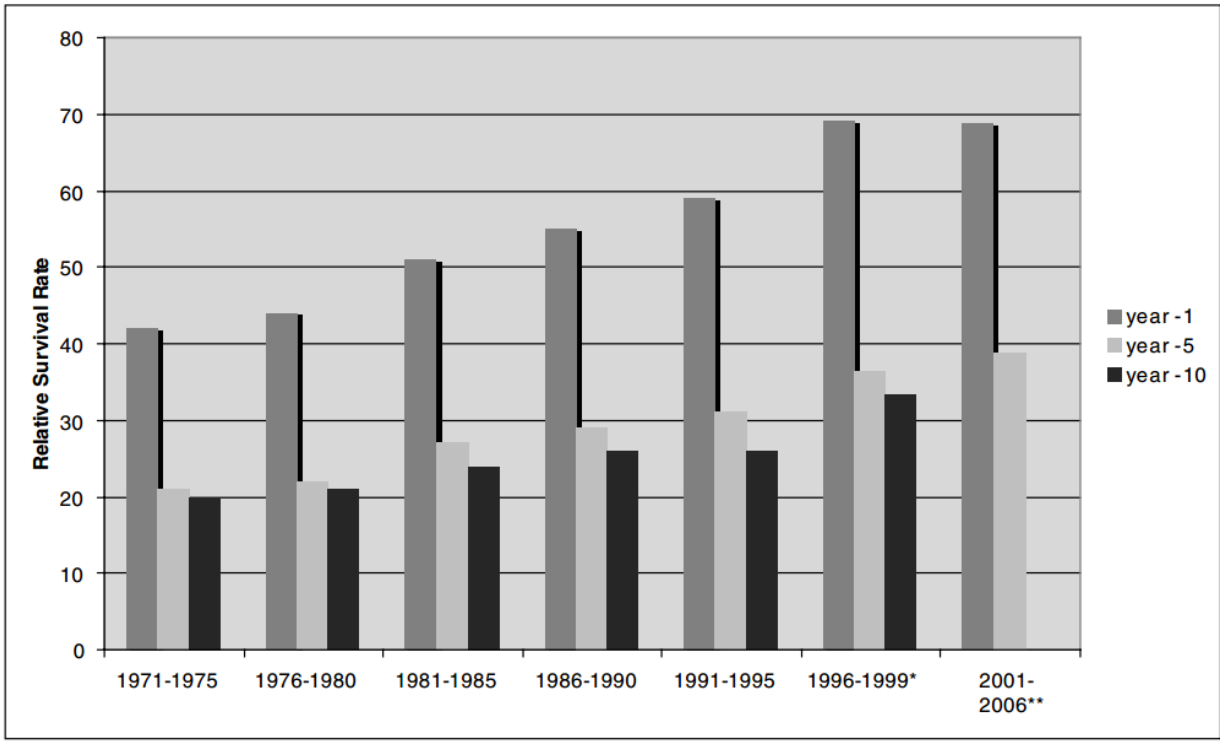

(* England only data, ** shows one year survival between 2001-2003 and five year survival between 2001-2006)
Data source: Office of National Statistics and Cancer Research UK

Figure 1.7 Survival rates of ovarian cancer in England and Wales (1971-2006)

1.3.1 Classifications of ovarian cancer

The histological classification of ovarian cancer according to world health organization (WHO) is based on the principle of histogenetic of the normal ovary [86]. This histogenetic classification groups ovarian neoplasms based on their derivation from coelomic surface epithelium, germ cells, and mesenchyme (the stroma and the sex cord). Epithelial ovarian cancer which is the primary malignant ovarian tumor in adult females and is classified into histological categories such as acute, mucinous, endometrioid, clear cell and transitional,

squamous, mixed and undifferentiated epithelial tumors[87]. Lesions that appear *in situ* in the surface epithelium or surface epithelial inclusion glands (SEIG) and preexisting benign epithelial ovarian endometriosis and tumors have been described as a possible precursor of ovarian surface epithelial lesions.

1.3.2 Epidemiology

There has been an increased incident of ovarian cancer in the United States, Europe, and Israel with the lowest in Japan and the developing countries[88]. The incidence of ovarian cancer in the united states is higher in Caucasian women than African-American and Asian American women[88], but there is evidence that the gap is narrowing every year. Compared to the native-born women, there is a gradual increased in the cases of ovarian cancer in women who migrated from low-risk countries of origin such as Asia to the high-risk countries like the United States[89].

1.3.3 Etiology

1.3.3.1 Family history

Family history of breast cancer is the most significant risk factor of ovarian cancer. The risk of the disease depends on the number of affected relatives as well as their age at diagnosis with ovarian or breast cancer[25a]. Most hereditary ovarian cancer cases occur as a result of mutation of BRCA genes, with almost two-thirds of the cases associated with BRCA1 gene mutation on chromosome 17q, and the rest linked to BRCA2 mutation found on chromosome 13q[90]. According to U.S. based population studies, the average lifetime risk for ovarian cancer is approximately 30% in BRCA1 carriers[91]. It has been estimated that about 5% of all ovarian cancer cases in women under the age of 40 can be associated with BRCA1 mutation while 4.4% and 1.1% rate are recorded in women between ages of

40 to 50 and above 50 years respectively[92]. However, there is approximately 87% cumulative risk of breast cancer in people from high-risk families with BRCA1 at the age of 70 [91]. The risk for ovarian and breast cancers in BRCA2 mutation carriers has been reported to be 20% and 84% respectively [93]

1.3.3.2 Reproductive factors

The concern of ovarian cancer in women is age independent, but late menopause has been confirmed to be one of the risk factors of ovarian cancer[94]. An increased risk of ovarian cancer has also been reported in women who have never given birth and therefore infertility is one of the significant risk factors for ovarian cancer[95]. Risk of ovarian cancer and the use of infertility drugs has been a considerable concern. There is a significantly increased risk of ovarian cancer in women with prolong use of infertility drug as compared to women who received a short term treatment[96].

1.3.3.3 Environmental and dietary factors

Varieties of factors such as the use of talc in genital hygiene, exposure to radiation, use of tobacco, psychotropic medications, the mumps, high-level physical activities[97], virus, dietary factors, and caffeine consumption, have been associated with ovarian cancer. Other studies suggested an excessive use of premenopausal estrogen as the leading risk factor of endometrioid ovarian cancer. However, there has not been any proven risk of ovarian cancer associated with the use of premenopausal hormone[98]. Moreover, risk factors such as the prior history of pelvic inflammatory disease[99], endometriosis and polycystic ovarian syndrome[100] have been linked to ovarian cancer.

1.3.3.4 Pharmacological agents

The use of oral contraceptive has shown to reduce the risk of ovarian cancer. Studies conducted revealed that the use of oral contraceptive by women for 4, 8 and 12 years reduces their risk of ovarian cancer by 40%, 53%, and 60%, respectively. Therefore, the risk of ovarian cancer decreases with increasing duration of the use of oral contraceptive and this protective effect continue to exist even after the patient discontinued use[101]. Cancer and Steroid Hormone studies (CASH) have revealed that women who have never given birth and have used an oral contraceptive for five or more years are less prone to ovarian cancer risks compared to those who have given birth and have never taken oral contraceptives. Prolong use of oral contraceptive (10 years and above) by women with a family history of ovarian cancer reduced their risk level below the general population baseline[102]. The use of oral contraceptives for six years or more in women with a high risk of BRCA1 and BRCA2 have resulted in about 60% risk reduction[103] **(Fig 1.8).** Acetaminophen and synthetic retinoid are the two pharmacological agents believed to reduce the risk of ovarian cancer but need to be studied further[104].

	Estimated risk (%)	Estimated relative risk
Baseline lifetime risk	1.4 to 1.8	1
Risk Factors		
Family history	9.4	5–7
BRCA1 mutation	30–40	18–29
BRCA2 mutation	27	16–19
Lynch II/HPNCC[a]	10	6–7
Infertility		2–5
Nulliparity		2–3
Late menopause		1.5–2
Early menarche		1–1.5
Protective Factors		
Multiparity		0.4–0.6
Oral contraceptive use		
× 4 years		0.6
× 8 years		0.5
× 12 years		0.4
Hysterectomy or tubal ligation		0.4–0.6

[a]HPNCC, hereditary nonpolyposis colorectal cancer.

Figure 1.8 Factors Influencing the Risk of ovarian cancer.

Adapted from Holschneider and Berek, Seminars in Surgical Oncology 2000; 19:3–10

1.3.4 Etiology of ovarian cancer: a proposed mechanism

The chronic injury and repairs cycle of ovarian surface epithelium (OSE) in connection with ovulation can lead to mutation in genes that regulate the OSE growth. A crypt is formed on the surface of the ovary lined with epithelial cells; these crypts can break through the underlying extracellular matrix during reproductive and premenopausal life and become internalized as epithelium line inclusion cyst into the stroma. Surface epithelial cells that are hidden in inclusion cyst in the ovarian stroma during the repair process of

OSE are eliminated by apoptosis and as results eliminate the potential sites of ovarian tumorigenesis. However, if the apoptotic elimination process is weekend or damaged, it results in the persistence of the inclusion cysts in the stroma leading to exposure of stroma-derived growth factors, steroids, and intragonadal peptides and cause propagation of mutation and proliferation of tumor formation[105].

Fas/Fas ligand system, a major apoptotic inducer in the immune system is a 48 kDa cell membrane protein which is part of tumor necrosis factor (TNF) and a family of nerve growth factor (NGF) receptor[106]. Cells that express Fas can induce apoptosis when they are exposed to either Fas ligand or an agonistic monoclonal Fas antibody[107]. The ovary in addition to the immune system, on the other hand, expresses the abundance level of Fas mRNA and is active in human and rat ovary[108 ،109]. Localization of Fas in the surface of epithelial cells section of normal human ovaries has been confirmed, and it has shown to express Fas and remain healthy and viable as long as they are prevented from making direct contact with the stroma by the underlying connective tissue[110]. As crypt is internalized and inclusion cyst is formed, the barrier becomes disrupted resulting in direct contact formation of surface epithelial cells with stromal cells that synthesized Fas ligands. This cell-cell contact between the mesenchymal cells with epithelial cells triggers Fas and signal transduction pathway induces apoptosis and death of inclusion cyst[110]. However, the persistence of the inclusion cysts in the stroma and onset of tumorigenesis occur when the Fas/Fas ligand system fails to operate[110].

1.3.5 Diagnosis and treatment of ovarian cancer

1.3.5.1 Diagnosis of ovarian cancer

The highest fatality rate of ovarian cancer is due to lack of early warning signs, effective detection techniques and the successful management of the disease. Many cancer networks and health institutions have recommended symptoms that trigger testing for ovarian cancer[111]. Women that show persistent symptoms of loss of appetite, frequent urinating, pelvic, abdominal pains, abdominal distension, early satiety, unexpected loss in weight, fatigue, change in bowel movement should be tested in the primary care setting and refer urgent cases to the secondary care for immediate diagnosis and treatment to enhance survival[112]. The use of serum markers (such as CEA, CDX2, CA 19-9, AFP, beta-HCG, and HE4) are essential and has improved in the early detection of ovarian cancer. It is recommended to conduct sequential testing of serum CA125 followed by abdominopelvic ultrasonography if the level of serum CA125 is higher than 35 IU/L and urgently refer women diagnosed with ascites and pelvic or abdominal masses for further testing[111]. However, CA125 does not diagnose the early stage of ovarian cancer with high accuracy and is prone to false results. As such, the need to identify additional markers is vital to the successful management of the disease. DNA chip technology is used to address this problem at the genomic level and provide accessibility to gene expression profiles. The studies of changes in proteins that result from pathological lesion such as cancer would, however, be the critical source of potential cancer biomarkers[113]. Sonography screening and serum test/imaging, mass spectrometry proteomic approach, the SELDI (surface-enhanced laser desorption/ ionization)[114], and protein chip system appear to be potential biomarker discovery and effective tools for ovarian cancer screening **(Fig 1.9)[115].** There is,

therefore, a need for a useful tool and techniques to detect early warning signs and successful treatment of ovarian cancer

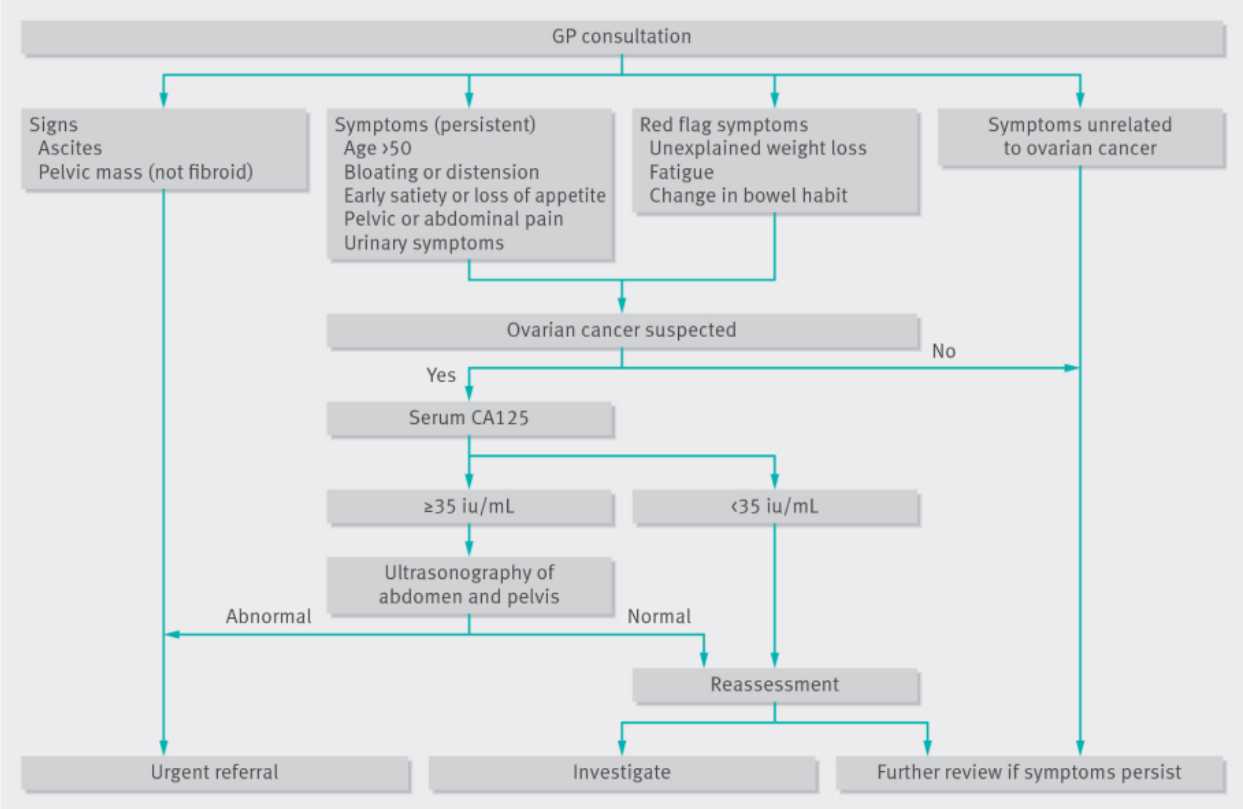

Figure 1.9 Floor chart for the diagnosis of ovarian cancer. Adapted from National Institute for Health and Care Excellence (NICE)

1.3.5.2 Treatment of ovarian cancer

The standard treatment of advanced ovarian cancer over the past decades includes surgical approaches followed by platinum and alkylating–based chemotherapy[116]. Manipulation of combinations dosages of existing drugs have resulted in marginal gains, but the use of these agents in standard therapy has not improved the overall survival of ovarian cancer patients. Several clinical controlled trials have predicted the platinum-paclitaxel combination

regimen as the initial treatment for advanced ovarian cancer with the responds rate of more than 80% and 40-60% complete responses[117]. However, a number of these patients suffer deterioration after a period of improvement (about 18 months)[118,119]. The disease-free period following patients' responds to the platinum compound is used to group patients into different prognoses categories such as platinum-resistant, platinum-sensitive, and platinum-refractory diseases. Since the platinum-resistant disease and platinum-refractory disease have less than 10-20% response rate to carboplatin, they are further treated with other agents such as gemcitabine, liposomal doxorubicin, topotecan, etoposide, and hormonal therapies[117]. The response rate, however, decreases at each subsequent relapse leading to drug resistance. A significant challenge in the treatment of ovarian cancer is the failure of current established therapies to treat the disease at the diagnosis stage. Other cytotoxic drugs including trabectedin, patupilone, and canfosfamide are recently used to overcome drug resistance in ovarian cancer, and the most effective has been the combination of trabectedin with doxorubicin[120]. The agents that currently being used to treat ovarian cancer have a different range of mechanical action such as binding to VEGFA or VEGF receptors, inhibition of receptor tyrosine kinase activation and downstream molecules[121].

1.3.5.2.1 Resistance to chemotherapy

Resistance to chemotherapy has been a significant threat to the treatment of ovarian cancer. This failure in treatment occur in more than 90% of patients with metastatic disease and have resulted in many death[117]. Drug resistance in clinical practice refers to the progressive disease that occurs at the dose associated with manageable toxicity. Most of these chemotherapeutic agents have very minimal therapeutic index such that small-fold changes

in the sensitivity of the patient tumor cells can result in clinical resistant. Reason for chemotherapeutic failure and clinical drug resistance can be categorized into three groups: (a) Pharmacokinetic, (b) tumor micro-environmental and (c) and cancer cell specific.

1.3.5.2.1.1 Pharmacokinetic

It has been established that the fraction of tumor cells killed in many cytotoxic agents is proportional to total drug exposure (**drug concentration x time of exposure = area under the curve** (AUC)). Insufficient intratumor drug concentration due to inter-patient differences in pharmacokinetic variables in some cases might result in drug resistance. First pass metabolism, conversion of prodrugs to active metabolites, renal clearance, hepatic drug metabolism, and tumor vascularity are some of the parameters for drug resistance[122,117]. Interpatient variation in drug effect has also been identified as a result of a change in gene expression and enzyme polymorphism[117].

1.3.5.2.1.2 Tumor microenvironment

Tumor microenvironment has been known to modulate tumor cell drug sensitivity while hypoxia has been identified to trigger radioresistance, chemoresistance implications[123], and might be related to cell arrest at G0 phase following hypoxic stress (limited free radicals generation, enhanced drug detoxification, increased genomic instability, and HIF1) mediated transcriptional activation of survival signals and inhibits apoptosis[124]. On the other hand, stromal cells can induce chemoresistance via antiapoptotic signaling pathway.[125]

1.3.5.2.1.3 Cancer- cell-specific

Tumor- cell-specific mechanisms have been the leading research emphasis on drug resistance as well as those that influence drug-target interactions and subsequent cell damage. The hypothesis has it that drug resistance develops due to progressively acquired somatic mutation or epigenetic changes inside the tumor cells as they develop gradually with time[126]. It is essential to consider the primary effectiveness of cytotoxic agent against rapid cell and tumor proliferation where a significant amount of cancer cells are in a quiescent state. These quiescence cells, however, show a degree of drug resistance[127] **(Fig 1.10).**

1.3.5.2.2 Cellular mechanism of multidrug resistance

The two main classifications of anticancer drug resistance are those that impair drug delivery to tumor cells and those that develop in the cancer cell itself as a result of genetic and epigenetic alterations that affect drug sensitivity. Poor absorption of orally administrated drugs can lead to impaired drug delivery since it can increase drug metabolism or excretion, results in lowering drug level in the blood and reduce diffusion of drugs from the blood into the tumor mass[128,129]. The important of the vasculature of the tumor and appropriate pressure gradient for effective drug delivery to cancer has extensively been studied [129]. Cells that are sensitive to chemotherapy as monolayer cells in culture become resistance when transplanted into animal model[125]; this supports the fact that environmental factors such as extracellular matrix or tumor geometry may play a part in drug resistance. The growth of cancer cells in cell culture as three-dimensional spheroids, imitating their *in vivo* geometry is another evidence of resistance to cancer drugs[125]. Cancer cell in culture can become resistant to a single or multidrug with similar

mechanical action, by altering the cellular target of the drug or increasing the repair of drug-induced damage frequent to DNA. Cells that are resistant to a single drug can also show cross-resistance to another drug that is different structurally and mechanistically- a situation called multi-drug resistant[130].

Many anticancer drugs currently in the market have shown multi-drug resistance problems in most cancer patients, and there is an urgent need for new and potent anticancer therapies to address the multi-drug resistant problem.

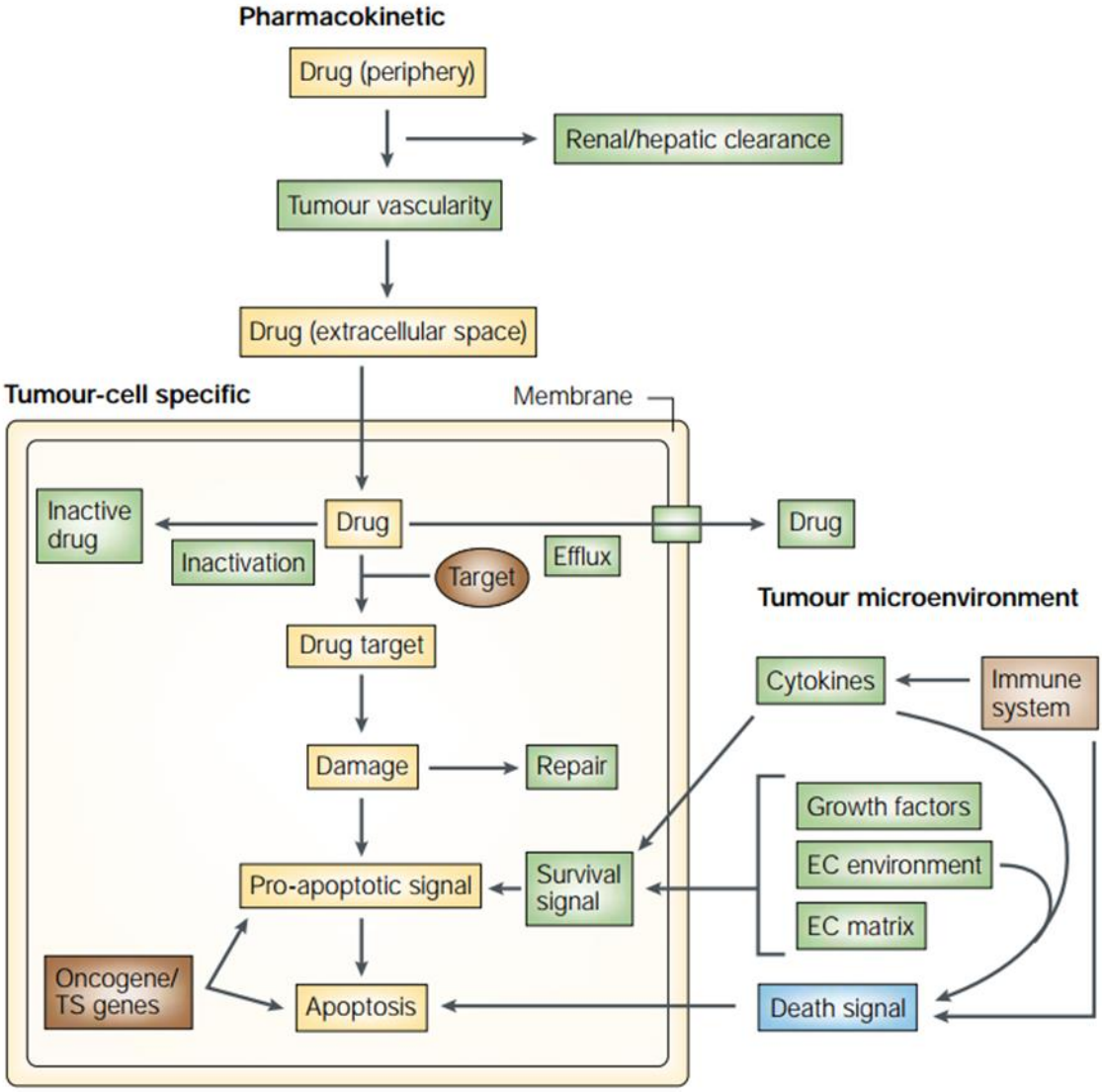

Figure 1.10 Drug resistance mechanism[130]

1.3.6 Molecular targets for the treatment of ovarian cancer

There has been a various range of molecular targets that have been discovered in different arrays of malignancies. Many therapeutic agents have been developed to target multiple processes such as cell cycle regulation, angiogenesis, protein translation, apoptosis induction, metastasis and signal transduction[84] **(Fig 1.11)**. However, there has been no

identification of specific gene amplification or gene mutation responsible for progression or initiation of the disease. The nonexistence of single pathogenic mutation is a challenge for target therapy[131] and the need for molecular targeted agents with cytotoxic regimens is likely to yield significant benefits towards the treatment of ovarian cancer. These agents include non-receptor tyrosine kinase, receptor tyrosine kinases inhibitors (RTK), transfereaces, serine-threonine kinases, selective inhibitors with either multiple or dual inhibitors, proteases and other pathways. The search for new and active molecular target anti-cancer agent for the treatment of ovarian cancer has become a significant area for research due to the urgent need to address the problem of drug toxicity and cellular resistance. Also, identification of the molecular target is vital for the discovery of potent treatment to overcome drug resistance and decreases the side effects. Several types of molecular targets for the treatment of ovarian cancer such as Erbb receptor pathway, VEGF family of receptors, PARP inhibitors and other pathways are elaborated in the next section.

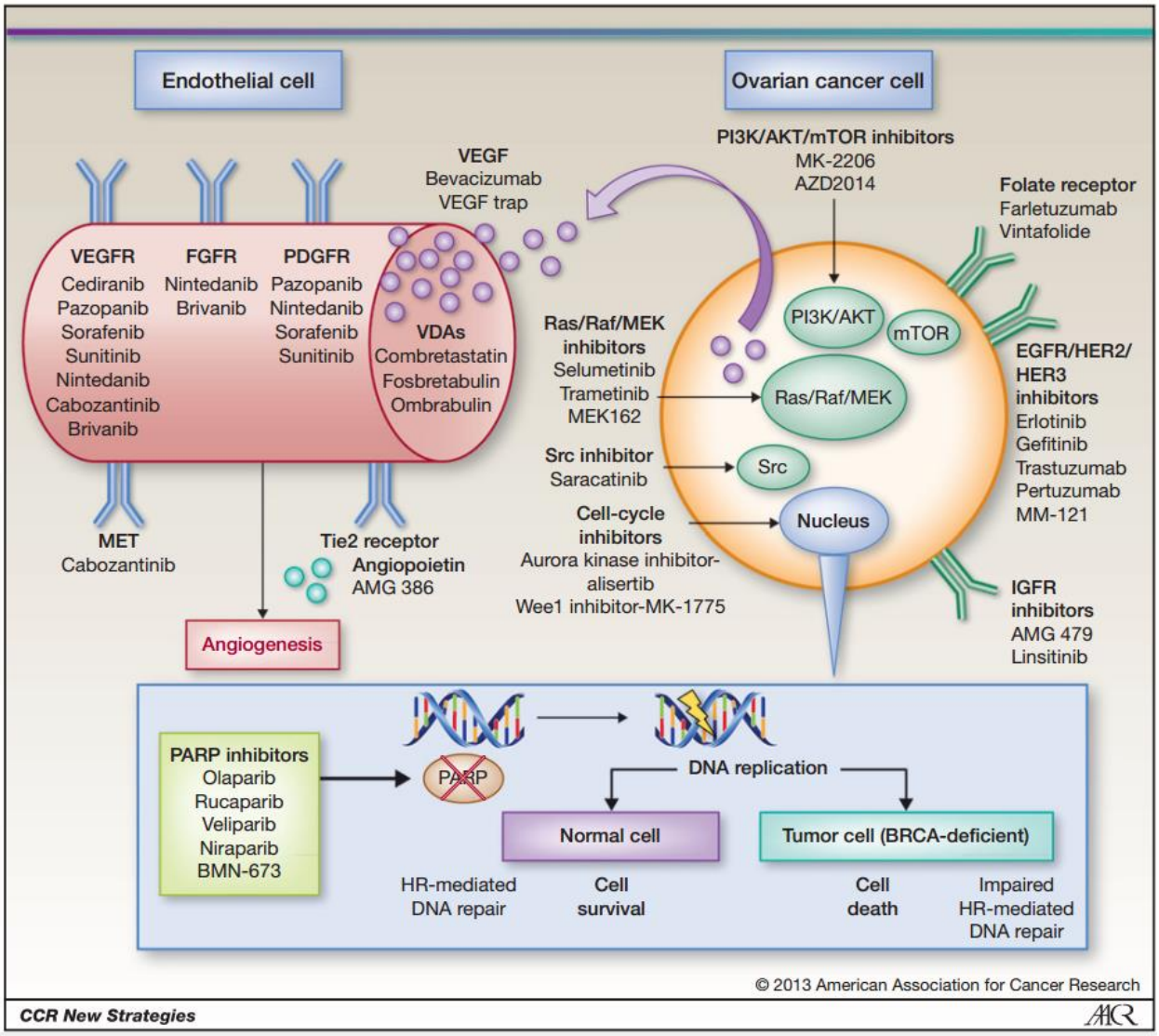

Figure 1.11 Target therapies for ovarian cancer

1.3.6.1.1 ErbB receptor pathway

Diverse signaling pathways and biological events are contributed by homo and heterodimerization within the ErbB family of RTK which are regulated by this class of receptors, and results in the activation of intracellular signaling pathways such as the phosphatidylinositol 3- kinase (P13K)-AKT and MAPK (mitogen-activated protein kinase pathways that involved in proliferation and survival of cells[132,133]. ErbB receptors and their ligands initiate tumorigenesis by inducing tumor survival, growth, invasion,

migration, vasculogenesis, angiogenesis and drug resistance. Several small molecular inhibitors and antibodies have been developed to inhibits various ErbB receptors[132,133]. High levels of several ErbB ligands such as EGF, HB-EGF, TGFα are expressed in ovarian cancer which can result in amplification and expression of EGFR and Her2, ErbB3 and ErbB4[134]. Among the small molecule inhibitors of EGFR are gefitinib and erlotinib. Gefitinib as a single agent is well tolerated, but its activity decreased in unscreened patients with recurrent ovarian or primary potential carcinoma[135]. However, the activity of erlotinib (similar EGFR inhibitor) marginally increased when used as a monotherapy and was well tolerated in patients with refractory, recurrent, EGFR-positive epithelial ovarian tumors who exhibited resistant to platinum-based chemotherapy[136].

1.3.6.1.2 VEGF family of receptors

Vascular endothelial growth factor receptor (VEGFR) and VGFR2 are members of the family of RTK activated by vascular endothelial growth factor (VEGFR), an angiogenic factor that involves a progression of malignancy and the formation of ascites in ovarian cancer. VEGF overexpression corresponds with microvessel density and has been linked to inferior survival[137,138]. Antibody against VEGF in pre-clinical murine models of bearing human xenografts was able to suppress and reverse the formation of ascites[139]. Also, a partial combination of VEGF-paclitaxel resulted in potential synergy and inhibited apoptosis[140]. Bevacizumab, a monoclonal antibody and small molecule inhibitors such as decoy receptors and sorafenib have been developed against VEGFR and VEGF.

1.3.6.1.3 c-Kit and PDGFR

Stem cell factor receptor, platelet-derived growth factor receptor (PDGFR)-α and PDGFR-β are RTK that stimulate the growth of tumor cell. Various small molecule inhibitors have

been developing as novel Abelson (ABL) inhibitors for imatinib mesylate-resistance tumors[141]. Studies have found out that c-kit and PDGFR with their respective ligands are expressed in ovarian cancer[137]. Furthermore, the overall survival rate in patients with PDGFR-α positive ovarian cancer is shorter compared to patients with PDGFR-α negative tumors[138].

1.3.6.1.4 PARP inhibitors

PARP is one of the inhibitors that target one of the genes in synthetic lethal pair while other is defective (e.g., BCRA mutation), selectively kills the tumor cells while sparing healthy cells and create a potential substantial therapeutic window[142]. Patients with BRCA1 or BRCA2 mutation are susceptible with the treatment of PARP inhibitors and has been supported by phase II trials of olaparib in patients with germ-line BRCA1 or BRCA2 mutation ovarian cancer as well as patients with platinum-resistance disease[143].

1.3.6.1.5 Ras/Raf/MEK/ERK pathway

Activation of mitogen-activated protein kinase (MAPK)/extracellular signal-regulated kinase-kinase (MEK) signaling pathway by RTK's, cytokines receptor and integrins is reported to suppress tumorigenesis by stimulating tumor growth, matrix degradation metalloproteinases (MMP) production and drug resistance[144]. These pathways are activated or mutated via autocrine and paracrine loops in ovarian cancer as well as other cancers. Expression of Raf is reported in various ovarian carcinomas, high expression of b-Raf has been associated with improved survival while high expression of c-Raf is related to poor prognosis[145].

1.3.6.1.6 PI3K/AKT/mTOR pathway

The phosphatidylinositol-3-kinase (PI3K) signaling pathway is reported to regulate growth-related cellular functions such as transcription membrane trafficking protein degradation, translation, and reorganization of the actin cytoskeleton[146]. Amplification or mutation of PI3KCA or ATK occurs in 40% of ovarian cancer cases, which leads to phosphorylation of ovarian mTOR and results in tumor cell survival[147]. PI3K mediates angiogenesis as well as vascular permeability in ovarian tumor and is associated with regulation of cisplatin resistance in ovarian cancer [148,149].

1.3.6.1.7 JAK/STAT pathway

Janus-activated kinase (JAK) family of tyrosine kinases are members of RTK and cytokine receptors which subsequently triggers the activation of members of the signal transducer and activator of transcription (STAT) family. JAK and STAT pathways regulate cellular processes such as cell survival, cell proliferation, angiogenesis and antitumor immunity that imitate tumorigenesis[150]. Overexpression and phosphorylation of STAT3 downstream of JAK2 are daily observations in an advanced stage of ovarian cancers[151]. Compared with early and normal ovarian cancer cells, STAT5 and STAT3 phosphorylation have also been reported in endothelial ovarian cancer as well as elevated tumor cell[152].

To understand the interaction between a small molecule and a protein at atomic level which allows us to characterize the behavior of compounds in the binding site of the target protein as well as predict the fundamental biochemical processes is essential. One of the techniques known to assist with the design and predict the interaction of compounds inside the molecular target is molecular modeling.

1.4 Molecular modeling

1.4.1 Introduction

Molecular docking is one of the critical components of structure-based drug design and has been used to design potential virtual drug candidates in silico by optimizing lead drug candidates targeted against the protein. The lead compound is identified using docking algorism that screen for optimal binding mode of the ligand within the active site of the macromolecule or a receptor. The purpose of docking in drug discovery is to identify a drug candidate that binds strongly to a given protein or receptor than the natural product and alter the biochemical process that catalyzes the molecular target[153]. A library of thousands of compounds is screened against a given receptor. This approach, although long, allows for cheaper and faster identification of drug candidate for immediate synthesis, toxicological studies, and clinical trials. Docking employs energy-based scoring function to identify the most stable ligand conformation as it binds to the receptor. The Lower the energy score, the better the protein-ligand binding affinity. Molecular docking can, therefore, be formulated as optimization of problem during identification of ligand-binding mode at the lowest energy. Docking remains one of the challenging issues as a high number of possible docking conformations prevents a systematic brute force[154]. The process starts with the applications of docking algorism that present small molecules to the active site and create a conformational degree of freedom. The degree of freedom must accurately be performed to identify an active and stable conformation for the receptor to achieve a docking run for thousands of compounds[155]. Algorithms are accompanied by scoring functions that are designed to predict the biological activity through the evaluation of interrelations between compounds and potential targets[155]

1.4.2 Molecular docking approaches

In docking, the main goal is to predict the best binding mode that allows a compound to fit into the binding site of a receptor. Docking involves two independent approaches: (1) Simulation approach, where the ligands position, conformation, and configuration are separated by certain distance to predict ligand pose within the binding site of a receptor; (2) Shape complementary approach, where the ranking is typically an arbitral reflection of how well the ligand is expected to bind to the receptor[155].

1.4.3 Molecular representations for docking

It is essential to consider the representation of protein and ligands before various docking is evaluated. There are three underlying receptor representations, and they include (1) Atomic, (2) surface and (3) grid[156]. Atomic representation, among these methods, is the only method that is used concurrently with potential energy function during the final ranking procedures. Surface-based docking programs, on the other hand, is not used in protein-protein docking. These methods align points on the surfaces by minimizing the angle between the surfaces of opposing molecules[157]. The grid methods, however, stores information about the energetic contribution of the receptor on the grid point which is read during ligand scoring.

1.4.4 Scoring functions in docking

One of the problems associated with molecular docking is to develop an energy scoring function that can accurately describe the protein-ligand interactions. The scoring function has three main applications in molecular docking: (1) Determination of site and binding mode ligand on protein, (2) Prediction of absolute binding affinity between protein and ligand, and (3) virtual library screening. Scoring functions that are commonly used are the

field of force, knowledge-based scoring function, consensus core, empirical scoring function and the like. However, all scoring functions suffer from a significant size dependent on the score, the larger the molecule, the higher the possibility that its score rank higher. Also, scoring function ignores entropic effects by assessing the interaction between a ligand and a rigid receptor without taking ensemble averages over many structures and also ignore the specific solvation and desolvation effects[158].

Molecular docking is one of the essential techniques in the computational methodology of drug discovery. It helps to find the appropriate conformational structure that binds to protein active site and score a higher binding affinity. Docking process provides a pattern or a set of compounds with specific pharmacophores as a result of how they interact with the target protein and may result in the discovery of potential drug candidates. Molecular docking process imitates by creating a database of molecules and a structure of target proteins to identify compounds with higher binding affinity. However, docking may take a long time to determine the hit compound which can be optimized to lead compound (LC), but it is cost effective technique that protects the research should help in case there is a failure to discover the lead compound; the study can go back to the database to find another hit molecule[159].

To this end, molecular modeling is one of the essential tool necessary to find the potential drug candidate for synthesis and structurally optimized. These candidates can be synthesized and biologically evaluated to provide the clinical form of the synthesized compounds. Virtual compounds that show higher calculated binding affinity to the molecular target can be synthesized and biologically evaluated for their activities.

1.5 Biological screening of active compounds

Compounds with high binding affinity during docking must be synthesized and biologically screened to ascertain their potency on the targeted molecular receptor. Antiproliferation assay is important tools in drug discovery to initially evaluate the anti-cancer activities of both natural product and synthesized derivatives. The biological assay can be performed on living animal (*in vivo*) or tissues (*in vitro*)[160]. Initial Screening of potential drug candidate by *in vitro* assay is less expensive compared to *in vivo* assay and has been used extensively in number primarily anti-cancer evaluations.

In vitro cytotoxicity assay is one of the most commonly used bioassays that measure the 50% growth inhibition concentration (IC_{50}) of a specific biological response and the most common, convenient and reliable among these methods is MTT assay. In MTT assay, 3-(4,5 dimethylthiazole-2-yl)-2,5-diphenyltetrazolium bromide is enzymatically reduced by dehydrogenase inside the living cells to form a colored formazan dye[161].

Enzyme immunoassay (EIA) and enzyme-linked immunosorbent assay (ELISA) are other quantitative methods used in drug discovery processes. These methods show antigen-antibody reactions through color change acquired using enzyme-linked conjugates and enzyme substrates that serve to identify the concentration and the presence of molecules such as protein, peptides, hormones, antibody, and antigens in biological fluid[162]

Applications of bioassays are essential to the protein and enzymes target as they measure the affinity of test compounds for a target receptor and has been used successfully by researchers and pharmaceutical for structural optimization, identification of hit and candidates molecules.

1.6 Project objectives

In this communication, we use ormeloxifene and novel analogs that have inhibitory activities towards epidermal growth factor receptor (EGFR) to develop a potential drug candidate for the treatment of ovarian cancer. Recent studies have reported the ability of ormeloxifene to attenuate the EGFR pathway in ovarian cancer cell lines. However, an effort to synthesize ormeloxifene analogs and biologically evaluated in ovarian cancer cell lines has not been reported.

The main objectives for this project are:

1. Study of ormeloxifene as a potential candidate targeting epidermal growth factor (EGFR) pathway towards the treatment of ovarian cancer using in silico molecular studies and biological evaluation.
2. Design a novel ormeloxifene analogs targeting epidermal growth factor receptor (EGFR) pathway using molecular docking studies.
3. Synthesis of novel ormeloxifene analogs
4. Examine the biological profile of synthesized novel ormeloxifene analogs targeting EGFR pathway towards the treatment of ovarian cancer.
5. Study structural activity relationships of synthesizing novel ormeloxifene analogs.

Docking studies were conducted to identify various binding modes with the receptors to facilitate the design of novel ormeloxifene analogs. The synthetic routes were outlined and put into effect using optimal structural design methods where different functionalities were installed on C-7, ring D and ring E of ormeloxifene scaffold. Different side chains were

installed employing mitsunobu reaction, hydroarylation, and condensation. The biological evaluation of the synthesized ormeloxifene analogs was executed to ascertain their inhibitory effects towards EGFR pathway.

1.7 References

1. Gul, S., Drug discovery programs.

2. Drews, J., Drug discovery: a historical perspective. *Science* **2000,** *287* (5460), 1960-1964.

3. Paul, S. M.; Mytelka, D. S.; Dunwiddie, C. T.; Persinger, C. C.; Munos, B. H.; Lindborg, S. R.; Schacht, A. L., How to improve R&D productivity: the pharmaceutical industry's grand challenge. *Nature reviews. Drug discovery* **2010,** *9* (3), 203.

4. Dickson, M.; Gagnon, J. P., Key factors in the rising cost of new drug discovery and development. *Nature reviews Drug discovery* **2004,** *3* (5), 417.

5. Choudhary, M. I.; Thomsen, W. J., *Bioassay techniques for drug development*. CRC Press: 2003.

6. Blass, B., *Basic principles of drug discovery and development*. Elsevier: 2015.

7. Newman, D. J.; Cragg, G. M.; Snader, K. M., Natural products as sources of new drugs over the period 1981− 2002. *Journal of natural products* **2003,** *66* (7), 1022-1037.

8. Newman, D. J.; Cragg, G. M.; Snader, K. M., The influence of natural products upon drug discovery. *Natural product reports* **2000,** *17* (3), 215-234.

9. (a) Dev, S., Ancient-modern concordance in Ayurvedic plants: some examples. In *Development of Plant-Based Medicines: Conservation, Efficacy and Safety*, Springer: 2001; pp 47-67; (b) Fallarino, M., Tibetan medical paintings: Illustrations to the blue beryl treatis of sangye gyamtso (1653-1705). *Herbalgram* **1994,** *31*, 38-44.

10. Harvey, A. L., Natural products in drug discovery. *Drug discovery today* **2008,** *13* (19-20), 894-901.

11. Harvey, A. L., *Natural Product Pharmaceuticals: A diverse approach to drug discovery*. PJB Publications: 2001.

12. Grifo, F.; Newman, D.; Fairfield, A. S.; Bhattacharya, B.; Grupenhoff, J. T., The origins of prescription drugs. *Biodiversity and human health* **1997**, 131-163.

13. Newman, D. J.; Cragg, G. M., Natural products as sources of new drugs over the 30 years from 1981 to 2010. *Journal of natural products* **2012,** *75* (3), 311-335.

14. Bansal, V.; Bansal, A.; Bansal, A. K., Efficacy of SEVISTA (Ormeloxifene) in treatment of mastalgia and fibrocystic breast disease. *International Journal of Reproduction, Contraception, Obstetrics and Gynecology* **2017,** *4* (4), 1057-1060.

15. Singh, M.; Kamboj, V., Fetal resorption in rats treated with an antiestrogen in relation to luteal phase nidatory estrogen secretion. *Acta endocrinologica* **1992,** *126* (5), 444-450.

16. Singh, M., Centchroman, a selective estrogen receptor modulator, as a contraceptive and for the management of hormone-related clinical disorders. *Medicinal research reviews* **2001,** *21* (4), 302-347.

17. Bhattacharyya, T. K.; Banerji, A., Efficacy of a Selective Estrogen Receptor Modulator:'Ormeloxifene'in Management of Dysfunctional Uterine Bleeding. *Journal of SAFOG with DVD* **2010,** *2* (3), 207-211.

18. Lal, J., Clinical pharmacokinetics and interaction of centchroman—a mini review. *Contraception* **2010,** *81* (4), 275-280.

19. Kumari, V.; Sahay, P. B., ORMELOXIFENE: A NEW DRUG TREATMENT MODALITY IN DUB AND ITS COMPARISON WITH NORETHISTERONE.

JOURNAL OF EVOLUTION OF MEDICAL AND DENTAL SCIENCES-JEMDS **2016,** *5* (83), 6199-6201.

20. Ray, S.; Tandon, A.; Dwivedy, I.; Wilson, S. R.; O'Neil, J. P.; Katzenellenbogen, J. A., An X-ray crystallographic study of the nonsteroidal contraceptive agent centchroman. *Journal of medicinal chemistry* **1994,** *37* (5), 696-700.

21. Jordan, V. C.; Murphy, C. S., Endocrine pharmacology of antiestrogens as antitumor agents. *Endocrine Reviews* **1990,** *11* (4), 578-610.

22. Salman, M.; Ray, S.; Anand, N.; Agarwal, A.; Singh, M.; Setty, S.; Kamboj, V., Studies in antifertility agents. 50. Stereoselective binding of d-and l-centchroman to estrogen receptors and their antifertility activity. *Journal of medicinal chemistry* **1986,** *29* (9), 1801-1803.

23. Camerman, N.; Chan, L. Y.; Camerman, A., Crystal and molecular structure of nafoxidine and stereochemical features of anticancer antiestrogens. *Journal of medicinal chemistry* **1980,** *23* (8), 941-945.

24. Ray, S.; Grover, P. K.; Kamboj, V. P.; Setty, B.; Kar, A. B.; Anand, N., Antifertility agents. 12. Structure-activity relation of 3, 4-diphenylchromenes and-chromans. *Journal of medicinal chemistry* **1976,** *19* (2), 276-279.

25. (a) Holschneider, C. H.; Berek, J. S. In *Ovarian cancer: epidemiology, biology, and prognostic factors*, Seminars in surgical oncology, Wiley Online Library: 2000; pp 3-10; (b) SIERKE, S. L.; CHENG, K.; Hong-Hee, K.; KOLAND, J. G., Biochemical characterization of the protein tyrosine kinase homology domain of the ErbB3 (HER3) receptor protein. *Biochemical Journal* **1997,** *322* (3), 757-763.

26. Kumar Gara, R.; Sundram, V.; C Chauhan, S.; Jaggi, M., Anti-cancer potential of a novel SERM ormeloxifene. *Current medicinal chemistry* **2013,** *20* (33), 4177-4184.

27. (a) Roy, S.; Datta, J., Nature of estrogenic and anti-estrogenic actions of centchroman on rat uterus. *Contraception* **1976,** *13* (5), 597-604; (b) Mehrotra, P.; Karkun, J.; Kar, A. B., Estrogenicity of some nonsteroidal compounds. *Contraception* **1973,** *7* (2), 115-124.

28. Srivastava, A.; Agnihotri, A.; Kamboj, V., Binding of centchroman—a nonsteroidal antifertility agent to human plasma proteins. *Cellular and Molecular Life Sciences* **1984,** *40* (5), 465-466.

29. Mishra, N.; Ratna, S.; Ray, S.; Roy, S., Distribution and excretion pattern of 14C-labelled centchroman in the rhesus monkey (Macaca mulatta). *Medical science research* **1992,** *20* (7), 259-260.

30. Paliwal, J.; Gupta, R., Tissue distribution and pharmacokinetics of centchroman. A new nonsteroidal postcoital contraceptive agent and its 7-desmethyl metabolite in female rats after a single oral dose. *Drug metabolism and disposition* **1996,** *24* (2), 148-155.

31. Ratna, S.; Mishra, N.; Ray, S.; Roy, S., Centchroman: tissue distribution and excretion profile in albino rats after oral and intravenous administration. *J Basic Appl Biomed* **1994,** *2*, 31-36.

32. Lal, J.; Asthana, O. P.; Nityanand, S.; Gupta, R. C., Pharmacokinetics of centchroman in healthy female subjects after oral administration. *Contraception* **1995,** *52* (5), 297-300.

33. Lal, J.; Nityanand, S.; Asthana, O.; Gupta, R., Multiple-dose pharmacokinetics of centchroman in female volunteers. *Indian J Pharmacol* **1998,** *30*, 120.

34. Arbatti, N.; Sheth, A.; Vaidya, R., Effect of L-dopa on Centchroman induced prolactin levels in female rats. *Indian journal of experimental biology* **1977,** *15* (12), 1193-1194.

35. Tripathi, S.; Dwivedy, I.; Dhar, J.; Dwivedy, A.; Ray, S., Evaluation of piperidinoethoxy moiety as an antiestrogenic substituent in non-steroidal anti-estrogens: Fertility regulation. *Bioorganic & Medicinal Chemistry Letters* **1997,** *7* (16), 2131-2136.

36. Anand, N. In *Molecules with restricted conformational mobility—an approach to drug design*, Proc. Indian Natn. Sci. Acad, 1983; pp 233-255.

37. Kole, P.; Ray, S.; Anand, N., STUDIES IN ANTIFERTILITY AGENTS: PART XX. 2, 3-CIS-3, 4-CIS-AND 2, 3-TRANS-3, 4-TRANS-2-METHYL-3-PHENYL-4-(4-(2-PYRROLIDINOETHOXY)) PHENYL-7-METHOXYCHROMAN. *ChemInform* **1979,** *10* (5).

38. Durani, S.; Anand, N., A possible basis for structure–function relationship of estrogens. *International Journal of Quantum Chemistry* **1981,** *20* (1), 71-83.

39. Durani, S.; Agarwal, A.; Saxena, R.; Setty, B.; Gupta, R.; Kole, P.; Ray, S.; Anand, N., Seco-oestradiols and some non-steroidal oestrogens: Structural correlates of oestrogenic action. *Journal of steroid biochemistry* **1979,** *11* (1), 67-77.

40. Ray, S.; Singh, M.; Agarwal, A.; Kamboj, V., Enhanced antifertility activity of non-steroidal molecules with 3-n-butylamino-2-hydroxypropyloxy side chain. *Contraception* **1987,** *35* (3), 283-287.

41. Coulter, A.; Kelland, J.; Peto, V.; Rees, M. C., Treating menorrhagia in primary care: an overview of drug trials and a survey of prescribing practice. *International journal of technology assessment in health care* **1995,** *11* (3), 456-471.

42. Dadich, S.; Agarwal, M. S., R. Jain. Role of ormeloxifene in medical management of dysfunctional uterine bleeding. *Asian Journal of Obs and Gynae Practice* **2012,** *6*, 28-31.

43. Biswas, S.; Saha, S.; Bag, T.; Ghosh Roy, S.; Roy, A.; Kabiraj, S., Ormeloxifene: A selective estrogen receptor modulator for treatment of dysfunctional menorrhagia. *J Obstet Gynecol Ind* **2004,** *54* (1), 56-59.

44. Higham, J. M.; O'Brien, P.; Shaw, R., Assessment of menstrual blood loss using a pictorial chart. *BJOG: An International Journal of Obstetrics & Gynaecology* **1990,** *97* (8), 734-739.

45. Gupta, N., Medical Management of Dysfunctional Menorrhagia: Is Ormeloxifene a Safe and Efficacious Therapeutic Choice? *Journal of SAFOMS* **2014,** *2* (2), 65.

46. Kanis, J. A.; Melton, L. J.; Christiansen, C.; Johnston, C. C.; Khaltaev, N., The diagnosis of osteoporosis. *Journal of bone and mineral research* **1994,** *9* (8), 1137-1141.

47. Slemenda, C. W.; Hui, S. L.; Longcope, C.; Wellman, H.; Johnston Jr, C. C., Predictors of bone mass in perimenopausal women. *Ann Intern Med* **1990,** *112* (2), 96-101.

48. Sato, M.; Grese, T. A.; Dodge, J. A.; Bryant, H. U.; Turner, C. H., Emerging therapies for the prevention or treatment of postmenopausal osteoporosis. *Journal of medicinal chemistry* **1999,** *42* (1), 1-24.

49. Nowak, J.; Sjogren, I.; Festersen, U.; Christensen, N. In *Effect of levormeloxifene, a partial estrogen receptor agonist, on body weight, food conversion efficacy, and uterus in the ovariectomized rat*, JOURNAL OF BONE AND MINERAL RESEARCH, BLACKWELL SCIENCE INC 350 MAIN ST, MALDEN, MA 02148: 1997; pp F482-F482.

50. Nowak, J.; Festersen, U.; Andersen, A.; Christensen, N. In *Effect of levormeloxifene, a partial estrogen receptor agonist, on serum cholesterol, osteocalcin and bone in the ovariectomized rat*, JOURNAL OF BONE AND MINERAL RESEARCH, BLACKWELL SCIENCE INC 350 MAIN ST, MALDEN, MA 02148: 1997; pp F483-F483.

51. Bjamason, K.; Skrumsager, B.; Kiehr, B. In *Levormeloxifene, a new partial estrogen receptor agonist demonstrates antiresorptive and antiatherogenic properties in postmenopausal women*, JOURNAL OF BONE AND MINERAL RESEARCH, BLACKWELL SCIENCE INC 350 MAIN ST, MALDEN, MA 02148: 1997; pp F479-F479.

52. Arshad, M.; Sengupta, S.; Sharma, S.; Ghosh, R.; Sawlani, V.; Singh, M., In vitro anti-resorptive activity and prevention of ovariectomy-induced osteoporosis in female Sprague–Dawley rats by ormeloxifene, a selective estrogen receptor modulator. *The Journal of steroid biochemistry and molecular biology* **2004,** *91* (1), 67-78.

53. SL, T.; GL, K., Effect of Centchroman administration in normospermic and oligospermic individuals. *Indian journal of experimental biology* **1977,** *15* (12), 1177-1181.

54. Holm, P.; Korsgaard, N.; Shalmi, M.; Andersen, H. L.; Hougaard, P.; Skouby, S. O.; Stender, S., Significant reduction of the antiatherogenic effect of estrogen by long-term inhibition of nitric oxide synthesis in cholesterol-clamped rabbits. *Journal of Clinical Investigation* **1997,** *100* (4), 821.

55. Dhawan, B.; Srimal, R., Anti-inflammatory and some other pharmacological effects of 3, 4-trans-2, 2-dimethyl-3-phenyl-4-[p-(β-pyrrolidinoethoxy)-phenyl]-7-methoxy-chroman (Centchroman). *British journal of pharmacology* **1973,** *49* (1), 64-73.

56. Srivastava, R.; Srimal, R., Biochemical mechanism of action of anti-inflammatory drugs. *Biol Mem* **1985,** *10*, 66-79.

57. Srivastava, R.; Puri, V.; Srimal, R.; Dhawan, B., Prostanoid mediated effects of centchroman, a non-steroidal oral contraceptive. *Inflammation Research* **1986,** *18* (5), 596-599.

58. Kamboj, V.; Setty, B.; Chandra, H.; Roy, S.; Kar, A., Biological profile of Centchroman--a new post-coital contraceptive. *Indian journal of experimental biology* **1977,** *15* (12), 1144-1150.

59. Mukerjee, S.; Sethi, N.; Srivastava, G.; Roy, A.; Nityanand, S.; Mukherjee, S., Chrinic toxicity studies of Centchroman in rats & rhesus monkeys. *Indian journal of experimental biology* **1977,** *15* (12), 1162-1166.

60. Sethi, N., Influence of Centchroman on prenatal development in mice & rabbits. *Indian journal of experimental biology* **1977,** *15* (12), 1182-1183.

61. Nityanand, S.; Anand, N., Centchroman: a nonsteroidal antifertility agent. *FOGSI (Fed Obstet Gynaecol Soc, India) FOCUS* **1996**, 8-10.

62. Ravibabu, K.; Palla, J.; Chintada, G. S., A study of efficacy of ormeloxifene in the pharmacological management of dysfunctional uterine bleeding. *Journal of clinical and diagnostic research: JCDR* **2013,** *7* (11), 2534.

63. Kamboj, V. P.; Ray, S.; Anand, N., Centchroman: A safe reversible postcoital contraceptive with curative and prophylactic activity in many disorders. *Frontiers in bioscience (Elite edition)* **2018,** *10*, 1-14.

64. Khurana, M.; Lal, J.; Kamboj, V. P.; Nityanand, S.; Gupta, R. C., Pharmacokinetic interaction of tetracycline with centchroman in healthy female volunteers. *Drugs in R & D* **2003,** *4* (5), 293-299.

65. Misra, N.; Nigam, P.; Gupta, R.; Agarwal, A.; Kamboj, V., Centchroman—a non-steroidal anti-cancer agent for advanced breast cancer: Phase-II study. *International journal of cancer* **1989,** *43* (5), 781-783.

66. Saha Roy, S.; Vadlamudi, R. K., Role of estrogen receptor signaling in breast cancer metastasis. *International journal of breast cancer* **2011,** *2012*.

67. Metzger-Filho, O.; Winer, E. P., The natural history of hormone receptor-positive breast cancer. *Oncology* **2012,** *26* (8), 688.

68. Srivastava, V. K.; Gara, R. K.; Bhatt, M.; Sahu, D.; Mishra, D. P., Centchroman inhibits proliferation of head and neck cancer cells through the modulation of PI3K/mTOR pathway. *Biochemical and biophysical research communications* **2011,** *404* (1), 40-45.

69. Nigam, M.; Ranjan, V.; Srivastava, S.; Sharma, R.; Balapure, A. K., Centchroman induces G 0/G 1 arrest and caspase-dependent apoptosis involving mitochondrial

membrane depolarization in MCF-7 and MDA MB-231 human breast cancer cells. *Life sciences* **2008,** *82* (11), 577-590.

70. (a) Khan, S.; Shukla, S.; Sinha, S.; Lakra, A. D.; Bora, H. K.; Meeran, S. M., Centchroman suppresses breast cancer metastasis by reversing epithelial-mesenchymal transition via downregulation of HER2/ERK1/2/MMP-9 signaling. *The international journal of biochemistry & cell biology* **2015,** *58*, 1-16; (b) Sharma, C.; Nusri, Q. E.-A.; Begum, S.; Javed, E.; Rizvi, T. A.; Hussain, A., (-)-Epigallocatechin-3-gallate induces apoptosis and inhibits invasion and migration of human cervical cancer cells. *Asian Pacific journal of cancer prevention* **2012,** *13* (9), 4815-4822.

71. Singh, N.; Zaidi, D.; Shyam, H.; Sharma, R.; Balapure, A. K., Polyphenols sensitization potentiates susceptibility of MCF-7 and MDA MB-231 cells to Centchroman. *PloS one* **2012,** *7* (6), e37736.

72. Siegel, R.; Naishadham, D.; Jemal, A., Cancer statistics for hispanics/latinos, 2012. *CA: a cancer journal for clinicians* **2012,** *62* (5), 283-298.

73. Schuller, D. E.; Abou-Issa, H.; Parrish, R., Estrogen and progesterone receptors in head and neck cancer. *Archives of Otolaryngology* **1984,** *110* (11), 725-727.

74. Shatalova, E. G.; Klein-Szanto, A. J.; Devarajan, K.; Cukierman, E.; Clapper, M. L., Estrogen and cytochrome P450 1B1 contribute to both early-and late-stage head and neck carcinogenesis. *Cancer Prevention Research* **2011,** *4* (1), 107-115.

75. Vivanco, I.; Sawyers, C. L., The phosphatidylinositol 3-kinase-AKT pathway in human cancer. *Nature reviews. Cancer* **2002,** *2* (7), 489.

76. Bussink, J.; van der Kogel, A. J.; Kaanders, J. H., Activation of the PI3-K/AKT pathway and implications for radioresistance mechanisms in head and neck cancer. *The lancet oncology* **2008,** *9* (3), 288-296.

77. Bhave, S. L.; Teknos, T. N.; Pan, Q., Molecular parameters of head and neck cancer metastasis. *Critical Reviews™ in Eukaryotic Gene Expression* **2011,** *21* (2).

78. Lissoni, P.; Vigano, P.; Vaghi, M.; Frontini, L.; Giuberti, C.; Manganini, V.; Casu, M.; Brivio, F.; Niespolo, R.; Strada, G., A phase II study of tamoxifen in hormone-resistant metastatic prostate cancer: possible relation with prolactin secretion. *Anticancer research* **2005,** *25* (5), 3597-3599.

79. Clarke, B. L.; Khosla, S., Modulators of androgen and estrogen receptor activity. *Critical Reviews™ in Eukaryotic Gene Expression* **2010,** *20* (4).

80. Rossi, V.; Bellastella, G.; De Rosa, C.; Abbondanza, C.; Visconti, D.; Maione, L.; Chieffi, P.; Della Ragione, F.; Prezioso, D.; De Bellis, A., Raloxifene induces cell death and inhibits proliferation through multiple signaling pathways in prostate cancer cells expressing different levels of estrogen receptorα and β. *Journal of cellular physiology* **2011,** *226* (5), 1334-1339.

81. Pal, P.; Kanaujiya, J. K.; Lochab, S.; Tripathi, S. B.; Bhatt, M. L.; Singh, P. K.; Sanyal, S.; Trivedi, A. K., 2-D gel electrophoresis-based proteomic analysis reveals that ormeloxifen induces G0–G1 growth arrest and ERK-mediated apoptosis in chronic myeloid leukemia cells K562. *Proteomics* **2011,** *11* (8), 1517-1529.

82. Ferlay, J.; Soerjomataram, I.; Dikshit, R.; Eser, S.; Mathers, C.; Rebelo, M.; Parkin, D. M.; Forman, D.; Bray, F., Cancer incidence and mortality worldwide: sources,

methods and major patterns in GLOBOCAN 2012. *International journal of cancer* **2015,** *136* (5).

83. Jemal, A.; Siegel, R.; Xu, J.; Ward, E., Cancer statistics, 2010. *CA: a cancer journal for clinicians* **2010,** *60* (5), 277-300.

84. Dinh, P.; Harnett, P.; Piccart-Gebhart, M. J.; Awada, A., New therapies for ovarian cancer: cytotoxics and molecularly targeted agents. *Critical reviews in oncology/hematology* **2008,** *67* (2), 103-112.

85. Jemal, A.; Murray, T.; Ward, E.; Samuels, A.; Tiwari, R. C.; Ghafoor, A.; Feuer, E. J.; Thun, M. J., Cancer statistics, 2005. *CA: a cancer journal for clinicians* **2005,** *55* (1), 10-30.

86. Scully, R. E.; Young, R. H.; Clement, P. B., Tumors of the Ovary, Maldeveloped Gonads, Fallopian Tube, and Broad Ligament. *International Journal of Gynecological Pathology* **1999,** *18* (3), 288.

87. Tavassoli, F. A., Tumours of the breast, neuroendocrine tumours. *World Health Organization classification of tumours, pathology and genetics of tumours of the breast and female genital organs* **2003**, 32-34.

88. Coleman, M. P.; Esteve, J.; Damiecki, P.; Arslan, A.; Renard, H., Trends in cancer incidence and mortality. *IARC scientific publications* **1993,** (121), 1-806.

89. Kliewer, E. V.; Smith, K. R., Ovarian cancer mortality among immigrants in Australia and Canada. *Cancer Epidemiology and Prevention Biomarkers* **1995,** *4* (5), 453-458.

90. Frank, T. S.; Manley, S. A.; Olopade, O. I.; Cummings, S.; Garber, J. E.; Bernhardt, B.; Antman, K.; Russo, D.; Wood, M. E.; Mullineau, L., Sequence analysis of

BRCA1 and BRCA2: correlation of mutations with family history and ovarian cancer risk. *Journal of Clinical Oncology* **1998,** *16* (7), 2417-2425.

91. Ford, D.; Easton, D. F.; Bishop, D. T.; Narod, S. A.; Goldgar, D. E., Risks of cancer in BRCA1-mutation carriers. *The Lancet* **1994,** *343* (8899), 692-695.

92. Ford, D.; Easton, D. F.; Peto, J., Estimates of the gene frequency of BRCA1 and its contribution to breast and ovarian cancer incidence. *American journal of human genetics* **1995,** *57* (6), 1457.

93. Ford, D.; Easton, D.; Stratton, M.; Narod, S.; Goldgar, D.; Devilee, P.; Bishop, D.; Weber, B.; Lenoir, G.; Chang-Claude, J., Genetic heterogeneity and penetrance analysis of the BRCA1 and BRCA2 genes in breast cancer families. *The American Journal of Human Genetics* **1998,** *62* (3), 676-689.

94. Franceschi, S.; La Vecchia, C.; Booth, M.; Tzonou, A.; Negri, E.; Parazzini, F.; Trichopoulos, D.; Beral, V., Pooled analysis of 3 european case-control studies of ovarian cancer: II. Age at menarche and at menopause. *International journal of cancer* **1991,** *49* (1), 57-60.

95. Wallach, E. E.; Bristow, R. E.; Karlan, B. Y., Ovulation induction, infertility, and ovarian cancer risk. *Fertility and sterility* **1996,** *66* (4), 499-507.

96. Harris, R.; Whittemore, A. S.; Itnyre, J.; Group, C. O. C., Characteristics relating to ovarian cancer risk: collaborative analysis of 12 US case-control studies: III. Epithelial tumors of low malignant potential in white women. *American Journal of Epidemiology* **1992,** *136* (10), 1204-1211.

97. Mink, P. J.; Folsom, A. R.; Sellers, T. A.; Kushi, L. H., Physical activity, waist-to-hip ratio, and other risk factors for ovarian cancer: a follow-up study of older women. *Epidemiology* **1996,** *7* (1), 38-45.

98. Whittmore, A. S.; Harris, R.; Itnyre, J.; Group, C. O. C., Characteristics relating to ovarian cancer risk: collaborative analysis of 12 US case-control studies: II. Invasive epithelial ovarian cancers in white women. *American journal of epidemiology* **1992,** *136* (10), 1184-1203.

99. Risch, H. A.; Howe, G. R., Pelvic inflammatory disease and the risk of epithelial ovarian cancer. *Cancer Epidemiology and Prevention Biomarkers* **1995,** *4* (5), 447-451.

100. Schildkraut, J. M.; Schwingl, P. J.; Bastos, E.; Evanoff, A.; Hughes, C., Epithelial ovarian cancer risk among women with polycystic ovary syndrome. *Obstetrics & Gynecology* **1996,** *88* (4), 554-559.

101. Schlesselman, J. J., Net effect of oral contraceptive use on the risk of cancer in women in the United States. *Obstetrics & Gynecology* **1995,** *85* (5), 793-801.

102. Gross, T. P.; Schlesselman, J. J., The estimated effect of oral contraceptive use on the cumulative risk of epithelial ovarian cancer. *Obstetrics & Gynecology* **1994,** *83* (3), 419-424.

103. Narod, S. A.; Risch, H.; Moslehi, R.; Dørum, A.; Neuhausen, S.; Olsson, H.; Provencher, D.; Radice, P.; Evans, G.; Bishop, S., Oral contraceptives and the risk of hereditary ovarian cancer. *New England Journal of Medicine* **1998,** *339* (7), 424-428.

104. De Palo, G.; Veronesi, U.; Camerini, T.; Formelli, F.; Mascotti, G.; Boni, C.; Fosser, V.; Vecchio, M. D.; Campa, T.; Costa, A., Can fenretinide protect women against ovarian cancer? *JNCI: Journal of the National Cancer Institute* **1995,** *87* (2), 146-147.

105. Heintz, A. P. M.; Hacker, N. F.; Lagasse, L. D., Epidemiology and etiology of ovarian cancer: a review. *Obstetrics & Gynecology* **1985,** *66* (1), 127-135.

106. Nagata, S.; Golstein, P., The Fas death factor. *Science* **1995,** *267* (5203), 1449.

107. Suda, T.; Takahashi, T.; Golstein, P.; Nagata, S., Molecular cloning and expression of the Fas ligand, a novel member of the tumor necrosis factor family. *Cell* **1993,** *75* (6), 1169-1178.

108. Guo, M. W.; Mori, E.; Xu, J. P.; Mori, T., Identification of Fas antigen associated with apoptotic cell death in murine ovary. *Biochemical and biophysical research communications* **1994,** *203* (3), 1438-1446.

109. Quirk, S. M.; Cowan, R. G.; Joshi, S. G.; Henrikson, K. P., Fas antigen-mediated apoptosis in human granulosa/luteal cells. *Biology of reproduction* **1995,** *52* (2), 279-287.

110. Ghahremani, M.; Foghi, A.; Dorrington, J., Etiology of ovarian cancer: a proposed mechanism. *Medical hypotheses* **1999,** *52* (1), 23-26.

111. Sundar, S.; Neal, R. D.; Kehoe, S., Diagnosis of ovarian cancer. *Bmj* **2015,** *351*, h4443.

112. De Pauw, B.; Walsh, T. J.; Donnelly, J. P.; Stevens, D. A.; Edwards, J. E.; Calandra, T.; Pappas, P. G.; Maertens, J.; Lortholary, O.; Kauffman, C. A., Revised definitions of invasive fungal disease from the European organization for research and treatment of cancer/invasive fungal infections cooperative group and the national institute of allergy and infectious diseases mycoses study group (EORTC/MSG) consensus group. *Clinical infectious diseases* **2008,** *46* (12), 1813-1821.

113. Vlahou, A.; Schorge, J. O.; Gregory, B. W.; Coleman, R. L., Diagnosis of ovarian cancer using decision tree classification of mass spectral data. *BioMed Research International* **2003,** *2003* (5), 308-314.

114. Reddy, G.; Dalmasso, E. A., SELDI proteinchip® array technology: protein-based predictive medicine and drug discovery applications. *BioMed Research International* **2003,** *2003* (4), 237-241.

115. Cancer, N. C. C. f., Ovarian cancer: the recognition and initial management of ovarian cancer. **2011**.

116. Bristow, R. E.; Tomacruz, R. S.; Armstrong, D. K.; Trimble, E. L.; Montz, F., Survival effect of maximal cytoreductive surgery for advanced ovarian carcinoma during the platinum era: a meta-analysis. *Journal of clinical oncology* **2002,** *20* (5), 1248-1259.

117. Agarwal, R.; Kaye, S. B., Ovarian cancer: strategies for overcoming resistance to chemotherapy. *Nature Reviews Cancer* **2003,** *3* (7), 502-516.

118. Greenlee, R. T.; Hill-Harmon, M. B.; Murray, T.; Thun, M., Cancer statistics, 2001. *CA: a cancer journal for clinicians* **2001,** *51* (1), 15-36.

119. Gore, M.; Fryatt, I.; Wiltshaw, E.; Dawson, T., Treatment of relapsed carcinoma of the ovary with cisplatin or carboplatin following initial treatment with these compounds. *Gynecologic oncology* **1990,** *36* (2), 207-211.

120. Monk, B., A randomized phase III study of trabectedin with pegylated liposomal doxorubicin (PLD) versus PLD in relapsed, recurrent ovarian cancer (OC). *CURRENT TREATMENT OPTIONS IN ONCOLOGY* **2008,** *9* (1), 30-30.

121. Yap, T. A.; Carden, C. P.; Kaye, S. B., Beyond chemotherapy: targeted therapies in ovarian cancer. *Nature Reviews Cancer* **2009,** *9* (3), 167-181.

122. Iyer, L.; Ratain, M., Pharmacogenetics and cancer chemotherapy. *European Journal of Cancer* **1998,** *34* (10), 1493-1499.

123. Tomida, A.; Tsuruo, T., Drug resistance mediated by cellular stress response to the microenvironment of solid tumors. *Anti-cancer drug design* **1999,** *14* (2), 169-177.

124. Teicher, B. A., Hypoxia and drug resistance. *Cancer and Metastasis Reviews* **1994,** *13* (2), 139-168.

125. Green, S. K.; Frankel, A.; Kerbel, R. S., Adhesion-dependent multicellular drug resistance. *Anti-cancer drug design* **1999,** *14* (2), 153-168.

126. Nowell, P. C., The clonal evolution of tumor cell populations. *Science* **1976,** *194* (4260), 23-28.

127. Shah, M. A.; Schwartz, G. K., Cell cycle-mediated drug resistance. *Clinical cancer research* **2001,** *7* (8), 2168-2181.

128. Pluen, A.; Boucher, Y.; Ramanujan, S.; McKee, T. D.; Gohongi, T.; di Tomaso, E.; Brown, E. B.; Izumi, Y.; Campbell, R. B.; Berk, D. A., Role of tumor–host interactions in interstitial diffusion of macromolecules: cranial vs. subcutaneous tumors. *Proceedings of the National Academy of Sciences* **2001,** *98* (8), 4628-4633.

129. Jain, R. K., Delivery of molecular and cellular medicine to solid tumors. *Advanced drug delivery reviews* **2001,** *46* (1), 149-168.

130. Gottesman, M. M.; Fojo, T.; Bates, S. E., Multidrug resistance in cancer: role of ATP–dependent transporters. *Nature Reviews Cancer* **2002,** *2* (1), 48-58.

131. Darcy, K. M.; Schilder, R. J., Relevant molecular markers and targets. *Gynecologic oncology* **2006,** *103* (2), 6-13.

132. Ciardiello, F., Epidermal growth factor receptor inhibitors in cancer treatment. **2005**.

133. Salomon, D. S.; Brandt, R.; Ciardiello, F.; Normanno, N., Epidermal growth factor-related peptides and their receptors in human malignancies. *Critical reviews in oncology/hematology* **1995,** *19* (3), 183-232.

134. Psyrri, A.; Kassar, M.; Yu, Z.; Bamias, A.; Weinberger, P. M.; Markakis, S.; Kowalski, D.; Camp, R. L.; Rimm, D. L.; Dimopoulos, M. A., Effect of epidermal growth factor receptor expression level on survival in patients with epithelial ovarian cancer. *Clinical Cancer Research* **2005,** *11* (24), 8637-8643.

135. Schilder, R. J.; Sill, M. W.; Chen, X.; Darcy, K. M.; Decesare, S. L.; Lewandowski, G.; Lee, R. B.; Arciero, C. A.; Wu, H.; Godwin, A. K., Phase II study of gefitinib in patients with relapsed or persistent ovarian or primary peritoneal carcinoma and evaluation of epidermal growth factor receptor mutations and immunohistochemical expression: a Gynecologic Oncology Group Study. *Clinical Cancer Research* **2005,** *11* (15), 5539-5548.

136. Gordon, A.; Finkler, N.; Edwards, R.; Garcia, A.; Crozier, M.; Irwin, D.; Barrett, E., Efficacy and safety of erlotinib HCl, an epidermal growth factor receptor (HER1/EGFR) tyrosine kinase inhibitor, in patients with advanced ovarian carcinoma: results from a phase II multicenter study. *International Journal of Gynecological Cancer* **2005,** *15* (5), 785-792.

137. Tonary, A. M.; Macdonald, E. A.; Faught, W.; Senterman, M. K.; Vanderhyden, B. C., Lack of expression of c-KIT in ovarian cancers is associated with poor prognosis. *International journal of cancer* **2000,** *89* (3), 242-250.

138. Henriksen, R.; Funa, K.; Wilander, E.; Bäckström, T.; Ridderheim, M.; Öberg, K., Expression and prognostic significance of platelet-derived growth factor and its receptors in epithelial ovarian neoplasms. *Cancer Research* **1993,** *53* (19), 4550-4554.

139. Coleman, R. L.; Broaddus, R. R.; Bodurka, D. C.; Wolf, J. K.; Burke, T. W.; Kavanagh, J. J.; Levenback, C. F.; Gershenson, D. M., Phase II trial of imatinib mesylate in patients with recurrent platinum-and taxane-resistant epithelial ovarian and primary peritoneal cancers. *Gynecologic oncology* **2006,** *101* (1), 126-131.

140. Uehara, H.; Kim, S. J.; Karashima, T.; Shepherd, D. L.; Fan, D.; Tsan, R.; Killion, J. J.; Logothetis, C.; Mathew, P.; Fidler, I. J., Effects of blocking platelet-derived growth factor-receptor signaling in a mouse model of experimental prostate cancer bone metastases. *Journal of the National Cancer Institute* **2003,** *95* (6), 458-470.

141. Lennartsson, J.; Ronnstrand, L., The stem cell factor receptor/c-Kit as a drug target in cancer. *Current cancer drug targets* **2006,** *6* (1), 65-75.

142. Ashworth, A., A synthetic lethal therapeutic approach: poly (ADP) ribose polymerase inhibitors for the treatment of cancers deficient in DNA double-strand break repair. *Journal of Clinical Oncology* **2008,** *26* (22), 3785-3790.

143. Audeh, M. W.; Carmichael, J.; Penson, R. T.; Friedlander, M.; Powell, B.; Bell-McGuinn, K. M.; Scott, C.; Weitzel, J. N.; Oaknin, A.; Loman, N., Oral poly (ADP-ribose) polymerase inhibitor olaparib in patients with BRCA1 or BRCA2 mutations and recurrent ovarian cancer: a proof-of-concept trial. *The Lancet* **2010,** *376* (9737), 245-251.

144. Weinstein-Oppenheimer, C. R.; Blalock, W. L.; Steelman, L. S.; Chang, F.; McCubrey, J. A., The Raf signal transduction cascade as a target for chemotherapeutic

intervention in growth factor-responsive tumors. *Pharmacology & therapeutics* **2000,** *88* (3), 229-279.

145. McPhillips, F.; Mullen, P.; Monia, B.; Ritchie, A.; Dorr, F.; Smyth, J.; Langdon, S., Association of c-Raf expression with survival and its targeting with antisense oligonucleotides in ovarian cancer. *British journal of cancer* **2001,** *85* (11), 1753-1758.

146. Schmelzle, T.; Hall, M. N., TOR, a central controller of cell growth. *Cell* **2000,** *103* (2), 253-262.

147. Cheng, J. Q.; Godwin, A. K.; Bellacosa, A.; Taguchi, T.; Franke, T. F.; Hamilton, T. C.; Tsichlis, P. N.; Testa, J. R., AKT2, a putative oncogene encoding a member of a subfamily of protein-serine/threonine kinases, is amplified in human ovarian carcinomas. *Proceedings of the National Academy of Sciences* **1992,** *89* (19), 9267-9271.

148. Hu, L.; Hofmann, J.; Jaffe, R. B., Phosphatidylinostol 3-kinase mediates angiogenesis and vascular permeability associated with ovarian carcinoma. *Clinical cancer research* **2005,** *11* (22), 8208-8212.

149. Yang, X.; Fraser, M.; Moll, U. M.; Basak, A.; Tsang, B. K., Akt-mediated cisplatin resistance in ovarian cancer: modulation of p53 action on caspase-dependent mitochondrial death pathway. *Cancer research* **2006,** *66* (6), 3126-3136.

150. Klampfer, L., Signal transducers and activators of transcription (STATs): Novel targets of chemopreventive and chemotherapeutic drugs. *Current cancer drug targets* **2006,** *6* (2), 107-121.

151. Savarese, T. M.; Campbell, C. L.; McQuain, C.; Mitchell, K.; Guardiani, R.; Quesenberry, P. J.; Nelson, B. E., Coexpression of oncostatin M and its receptors and

evidence for STAT3 activation in human ovarian carcinomas. *Cytokine* **2002,** *17* (6), 324-334.

152. Chen, H.; Ye, D.; Xie, X.; Chen, B.; Lu, W., VEGF, VEGFRs expressions and activated STATs in ovarian epithelial carcinoma. *Gynecologic oncology* **2004,** *94* (3), 630-635.

153. Thomsen, R.; Christensen, M. H., MolDock: a new technique for high-accuracy molecular docking. *Journal of medicinal chemistry* **2006,** *49* (11), 3315-3321.

154. Huang, S.-Y.; Zou, X., Advances and challenges in protein-ligand docking. *International journal of molecular sciences* **2010,** *11* (8), 3016-3034.

155. Kitchen, D. B.; Decornez, H.; Furr, J. R.; Bajorath, J., Docking and scoring in virtual screening for drug discovery: methods and applications. *Nature reviews Drug discovery* **2004,** *3* (11), 935-949.

156. Halperin, I.; Ma, B.; Wolfson, H.; Nussinov, R., Principles of docking: An overview of search algorithms and a guide to scoring functions. *Proteins: Structure, Function, and Bioinformatics* **2002,** *47* (4), 409-443.

157. Norel, R.; Wolfson, H.; Nussinov, R., Small molecule recognition: solid angles surface representation and molecular shape complementarity. *Combinatorial Chemistry and High Throughput Screening* **1999,** *2*, 223-236.

158. Schulz-Gasch, T.; Stahl, M., Scoring functions for protein–ligand interactions: a critical perspective. *Drug Discovery Today: Technologies* **2004,** *1* (3), 231-239.

159. Shoichet, B. K.; McGovern, S. L.; Wei, B.; Irwin, J. J., Lead discovery using molecular docking. *Current opinion in chemical biology* **2002,** *6* (4), 439-446.

160. Gaddum, J., Bioassays and mathematics. *Pharmacological reviews* **1953,** *5* (1), 87-134.

161. Berg, K.; Zhai, L.; Chen, M.; Kharazmi, A.; Owen, T., The use of a water-soluble formazan complex to quantitate the cell number and mitochondrial function ofLeishmania major promastigotes. *Parasitology research* **1994,** *80* (3), 235-239.

162. Paulie, S.; Perlmann, H., Enzyme-Linked Immunosorbent Assay. *eLS* **2003**.

Chapter 2

Design of Ormeloxifene analogs, a potential drug candidate targeting epidermal growth factor Receptor (EGFR) pathway

2 Introduction

2.1 Ormeloxifene (Centchroman)

Ormeloxifene is a reversible post-coital/weekly oral contraceptive (half-life 168 hours), designed and developed at Central Drug Research Institute (CDRI) Lucknow India. It is the only non-steroidal oral contraceptive in clinical use in the world today. Ormeloxifene was synthesized in 1967, and pre-clinical and clinical studies were completed in 1989. The drug was approved for marketing in 1991, social marketing in 1995 and non-pollinating fig wasps (NPFW) in April 2016[1]. It acts by suppressing implantation of the blastocyst in endometrium[2]. Ormeloxifene is the only contraceptive that neither suppresses ovulation nor interferes with the hypothalamic-pituitary-ovarian axis. It has a high level of safety, and it is virtually free from side effects except for a delay in about 8% menstrual cycles which is not confined to any woman[3]. However, ormeloxifene is currently banned in the United States due to the concern of causing cardiovascular problems.

Ormeloxifene is a white powder with a melting point of 163°C -166°C. It is very stable under room temperature. The pyrrolidine moiety in ormeloxifene is optimal and is responsible for its antagonistic activity. The receptor binding ability and estrogen agonistic activity of ormeloxifene are as a result of its benzopyran base. The strategy has led to the development of a pharmacophore model that attributes the differences in effects on the

uterus. Ormeloxifene competes with estradiol for binding the cytosol receptors. Unlike other SERM, the action of ormeloxifene last longer even after the drug has been withdrawn[4]. Studies have confirmed the effectiveness of ormeloxifene in advanced breast cancer cell lines, as well as other tumor cells and one of the advantages, is, it does not exhibit progestational, androgenic or antiandrogenic properties and does not affect the secretion of some hormones in the usual therapeutic dosage[5].

2.1.1 Ormeloxifene as selective estrogen receptor modulator (SERM)

Estrogen receptors (ER) regulates mammalian hormonal and physiological processes by interacting with steroid hormone 17-β-estradiol (E2)[6]. The two central estrogen receptors are ERα and ERβ with each showing distinct expression. ERα is expressed in the bone, breast and the uterine while ERβ is distributed in the lungs, prostate, the cardiovascular system, and the central nervous system[7]. Studies have shown that ERs are responsible for several estrogen-related diseases such as breast cancer, ovarian cancer, prostate cancer, and other inflammatory diseases[7b]. ER modulators have been used in several hormonal replacement therapies (HRT) to treat postmenopausal disease caused by a lack of naturally occurring hormones. SERMs are a class of compounds that shows tissues specific estrogenic activities with the possibility of selectively exert agonistic or antagonistic estrogen-like actions in various tissues [8]. One of such SERMs is ormeloxifene, a marked ER modulator with estrogenic effect on bone and anti-estrogenic on breast and uterus and its ability to suppress uterus and breast cancer has been reported (**Fig.2.1**)[8]. Studies have also shown that ormeloxifene can suppress breast and ovarian cancer by targeting EGFR pathway[9].

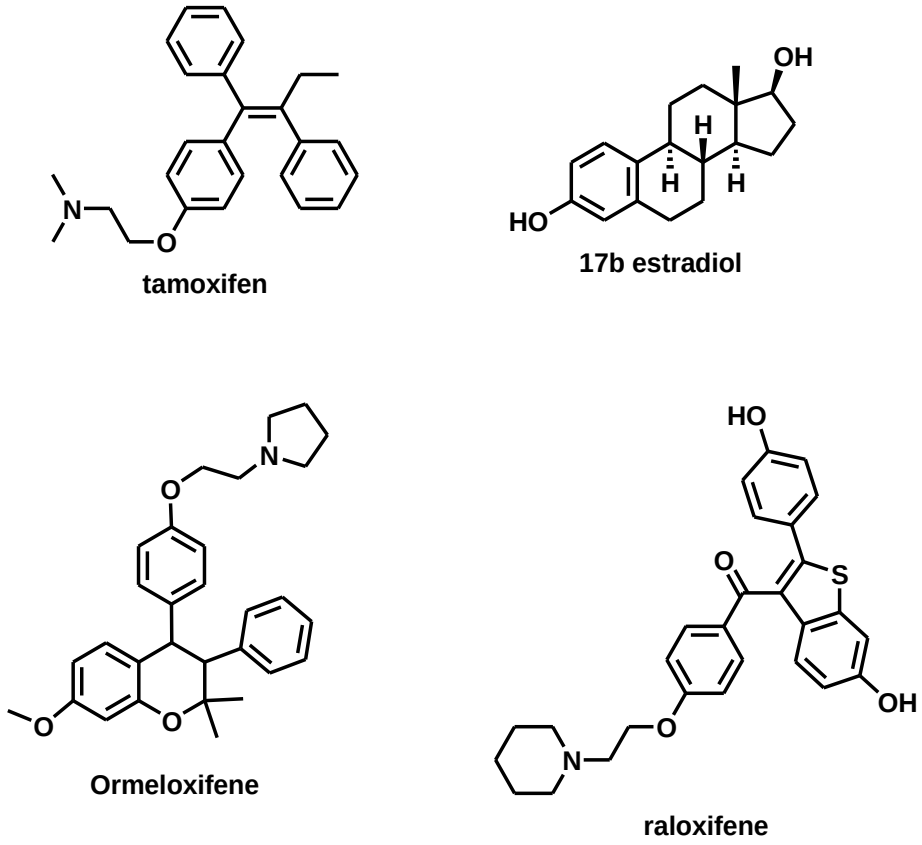

Figure 2.1 Structure of 17β-estradiol and some selected SERMs

2.2 The epidermal growth factor receptor (EGFR).

The family of epidermal growth factor receptor (EGFR) is made up of extracellular ligand binding domain, an intracellular region which contains kinase domain and single transmembrane spanning region (Fig)[10,11,12]. More than 30 ligands that bind to EGFR have been identified in humans, these include EGF and EGF-like ligands, transforming growth factor (TGF)-α, and heregulins[13] **(Fig 2.2)**. The EGFR become activated after binding with a ligand, this leads to a conformational change in the extracellular domain, which results in homo or heterodimerization with another EGFR family member. Binding of EGFR to a partner mostly depends on many properties such as members of EGRF family in the

membrane, type, and proportion ligand and cell lineage which relate in the expression of additional members of the signaling processes[13,14]. The preferred binding partner of all the EGFR family is HER2, while HER3 acts as an obligatory partner which is inactive of its own or as a homodimer since it lacks intrinsic kinase activity as a result of mutation of critical amino acids in the kinase domain[15]. Activation of the EGFR Family member can lead to transduction of EGFR signals such as mitogen-activated protein kinase (MAPKs) and activated protein kinase B (AKT) which can alter multiple cellular responses such as cell proliferation, differentiation, cell survival, and motility[16]. The EGFR family members can also be activated by other signaling proteins such as receptor tyrosine kinase (RTKs), tyrosine kinase B receptor (TRKB) and G-protein-coupled receptors (GPCRs)[17,18,19].

2.2.1 Targeting the EGFR pathway in ovarian cancer

In ovarian cancer cells, EGFR and its downstream effectors may be activated directly or indirectly by several other signaling molecules. Some functions of antibodies such as their action as modulators of the immune response, molecular carriers and pharmacological agents that interfere directly with activation of the receptors and its downstream pathways can contribute to their effectiveness as anticancer agents[20]. Anti-EGFR mAbs used in the treatment of ovarian cancer normally binds to the extracellular domain of EGFR[21]. However there are potentially different mechanisms of inhibitions where the antibodies prevent ligand binding (wild type EGFR), promotes antibody-receptor complex internalization, alter transient decrease of EGFR expression[22], inhibits EGFR heterodimerization and trigger ubiquitin-mediated degradation[23]. The inhibition of EGFR

downstream dependent cancer cells can result in decreased TGF-α secretion, angiogenesis, cell migration, cell invasion, and apoptotic induction[24,25].

Small molecular inhibitors have been developed using structure-based drug design (such as Ormeloxifene) which appear to act intracellularly through ATP binding in the catalytic region of the kinase domain and evade an enzymatic activity of the kinase and its subsequent downstream signaling effects[26]. In this communication, we report the development of novel ormeloxifene analogs as small molecular inhibitors to suppress ovarian cancer cell line via the EGFR pathway **(Fig 2.3).**

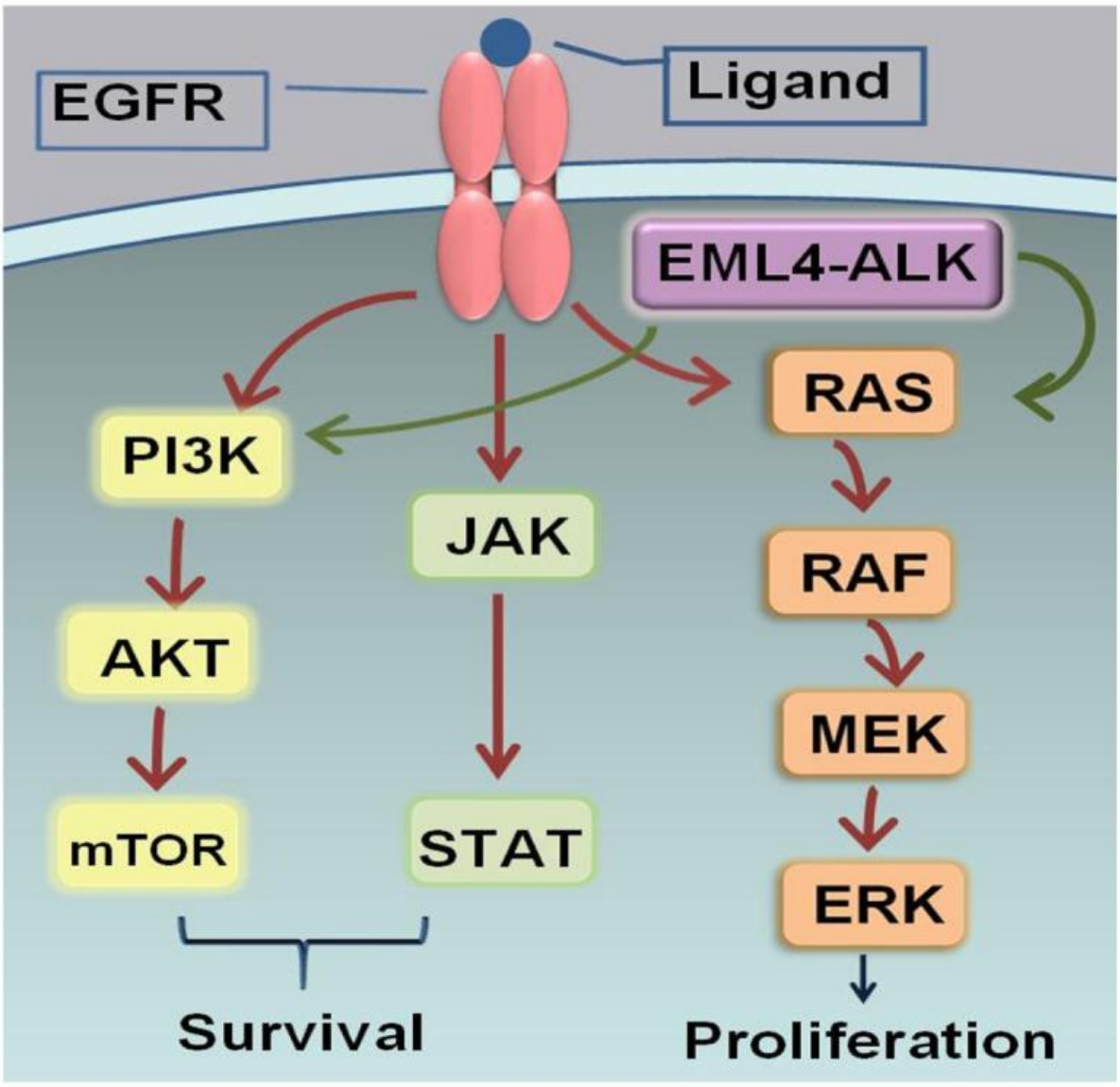

Figure 2.2 EGFR pathway Adapted from (Wu et al. 2012 #526)

2.3 Mechanism of action of ormeloxifene as cytotoxic agents

Several studies have been conducted on the cytotoxic activity of ormeloxifene on ovarian cancer cell lines. It has been reported that ormeloxifene can decrease Akt phosphorylation and modulate the expression and localization of CDK2 [27]. It is believed that the benzopyran base structure of ormeloxifene is responsible for its estrogen activity and receptor binding ability.

Recent studies have revealed that ormeloxifene inhibits epithelial-mesenchymal transition (EMT) process by suppressing the β-catenin/TCF-4 transcriptional activity and influence the expression of Pgsk3β[28].

Currently, Ormeloxifene is being investigated to target the Akt/mTOR/PIK3 pathways, and the ability of ormeloxifene to inhibit Akt phosphorylation in Head and neck squamous cell carcinomas (HNSCC)[29] has been reported. Activation of mTOR induces phosphorylation of effector molecule P70S6K and S6 ribosomal proteins, which effectively results in mTOR dependent gene transcription that control cell proliferation, metabolism, and protein synthesis [30]. The knowledge of varying inhibitory activity of ormeloxifene on multiple pathways is a possible lead towards the discovery of potential anticancer agent; we propose that ormeloxifene framework can be altered to generate possible drug candidates, which can affect multiple targets following multi-faceted drug strategies to combat ovarian cancer.

2.4 Molecular modeling

Molecular modeling study calculations were achieved using HP Pavilion 27xi with window 7, Intel ® Core ™ processor, 8.0 GB installed memory (RAM) and 64-bit operating system. Open Eye ® scientific software which is semi-flexible docking program was utilized in this study. MMF94 semi-empirical calculation was employed to conduct energy minimization, followed by processing using OMEGA, FRED, and VIDA applications.

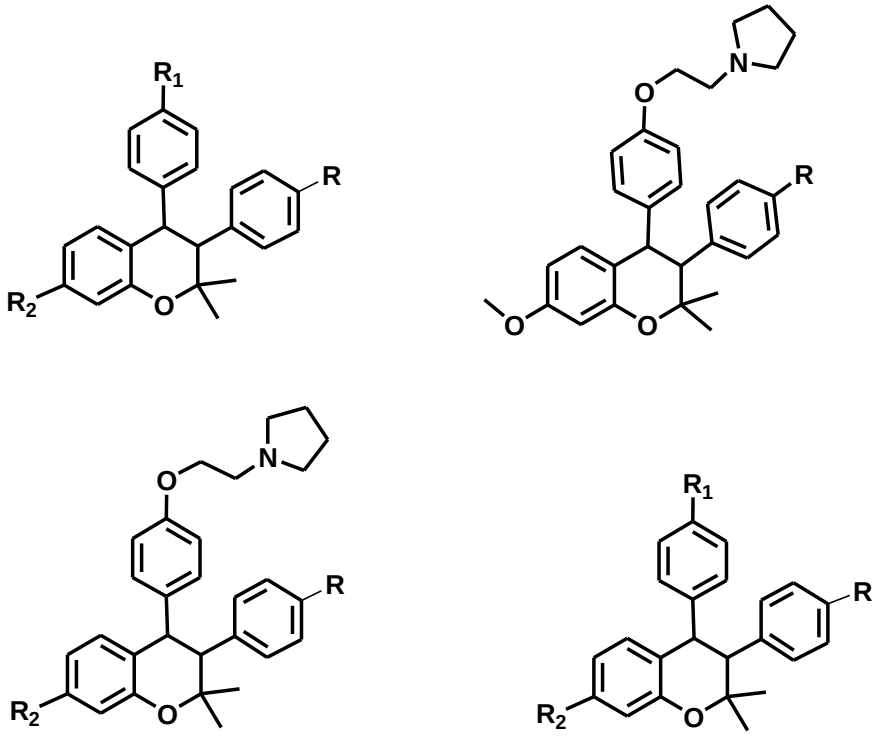

R = H, CH_2, OH, NH_2, F,Cl, Br, I, CF_3, OCF_3

R_1 = OCH_3, OCF_3, NH_2, OH

R_2 = 4-(2-hydroxyethyl)phenol, benzotrifluoride

5-methylthiophene, anisole, 1-Fluoro-benzene

Figure 2.3 Proposed ormeloxifene analogs

2.4.1 Creating a virtual library

A virtual library of 900 ormeloxifene analogs including ormeloxifene as a standard and EGFR inhibitors were prepared and their energy using Chemoffice® 2012. MMF94 energy minimization of the compounds was calculated to develop structural conformation (3-D) of each compound.

2.4.2 Using Omega to generate conformers

The energy minimized compounds were converted to *pdb file maintaining all heavy atoms. All the *pdb files were converted into one continuous *pdb file to be used as an impute parameters for Omega calculations. Omega produces different conformers of each molecule in the virtual library to generate ligand flexibility in a rigid model. Omega produces an optimal balance between speed and performance when used in a large library of compounds and reproduce the desired conformations[31],[32].

2.4.3 Receptor preparation using FRED

The PDB files of receptors such as EGFR (PDB ID # 1M17), GSK3β (PDB ID # 1Q3D), ERK (PDB ID # 2OJG), CDK2 (PDB ID # 3QLS), mTOR (PDB ID # 4JSV), Akt (PDP ID # 3MV5), PI3K (PDB ID # 3L54), STAT3 (PDB ID # 1BG1), Era (PDB ID # 1A52), Erb (PDB ID # 3OLS) were downloaded from the protein data bank (PDB) (**Fig 2.5**) and were prepared using FRED receptor software. The FRED program uses a search algorithm that searches for translations and rotations of each conformer of the ligand within the active site at a specific resolution.

In the preparation of our receptor, the receptor of interest is loaded into FRED which makes receptor application and converts the *pdb file into three-dimensional view (3-D) of the receptor chain which includes the binding ligand as well as the co-factors. After locating the binding pocket and the co-crystallized ligand, the grid box is generated to a specific range, not more than 60,000 A°. In a situation where the grid box requires more than 60,000 A°, it is divided into two boxes to avoid inaccurate or docking irregularities. The mode selection window finally specified the pocket shape to allow the docking program to recognize both the inner and outer contours. The ligand input file and the receptor input files are moved into FRED application to initiate molecular docking process. Multiple scoring functions such as consensus score, oechemscore, shapeguass, shapegauss3, screen score, and PLP were used to achieve a consensus structure. Visual representation, in 3-D mode, of docking results, can be obtained using OprnEye® VIDA application. All information about OpenEye® FRED application can be found at www.eyesopen.com/prpducts.

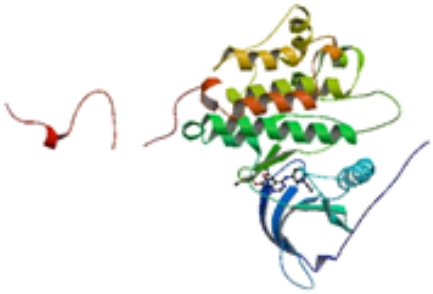

PDB ID: 1M17
Epidermal Growth Factor Receptor tyrosine kinase domain with 4-anilinoquinazoline inhibitor erlotinib

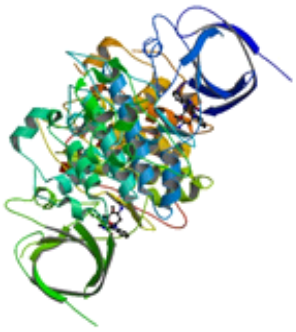

PDB ID:1Q3D
GSK-3 Beta complexed with Staurosporine

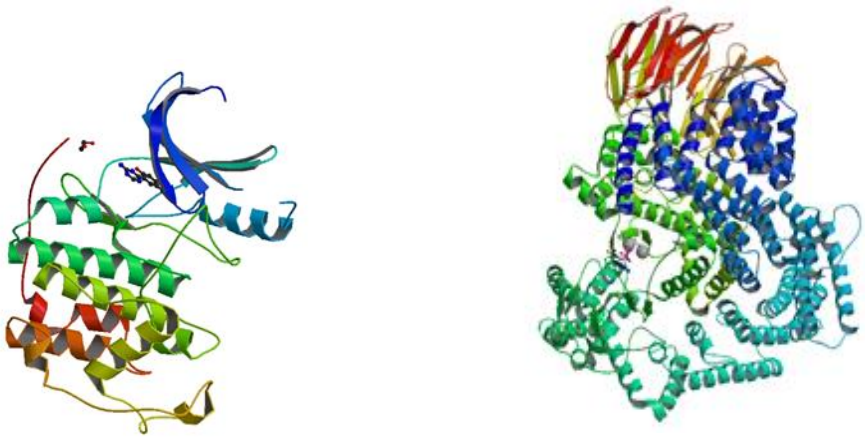

Figure 2.4 3-D structure of proteins co-crystallized with standard inhibitors, (Downloaded from protein data bank)

2.5 Results and discussion of molecular modeling

The virtual library of compounds including ormeloxifene and known standard inhibitors were docked against 12 different proteins including EGFR and downstream EGFR pathways such as Akt, ERK, GSK3β, CDK2, STAT3, mTOR, and others. Ormeloxifene analogs were designed base on the benzopyran and the pyrrolidine moieties that are responsible for its pharmacological and biological interactions. While maintaining the benzopyran base, modifications of the main skeleton were made mainly at three positions. Incorporation of various side chains such as methytlhiophene, benzotrifluoride, anisole, hydroxylethylphenol, and pyrrolidine side chains at C-7 resulted in alteration of pharmacophore of the compound. Also, the para position of 3-phenyl-2H-chromen was substituted with halogens as well as stronger activating (electron donating group) OH, NH_2,

and deactivating (electron withdrawal group) CF_3. Finally, the phenoxy position was installed with other functionalities to alter pharmacophore of ormeloxifene scaffold (**Fig 2.4**).

In average, a total of 80 analogs exhibited better receptor-ligand binding affinity (lower consensus scores) than the known inhibitors.

The designed virtual library was grouped into three categories. (1) Installing various functionalities such as halogens, electron donating and electron withdrawing groups para to 3-phenyl-2H-chromen position while maintaining the rest of ormeloxifene framework (**Fig 2.6**). (2) Switching the pyrrolidine side chain to C-7 and install electron donating, withdrawing and other functional substituents at phenoxy position (**Fig 2.7**) and (3) Substituting the ormeloxifene side chain at C-7 and phenoxy position with aromatic functional groups as well as hydroxyl, methyl and trifluoromythylated moieties (**Fig 2.8**). Full docking results are discussed in the next sections.

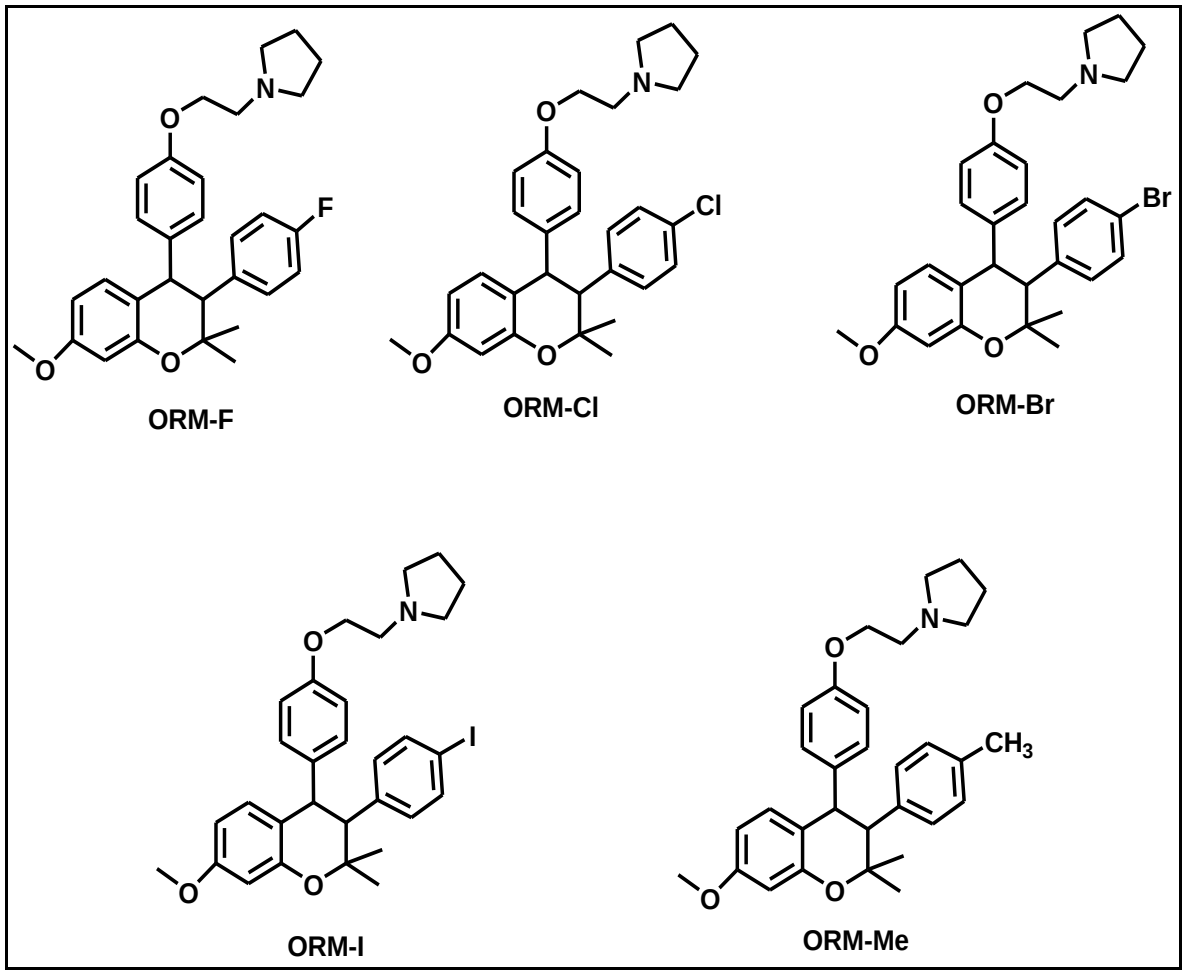

Figure 2.5. First set of synthesized compounds containing halogens, electron donating or electron withdrawing group para to 3-phenyl-2H-chromen position while maintaining the rest of ormeloxifene framework.

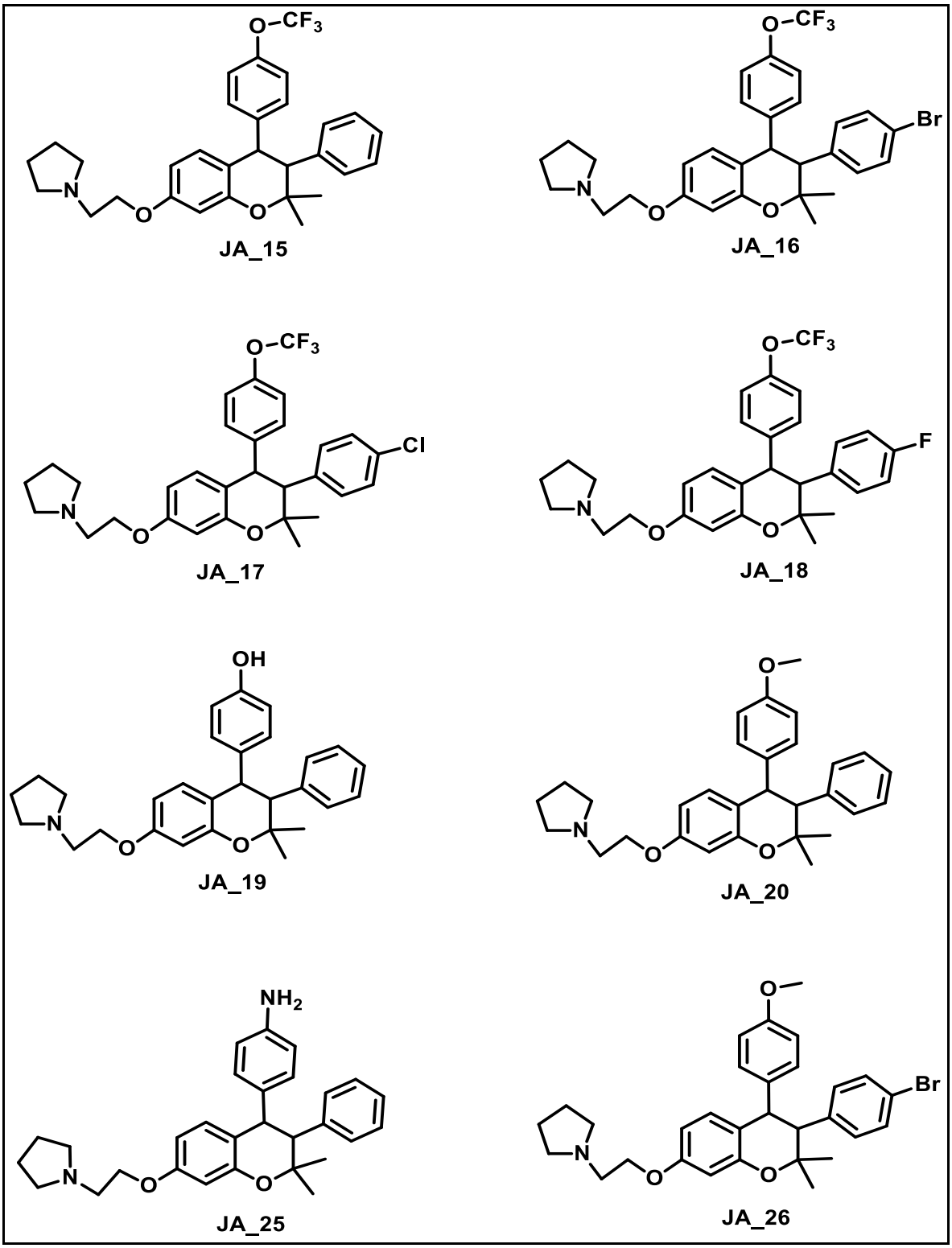

Figure 2.6 Second synthesized analogs. Switching the pyrrolidine side chain to C-7 and install electron donating, withdrawing and other functional substituents at phenoxy position

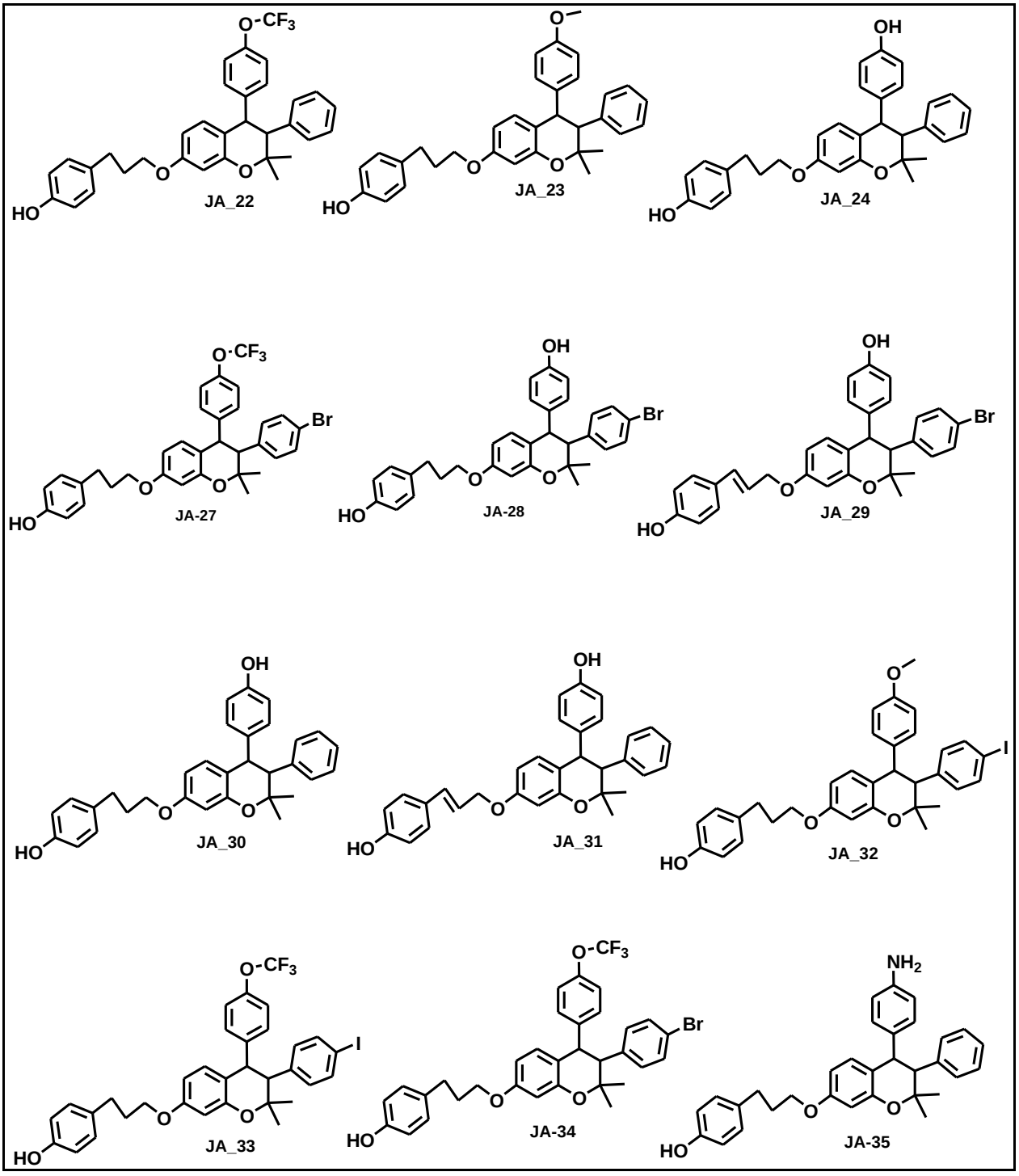

Figure 2.7 Third synthesized analogs substituting the ormeloxifene side chain at C-7 and phenoxy position with aromatic functional groups as well as hydroxyl, methyl and trifluoromythylated moieties

2.5.1 Results of molecular modeling of ormeloxifene analogs on cyclin-dependent kinase inhibitor protein (CDK2).

Molecular docking results on **CDK2** crystal structure revealed a significant increase in binding affinity of ormeloxifene analogs relative to known estrogen receptor modulator ormeloxifene (**Table 2.1**). Replacing the (ethyl)pyrrolidine moiety at the phenoxy position with trifluoromethoxy group and substitution of methoxy group at **C-7** with (ethyl)pyrrolidine moiety such as in **JA_15, JA_16, JA_17,** and **JA_18** demonstrated significant binding mode with CDK2 pocket by forming hydrogen bond with **HIS:84: A**, the same amino acid in CDK2 pocket that ormeloxifene binds to induce its anticancer activity. It is fascinating to note that the substitution of halogen at the para position of the aromatic ring at C-3 altered the binding affinity of the entire compound in the CDK2 pocket. As the size of the halogen atom at para position increases (from F to I), the binding affinity of the compound in CDK2 pocket decreases. Also, **JA_15** which is an unsubstituted analog exhibited higher binding affinity relative to the halogenated analogs (**JA_16, JA_17, JA_18) (Fig 2.9).**

Table 2.1 Sample of consensus score of FRED docking in CDK2 receptor

VIDA Name	VIDA ID	PLP	Chemgauss3	OEChemscore	Screenscore	Consensus Score
JA_15_8	2	-62.1912	-98.9223	-50.9355	-161.426	4
JA_23_65	3	-63.1604	-85.4124	-53.3115	-148.521	9
JA_18_194	4	-55.5819	-94.061	-49.7552	-156.399	15
JA_31_197	5	-58.7091	-78.7798	-50.6628	-138.252	31
ORM_Me_70	6	-58.9203	-88.0918	-48.9543	-130.846	31
JA_17_124	7	-60.2571	-82.0704	-46.9993	-151.993	33

JA_30_136	8	-54.9044	-82.1141	-49.7006	-133.778	34
JA_20_91	9	-55.1979	-82.9193	-52.6244	-128.111	34
JA_29_196	10	-56.4896	-74.7738	-51.4356	-136.43	37
JA_22_18	11	-57.7173	-76.0436	-49.6441	-141.795	38
JA_24_136	12	-54.9044	-82.1141	-49.7006	-133.778	38
JA_16_118	13	-50.2681	-89.5709	-47.0727	-145.829	41
JA_19_43	14	-51.9849	-86.1558	-49.8197	-128.74	41
JA_33_173	15	-52.6577	-80.5097	-48.3041	-139.799	43
JA_35_136	16	-49.7391	-81.7393	-46.085	-134.599	58
JA_25_26	17	-52.629	-76.5679	-47.4447	-128.804	63
JA_28_130	18	-52.1154	-73.6299	-49.4652	-122.123	65
JA_26_58	19	-50.8557	-75.0371	-48.8462	-128.441	65
JA_32_166	20	-49.3175	-79.5876	-48.1438	-121.453	68
JA_34_4	21	-48.3862	-71.7791	-48.2779	-130.937	69
ORM_188	22	-46.7276	-86.295	-45.0742	-110.072	69
JA_27_4	23	-48.3862	-71.7791	-48.2779	-130.937	73
ORM_F_106	24	-54.664	-70.7967	-42.5575	-119.368	79
ORM_Cl_107	25	-46.5579	-78.3947	-41.5806	-103.429	86
ORM_Br_166	26	-36.8834	-79.3884	-41.2741	-92.8488	87
ORM_I_109	27	-30.6345	-79.4347	-40.6518	-85.7905	89

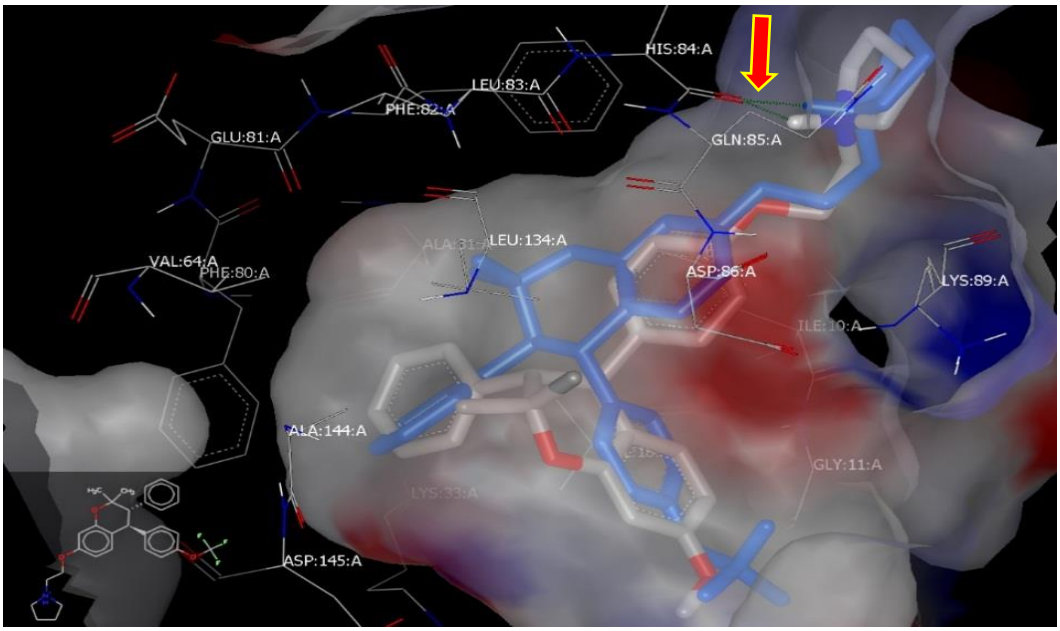

Figure 2.8. Ormeloxifene (**Gray**) and JA_**15** (**Blue**). The two compounds overlaid and their nitrogen forming hydrogen bonding with His: 84: A in CDK2 binding pocket

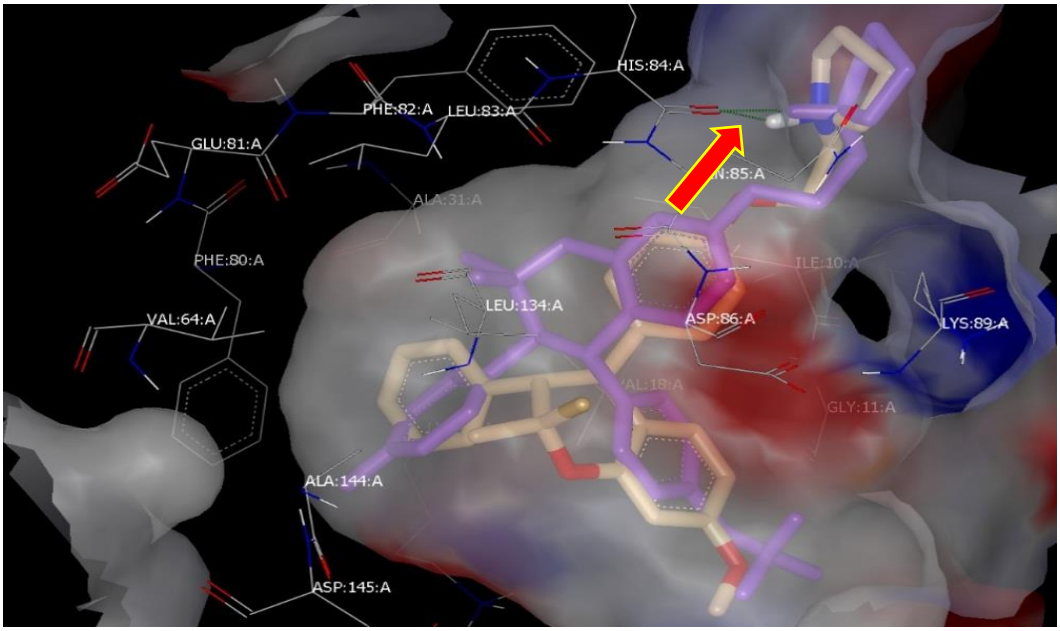

Figure 2.9 Ormeloxifene (**Gray**) and JA_18 (**Purple**) showing hydrogen bonding with His:84: A in CDK2 binding pocket

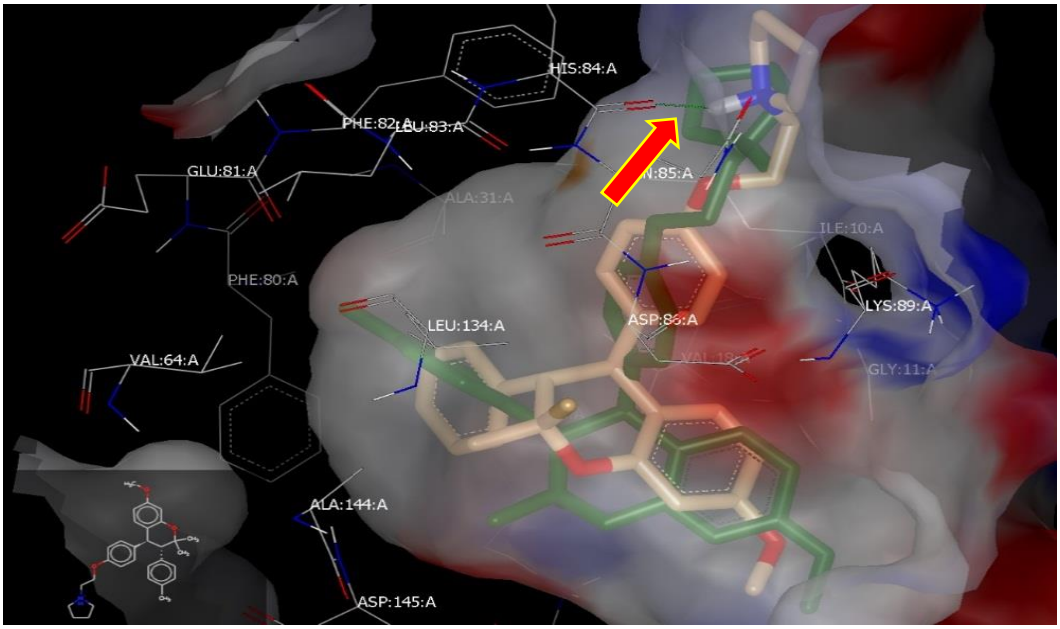

Figure 2.10 ORM (Gray) and ORM-CH_3 (Blue) with nitrogen forming hydrogen bonding with His: 84:A in CDK2 pocket

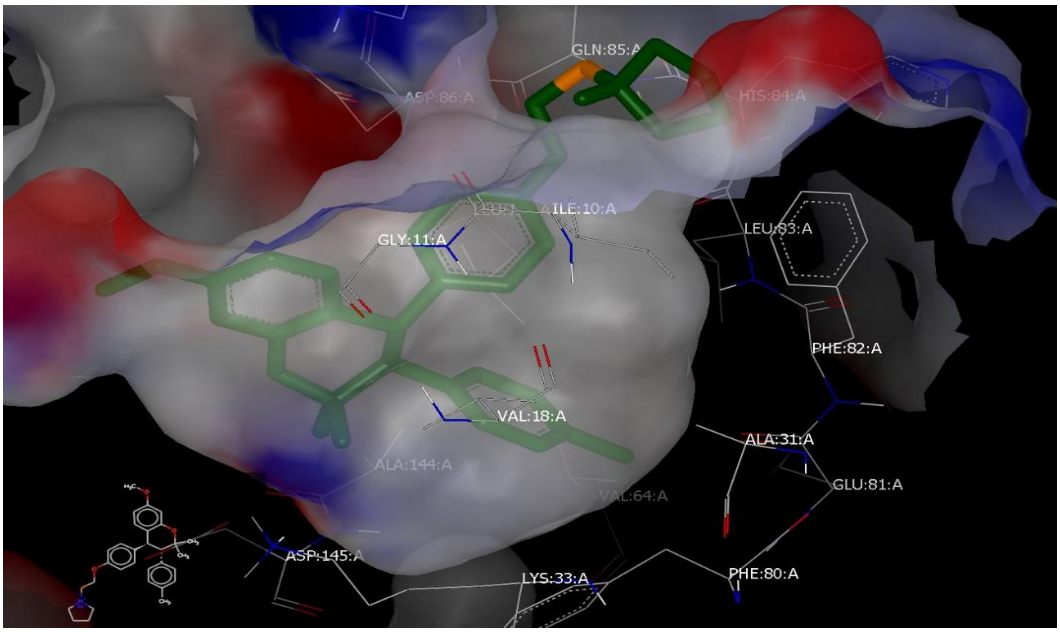

Figure 2.11 ORM-CH_3 in fitting inside the hydrophobic pocket of CDK2 with no observed hydrogen bonding or non-covalent interaction.

Analogs with 4-(3-hydroxypropyl) phenol and (E)-4-(3-hydroxyprop-1-en-1-yl) phenol at **C-7** and phenol at C-4 such as **JA_24, JA_29, JA_30, and JA_31** showed hydrophobic interaction mode in CDK2 pocket. Presence of double bond at C-1' Position played a significant role in binding to the crystal structure of CDK2 as demonstrated in **JA_31** and **JA_29**. The binding affinity of **JA_31** and **JA_29** were significantly higher (lower consensus score) compared to the counterparts JA**_24,** and **JA_30.** Generally, the **ORM-series (ORM-Br, ORM-Cl, ORM-F, ORM-CH_3, ORM-I) (Fig 2.6)** of compounds displayed an exciting trend in CDK2 binding site. Incorporation of electron donation group (EDG) at the para position of aromatic C-3 resulted in higher binding affinity with hydrophobic interaction in CDK2 binding pocket as shown in **ORM-CH_3**. However, the binding affinity of ORM-series forming hydrogen bond with **HIS:84: An** in the crystal structure of CDK2 binding site decreases when the para position of aromatic C-3 was either unsubstituted or substituted with electron withdrawing groups (EWG) such as F, Cl, Br, and I as indicated in **ORM, ORM-F, ORM-Cl, ORM-Br, ORM-I.**

Analogs such as **JA_32, JA_33,** and **ORM-I** showed an outstanding hydrophobic interaction and hydrogen bonding with **HIS:84: A** in the CDK2 pocket and showed a drastic decreased in binding mode with the crystal structure of CDK2 when iodine moiety was incorporated at the para position of aromatic C-3. The decrease in binding affinity of these analogs may be attributed to the larger size of iodine which is sticking out of the hydrophobic pocket of CDK2. **(Fig 2.13).** Analogs with trifluoromethyl group at phenoxy position and (ethyl)pyrrolidine moiety at C-7 such as **JA_15, JA_18, JA_17, and JA_16** showed higher binding affinity by forming hydrophobic interaction as well as hydrogen bonding in the crystal structure of CDK2.

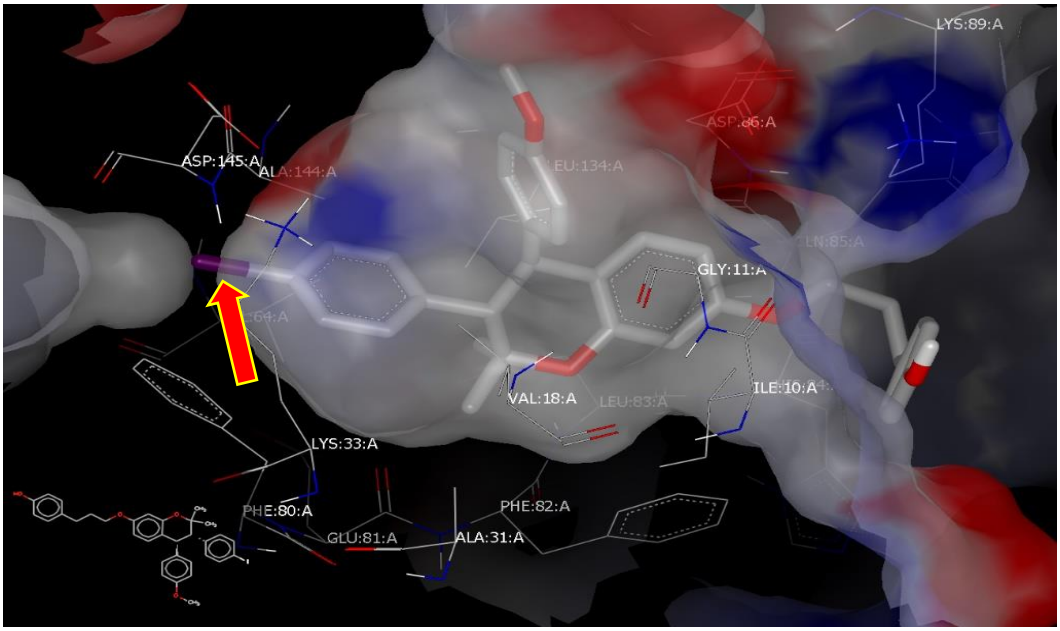

Figure 2.12 JA_23 in CDK2 Pocket with Iodine (**purple**) sticking out of the hydrophobic pocket

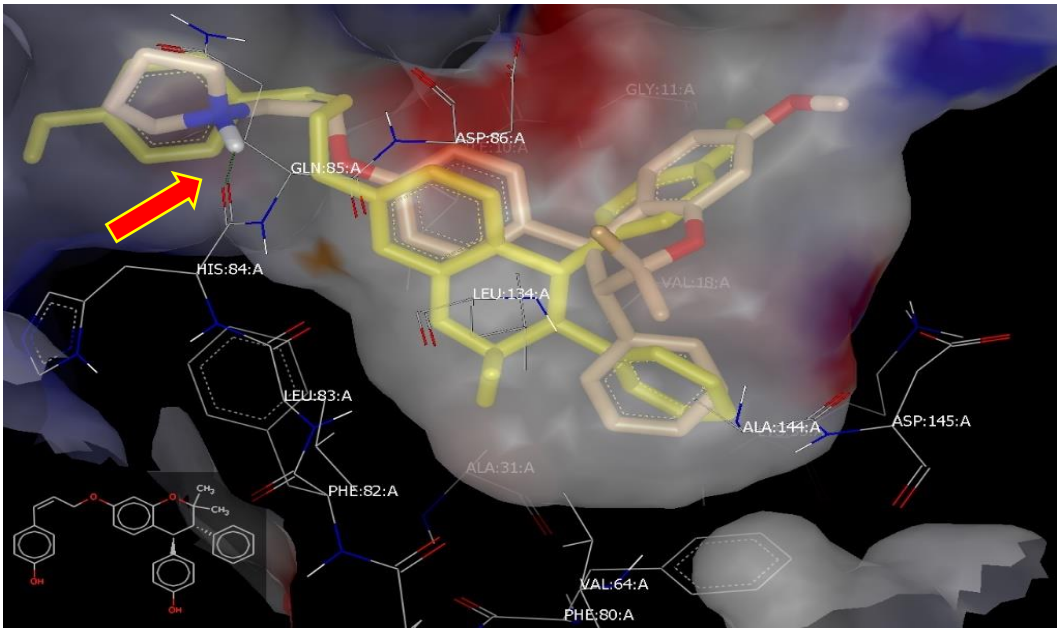

Figure 2.13 Ormeloxifene (**gray**) and JA_31 (**yellow**) overlaying each other, however, JA_31showed no hydrogen bonding in CDK2 binding pocket

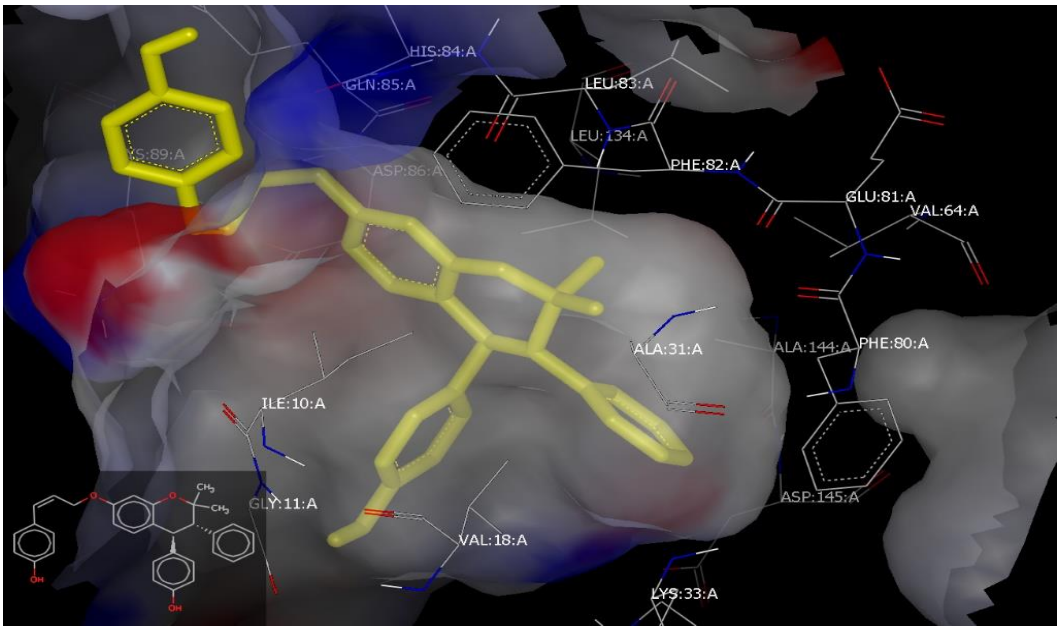

Figure 2.14. JA_31 forming hydrophobic interactions inside CDK2 binding Pocket, however no hydrogen bonding or non-covalent interactions were observed.

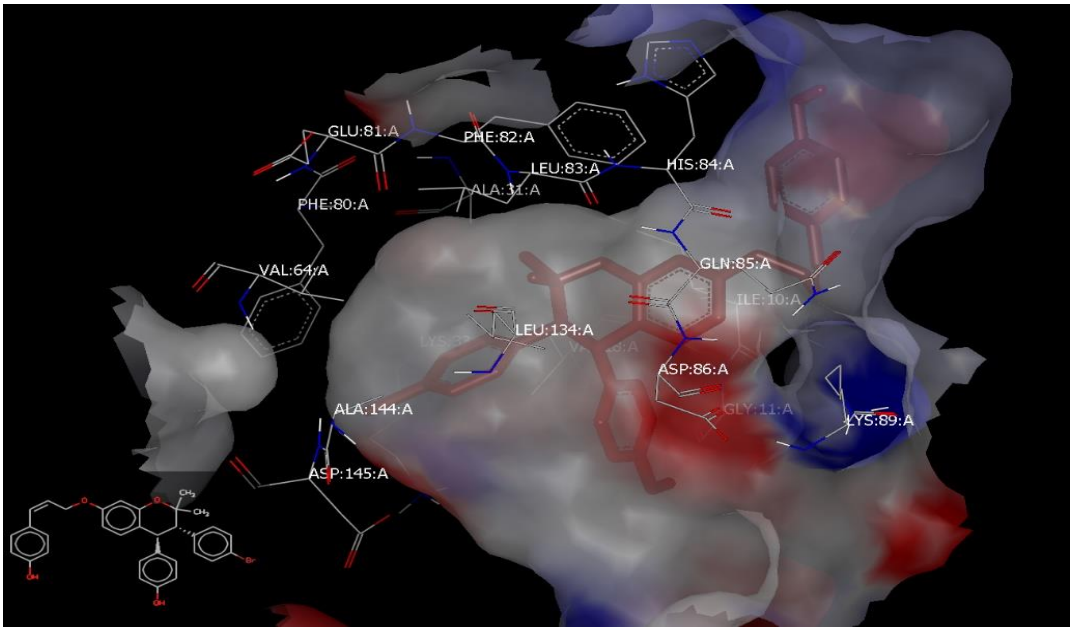

Figure 2.15 JA_29 displaying hydrophobic interaction in CDK2 Pocket. The double bond on C-1' improved its receptor binding affinity.

In conclusion, analogs with trifluoromethyl group at phenoxy position and (ethyl)pyrrolidine moiety at C-7 such as **JA_15, JA_16, JA_17,** and **JA_18** showed higher binding affinity by forming hydrophobic interaction as well as hydrogen bonding toward the crystal structure of CDK2. Analogs with 4-(3-hydroxypropyl) phenol at C-7 demonstrated significant binding mode in the CDK2 binding pocket relative to ormeloxifene. However, halogenated ormeloxifene although with both hydrogen bonding and hydrophobic interactions showed lower in binding activities towards the CDK2 pocket compared to Ormeloxifene. Orm_CH_3 (**Fig 2.12**) on the other hand performed better among the ORM- series in the CDK2 binding pocket. Finally, analogs with (E)-4-(3-hydroxyprop-1-en-1-yl) phenol as C-7 such as **JA_31** and **JA_29** had an outstanding binding affinity with the crystal structure of CDK2 than similar analogs with no double bond (**Fig 2.16, Fig 2-17**).

2.5.2 Molecular modeling of ormeloxifene analogs on EGFR

Docking on EGFR showed that, compounds with 4-(3-hydroxypropyl) phenol and (E)-4-(3-hydroxyprop-1-en-1-yl) phenol at **C-7** and phenol at C-4 such as **JA_31, JA_29, JA_30, JA_33 and JA_24** formed hydrogen bond and hydrophobic interaction in EGFR pocket. **JA_31** binds significantly with amino acids such as **ASP:292: A** and **THR:291: A** in the EGFR binding site (**Fig 2.18**). However, the introduction of bromine atom at C-4$^{'}$ position such as **JA_29** (**Fig 2.21**) led to the loss of hydrogen bonding and reduction in binding affinity in EGFR binding pocket and may have something to do with the size of bromine and its electron withdrawing effect.

The binding affinity of Orm-series such as **ORM-CH_3**, **ORM-Cl, ORM-F,** and **ORM-Br**, significantly improved by forming a hydrogen bond with THR:291: A inside of EGFR pocket in comparison with Ormeloxifene which showed no hydrogen bonding with EGFR.

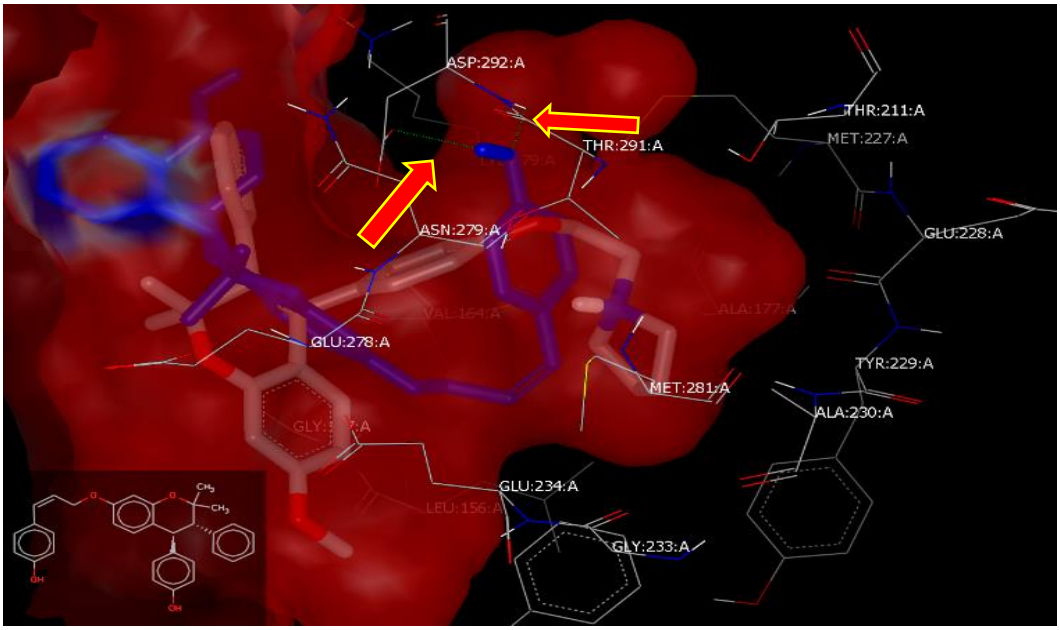

Figure 2.16 JA_31 (**blue**) and **ORM** forming two hydrogen bonding with THR:291: A and ASP;292: A in EGFR binding pocket

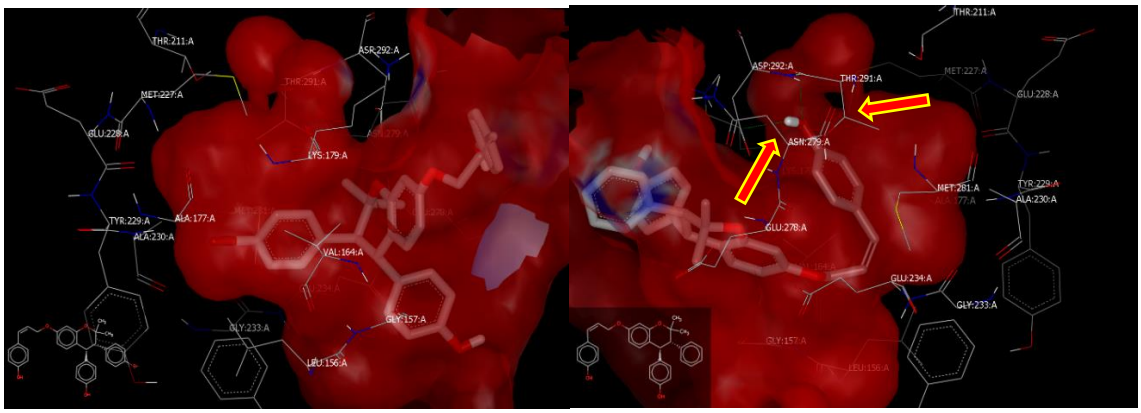

Figure 2.17 JA_29 (**left**) with no hydrogen bond and JA-31 (**right**) with two hydrogen bonds in EGFR pocket

Introduction of (ethyl)pyrrolidine moiety at the C-7 position, and installing moieties such as anisole and aniline at C-4 as in **JA_25** and **JA_19** improved binding activities as it formed hydrophobic interaction with EGFR binding pocket. But binding affinity with EGFR decreases when phenol and trifluoromethoxy benzene moieties were installed at C-4 position as shown in **JA_23,JA_20, JA_15,JA_16, JA_17, JA_18, JA_22** and **JA_26 (Fig 2.17, 2.18, 2.21)** Although there was strong hydrogen bonding of **JA_15** and **JA_17** with **GLU: 234: A** in the crystal structure of EGFR, this factor did not improve the binding affinities of these analogs in EGFR binding pocket. In the case of the crystal structure of EGFR, the trend of halogen atomic size as well as electron donating and electron withdrawing groups did not show any consistency.

2.5.3 Results of molecular modeling of ormeloxifene analogs on Glycogen synthase kinase three beta (GSK3B)

Molecular docking results of ormeloxifene analogs with GSK3B protein demonstrated different binding modes. Analogs with (ethyl)pyrrolidine side chain at C-7 of Ormeloxifene scaffolds such as **JA_20, JA_25 JA_15, JA_18, JA_19,** and **JA_17** showed both hydrophilic and hydrophobic interactions in GSK3B binding pocket. For instance, **JA_20** and **JA_25** with anisole and aniline respectively at C-4 of Ormeloxifene scaffolds showed the highest binding affinity and forms two hydrogen bonds with **LYS:85: B** and **ASP:200: B** in GSK3B binding pocket **(Fig 2.22).**

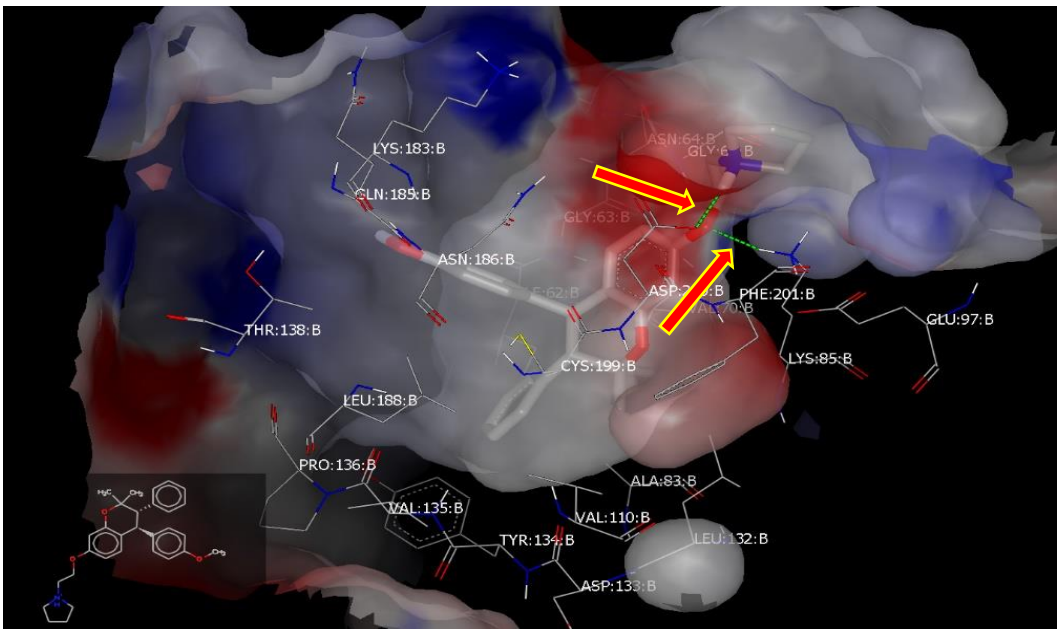

Figure 2.18 JA-20 showing oxygen at position number 1forming two hydrogen bonding with GLY:68: B and PHE:201: B in GSK3B pocket

Meanwhile, analogs with trifluoromethoxy benzene at C-4 of Ormeloxifene scaffold such as **JA_22, JA_15,** and **JA_33**, formed hydrogen bond with **LYS: 85: B** and **ASP: 200: B** in GSK3B binding pocket. However, the introduction of halogen at the para position of aromatic C-3 such as **JA_18, JA_17** resulted in the loss of hydrogen bond with ASP**: 200: B** in GSK3B binding pocket (**Fig 2.24**). Ormeloxifene analogs with 4-(3-hydroxypropyl) phenol at C-7 as shown in **JA_33, JA_35, JA_25, 28, JA_22** and **JA_28** demonstrated a higher binding affinity by forming hydrogen bonds with **LYS:85: B** and **LYS:183: B** in the GSK3B binding pocket. **JA_35**, on the other hand, showed an outstanding binding affinity in the crystal structure of GSK3B when the **C-4** position was substituted with aniline which leads to the formation of three hydrogen bonds with **LYS: 85: B, LYS: 183: B** and **ASN: 186: B (Fig 2.23).**

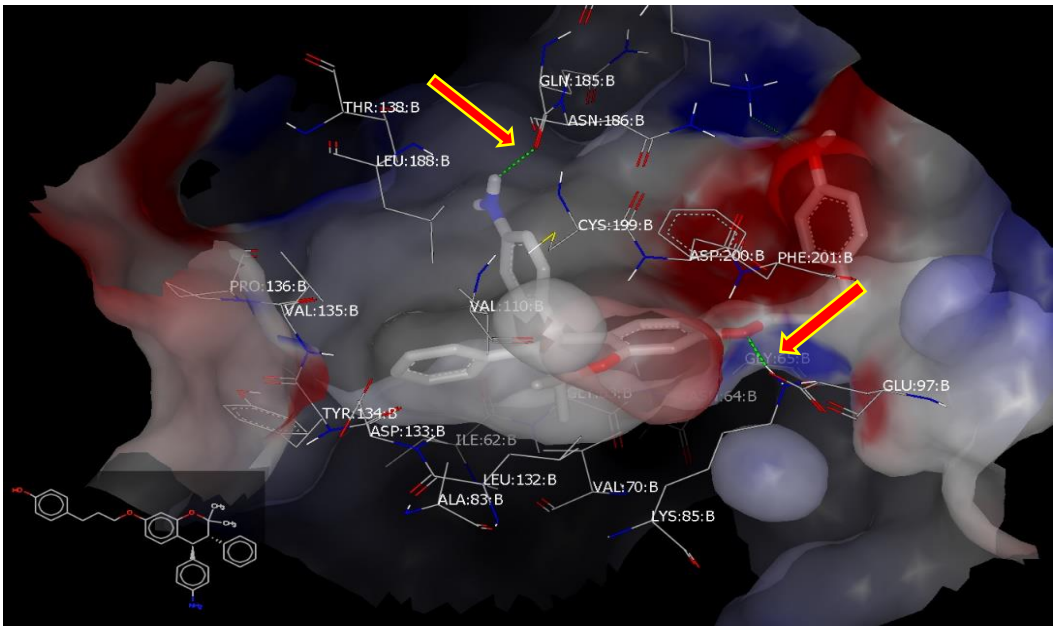

Figure 2.19. The nitrogen on JA_35 showed hydrogen bonding ASN:186: B. Meanwhile, the oxygen at the para position of the aromatic ring formed hydrogen bond with LYS:183: B in GSK3B pocket

Also, **ORM-series** of compounds also performed very well in the crystal structure of GSK3B by forming hydrophobic interaction as well as hydrogen bonding relative to ormeloxifene. Introduction of halogens at the para position of the aromatic ring at C-3 as in **ORM-Cl, ORM-F** and **ORM-Br** led to the formation of a hydrogen bond with **ASP: 200: B** inside GSK3B binding pocket. Binding affinities of these analogs increase with increasing the size of the halogenated substituent in the GSK3B pocket (**Fig.2.24**).

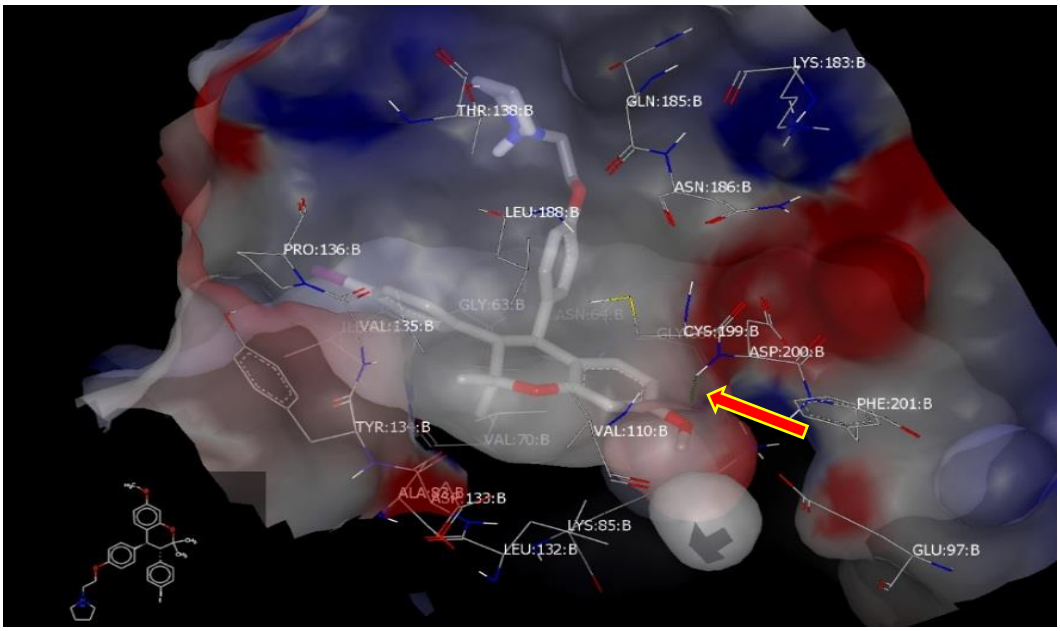

Figure 2.20. Orm-I forming hydrogen bond with ASP: 200: B in GSK3B pocket. However, the large size of iodine caused the loss in receptor binding affinity.

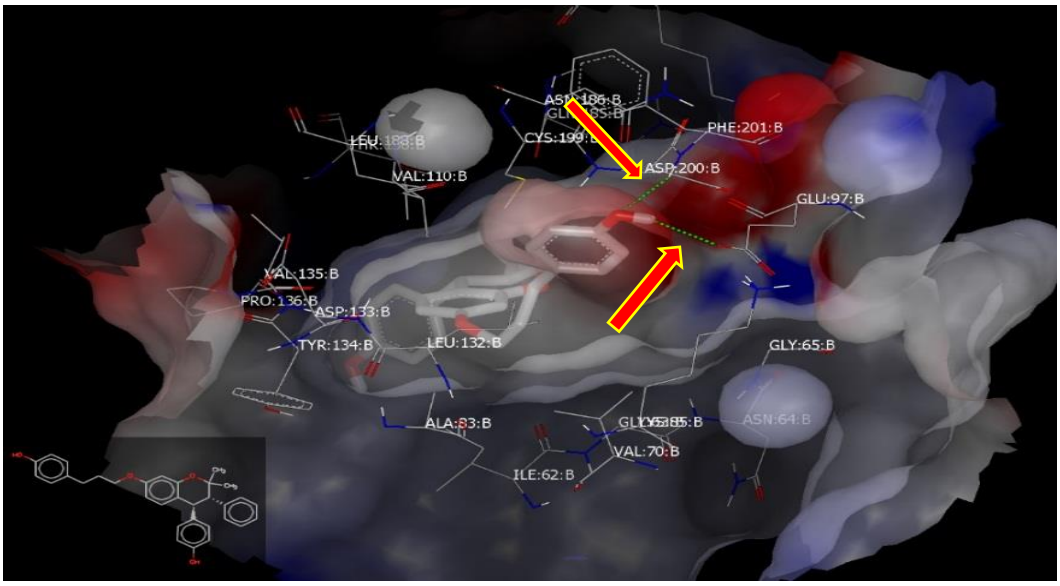

Figure 2.21. Oxygen at the para position of JA_24 Formed two hydrogen bonds with ASP:200: B and GLU:97; B in the crystal structure of GSK3B.

It is interesting to note that the introduction of phenol at **C-4** and substitution of 4-(3-hydroxypropyl) phenol at the **C-7** position of ormeloxifene scaffold resulted in higher binding mode with the crystal structure of **GS3KB**. The hydroxyl group of 4-(3-hydroxypropyl) phenol **JA-24** formed two hydrogen bonds with **GLU: 97: B** and **PHE: 201: B** in the crystal structure of GSK3B (**Fig 2.25**).

2.5.4 Results of molecular modeling of ormeloxifene analogs on the mammalian target of rapamycin (mTOR)

Molecular modeling of analogs **JA_22, JA_19, JA_15, JA_30, JA_29** and **JA_23** towards mTOR showed various binding modes. The first set of ormeloxifene analogs with trifluoromethoxy benzene at C-4 and (ethyl)pyrrolidine side chain at C-7 of Ormeloxifene frameworks such as **JA_19** and **JA_15** performed better compared with Ormeloxifene. **JA_15** formed three hydrogen bonds with **SER:21655: B, LYS:2187: B** and **THR:2245:**

B whiles **JA_19** exhibited three hydrogen bonds with two amino acids, two bonds with **THR:2245: B** and another bond with **LYS:2187: B** in mTOR binding pocket (**Fig 2.26**)

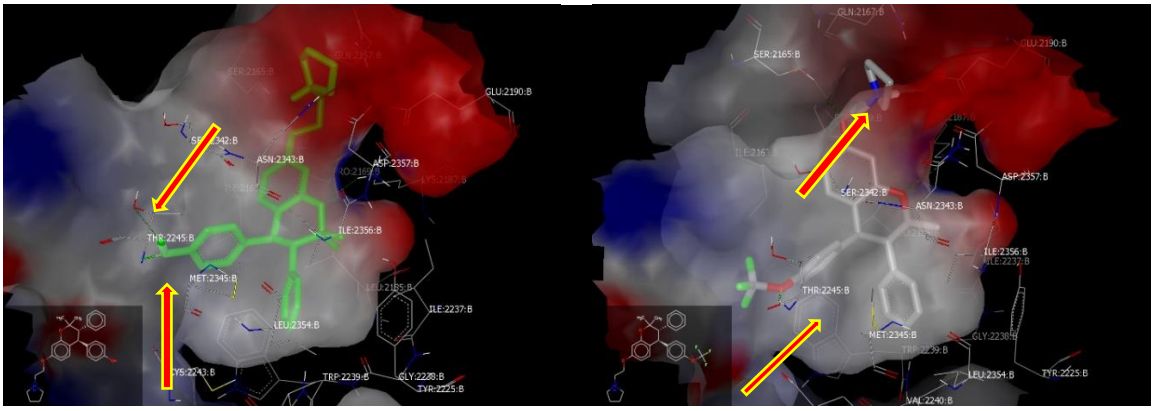

Figure 2.22. JA_19 (Blue) and JA_15 each forming two hydrogen bonding with THR:2245: B and LYS: 2187: B in mTOR binding pocket

The second set of analogs with 4-(3-hydroxypropyl) phenol and (E)-4-(3-hydroxyprop-1-en-1-yl) phenol at **C-7** and phenol, aniline and anisol moieties at C-4 position such as **JA_22, JA_29, JA_30,** and **JA_23** showed better binding affinities relative to ormeloxifene. These analogs formed both hydrogen bonds as well as hydrophobic interaction with the crystal structure of mTOR (**Fig 2.27).**

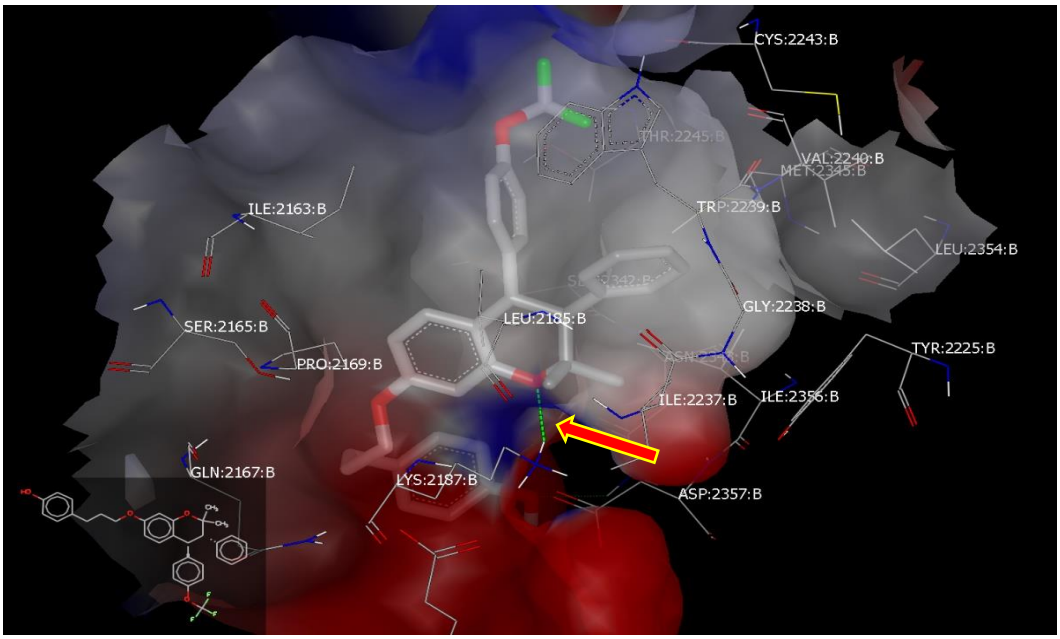

Figure 2.23. JA_22 forming hydrogen bonding with LYS:227: B in mTOR binding pocket

The third series of ormeloxifene analogs such as **ORM-CH_3, ORM-Cl, ORM-F,** and **ORM-Br** performed poorly with the crystal structure of mTOR compared to ormeloxifene. They showed hydrophobic interaction in the mTOR binding pocket with no hydrogen bonding.

2.5.5 Results of molecular modeling of ormeloxifene analogs on ERK

In the crystal structure of ERK, only the first set of ormeloxifene analogs that have anisole, phenol and trifluoromethoxy benzene at C-4 and (ethyl)pyrrolidine side chain at C-7 of Ormeloxifene scaffolds such as **JA_19**, **JA_17, JA-20,** and **JA_15** performed better in ERK binding pocket as compared to the known inhibitor Ormeloxifene. JA_20 formed a

hydrogen bond with **ASP: 109: B,** meanwhile the remaining analogs formed hydrophobic interaction inside ERK pocket(**Fig 2.29**).

The second and the third series of ormeloxifene analogs (ORM-series and JA-24 to JA-31), although they showed both hydrogen bonding and hydrophobic interaction with the crystal structure of ERK did not perform better compare to ormeloxifene.

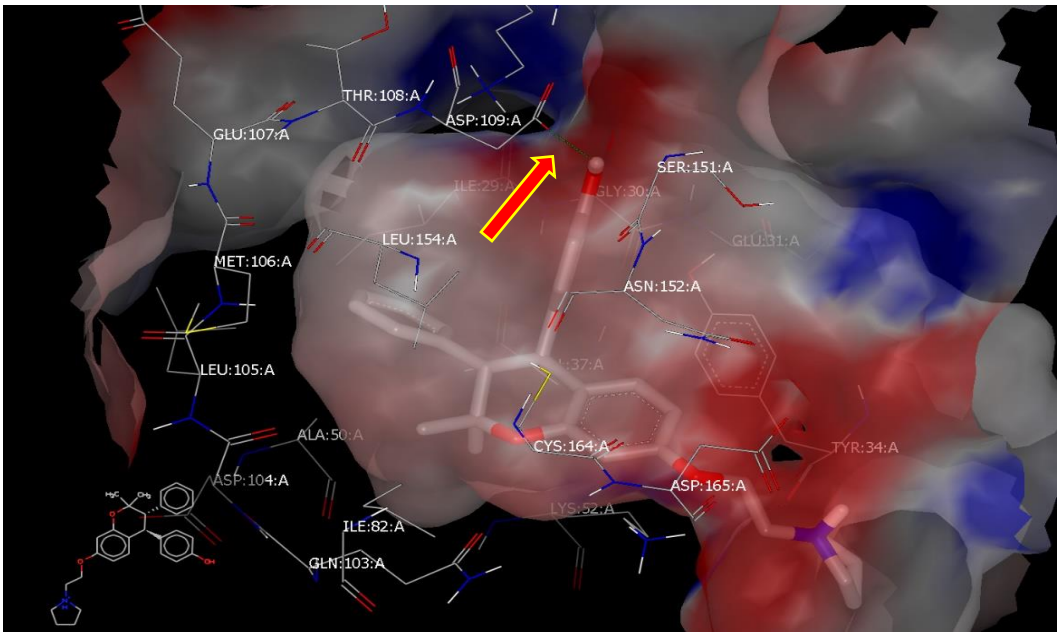

Figure 2.24 JA_19 showing hydrogen bonding with ASP:109: A in ERK binding pocket

2.5.6 Results of molecular modeling of ormeloxifene analogs on the β-catenin

Molecular docking studies of ormeloxifene analogs on beta-catenin binding pocket revealed various binding modes. For instance, analogs with trifluoromethyl at the para position of the aromatic ring at C-3 such as JA-33, JA-27, and JA-34 showed higher binding affinity towards the beta-catenin binding pocket. However, these analogs only

exhibited hydrophobic interaction inside the binding pocket. The reasons for their higher binding activities may be attributed to the higher covalent bonding between the tree fluorine atom and the receptor binding pocket of beta-catenin (**Fig 2.25**).

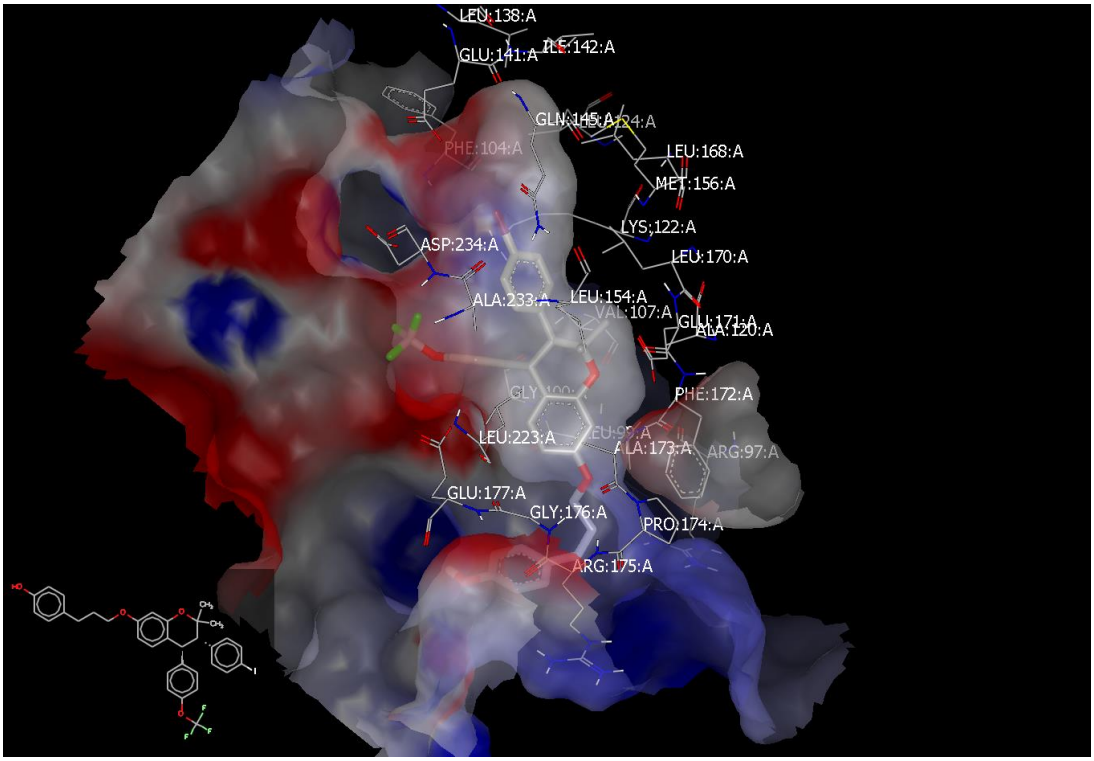

Figure 2.25. JA-33 forming hydrophobic interactions inside beta-catenin binding pocket. However, there was no evidence of hydrogen bonding.

Analog ORM-Br (**Fig 2.26**), among ORM-series, performed relatively better in the beta-catenin binding pocket with lower consensus score (higher binding affinity) compared to ormeloxifene. This analog showed only hydrophobic interactions in the beta-catenin binding site. It is interesting to note that analogs with halogens have a higher affinity towards beta-catenin. Other analogs without halogens such as ORM-CH_3, JA-28, performed moderately well inside the beta-catenin binding site with better binding affinity than ormeloxifene.

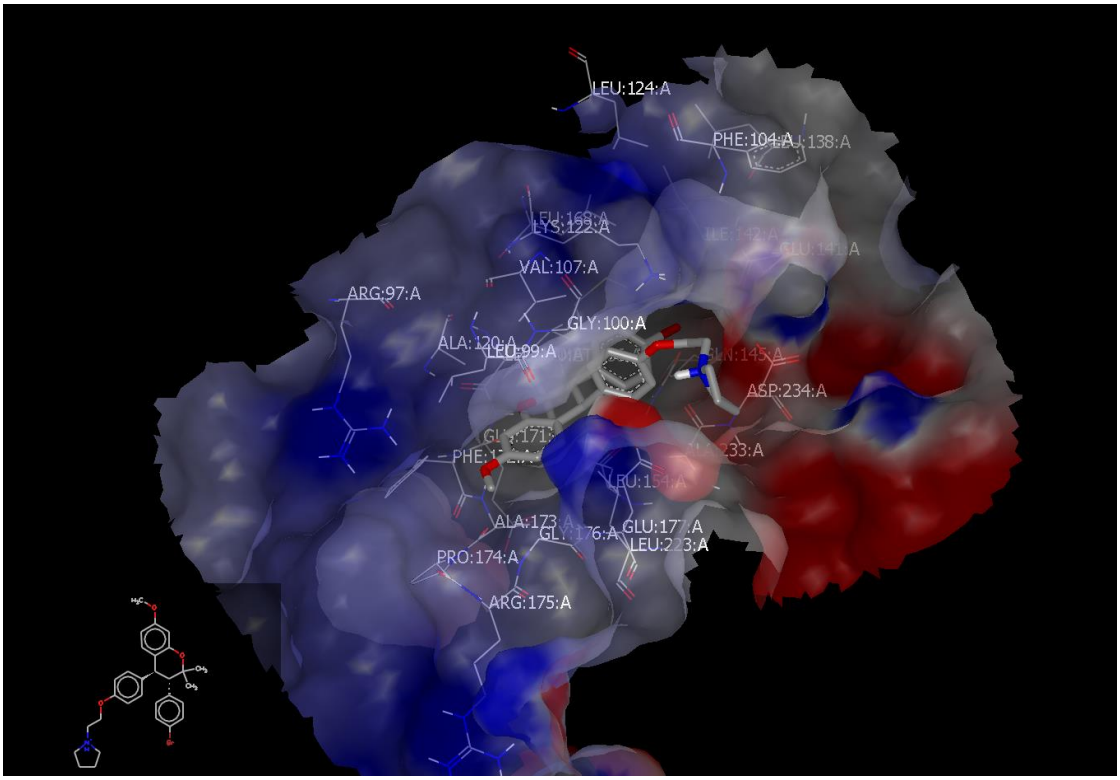

Figure 2.26. Visual representation of ORM-Br inside beta-catenin binding pocket. The analog fit perfectly inside the hydrophobic pocket resulting in stronger hydrophobic interactions

2.6 Conclusion

Molecular modeling is important to approach to identify and discover compounds exhibiting high specificity of recent potential drug candidates from the basis of the structure-based drug design approach. In our docking studies, the proposed analogs were docked against the molecular target that causes ovarian cancer. The in-silico study outlined the basis of designing analogs which will filter out and helps us focus on synthesizing with higher binding affinity to the molecular targets.

Molecular docking studies revealed that replacing the methoxy group at C-7 with pyrrolidine side chain improved the binding affinity in almost all the receptors downstream

EGFR (CDK2, ERK, mTOR, GSK3B). Analogs **JA-15, JA_18** and **JA_17** showed significant binding affinity in all the receptors relative to other analogs. The size of halogens, on the other hand, had a significant effect on most of the receptors. For instant presences of halogen with larger atomic size such as iodine reduces the binding affinity in **CDK2** binding pockets while the larger size of halogen favors higher binding affinity in GSK3B. Presence of double bonds at C-1' also played an important role in **CDK2, GSK3B** and **EGFR**, analogs with double bonds on (E)-4-(3-hydroxyprop-1-en-1-yl)phenol at C-7 improved the binding affinity in these receptors compared to similar analogs without double bonds. Analogs with halogen at the para position of aromatic rings at C-3 and C-4' such as **JA-33, JA-34, JA-27,** and **ORM-Br** increased binding affinity in the beta-catenin binding pocket.

On the other hand, docking studies assisted in exploring different aromatic substituents at C-4, ortho and meta substituents led to a drastic reduction in binding activity in all the receptors. Meanwhile, binding activity in all receptors increases with para-substituted aromatic moieties. Also, para-substituted aromatic moieties and trifluoromethoxy benzene showed higher binding affinity in all receptors by forming hydrogen bonding and hydrophobic interactions. These results help us to assemble various aromatic and aliphatic groups at **C-7** and **C-4** of ormeloxifene scaffold.

Finally, the result of molecular docking provided an opportunity to outline the synthetic schemes towards the installation of different functionalities and side chains on ormeloxifene framework. It also proved as a reliable tool for designing drug candidates for the inhibition of **EGFR, ERK, GSK3B, CDK2, mTOR** and all downstream proteins.

2.7 References

1. Kamboj, V. P.; Ray, S.; Anand, N., Centchroman: A safe, reversible postcoital contraceptive with curative and prophylactic activity in many disorders. *Frontiers in bioscience (Elite edition)* **2018,** *10*, 1-14.

2. LERNER, L. J.; HOLTHAUS, F. J.; THOMPSON, C. R., A non-steroidal estrogen antagonist l-(p-2-diethylaminoethoxyphenylh-phenyl-2-p-methoxyphenyl ethanol. *Endocrinology* **1958,** *63* (3), 295-318.

3. Singh, M., Centchroman, a selective estrogen receptor modulator, as a contraceptive and for the management of hormone-related clinical disorders. *Medicinal research reviews* **2001,** *21* (4), 302-347.

4. Karmakar, S.; Deshpande, H., Ormeloxifene-A new treatment modality in Dysfunctional Uterine Bleeding: efficacy and safety. *Indian Journal of Obstetrics and Gynecology Research* **2016,** *3* (3), 225-228.

5. Sharma, S.; Kaur, D.; Mahajan, A.; Tandon, V., Selective oestrogen receptor modulators. *Asian Journal of obstetrics and gynaecology practice* **2006,** *10* (3), 30-36.

6. Kuiper, G.; Enmark, E.; Pelto-Huikko, M.; Nilsson, S.; Gustafsson, J.-A., Cloning of a novel receptor expressed in rat prostate and ovary. *Proceedings of the National Academy of Sciences* **1996,** *93* (12), 5925-5930.

7. (a) Lin, Z.; Shen, H.; Huang, J.; Chen, S.; Chen, L.; Chen, J.; Liu, G.; Jiang, H.; Shen, X., Butyl 4-(butyryloxy) benzoate functions as a new selective estrogen receptor β agonist and induces GLUT4 expression in CHO-K1 cells. *The Journal of steroid biochemistry and molecular biology* **2008,** *110* (1), 150-156; (b) Korach, K. S.; Emmen,

J. M.; Walker, V. R.; Hewitt, S. C.; Yates, M.; Hall, J. M.; Swope, D. L.; Harrell, J. C.; Couse, J. F., Update on animal models developed for analyses of estrogen receptor biological activity. *The Journal of steroid biochemistry and molecular biology* **2003,** *86* (3), 387-391.

8. McKie, J. A.; Bhagwat, S. S.; Brady, H.; Doubleday, M.; Gayo, L.; Hickman, M.; Jalluri, R. K.; Khammungkhune, S.; Kois, A.; Mortensen, D., Lead identification of a potent benzopyranone selective estrogen receptor modulator. *Bioorganic & medicinal chemistry letters* **2004,** *14* (13), 3407-3410.

9. (a) Khan, S.; Shukla, S.; Sinha, S.; Lakra, A. D.; Bora, H. K.; Meeran, S. M., Centchroman suppresses breast cancer metastasis by reversing epithelial–mesenchymal transition via downregulation of HER2/ERK1/2/MMP-9 signaling. *The international journal of biochemistry & cell biology* **2015,** *58*, 1-16; (b) Kaushik, S.; Shyam, H.; Sharma, R.; Balapure, A. K., Genistein synergizes centchroman action in human breast cancer cells. *Indian journal of pharmacology* **2016,** *48* (6), 637.

10. Maihle, N. J.; Baron, A.; Barrette, B. A.; Boardman, C.; Christensen, T.; Cora, E.; Faupel-Badger, J.; Greenwood, T.; Juneja, S.; Lafky, J., EGF/ErbB receptor family in ovarian cancer. In *Ovarian cancer*, Springer: 2002; pp 247-258.

11. Yarden, Y.; Ullrich, A., Growth factor receptor tyrosine kinases. *Annual review of biochemistry* **1988,** *57* (1), 443-478.

12. van Delft, S.; Verkleij, A. J.; Boonstra, J.; en Henegouwen, P. M. v. B., Epidermal growth factor induces serine phosphorylation of actin. *FEBS letters* **1995,** *357* (3), 251-254.

13. Yarden, Y., The EGFR family, and its ligands in human cancer: signaling mechanisms and therapeutic opportunities. *European journal of cancer* **2001,** *37,* 3-8.

14. Prenzel, N.; Fischer, O.; Streit, S.; Hart, S.; Ullrich, A., The epidermal growth factor receptor family as a central element for cellular signal transduction and diversification. *Endocrine-related cancer* **2001,** *8* (1), 11-31.

15. (a) Tzahar, E.; Waterman, H.; Chen, X.; Levkowitz, G.; Karunagaran, D.; Lavi, S.; Ratzkin, B. J.; Yarden, Y., A hierarchical network of interreceptor interactions determines signal transduction by Neu differentiation factor/neuregulin and epidermal growth factor. *Molecular and cellular biology* **1996,** *16* (10), 5276-5287; (b) Guy, P. M.; Platko, J. V.; Cantley, L. C.; Cerione, R. A.; Carraway, K. L., Insect cell-expressed p180erbB3 possesses an impaired tyrosine kinase activity. *Proceedings of the National Academy of Sciences* **1994,** *91* (17), 8132-8136; (c) Plowman, G. D.; Whitney, G. S.; Neubauer, M. G.; Green, J. M.; McDonald, V. L.; Todaro, G. J.; Shoyab, M., Molecular cloning and expression of an additional epidermal growth factor receptor-related gene. *Proceedings of the National Academy of Sciences* **1990,** *87* (13), 4905-4909.

16. Morandell, S.; Stasyk, T.; Skvortsov, S.; Ascher, S.; Huber, L. A., Quantitative proteomics and phosphoproteomics reveal novel insights into complexity and dynamics of the EGFR signaling network. *Proteomics* **2008,** *8* (21), 4383-4401.

17. Jones, H. E.; Gee, J. M.; Hutcheson, I. R.; Knowlden, J. M.; Barrow, D.; Nicholson, R. I., Growth factor receptor interplay and resistance in cancer. *Endocrine-related cancer* **2006,** *13* (Supplement 1), S45-S51.

18. Qiu, L.; Zhou, C.; Sun, Y.; Di, W.; Scheffler, E.; Healey, S.; Kouttab, N.; Chu, W.; Wan, Y., Crosstalk between EGFR and TrkB enhances ovarian cancer cell migration and proliferation. *International journal of oncology* **2006,** *29* (4), 1003-1011.

19. Gschwind, A.; Zwick, E.; Prenzel, N.; Leserer, M.; Ullrich, A., Cell communication networks: epidermal growth factor receptor transactivation as the paradigm for interreceptor signal transmission. *Oncogene* **2001,** *20* (13), 1594-1600.

20. Nicodemus, C. F.; Berek, J. S., Monoclonal antibody therapy of ovarian cancer. *Expert review of anticancer therapy* **2005,** *5* (1), 87-96.

21. Johns, T. G.; Adams, T. E.; Cochran, J. R.; Hall, N. E.; Hoyne, P. A.; Olsen, M. J.; Kim, Y.-S.; Rothacker, J.; Nice, E. C.; Walker, F., Identification of the epitope for the epidermal growth factor receptor-specific monoclonal antibody 806 reveals that it preferentially recognizes an untethered form of the receptor. *Journal of Biological Chemistry* **2004,** *279* (29), 30375-30384.

22. Murthy, U.; Basu, A.; Rodeck, U.; Herlyn, M.; Ross, A. H.; Das, M., Binding of an antagonistic monoclonal antibody to an intact and fragmented EGF-receptor polypeptide. *Archives of biochemistry and biophysics* **1987,** *252* (2), 549-560.

23. Lu, Y.; Li, X.; Liang, K.; Luwor, R.; Siddik, Z. H.; Mills, G. B.; Mendelsohn, J.; Fan, Z., Epidermal growth factor receptor (EGFR) ubiquitination as a mechanism of acquired resistance escaping treatment by the anti-EGFR monoclonal antibody cetuximab. *Cancer research* **2007,** *67* (17), 8240-8247.

24. Karamouzis, M. V.; Grandis, J. R.; Argiris, A., Therapies directed against epidermal growth factor receptor in aerodigestive carcinomas. *Jama* **2007,** *298* (1), 70-82.

25. Huang, S.-M.; Bock, J. M.; Harari, P. M., Epidermal growth factor receptor blockade with C225 modulates proliferation, apoptosis, and radiosensitivity in squamous cell carcinomas of the head and neck. *Cancer research* **1999,** *59* (8), 1935-1940.

26. Rowinsky, E. K., The erbB family: targets for therapeutic development against cancer and therapeutic strategies using monoclonal antibodies and tyrosine kinase inhibitors. *Annu. Rev. Med.* **2004,** *55*, 433-457.

27. Maher, D. M.; Khan, S.; Nordquist, J. L.; Ebeling, M. C.; Bauer, N. A.; Kopel, L.; Singh, M. M.; Halaweish, F.; Bell, M. C.; Jaggi, M., Ormeloxifene efficiently inhibits ovarian cancer growth. *Cancer letters* **2015,** *356* (2), 606-612.

28. Hafeez, B. B.; Ganju, A.; Sikander, M.; Kashyap, V. K.; Hafeez, Z. B.; Chauhan, N.; Malik, S.; Massey, A. E.; Tripathi, M. K.; Halaweish, F. T., Ormeloxifene suppresses prostate tumor growth and metastatic phenotypes via inhibition of oncogenic β-catenin signaling and EMT progression. *Molecular cancer therapeutics* **2017,** *16* (10), 2267-2280.

29. Srivastava, V. K.; Gara, R. K.; Bhatt, M.; Sahu, D.; Mishra, D. P., Centchroman inhibits proliferation of head and neck cancer cells through the modulation of PI3K/mTOR pathway. *Biochemical and biophysical research communications* **2011,** *404* (1), 40-45.

30. Huang, S.; Houghton, P. J., Targeting mTOR signaling for cancer therapy. *Current opinion in pharmacology* **2003,** *3* (4), 371-377.

31. Hawkins, P. C.; Skillman, A. G.; Warren, G. L.; Ellingson, B. A.; Stahl, M. T., Conformer generation with OMEGA: algorithm and validation using high quality

structures from the Protein Databank and Cambridge Structural Database. *Journal of chemical information and modeling* **2010,** *50* (4), 572-584.

32. Kristam, R.; Gillet, V. J.; Lewis, R. A.; Thorner, D., Comparison of conformational analysis techniques to generate pharmacophore hypotheses using catalyst. *Journal of chemical information and modeling* **2005,** *45* (2), 461-476.

Chapter 3

Design, synthesis and biological evaluation of ormeloxifene Analogs: Potential Protein kinase inhibitors

3 Introduction

Despite the recent advancement in diagnosis and improved strategies for the treatment of cancer, the disease is still the leading cause of death for much of the world population. The occurrence and death rate continues to increase for several cancer types, which is costing billions of dollars every year. The estimated national expenditure for cancer care in the United States in 2010 alone was about 125 billion dollars, and it is expected to skyrocket to about 156 billion dollars in 2020[1]. Several clinical studies and research on the fight against cancer have led to the discovery of many anticancer drugs and therapies. However, they are associated with severe side effects and high cost. Among these drugs is Tamoxifen, a molecular treatment targeting the estrogen receptor (ER) by a Selective Estrogen Receptor Modulator (SERM). The drug is effective in reducing risk of breast cancer but also found to increase the risk of adverse effects such as lower-limb lymphedema, increase risk of bone loss in premenopausal women, and has been linked to endometrial cancer in some women[2]. The need for a potent and cost-effective drug candidate to fight against the proliferation of ovarian cancer has become a significant concern to humanity. Ormeloxifene, one of the Selective Estrogen Receptor Modulator (SERM) that acts on the estrogen receptor, has been available as an oral contraceptive with trade names Saheli, novex-DS, sevista. Studies have shown its effectiveness for abnormal uterine bleeding

(AUB), fibroadenomas, and advanced breast cancer with excellent therapeutic index and safety for chronic administration[3]. Anti-tumorigenic effect of ormeloxifene in different cancers, such as breast, ovarian, head and neck, and chronic myeloid leukemia had been confirmed. To date, there is no proven evidence of an adverse effect, but there are concerns that ormeloxifene may cause a delay in menstruation, which has not yet proven[4]. These advantages of ormeloxifene over tamoxifen has made it an excellent candidate for the treatment of cancer**.**

In previous studies, it was confirmed that ormeloxifene could decrease Akt phosphorylation and increase p53 phosphorylation[5]. Phosphorylation of Akt by PI3K activates the protein to signal for cell survival (by resisting apoptosis), proliferation, growth, motility, and angiogenesis. Levels of p53 increase in response to hypoxia or physiologic signals that damage DNA, to prevent the progression of the cell cycle and in some cases, they promote apoptosis. Phosphorylation of p53 protects it from degradation from the Mdm2 protein, hence contributing to the increase of p53 levels in the cell[6]. Mdm2 activity is influenced by Akt signaling activity. Akt is one of the many signal-transducing proteins among a web of kinases that signal for cell growth and proliferation downstream of the EGFR kinase. Cytotoxic activity of ormeloxifene on ovarian cancer cell lines has demonstrated its ability to significantly decrease Akt phosphorylation and modulate the expression and localization of CDK2[5].

The standard treatment of ovarian cancer includes surgical approaches followed by platinum and alkylating–based chemotherapy[7]. Manipulation of combinations dosages of existing drugs have resulted in marginal gains, but the use of these agents in standard

therapy has not improved the overall survival of ovarian cancer patients. Several clinical controlled trials have predicted the platinum-paclitaxel combination regimen as the initial treatment for advanced ovarian cancer with the responds rate of more than 80% and 40-60% complete responses[8]. However, a number of these patients suffer deterioration after a period of improvement. The established records of the safety of Ormeloxifene along with its favorable bioavailability and ability to inhibit rapid cell proliferation in the endometrium during embryonic implantation has made it one of the best drug candidate for controlling undesirable rapid cell growth such as endometriosis and cancerous tumor conditions[9]. Previous studies have confirmed the effectiveness of Ormeloxifene in preventing and suppressing ovarian cancer cell lines due to its potent estrogen agonist and antagonist's functions of the reproductive tissues as well as non-reproductive tissues[10]. In this communication, a novel ormeloxifene analogs with inhibitory activities towards epidermal growth factor receptor **(EGFR)** is studied to develop a potential drug candidate for the treatment of ovarian cancer. Introduction of electron withdrawing groups such as halogens at the para position of the aromatic ring at **C-3** of the benzopyran framework improved the inhibitory activity of the compound in different proteins relative to Ormeloxifene. The knowledge of varying inhibitory activity of ormeloxifene on multiple pathways provided a possible lead towards the discovery of a potential anticancer agent.

Computational chemistry (Molecular modeling) is a valuable tool that provides an understanding of various interactions made by known ligand and to examine the potential new interactions of designed ligand[11,12]. The desire to understand and predict these interactions outlined a successful virtual screening, structure-based drug design, and

accurate ligand placement proved to be very important[12]. This tool is vital to determine the energy parameters for various molecules. A potential anticancer agent such as ormeloxifene was obtained from structural modification of benzopyran framework and allowed for the formation of the hypothesis that benzopyran framework containing receptor binding affinity and agnostic properties for selective estrogen receptors modulators (SERM'S) related to ormeloxifene could be applied to inhibit EGFR pathway **(Fig 3.1)**.

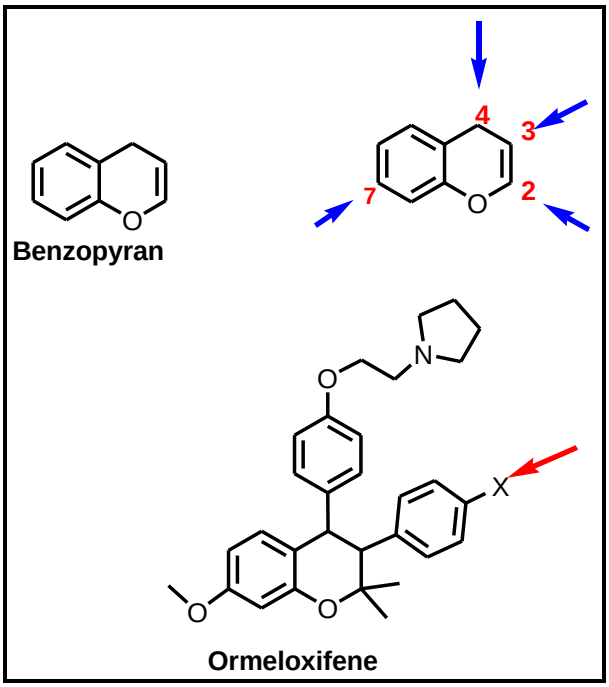

Figure 3.1 Benzopyran, Ormeloxifene, and significant sites for activity

Ormeloxifene has demonstrated a wide range of biological activities as illustrated from the antiproliferation activities via ER-dependent and ER-independent pathways on various cancer cell lines as well as their potency on different biological pathways[10]. The pyrrolidine moiety in ormeloxifene is favorable and is responsible for its antagonistic activity. The receptor binding ability and estrogen agonistic activity of ormeloxifene are due to its benzopyran base[13]. This design by (Central Drug Research Institute) CDRI led to the

development of ormeloxifene which compete with estradiol for binding the cytosol receptors[3]. In our study modification of the structure of ormeloxifene was based on the concept of bioisosterism to systematically design and installed different functionalities on the ormeloxifene core as well as the benzopyran base to increase the potency and reduce any undesirable side effects.

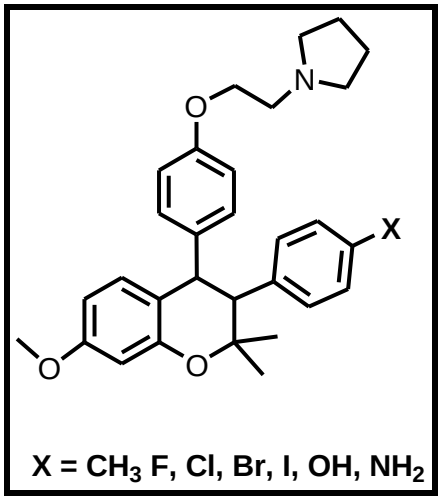

Figure 3.2. Proposed ormeloxifene analogs

3.1 Results and discussion

3.1.1 Results of molecular docking of Halogenated ormeloxifene on EGFR and its downstream

Molecular docking results revealed that introduction of electron donating (particularly methyl, amine and hydroxyl) groups at C-4' as in **ORM-CH_3**, **ORM-OH, ORM-NH_2** increased the binding affinity two folds towards EGFR (**ORM-CH_3, ORM-OH**) in comparison to ormeloxifene **(Fig 3.3), (Table 3.1).** **ORM-CH_3** (**Fig 3.4**) formed hydrophobic interaction with EGFR binding pocket, but there was no evidence of hydrogen

bonding inside EGFR binding pocket. Installing halogen electron withdrawing groups (**F, Cl, Br, and I**) at C-4' position as in **ORM-F, ORM-Cl, ORM-Br,** and **ORM-I** resulted in stronger hydrophobic interactions inside EGFR binding pocket. It is worth mentioning that, as the size of halogens on an aromatic ring on C-3 increases, the strength of hydrophobic interactions with the crystal structure of EGFR decreases and results in a decrease in binding affinity inside the EGFR binding pocket (**Increasing binding affinity with decreasing size: trend: ORM-I** < **ORM-Br < ORM-Cl < Orm-F**). Among all the docked compounds, **ORM-CH_3, ORM-OH, ORM-NH_2,** and **ORM-F** were identified to have the highest calculated binding affinity towards EGFR. Ligand-protein interactions of para-substituted analogs such as **ORM-Br, ORM-F, ORM-OH, ORM-NH_2,** and **ORM-CH_3** had higher binding affinity to EGFR compared to meta and ortho-substituted analogs. Molecular docking results revealed that **ORM-Br** and **ORM-F** forms hydrogen bond with **Glu:234: A** inside the hydrophobic pocket of Akt kinase via the nitrogen on the pyrrolidine group in comparison to ormeloxifene showed no hydrogen bond in the Akt kinase binding pocket. **ORM-F, ORM-Cl, ORM-Br,** and **ORM-I** exhibited strong binding affinity as they fill the entire hydrophobic pocket of Akt. Compounds **ORM-Br** and **ORM-I** were also predicted to have enhanced ligand-protein interactions with GSK3B binding pocket, which is also downstream of the EGFR pathway. **ORM-Br** and **ORM-I** form hydrogen bonding with **ASP:200: B** as well as strong hydrophobic interactions inside GSK3B binding pocket (**Fig 3.7**). These results imply that para-substituted halogen analogs are more likely to inhibit EGFR pathway activity than ormeloxifene. Also, inside the binding pocket of beta-catenin, **ORM-Br** exhibited outstanding hydrophobic interaction compared to ormeloxifene although there was no evidence of hydrogen bonding between beta-catenin

and these analogs **(Fig. 3.5).** All compounds showing lower consensus scores (higher binding affinity) will be chemically synthesized to be evaluated biologically as an anti-cancer candidate (**Table 3.1**).

Table 3.1 Sample of consensus score of FRED docking in the EGFR receptor

VIDA Name	VIDA ID	PLP	Chemgauss 3	OEChemscore	Screenscore	Consensus Score
JA_31_1	2	-45.247	-68.4535	-38.6503	-104.501	3
JA_30_39	3	-44.9719	-60.5825	-40.8394	-90.4211	13
JA_24_39	4	-44.9719	-60.5825	-40.8394	-90.4211	15
JA_35_39	5	-44.6895	-62.8689	-38.1707	-92.5443	15
ORM_Me_190	6	-41.6986	-53.6256	-36.454	-106.272	17

JA_25_38	7	-44.7585	-57.4479	-34.8473	-101.471	17
JA_19_38	8	-42.0043	-58.1483	-33.9175	-99.8021	20
ORM_F_51	9	-38.6906	-45.5903	-35.0408	-96.5411	30
ORM_Br_51	10	-39.0345	-48.4712	-33.0672	-97.0094	31
ORM_Cl_52	11	-36.6162	-47.8941	-32.9173	-98.0451	34
JA_29_122	12	-33.8423	-36.6207	-35.0655	-83.5629	40
ORM_69	13	-33.8104	-42.1914	-33.7609	-92.4648	40

ORM_I_51	14	-34.1445	-41.1615	-33.5722	-76.1835	44
JA_20_65	15	-31.0004	-54.6548	-30.0644	-68.121	47
JA_15_175	16	-17.8434	-36.0847	-28.6275	-60.5747	60
JA_28_177	17	-20.2947	-25.438	-30.9079	-65.3065	61
JA_23_90	18	-9.9837	-34.0844	-31.1391	-31.8667	63
JA_26_45	19	-7.8375	-28.432	-22.4842	-36.7958	68
JA_17_10	20	-5.1128	-31.1933	-17.2967	-41.8368	69
JA_22_165	21	-2.1763	-25.8179	-17.5796	-33.7014	73

JA_18_177	22	0.6849	-24.4723	-16.1185	-27.703	80
JA_16_178	23	24.8383	-15.6823	-13.7416	-4.1119	84

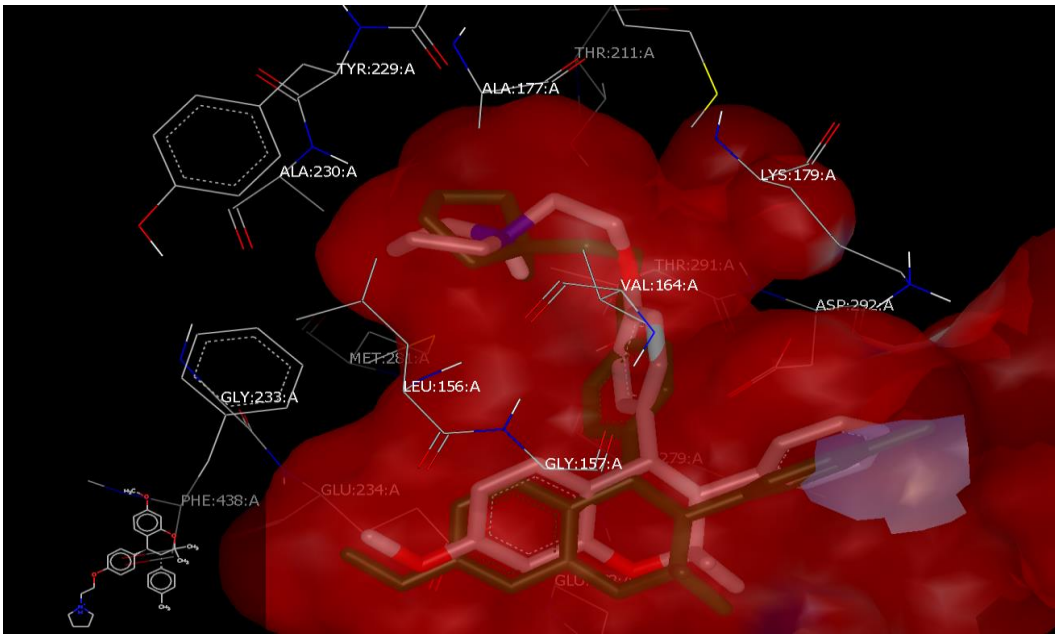

Figure 3.3 ORM (**purple**) and ORM-CH_3 (**green**) overlaying inside hydrophobic pocket of EGFR and no hydrogen bonding were observed.

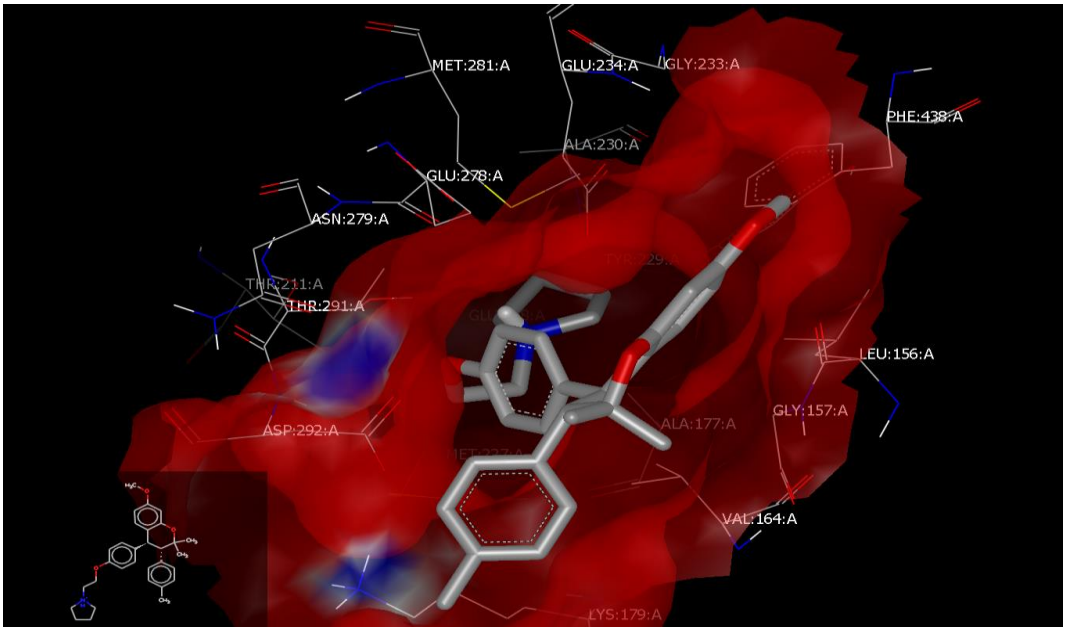

Figure 3.4 ORM-CH_3 inside the hydrophobic pocket of EGFR with no observed hydrogen bonding and non-covalent interactions.

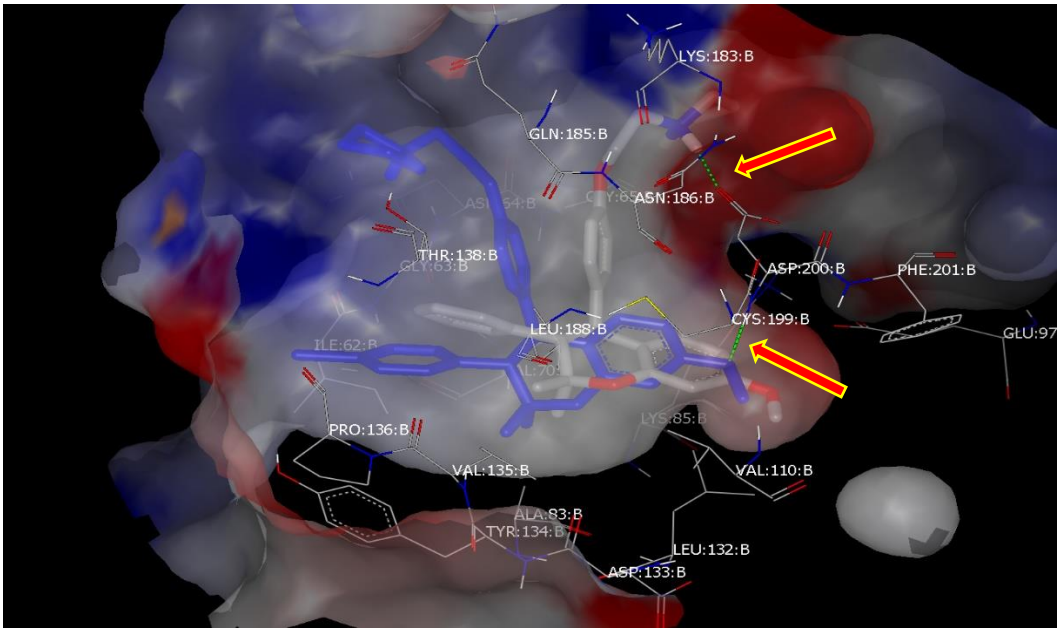

Figure 3.5 ORM and ORM-Br bonding to different amino acids GSK3B binding pocket.

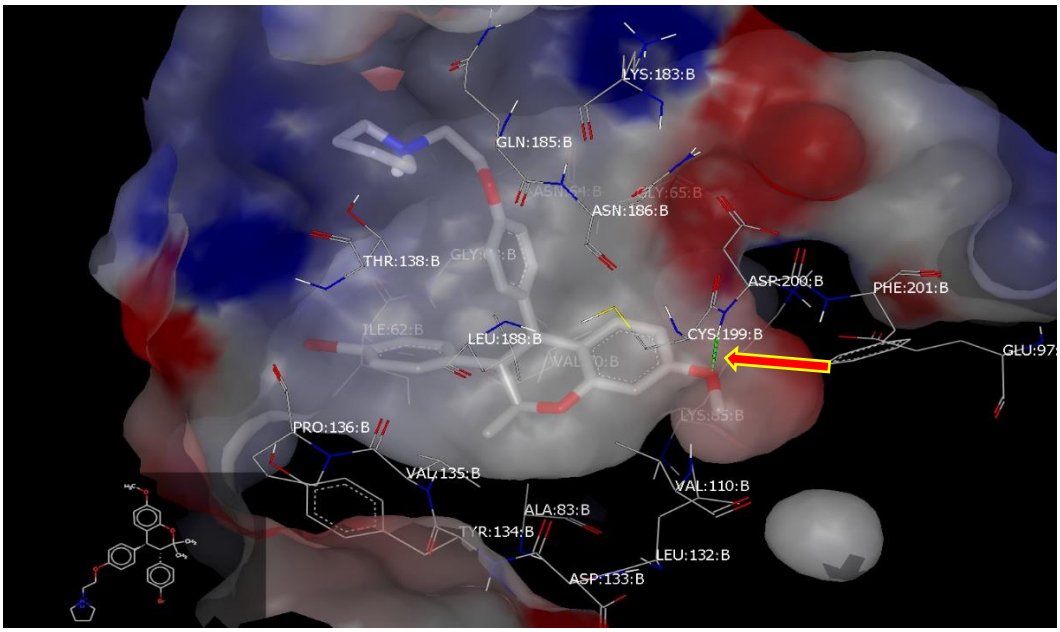

Figure 3.6 Orm-Br forming hydrogen bonding with ASP: 200: B in GSK3B binding pocket

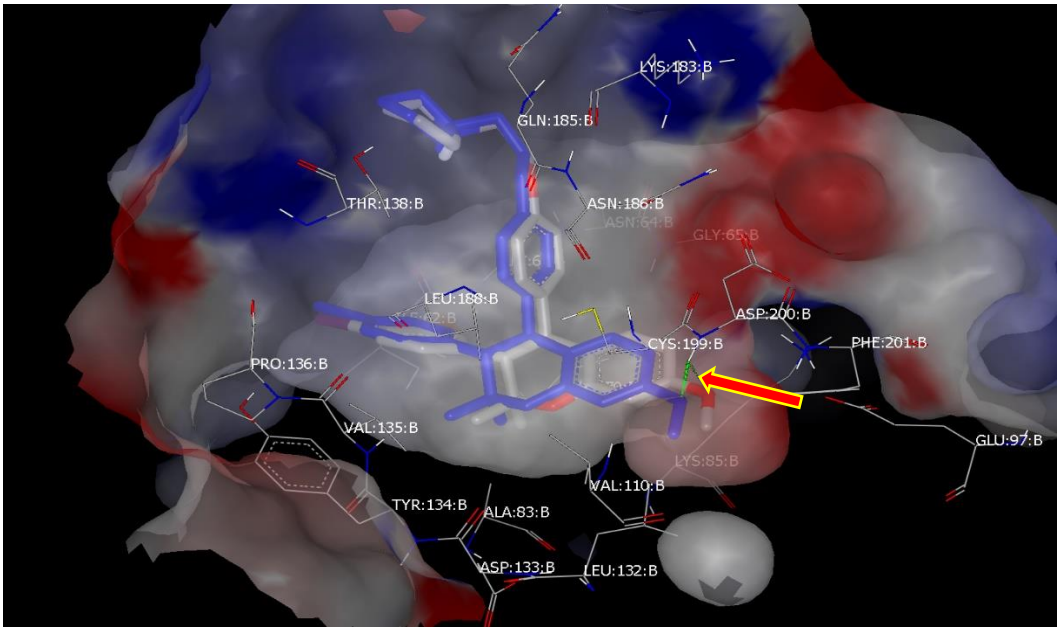

Figure 3.7 ORM-I (ash) and ORM-Br (blue) binding to ASP:200: B in GSK3B binding pocket.

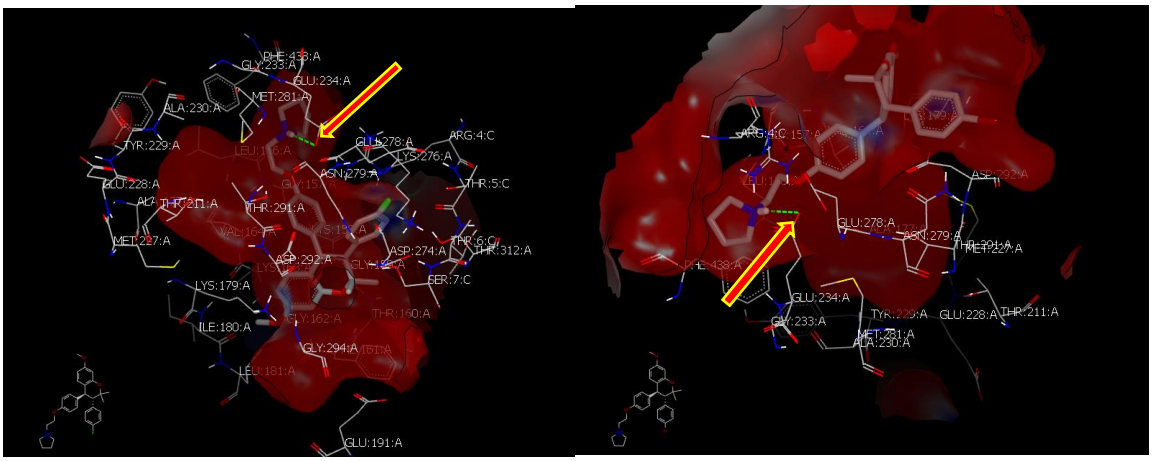

Figure 3.8 ORM-F (left) and ORM-Br (right) in ATK Kinase showing hydrogen bonding with Glu: 234: A

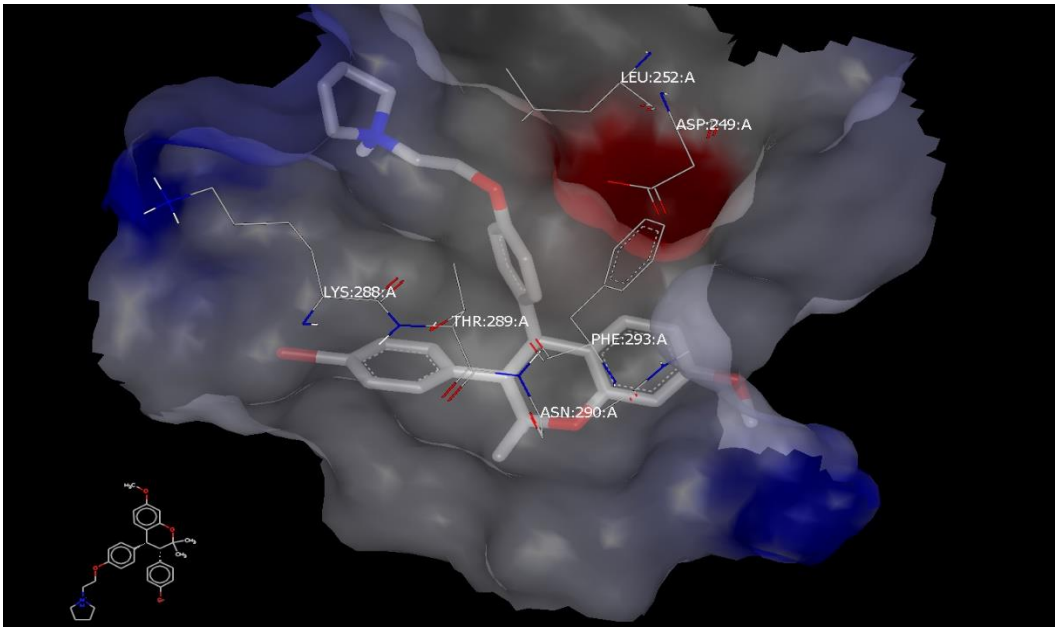

Figure 3.9 ORM-Br forming hydrophobic interaction in the β-catenin binding pocket, however no hydrogen bond with various amino acids were observed.

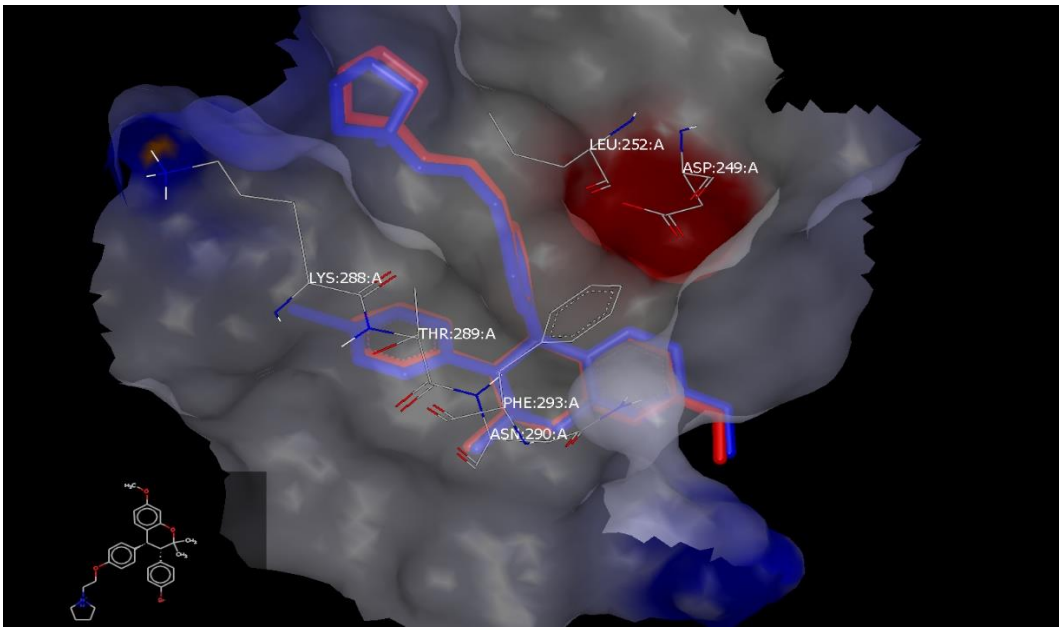

Figure 3.10 Ormeloxifene and ORM-Br overlaying inside beta-catenin binding pocket; however, no hydrogen bonding was observed.

3.1.2 Synthesis of methyl, hydroxyl, amine, and halogenated ormeloxifene

To synthesis of various analogs of ormeloxifene, several synthetic approaches were employed to arrive at successful and productive synthetic routes. The initial synthesis proceeded using the published synthetic route by ***suprabhat et al.,1975*** **(Scheme 3.1)** where Ormeloxifene was synthesized by Friedel-Crafts like acylation of 4-hydroxybenzoic acid and 3-methoxyphenol to give (2-hydroxy-4-methoxyphenyl)(4-hydroxyphenyl)methanone **(a)**[14,15]. Nucleophilic addition-elimination of **(a)** with phenylacetic acid in the presence of triethylamine to produce cis-3-phenyl-4-p-acetoxyphenyl-7-methoxy-3,4-dihydrocoumarin **(b).** Grignard reaction of **(b)** using methyl magnesium iodide with THF as a solvent to provide 2-(3-hydroxy-1-(4-hydroxyphenyl)-3-methyl-2-phenylbutyl)-5-methoxyphenol **(c)**[16]. This step gave varieties of side reactions

which resulted in low yield. Cyclization of compound **(c)** with polyphosphoric acid at a temperature of 75 - 80°C to produce **(d).** Condensation of 1-(2-chloroethyl) pyrrolidine with potassium carbonate (K_2CO_3) in acetone at 60 °C yields **(e)** and isomerization of **(e)** with n-butyl lithium DMSO afforded centchroman **(f)**[17]. This synthetic route, although successful was discontinued due to the use of unfriendly environmental reagents such as polyphosphoric acid, phosphorus trichloride acid, and n-butyl lithium. The reaction was also cost ineffective and time-consuming relative to the yield obtained. It was essential to find an alternative and improved synthetic procedure with excellent yield, atom economy and environmentally friendly.

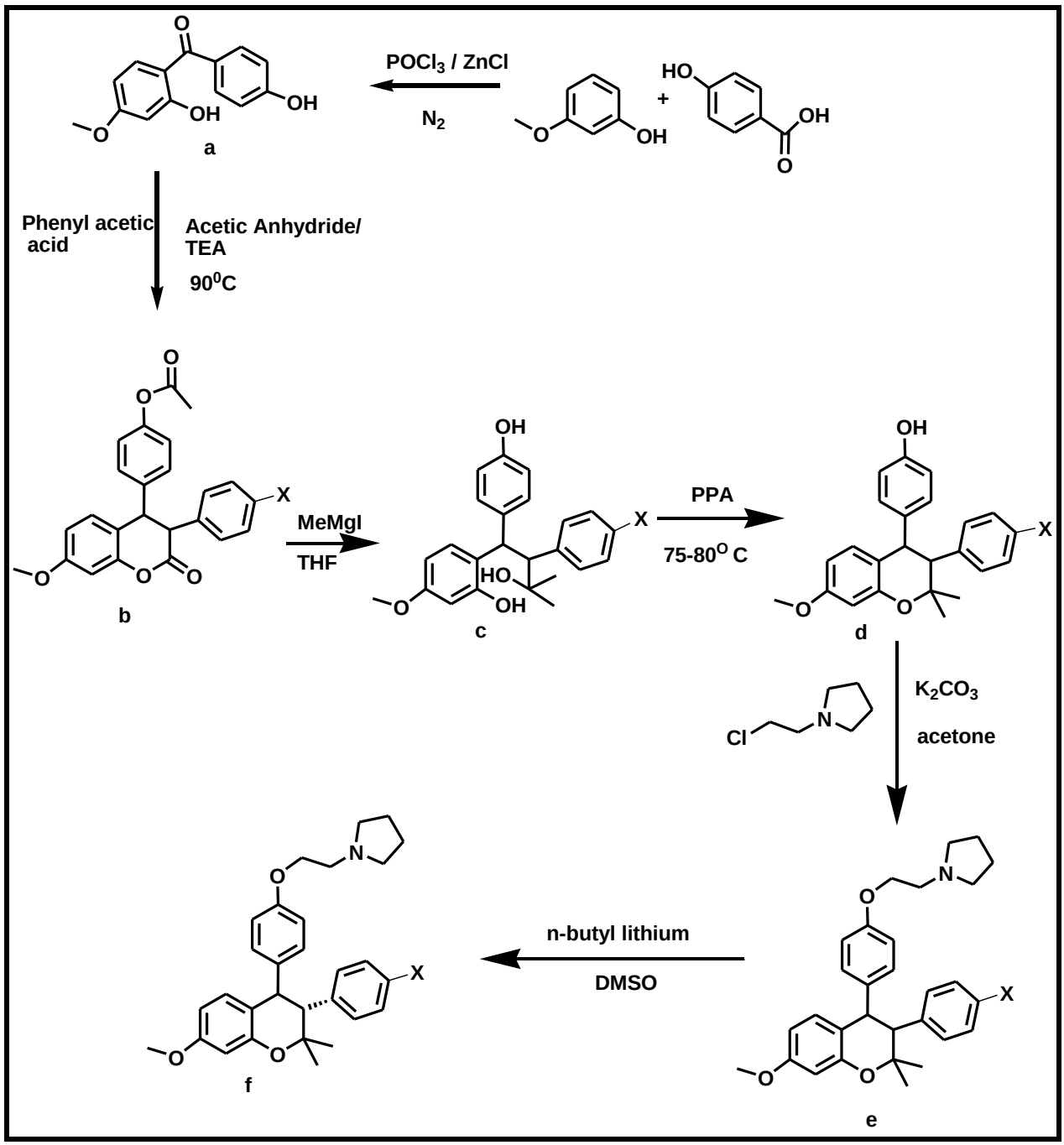

Scheme 3.1 Total synthesis of ormeloxifene (Centchroman), proposed by ***suprabhat et al.,1975***

Synthesis of Ormeloxifene analogs started again by employing the synthetic procedure proposed by ***XS Ji et al.*,1998** ORM-X as outlined in **Scheme 2** [18,19]. Commercially available 2, 4-hydroxybenzaldehyde and various derivatives of phenylacetic acid undergo nucleophilic addition-elimination in the presence of triethylamine and acetic anhydride to give compound **(1).** Hydrolysis of **(1)** with triethylamine using methanol as a solvent gave compound **(2),** followed by alkylation using methyl iodide in the presence of K_2CO_3 and acetone to produce **(3).** Grignard reaction of **(3)** with methylmagnesium bromide in THF produced **(4),** followed by intramolecular dehydration with TFA and $NaHCO_3$ to give **(5)**[20]**.** Hydroarylation of phenol with **(5)** in benzene and cyclohexane afforded a 1:1 (w/w) racemic mixture of D- and L- enantiomers **(6).** Previous studies[17] have shown that these racemic mixtures can be resolved into D- and L- enantiomers with L-isomer showing more receptor binding potency and about two-fold higher anti-implantation activity in rat than D- and DL- ormeloxifene[17]. The presence of halogens para to the aromatic ring at C-3 changed the confirmation of ormeloxifene analogs and improved the binding affinity toward EGFR binding pocket. Condensation of **(6)** with 1-(2-chloroethyl)-pyrrolidine.HCl (responsible for antagonistic activity) in the presence of NaH and DMF finally gave the titled compounds **ORM-X** in approximately 70% yield. Analogs such as **ORM-Br, ORM-F, ORM-OH,** and **ORM-CH_3** were synthesized via synthetic route outlined in **(Scheme 3.2)** which resulted in higher percentage yield. On the other hand, Grignard reaction of tert-butyl 4-(7-methoxy-2-oxo-2H-chromen-3-yl) phenyl carbamate **(3a)** produced a lower yield (3%) **(Scheme 3.3)** which resulted in dropping out of this synthetic route **(Scheme 3.3).**

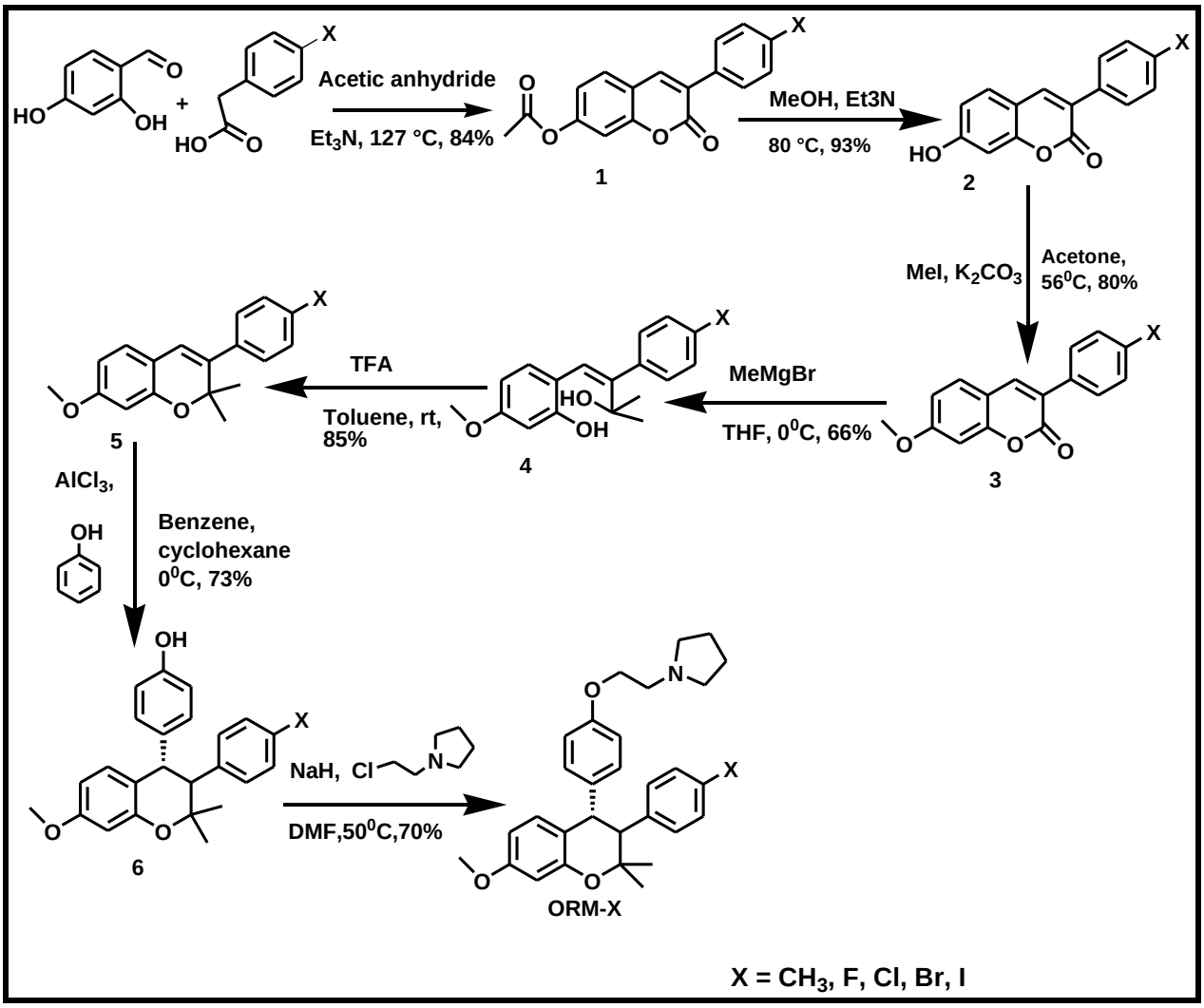

Scheme 3.2 Reagents and conditions: An improved synthesis of ormeloxifene analogs

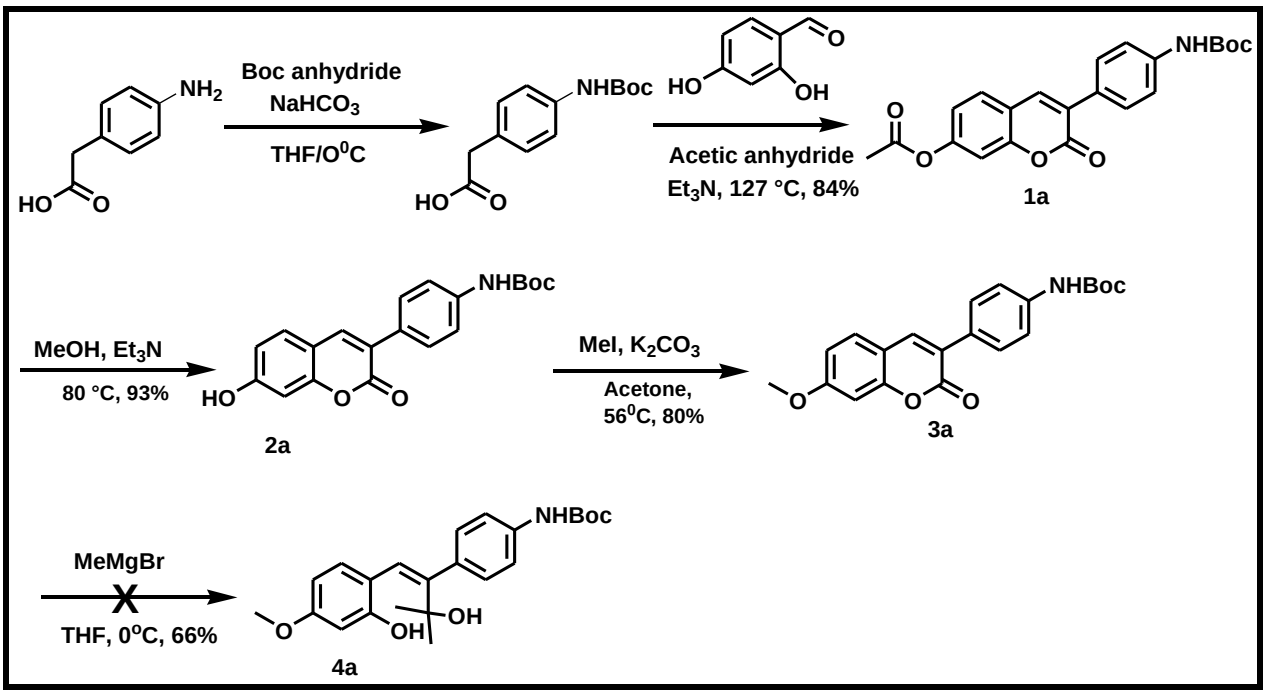

Scheme 3.3 Synthesis of compound 4a

Table 3.2 First series of ormeloxifene analogs showing various substituents at C-4'' (X) position and their percentage yields

Compound	**(X) = Halogen, CH_3**	**% Yield**
ORM-F	F	85
ORM-Cl	Cl	87
ORM-Br	Br	70
ORM-I	I	68
ORM-CH_3	CH_3	86
ORM-OH	OH	62

3.1.3 Biological evaluation of ormeloxifene analogs.

The biological assay was conducted to study the antiproliferation of ORM- analogs in comparison to standard (ormeloxifene). MTT cell viability assay was first undertaken to measure the cytotoxicity and anti-proliferation activity of synthesized analogs. Among all the analogs, **ORM-Br** showed stronger cytotoxicity on ovarian cancer cell line (A2780) with an IC_{50} value of 11.2 µM relative to ormeloxifene which showed IC_{50} of 17.5 µM **(Table 3.2).** However, compounds such as **ORM-F** and **ORM-CH_3** moderate cytotoxicity on ovarian cancer cell lines with IC_{50} value 36.3 µM and 37.9 µM respectively as compared to ormeloxifene. However, compounds such as **ORM-Cl, ORM-I,** and **ORM-OH** showed no cytotoxicity on ovarian cancer cell lines. This result demonstrated that the presence of a bromine atom at the para position of aromatic at C-3 improves the overall cytotoxicity activity of the compound on the ovarian cancer cell line. The higher cytotoxicity of Br can be explained in two ways. First, the size of the Bromine atom is a perfect fit for receptor binding pocket which resulted in the formation of hydrogen bonding with ASP:200: A (**Fig**

3.6). Second, the electronegativity of the Bromine atom on ORM-Br might be a contributing factor for its cytotoxicity.

Table 3.3 MTT Cell viability results for ORM-analogs tested against A2780 ovarian cancer Cell line

Compound	**IC_{50} (μM)**	**Compound**	**IC_{50} (μM)**
Ormeloxifene	17.5 μM	ORM-CH_3	37.9 μM
ORM-Br	11.2 μM	ORM-I	NA
ORM-F	36.3 μM	ORM-OH	NA
ORM-Cl	NA		

To further understand the anti-proliferation mechanism of ORM-Br, further biological assay was conducted using cervical cancer cell lines CaSki and SiHa. Western blot analysis was conducted to investigate the effect of ormeloxifene analogs on protein levels of β-catenin on the ovarian cancer cell line. Ovarian cancer cell (70 – 80% confluent) were treated with 10-20mmol/L of ormeloxifene analogs for 72 hours. The control was treated with 0.1% DMSO. Total lysates were prepared as reported by ***M Sikander et al., 2016.***

Western blot analysis conducted to determine the effect of ORM-Br on β-catenin degradation, Using ORM-Br and translational inhibitor (cycloheximide) as control, the result showed a significant decrease in protein levels of β-catenin in CaSki and SiHa cells

relative to cycloheximide treatment **(Fig 3.12a).** On the other hand, to study the effectiveness of ORM-Br on survival and proliferation of cervical cancer cell, clonogenic assay was conducted. The results showed that ORM-Br suppresses the clonogenic potential of CaSki and SiHa cell lines (**Fig 3.13)**. Also, ORM-Br inhibits the migration of cervical cancer cells as indicated by agarose bead assay **(Fig 3.15a).** Boyden chamber and xCELLigence assay revealed that Br-ORM inhibits the invasion of cervical cancer (CaSki and SiHa) cells **(Fig 3.17a)**. There was a decrease in expression of nuclear β-catenin in the cytoplasm (Ai and Bi) of cervical cancer cell lines when subjected to western blot analysis to detect the protein levels of β-catenin (**Fig 3.17b).** Also, cell lysates and western blot analysis conducted for EMT markers and MMPs analysis showed that ORM-Br inhibits the EMT associated markers in both CaSki and SiHa cell lines (**Fig 3.18).**

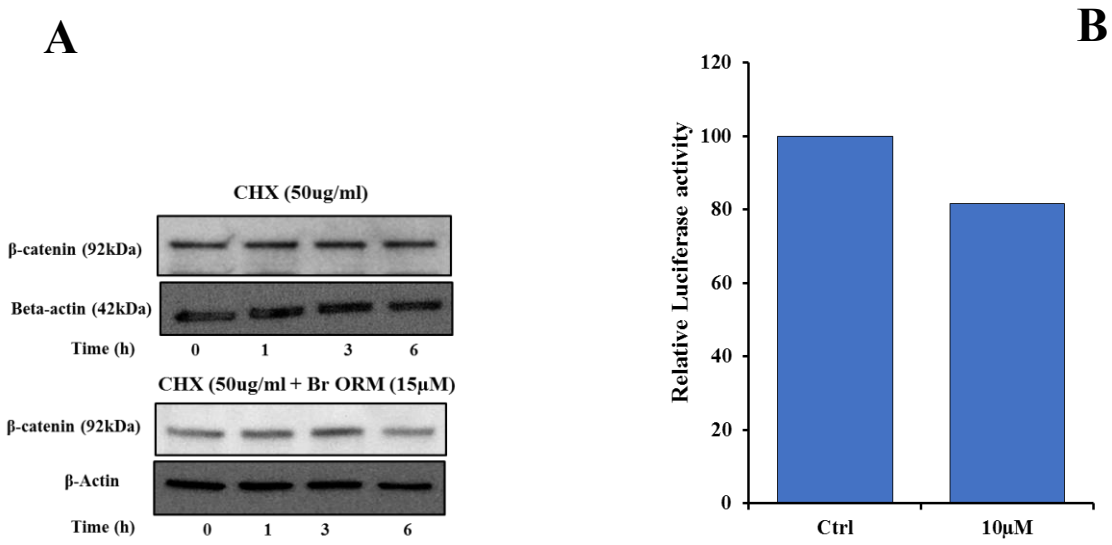

Figure 3.11. Effect of ORM-Br on β-catenin degradation analyzed by pulse-chase experiment.

SiHa cells were treated with cycloheximide (CHX: 50 mg) alone or in combination with ORM-Br (15 mmol/L) at indicated time points. Protein lysates were prepared and subjected to western blot analysis to ascertain the levels of protein of β-catenin in cycloheximide-treated (**top**) and ORM-Br and cycloheximide-treated (**bottom**).

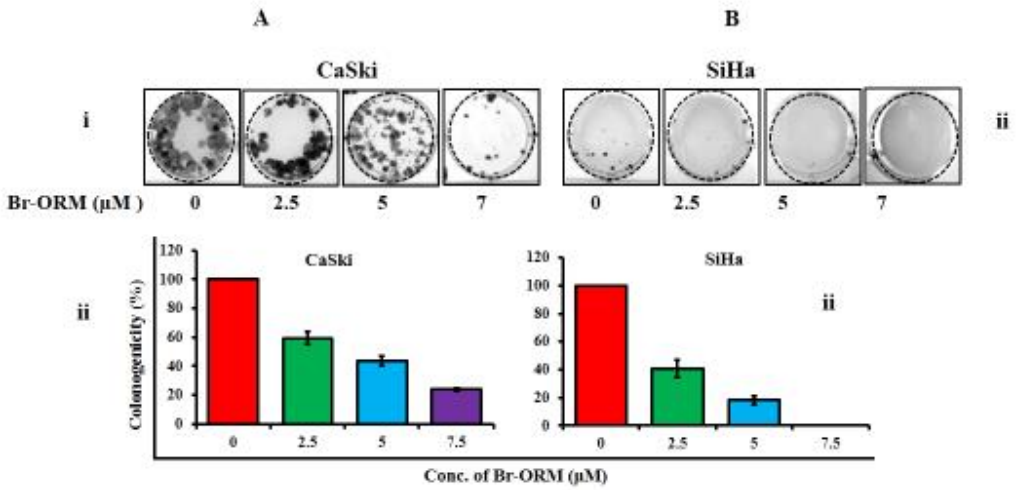

Figure 3.12. A and B represent the effect of Br-ORM on the clonogenic potential of cervical cancer cells. Representative colony images of control and Br-ORM treated CaSki (Ai) and SiHa (Bi) cells. The bar graphs represent the quantification of colony formation in CaSki (Aii) and SiHa (Bii) cells.

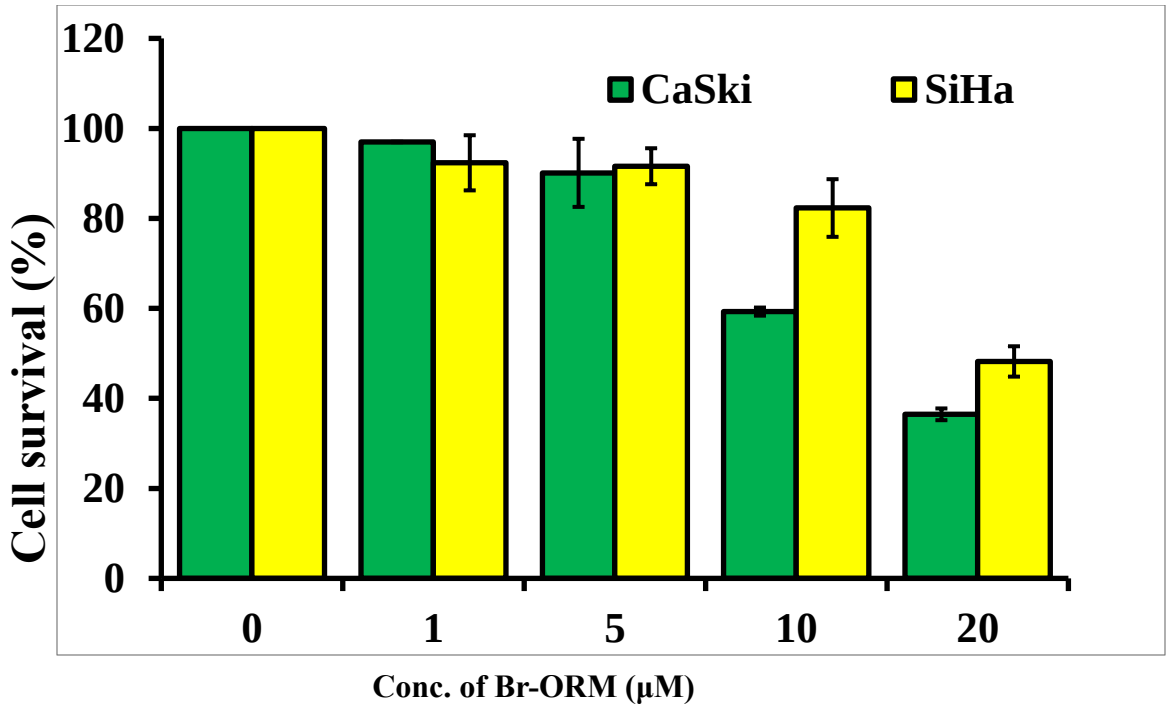

Figure 3.13 Br-ORM inhibits the growth of cervical cancer (CaSki and SiHa) cells

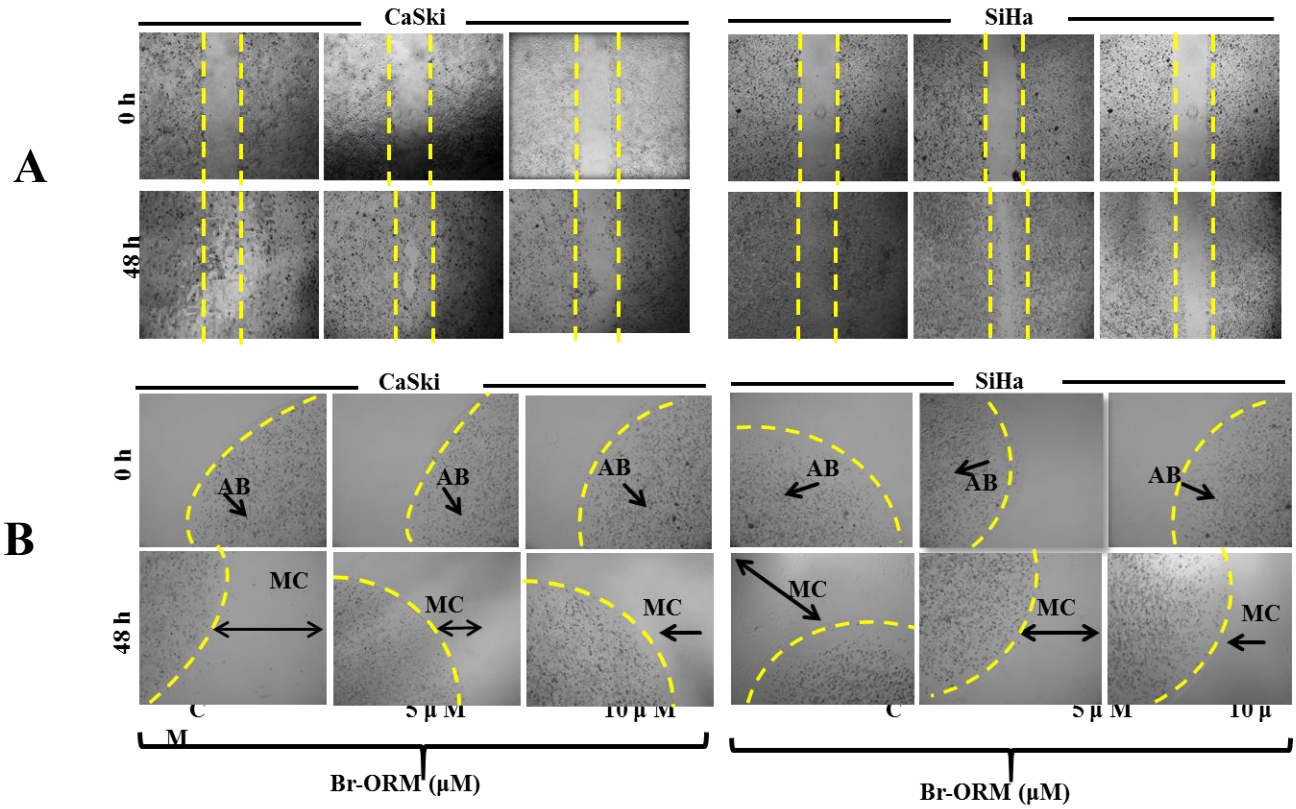

Figure 3.14 (A) Br-ORM inhibits the migration of cervical cancer (CaSki and SiHa) cell.

(B) Effect of ORM-Br on motility potential of CaSki and SiHa cells as predicted by agarose bead assay. Images represent the migratory cells (MC) in control, and ORM-Br treated groups at 0 and 48 hours. AB means agarose beads. Images magnification were at 4.

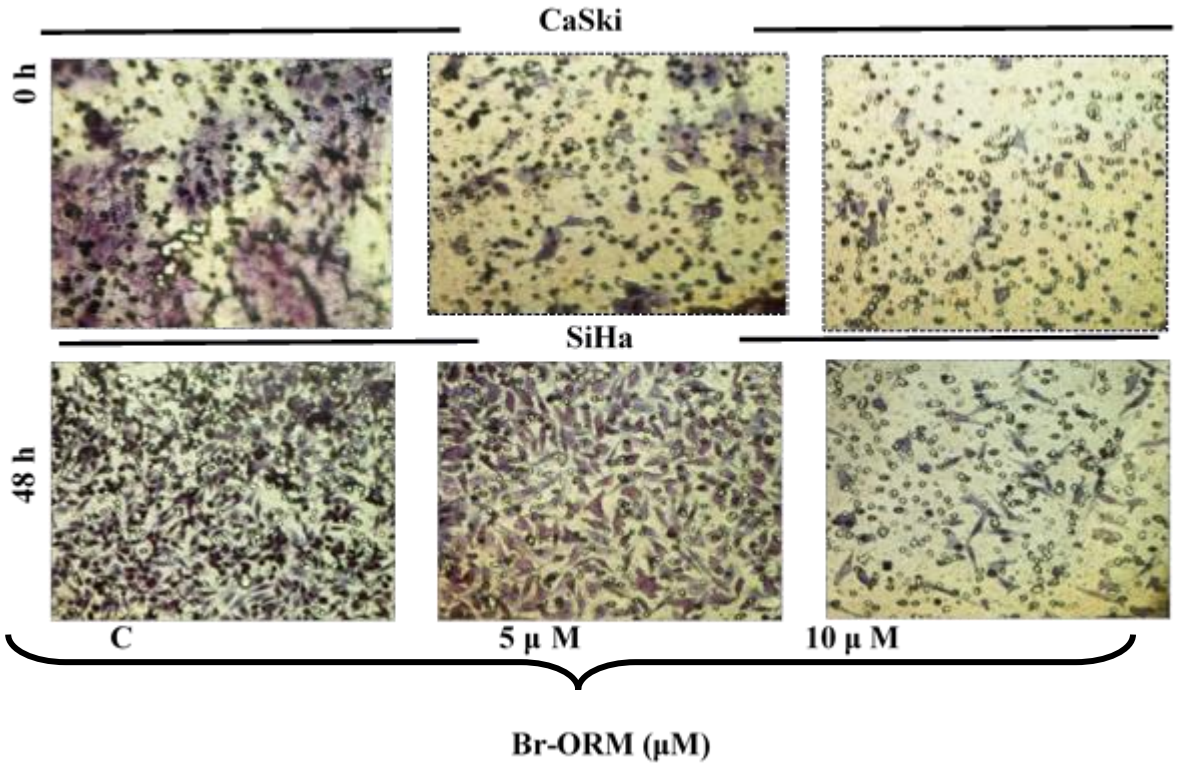

Figure 3.15 Effect of ORM-Br on the invasion of CaSki and SiHa cell lines in the Boyden chamber and xCELLigence assay. Images represent the invaded cells of control and ORM-Br-treated CaSki and SiHa cells as determined by Boyden Chamber kit. Image magnification was set at 20.

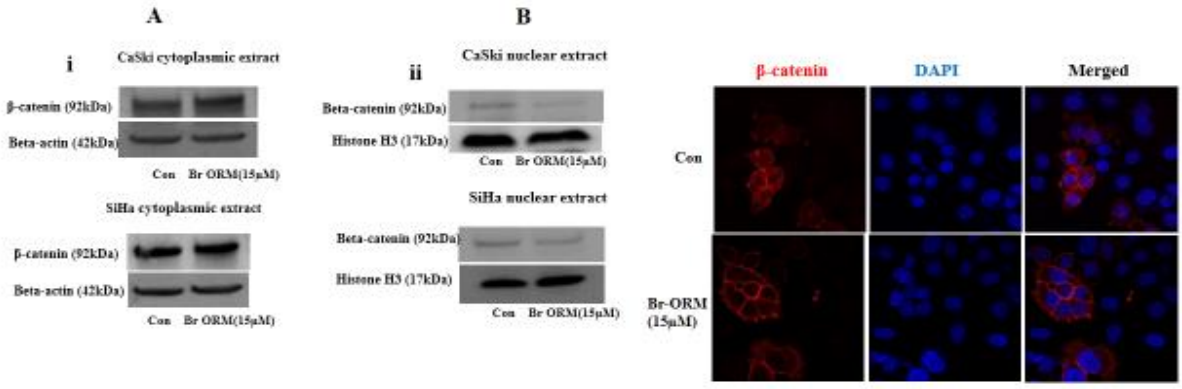

Figure 3.16 Effect of **ORM-Br** on β-catenin distribution in the cytoplasm and nucleus of CaSki and SiHa cell lines. Cells were subjected to treatment with a 15μM concentration of ORM-Br for 24 hours, nuclear extracts were prepared, and western blot analysis was used to detect the protein levels of β-catenin. The results revealed a decrease in the expression of nuclear β-catenin and increased expression of β-catenin in the cytoplasm (Ai and Bi) of CaSki and SiHa cells. Western blots were reprobed with β-actin and Histone H3 antibodies as an internal control. Effect of ORM-Br on β-catenin localization in CaSki cells as illustrated by confocal microscopy (c).

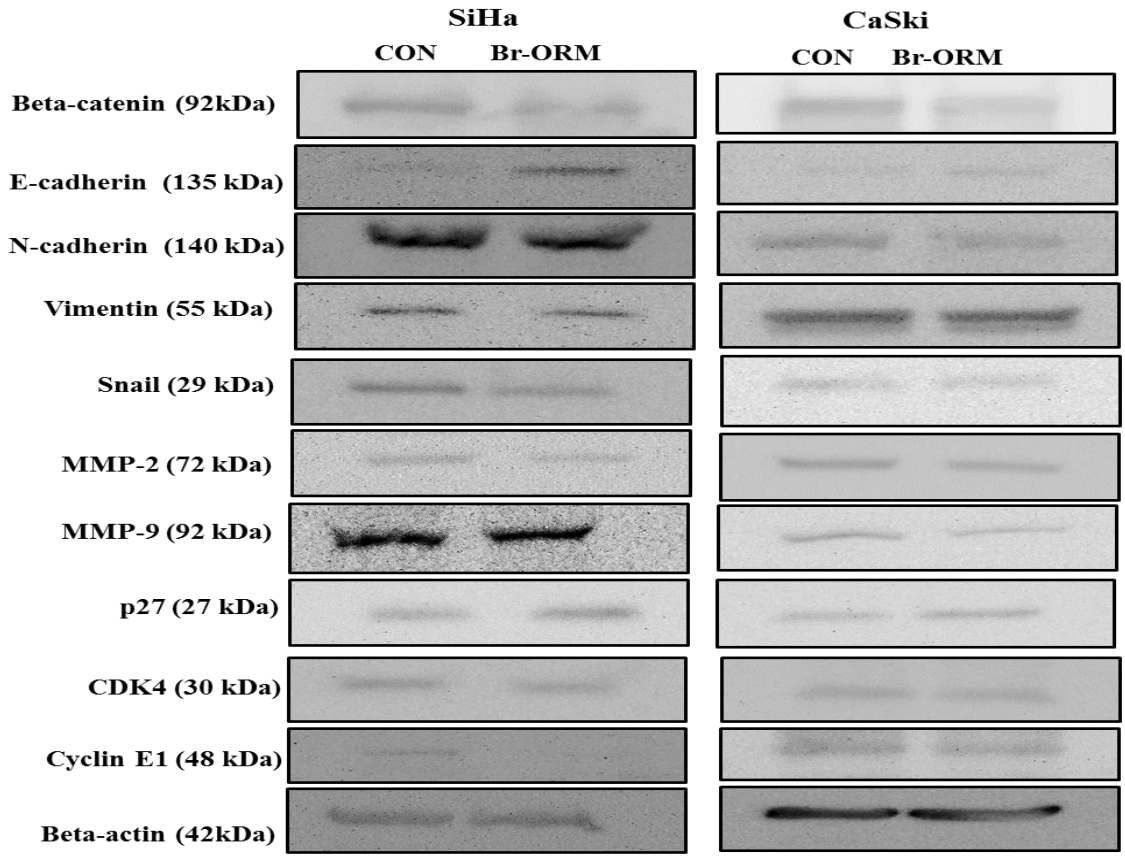

Figure 3.17. Effect of ORM-Br on EMT markers. About 70% of confluent SiHa and CaSki were treated with ORM-Br (10-20 mmol/L) for 24 hours. Cell lysates were prepared, and western blot analysis was conducted for EMT markers and MMPs analysis. Effect of ORM-Br on protein levels of cell-cycle regulatory proteins (cyclin E1 and p27) in both CaSki and SiHa cell lines.

3.2 Conclusion

In summary, analogs of ormeloxifene ORM-F, ORM-Br, ORM-Cl, ORM-I, ORM-OH, and ORM-CH_3 were designed using structural based drug design (SBDD). Docking studies revealed that the installation of halogens on the ormeloxifene scaffold improved both binding affinity in GSK3B, EGFR, and CDK2 binding pockets and, this prediction was also confirmed by biological evaluation. The IC_{50} of ORM-Br (11.2 µM) was superior to all other analogs including ormeloxifene in MTT analysis. Further biological studies

confirmed that ORM-Br inhibits the localization and invasion of β-catenin in cervical cancer cell lines. We, therefore, conclude that it is essential to conduct further studies on the potency of ORM-Br on various cancer cell lines.

3.3 Experimental section

3.3.1 General

Based on the current literature and related organic synthetic approach, various synthetic routes were optimized for the synthesis of halogenated ormeloxifene analogs. Standard spectroscopic, analytical and chromatographic procedures were employed to achieve better results. The melting points were determined using Meltemp apparatus was used and uncorrected. Analytical TLC was performed using silica gel with a fluorescent indicator coated on a 1x3 inch flexible plate with 0.2 mm thickness. Column chromatography separations were carried out on standard silica gel 60-120 mesh. IR spectra were performed with a Perkin Elmer Spectrum one FT-IR Spectrometer and all solid samples recorded using a salt plate. The molecular weights of the compounds were determined on a high-performance Varian 500-MS. 1H NMR and 13C NMR were conducted using Bruker Avance – 600, 400 MHz Spectrometer. The samples were dissolved in $CDCL_3$ containing 0.03% tetramethylsilane (TMS) as internal standard and chemical shift recorded in δ (ppm) relative to tetramethylsilane signal. Coupling constant (J) was measured in Hz and the multiplicities of the signals recorded as follows: singlet(s), doublet (d) doublet of doublet (dd), triplet (t), and multiple (m). The chemicals obtained from Aldrich and Fisher Scientific were used without purification.

3.3.2 Synthesis of 3-(4-bromophenyl)-2-oxo-2H-chromen-7-yl acetate

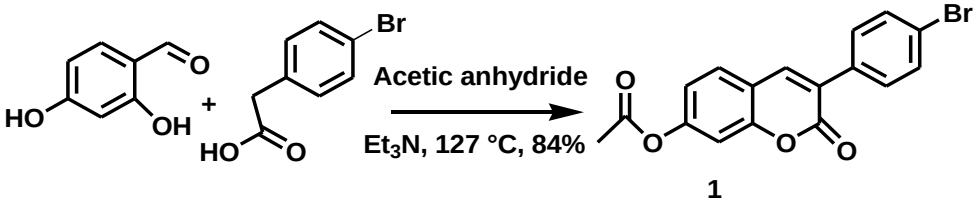

1

To a round bottom flask with a stir bar under nitrogen was added 2, 4-dihydroxybenzaldehyde (5g, 36.20 mmol) followed by 4-bromophenylacetic acid (5.1g, 23.72 mmol) and acetic anhydride (11.30ml). Triethylamine (6.6 ml, 65.22 mmol) was slowly added, and the mixture was refluxed at 127°C for 7 hours. The reaction was monitored by TLC till completion and quenched with distilled water (89 ml) to give a gray solid. The solid was crushed and recrystallized using methanol (100 ml) to afford (7.2g) 84% of the desired product as white solid.

^{1}H NMR (400Mz, $CDCl_3$, δ ppm) 2.25 (s, 3H), 6.99 (s, 1H), 7.03 (d, J = 2.27, 1H), 7.07 (d, J = 2.27), 7.19 (s, 1H), 7.46 (d, J = 8.56), 7.72 (s, 1H). ^{13}C NMR (400Mz, $CDCl_3$ δ ppm) 168, 160, 154.1, 153.3, 139.5, 133.4, 131.8, 130.3, 128.9, 126.5, 123.3, 118.7, 117.3, 109.9, 20.9.

3.3.3 Synthesis of 3-(4-Bromo-phenyl)-7-hydroxy-chromen-2-one

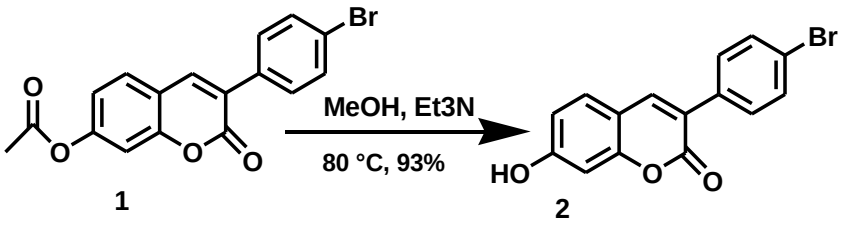

To a stirred solution of methanol (39.3 ml) and triethylamine (3.93 ml, 38.83 mmol) in a round bottom flask under nitrogen atmosphere was added 3-(4-bromophenyl)-2-oxo-2H-chromen-7-yl acetate (4.0g, 11.17 mmol). The reaction mixture was refluxed at 80ºC for 24 hours. After the reaction was completed as shown by TLC, it was quenched by adding 1M HCl until the pH became acidic. The mixture was extracted using ethyl acetate, water (25 mil) and recrystallized using methanol (70 ml) to give (3.28) 93% expected compound.

^{1}H NMR (400Mz, $CDCl_3$) 5.15 (s, 1H) 6.78 (s, 1H), 6.79 (d, J = 2.52 Hz ,1H), 7.19 (s, 1H), 7.36 (d, J = 8.31 Hz, 1H), 7.51 (d, J = 4.03 Hz, 1H), 7.70 (s, 1H).) ^{13}C NMR (400Mz, $CDCl_3$ δ ppm) 161.3, 159.8, 155.4, 139.6, 131.7, 129.4, 128.4, 127. 5, 123.5, 117. 1, 107.4, 102.9

3.3.4 Synthesis of 3-(4-bromophenyl)-7-methoxy-2H-chromen-2-one

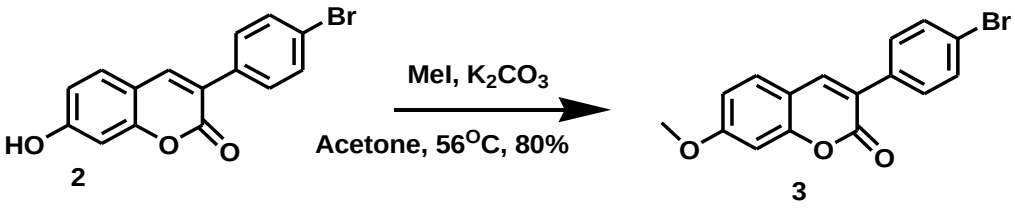

To a stirred solution of acetone (16.5 ml) was added 3-(4-bromophenyl)-7-hydroxy-2H-chromen-2-one (1.18g, 4.933 mmol) under nitrogen atmosphere. K_2CO_3 (1.362g, 9.89 mmol) was added while stirring followed by careful addition of MeI (0.614 ml, 9.86 mmol) and the mixture was refluxed overnight at 56ºC. Excess acetone was evaporated under reduced pressure after completion of the reaction, and the mixture dissolved in CH_2Cl_2, washed with water (15 ml x 3), dried over $MgSO_4$ and evaporated under reduced pressure to give a yellow solid (1.164g) of 90% yield. ^{1}H NMR (400Mz, $CDCl_3$, δ ppm) 3.83 (s, 3H), 6.78 (s, 1H), 6.79 (d, J = 2.52 Hz, 1H), 7.19 (s, 1H), 7.36 (d, J = 8.31 Hz, 1H), 7.51 (d, J = 4.03 Hz, 1H), 7.70 (s, 1H).) ^{13}C NMR (400Mz, $CDCl_3$ δ ppm) 161.3, 159.8, 155.4, 139.6, 131.7, 129.4, 128.4, 127. 5, 123.5, 117. 1, 107.4, 102.9, 56.8

3.3.5 Synthesis of 2-((Z)-2-(4-bromophenyl)-3-hydroxy-3-methylbut-1-enyl)-5-methoxyphenol

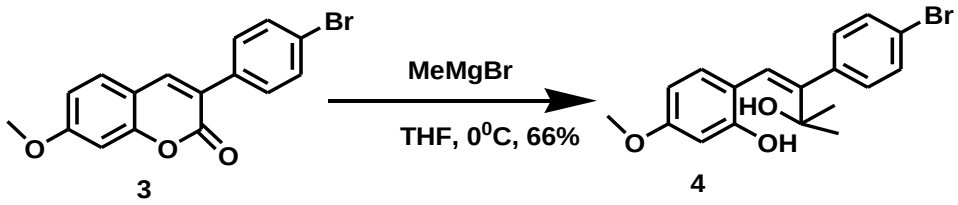

To a stirred solution of 3-(4-bromophenyl)-7-methoxy-2H-chromen-2-one (0.51g, 1.5 mmol) in THF (10 ml) under nitrogen atmosphere at -20°C was added MeMgBr (in 3M diethyl ether, 1 ml, 0.60 mmol) and stirred for 45 min. The reaction mixture was warmed to -10°C and monitored by TLC for 7 hours. After completion, the reaction mixture was quenched with saturated aqueous NH_4Cl solution (40 ml) and extracted with ethyl acetate (60 ml). The organic layer was separated, and the aqueous layer was again extracted with ethyl acetate (25 ml). The combined organic layer was dried over anhydrous $MgSO_4$ concentrated under reduced pressure and purified by column chromatography (20% ethyl acetate: 80% hexane) to give a semi-solid (0.37g) with 66% yield.

^{1}H NMR (400Mz, $CDCl_3$) 1.45 (s, 3H), 1.96 (s, 1H), 3.68 (s, 3H), 5.01 (s, 1H), 6.23 (s, 1H), 6.42 (s, 1H), 6.46 (d, J = 8.45, 1H), 6.89 (d, J = 8.31 Hz, 1H), 7.08 (d, J = 8.03 Hz, 1H), 7.38 (d, J = 8.06 Hz, 1H). ^{13}C NMR (400Mz, $CDCl_3$ δ ppm) 161, 156.4, 138.8, 131.6, 129.9, 127.4, 122.5, 115. 8, 107.4, 102.9, 73.6, 55.2, 26.8

3.3.6 3-(4-bromophenyl)-7-methoxy-2,2-dimethyl-2H-chromene

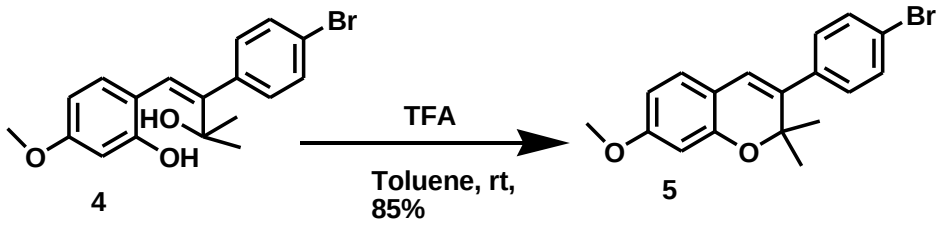

To a solution of 2-((Z)-2-(4-bromophenyl)-3-hydroxy-3-methylbut-1-enyl)-5-methoxyphenol (0.1199g, 0.11 millimole) , toluene (5.25 ml) were added TFA (0.021 ml, 0.26 mmol) and refluxed for 30 minutes mixture was diluted with ethyl acetate (13.20 ml) followed by 5% aqueous $NaHCO_3$ (18.4 ml) and stirred continuously until the reaction was completed (TLC). The organic layer was separated, and the aqueous layer was extracted with ethyl acetate (15 ml), and the combined organic layer was dried with anhydrous Na_2SO_4 and evaporated under reduced pressure. The mixture was purified by column chromatography (70% hexane: 30% ethyl acetate) to give a semi-solid (0.971g) with 85% yield.

^{1}H NMR (400Mz, $CDCl_3$ δ ppm) 1.47 (s, 3H), 3.66 (s, 3H), 6.23 (s, 1H), 6.42 (s, 1H), 6.46 (d, J = 8.45, 1H), 6.89 (d, J = 8.31 Hz, 1H), 7.08 (d, J = 8.03 Hz, 1H), 7.38 (d, J = 8.06 Hz,

1H). ^{13}C NMR (400Mz, $CDCl_3$ δ ppm) 161, 154.3, 138.8, 131.6, 129.9, 127.4, 122.5, 115. 8, 107.4, 102.9, 78.7, 55.2, 22.3.

3.3.7 Synthesis of 4-(3-(4-bromophenyl)-1, 2, 3, 4-tetrahydro-7-methoxy-2,2-dimethylnaphthalen-4-yl)phenol

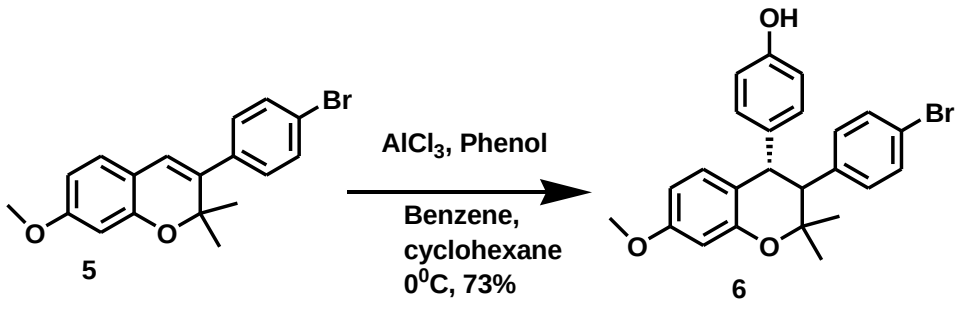

To a stirred solution of 3-(4-bromophenyl)-7-methoxy-2, 2-dimethyl-2H-chromene (0.4g, 1.12 mmol) and phenol (0.24 g, 2.25 mmol) in benzene-cyclohexane mixture (1:1 ratio, 15 ml) at 0°C was added anhydrous aluminum chloride (0.24 g, 1.8 mmol) in portions. A solution of phenol (0.117 g, 1.25 mmol) in benzene- cyclohexane mixture (1:1 Ratio, 15 ml) was added after 30 min, and the mixture further stirred for 8 hrs. The reaction mixture was quenched by adding a mixture of ice and cone. Hydrochloric acid (0.4 ml) and the organic layer was separated. The aqueous layer was re-extracted three times with dichloromethane (5 ml). The combined extract was washed with $NaHCO_3$ (10 %, 5 ml), dried over anhydrous Na_2SO_4, filtered and concentrated under reduced pressure. The semi-

solid obtained was purified by column chromatography (70% hexane: 30% ethyl acetate) to obtain the title compound (0.38g) with 73% yield.

^{1}H NMR (400Mz, $CDCl_3$, δ ppm) 1.17 (s, 3H) 1.29 (s, 3H), 3.84 (s, 3H), 4.27 (d, J = 12.34 Hz, 1H), 4.81 (s, 1H), 6.24 (dd, J = 8.06, 2.52 Hz, 1H), 6.31 (d, J = 2.5 Hz, 1H), 6.47 (d, J = 8.3 Hz, 2H), 6.59 (dd, J = 7.30, 1.05 Hz, 1H), 6.78 (d, J = 8.56 Hz, 2H), 7.24 (d, J = 8.31 Hz, 2H). ^{13}C NMR (400Mz, $CDCl_3$ δ ppm) 158.9, 155.2, 153.7, 138.3, 135.6, 131.1, 131.1, 129.7, 128.3, 120.9, 120.2, 115.6, 102.1, 78.4, 60.7, 55.5, 32.4, 23.4.

3.3.8 1-(2-(4-(3-(4-bromophenyl)-1,2,3,4-tetrahydro-7-methoxy-2,2-dimethylnaphthalen-4-yl)phenoxy)ethyl)pyrrolidine

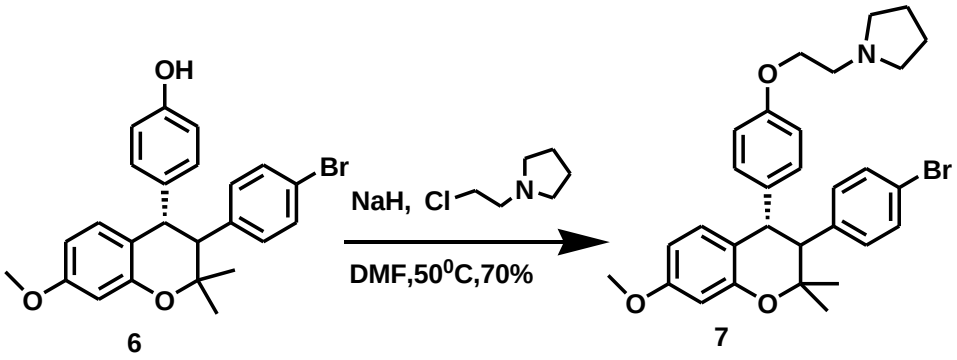

To a stirred solution of 4-(3-(4-bromophenyl)-1, 2, 3, 4-tetrahydro-7-methoxy-2,2-dimethylnaphthalen-4-yl)phenol (1.84 g, 3.44 mmol) and DMF (49 ml) was added NaH (0.74 g, 30.72 mmol) under nitrogen atmosphere. The reaction mixture was vented with a needle for 20 min to allow the evolution of H_2 gas and then quenched with methanol (2 ml). After the evolution of all H_2 gas, 1-(2-chloroethyl) pyrrolidine hydrochloride was

added sequentially, and the reaction mixture was heated at 50°C overnight. After completion as indicated by TLC, the reaction mixture was quenched at 0°C by dropwise addition of $NaHCO_3$ over 20 min. It was then extracted with ethyl acetate (3x 15 ml) and the organic layer washed with water (3 x 25 ml). The organic layer was washed with brine, dried over $MgSO_4$, evaporated and purified by column chromatography (30% ethyl acetate: 70% hexane) to afford a semi-solid (1.751g) with 70% yield. **HR-FT-MS calcd for $C_{30}H_{34}BrNO_3$ 536.49 found 536.41**

^{1}H NMR (400 MHz, Chloroform-*d*) δ 0.87 (q, *J* = 8.4, 7.2 Hz, 6H), 0.95 (td, *J* = 8.4, 7.3, 5.0 Hz, 2H), 1.08 (s, 1H), 1.15 (s, 2H), 1.22 (d, *J* = 10.2 Hz, 4H), 1.29 (d, *J* = 22.1 Hz, 15H), 1.65 – 1.71 (m, 1H), 1.71 – 1.86 (m, 11H), 2.55 – 2.70 (m, 10H), 2.77 – 2.95 (m, 8H), 3.12 (dd, *J* = 12.2, 3.1 Hz, 1H), 3.63 – 3.78 (m, 3H), 3.96 (t, *J* = 5.9 Hz, 1H), 4.08 (t, *J* = 5.9 Hz, 4H), 4.20 (dd, *J* = 16.1, 12.1 Hz, 1H), 6.34 (d, *J* = 8.5, 2.6 Hz, 1H), 6.38 – 6.47 (m, 1H), 6.49 – 6.68 (m, 2H), 6.70 – 7.05 (m, 12H), 7.06 – 7.17 (m, 2H), 7.17 – 7.23 (m, 3H), 7.23 – 7.35 (m, 3H). ^{13}C NMR (400Mz, $CDCl_3$ δ ppm) 159.3, 156.9, 153.9, 138.5, 135.6, 130.9, 129.9, 129.4, 120.5, 118.1, 114.7, 107.8, 101.3, 77.9, 71.2, 66.5, 56.9, 54.6, 44.4, 28.7, 23.4, 20.2.

3.3.9 Synthesis of 3-(4-fluoro-phenyl)-2-oxo-2H-chromen-7-yl acetate

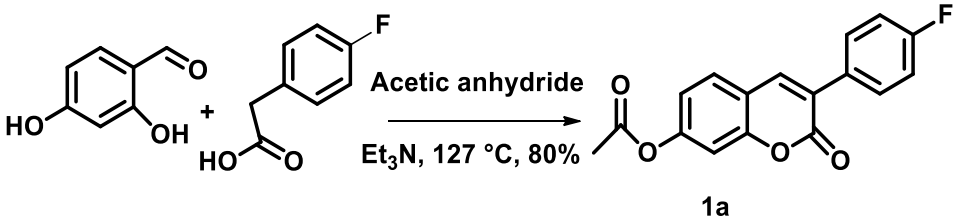

1a

To a round bottom flask with a stir bar under nitrogen was added 2, 4-dihydroxybenzaldehyde (3g, 19.5 mmol) followed by 4-fluorophenyacetic acid (3.0g, 19.5 mmol) and acetic anhydride 7.0 ml). Triethylamine (3.5 ml, 34.60 mmol) was slowly added, and the mixture was refluxed at 127°C for 7 hours. The reaction was monitored by TLC till completion and quenched with distilled water (50 ml) to give a yellow solid. The solid was crushed and recrystallized using methanol (80 ml) to afford (4.12g) 80% of the desired product as a cream solid.

^{1}H NMR (400Mz, $CDCl_3$, δ ppm) 2.05 (s, 3H), 6.90 (s, 1H), 6.94 (d, J = 2.27, 1H), 7.07 (d, J = 2.27), 7.19 (s, 1H), 7.62 (d, J = 8.56), 7.97 (s, 1H). ^{13}C NMR (400Mz, $CDCl_3$ δ ppm) 168.1, 162.2, 161.3, 153.4, 151.6, 135.5, 131.4, 130.3, 128.9, 127.2, 123.9, 118.7, 115.0, 114.1, 17.6.

3.3.10 Synthesis of 3-(4-Fluoro-phenyl)-7-hydroxy-chromen-2-one

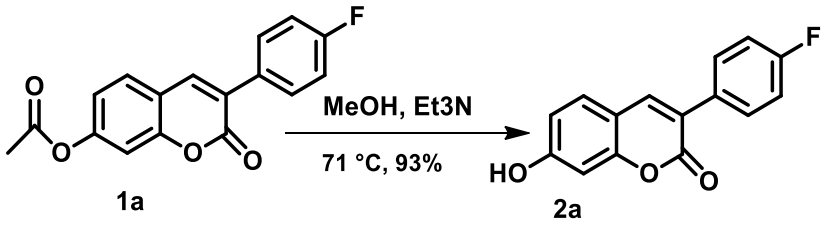

To a stirred solution of methanol (49.3 ml) and triethylamine (4.8 ml, 47.40 mmol) in a round bottom flask under nitrogen atmosphere was added 3-(4-fluoro-phenyl)-2-oxo-2H-chromen-7-yl acetate (4.9g, 16.43 mmol). The reaction mixture was refluxed at 80ºC for 24 hours. After the reaction was completed as shown by TLC, it was quenched by adding 1M HCl until the pH became acidic. The mixture was extracted using ethyl acetate (20 x 3 ml) and water (35 mil) and recrystallized with methanol (70 ml) to give (2.98) 71% expected compound.

^{1}H NMR (400Mz, $CDCl_3$) 5.15 (s, 1H) 6.65 (s, 1H), 6.68 (d, J = 2.52 Hz, 1H), 7.19 (s, 1H), 7.38 (d, J = 8.31 Hz, 1H), 7.47 (d, J = 4.03 Hz, 1H), 7.98 (s, 1H).) ^{13}C NMR (400Mz, $CDCl_3$ δ ppm) 161.8, 161.5, 159.7, 155.6, 134.3, 130.7, 129.4, 128.4, 127. 3, 120.5, 115. 2, 102.3, 107.9.

3.3.11 Synthesis of 3-(4-Fluoro-phenyl)-7-methoxy-chromen-2-one

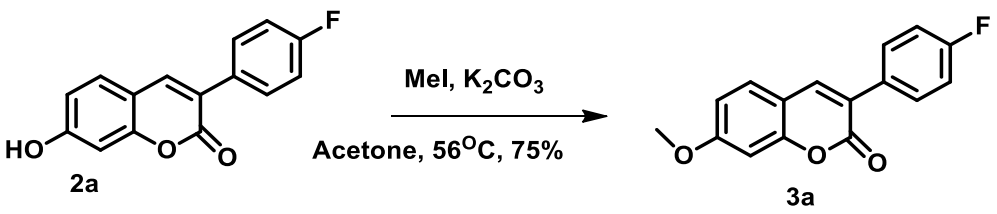

To a stirred solution of acetone (16.5 ml) was added 3-(4-fluorophenyl)-7-hydroxy-2H-chromen-2-one (2.50g, 9.25 mmol) under nitrogen atmosphere. K_2CO_3 (2.9g, 20.9 mmol) was added while stirring followed by careful addition of MeI (1.30 ml, 9.16 mmol) and the mixture was refluxed overnight at 56ºC. Excess acetone was evaporated under vacuum after completion of the reaction, and the mixture dissolved in CH_2Cl_2, washed with water (15 ml x 3), dried over $MgSO_4$ and evaporated under reduced pressure to give a yellow solid (1.80 g) of 75% yield.

^{1}H NMR (400Mz, $CDCl_3$, δ ppm) 3.83 (s, 3H), 6.72 (s, 1H), 6.93 (d, J = 2.52 Hz, 1H), 6.98 (s, 1H), 7.30 (d, J = 8.31 Hz, 1H), 7.51 (d, J = 4.03 Hz, 1H), 7.94 (s, 1H). ^{13}C NMR (400Mz, $CDCl_3$ δ ppm)161.9 161.3, 159.7, 151.4, 139.6, 133.8, 129.4, 128.4, 127. 9, 120.5, 115. 4, 110.3, 106.5, 55.2

3.3.12 Synthesis of 2-((Z)-2-(4-flourophenyl)-3-hydroxy-3-methylbut-1-enyl)-5-methoxyphenol

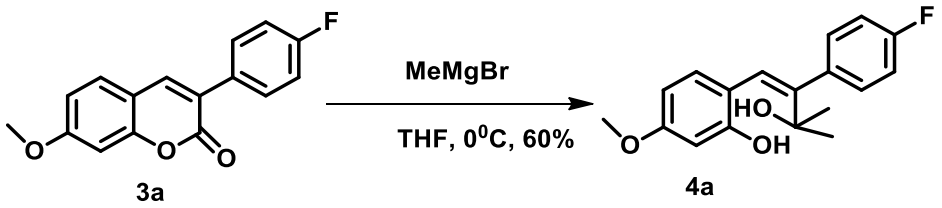

To a stirred solution of 3-(4-fluorophenyl)-7-methoxy-2H-chromen-2-one (1g, 3.30 mmol) in THF (20 ml) under nitrogen atmosphere at -20°C was added MeMgBr (in 3M diethyl ether, 2.38 ml, 19.9 mmol) and stirred for 45 min. The reaction mixture was warmed to -10°C and monitored by TLC for 7 hours. After completion, the reaction mixture was quenched with saturated aqueous NH_4Cl solution (50 ml) and extracted with ethyl acetate (65 ml). The organic layer was separated, and the aqueous layer was again extracted with ethyl acetate (25 ml). The combined organic layer was dried over anhydrous $MgSO_4$ concentrated under reduced pressure and purified by column chromatography (20% ethyl acetate: 80% hexane) to give a semi-solid (0.60g) with 60% yield.

^{1}H NMR (400Mz, $CDCl_3$) 1.35 (s, 3H), 1.96 (s, 1H), 3.64 (s, 3H), 5.01 (s, 1H), 6.23 (s, 1H), 6.26 (d, J = 8.45, 1H), 7.13 (d, J = 8.31 Hz, 1H), 7.24 (d, J = 8.03 Hz, 1H), 7.39 (d, J = 8.06 Hz, 1H). ^{13}C NMR (400Mz, $CDCl_3$ δ ppm) 161.9, 161.8, 156.4, 143.8, 130.6, 128.6, 127.8, 127.3, 115. 8, 104.4, 102.9, 73.6, 5582, 26.9.

3.3.13 Synthesis of 3-(4-fluorophenyl)-7-methoxy-2,2-dimethyl-2H-chromene

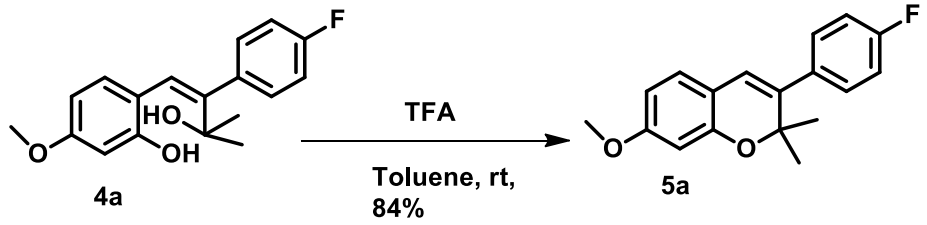

To a solution of 2-((Z)-2-(4-fluorophenyl)-3-hydroxy-3-methylbut-1-enyl)-5-methoxyphenol (1.25g, 4.13 mmol) in toluene (15.8 ml) was added TFA (0.22 ml, 1.92 mmol) stirred for 30 min. The reaction mixture was diluted with ethyl acetate (20.0 ml) followed by 5% aqueous $NaHCO_3$ (23.1 ml) and stirred vigorously until the reaction was completed (TLC). The organic layer was separated, and the aqueous layer was extracted with ethyl acetate (32 ml), and the combined organic layer was dried with anhydrous Na_2SO_4 and evaporated under reduced pressure. The mixture was purified by column chromatography (70% hexane: 30% ethyl acetate) to give a semi-solid (0.98g) with 84% yield.

^{1}H NMR (400Mz, $CDCl_3$ δ ppm) 1.57 (s, 3H), 3.56 (s, 3H), 6.23 (s, 1H), 6.38 (s, 1H), 6.91 (d, J = 8.45, 1H), 6.95 (d, J = 8.31 Hz, 1H), 7.22 (d, J = 8.03 Hz, 1H), 7.39 (d, J = 8.06 Hz, 1H). ^{13}C NMR (400Mz, $CDCl_3$ δ ppm) 161.5, 161.2 157.2, 131.8, 129.9, 227.9, 127.4, 121.5, 115. 4, 107.4, 102.9, 79.7, 56.2, 23.3.

3.3.14 Synthesis of 4-(3-(4-fluorophenyl)-1, 2, 3, 4-tetrahydro-7-methoxy-2,2-dimethylnaphthalen-4-yl) phenol

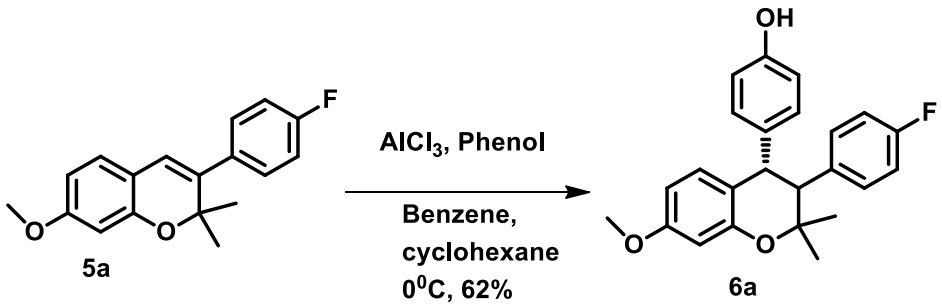

To a stirred solution of 3-(4-fluorophenyl)-7-methoxy-2, 2-dimethyl-2H-chromene (0.4g, 1.05 mmol) and phenol (0.24 g, 2.25 mmol) in benzene-cyclohexane mixture (1:1 ratio, 15 ml) at 0°C was added anhydrous aluminum chloride (0.24 g, 1.8 mmol) in portions. A solution of phenol (0.117 g, 1.25 mmol) in benzene- cyclohexane mixture (1:1 Ratio, 15 ml) was added after 30 min, and the mixture further stirred for 8 hrs. The reaction mixture was quenched by adding a mixture of ice and cone. Hydrochloric acid (0.4 ml) and the organic layer was separated. The aqueous layer was re-extracted three times with dichloromethane (5 ml). The combined extract was washed with $NaHCO_3$ (10 %, 5 ml), dried over anhydrous Na_2SO_4, filtered and concentrated under reduced pressure. The semi-solid obtained was purified by column chromatography (70% hexane: 30% ethyl acetate) to obtain the title compound (0.32g) with 62% yield.

^{1}H NMR (400Mz, $CDCl_3$, δ ppm) 1.26 (s, 3H) 1.29 (s, 3H), 3.84 (s, 3H), 4.29 (d, J = 12.34 Hz, 1H), 4.71 (s, 1H), 6.27 (dd, J = 8.06, 2.52 Hz, 1H), 6.67 (d, J = 2.5 Hz, 1H), 6.87 (d, J = 8.3 Hz, 2H), 6.90 (dd, J = 7.30, 1.05 Hz, 1H), 6.98 (d, J = 8.56 Hz, 2H), 7.10 (d, J = 8.31 Hz, 2H). ^{13}C NMR (400Mz, $CDCl_3$ δ ppm) 159.9, 159.3, 158.8, 155.2, 153.7, 138.3, 136.6, 135.1, 130.1, 129.7, 128.3, 121.0, 116.2 114.6, 102.1, 78.4, 60.7, 55.5, 33.1, 22.9

3.3.15 1-(2-(4-(3-(4-fluorophenyl)-1,2,3,4-tetrahydro-7-methoxy-2,2-dimethylnaphthalen-4-yl)phenoxy)ethyl)pyrrolidine

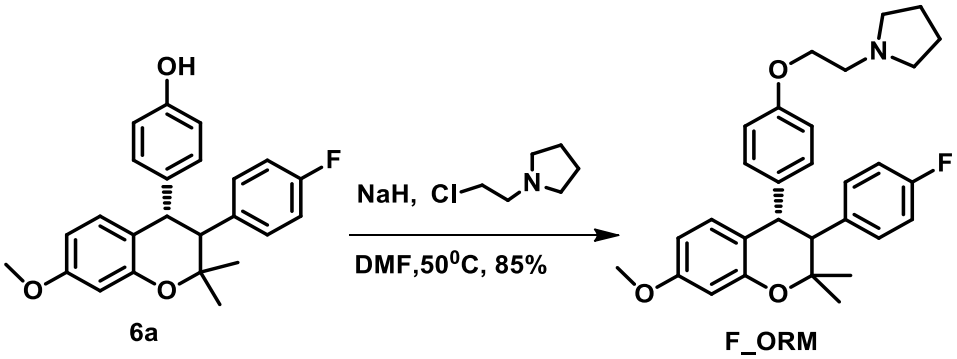

To a stirred solution of 4-(3-(4-fluorophenyl)-1, 2, 3, 4-tetrahydro-7-methoxy-2,2-dimethylnaphthalen-4-yl)phenol (0.1 g, 0.21 mmol) and DMF (2.7 ml) was added NaH (0.04 g, 16.67 mmol) under nitrogen atmosphere. The reaction mixture was vented with a needle for 20 min to allow the evolution of H_2 gas and then quenched with methanol (0.3 ml). After the evolution of all H_2 gas, 1-(2-chloroethyl) pyrrolidine hydrochloride (0.102

g) was added sequentially, and the reaction mixture was heated at 50°C overnight. After completion as indicated by TLC, the reaction mixture was quenched at 0°C by dropwise addition of $NaHCO_3$ over 20 min. It was then extracted with ethyl acetate (3x 5 ml) and the organic layer washed with water (3 x 3 ml). The organic layer was washed with brine, dried over $MgSO_4$, evaporated and purified by column chromatography (30% ethyl acetate: 70% hexane) to afford a semi-solid (0.084g) with 85% yield.

^{1}H NMR (400 MHz, Chloroform-*d*) δ 0.77 – 0.99 (m, 7H), 1.04 – 1.08 (m, 1H), 1.09 (s, 1H), 1.17 – 1.44 (m, 17H), 1.59 (t, *J* = 6.5 Hz, 1H), 1.68 – 1.73 (m, 1H), 1.74 – 1.87 (m, *J* = 4.0, 3.2 Hz, 12H), 2.57 – 2.75 (m, 12H), 2.80 – 2.99 (m, 6H), 3.63 – 3.76 (m, 3H), 3.76 – 3.85 (m, 1H), 3.97 (t, *J* = 5.7 Hz, 1H), 4.09 (t, *J* = 5.9 Hz, 5H), 6.36 (ddt, *J* = 9.0, 4.9, 2.3 Hz, 1H), 6.40 – 6.54 (m, 2H), 6.56 – 6.64 (m, 1H), 6.70 – 6.96 (m, 14H), 6.97 – 7.05 (m, 2H), 7.06 – 7.30 (m, 9H). ^{13}C NMR (400Mz, $CDCl_3$ δ ppm) 160.3, 159.9, 158.156.1, 136.4, 134.6, 130.9, 129.9, 129.4, 120.5, 118.1, 114.7, 114.6, 107.8, 101.3, 78.1, 71.9, 61.2, 56.9, 54.6, 44.4, 28.7, 23.6, 21.4. **HR-FT-MS calcd for $C_{30}H_{34}FNO_3$ 475.25 found 475.28**

3.3.16 Synthesis of 3-(4-Iodo-phenyl)-2-oxo-2H-chromen-7-yl acetate

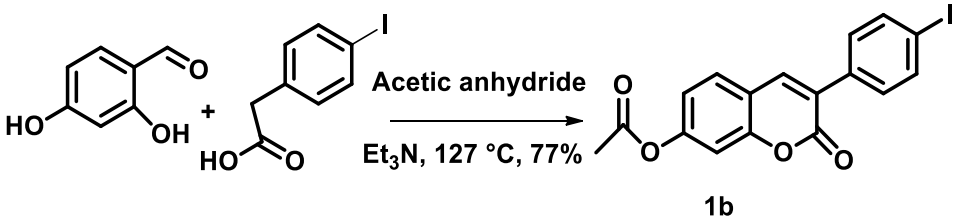

1b

To a round bottom flask with a stir bar under nitrogen was added 2, 4-dihydroxybenzaldehyde (1g, 6.4 mmol) followed by 4-Iodo-phenylacetic acid (1.02g, 3.90 mmol) and acetic anhydride 2.26 ml). Triethylamine (1.32 ml, 13.06 mmol) was slowly added, and the mixture was refluxed at 127°C for 7 hours. The reaction was monitored by TLC till completion and quenched with distilled water (30 ml) to give a yellow solid. The solid was crushed and recrystallized using methanol (60 ml) to afford (1.27g) 77% of the desired product as brown solid.

^{1}H NMR (400Mz, $CDCl_3$, δ ppm) 2.19 (s, 3H), 6.99 (s, 1H), 7.03 (d, J = 2.27, 1H), 7.07 (d, J = 2.27), 7.19 (s, 1H), 7.63 (d, J = 8.56), 8.01 (s, 1H). ^{13}C NMR (400Mz, $CDCl_3$ δ ppm) 168.2, 161.9, 153.1, 151.3, 137.5, 133.4, 130.3, 127.9, 127.3, 126.5, 124.3, 118.7, 117.3, 96.0, 17.1.

3.3.17 Synthesis of 3-(4-Iodo-phenyl)-7-hydroxy-chromen-2-one

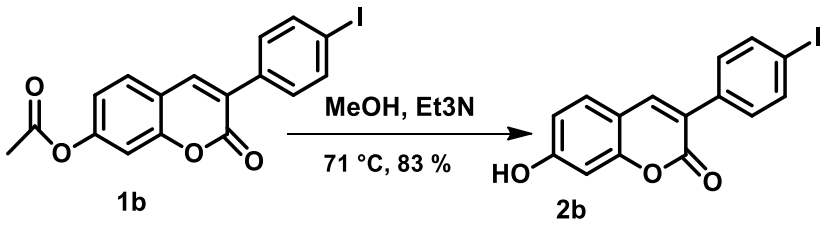

1b 2b

To a stirred solution of methanol (9.7 ml) and triethylamine (0.98g. 9.68mmol) in a round bottom flask under nitrogen atmosphere was added 3-(4-Iodo-phenyl)-2-oxo-2H-chromen-

7-yl acetate (1.27g, 3.0 mmol). The reaction mixture was refluxed at 80ºC for 24 hours. After the reaction was completed as shown by TLC, it was quenched by adding 1M HCl until the pH became acidic. The mixture was extracted using ethyl acetate (15 x 3 ml) and water (11 ml) and recrystallized with methanol (50 ml) to give (0.95g) 83% expected compound.

^{1}H NMR (400Mz, $CDCl_3$) 5.10 (s, 1H) 6.78 (s, 1H), 6.79 (d, J = 2.52 Hz, 1H), 7.10 (s, 1H), 7.36 (d, J = 8.31 Hz, 1H), 7.62 (d, J = 4.03 Hz, 1H), 7.89 (s, 1H).) ^{13}C NMR (400Mz, $CDCl_3$ δ ppm) 161.9, 157.8, 152.1, 137.6, 133.2, 129.4, 128.4, 125. 1, 121.5, 117. 1, 107.4, 96.2

3.3.18 Synthesis of 3-(4-Iodo-phenyl)-7-methoxy-chromen-2-one

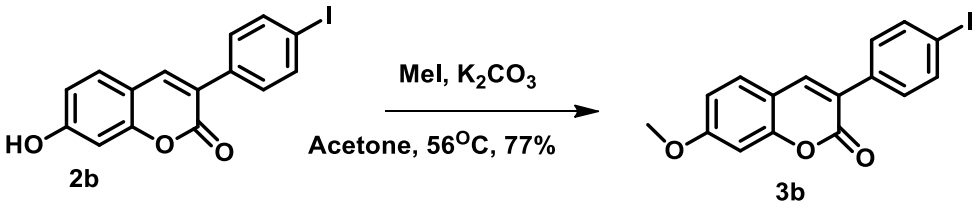

To a stirred solution of acetone (13.3 ml) was added 3-(4-Iodo-phenyl)-7-hydroxy-2H-chromen-2-one (0.95g, 2.60 mmol) under nitrogen atmosphere. K_2CO_3 (1.10g, 8.0 mmol) was added while stirring followed by careful addition of MeI (0.49 ml, 3.50 mmol) and the mixture was refluxed overnight at 56ºC. Excess acetone was evaporated under vacuum after completion of the reaction and the mixture dissolved in CH_2Cl_2, washed with water

(8.0 ml x 3), dried over $MgSO_4$ and evaporated under reduced pressure to give a yellow solid (0.76) of 77% yield.

^{1}H NMR (400Mz, $CDCl_3$, δ ppm) 3.70 (s, 3H), 6.68 (s, 1H), 6.71 (d, J = 2.52 Hz ,1H), 7.19 (s, 1H), 7.49 (d, J = 8.31 Hz, 1H), 7.61 (d, J = 4.03 Hz, 1H), 7.98 (s, 1H).) ^{13}C NMR (400Mz, $CDCl_3$ δ ppm) 161.9, 160.0, 152.4, 137.6, 132.7, 129.4, 128.4, 127. 5, 123.5, 117. 1, 107.4, 96.1, 55.8

3.3.19 Synthesis of 2-((Z)-2-(4-Iodophenyl)-3-hydroxy-3-methylbut-1-enyl)-5-methoxyphenol

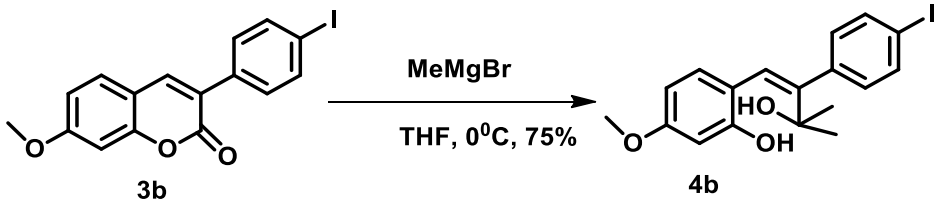

To a stirred solution of 3-(4-Iodo-phenyl)-7-methoxy-2H-chromen-2-one (0.3g, 0.79 mmol) in THF (11.0 ml) under nitrogen atmosphere at -20°C was added MeMgBr (in 3M diethyl ether, 1.5 ml, 12.5 mmol) and stirred for 45 min. The reaction mixture was warmed to -10°C and monitored by TLC for 7 hours. After completion, the reaction mixture was quenched with saturated aqueous NH_4Cl solution (40 ml) and extracted with ethyl acetate (60 ml). The organic layer was separated, and the aqueous layer was again extracted with ethyl acetate (20 ml). The combined organic layer was dried over anhydrous $MgSO_4$

concentrated under reduced pressure and purified by column chromatography (20% ethyl acetate: 80% hexane) to give a semi-solid (0.24g) with 75% yield.

^{1}H NMR (400Mz, $CDCl_3$) 1.35 (s, 3H), 1.98 (s, 1H), 3.68 (s, 3H), 5.00 (s, 1H), 6.27 (s, 1H), 6.38 (s, 1H), 6.86 (d, J = 8.45, 1H), 6.99 (d, J = 8.31 Hz, 1H), 7.19 (d, J = 8.03 Hz, 1H), 7.61 (d, J = 8.06 Hz, 1H). ^{13}C NMR (400Mz, $CDCl_3$ δ ppm) 158.0, 156.5,141.2 137.2, 133.6, 129.9, 127.4, 122.5, 115. 8, 107.4, 95.9, 73.1, 55.8, 27.2.

3.3.20 Synthesis of 3-(4-Iodo-phenyl)-7-methoxy-2,2-dimethyl-2H-chromene

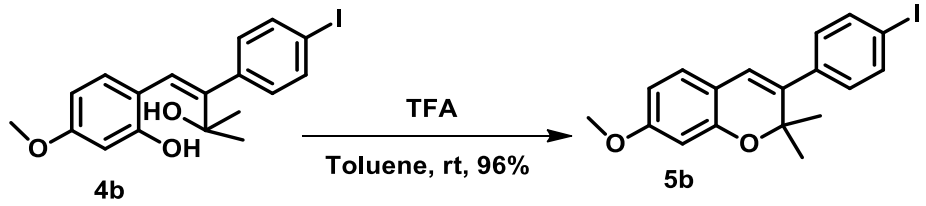

To a solution of 2-((Z)-2-(4-Iodo-phenyl)-3-hydroxy-3-methylbut-1-enyl)-5-methoxyphenol (.383g, 0.93 mmol) in $CHCl_3$ (13.6 ml) was added para-toluene sulfonic acid (0.077 ml, 0.45 mmol) stirred overnight at 0°C. The reaction mixture was diluted with ethyl acetate (20.0 ml) followed by saturated aqueous $NaHCO_3$ (10.0 ml) and stirred vigorously until the reaction was completed (TLC). The organic layer was separated, and the aqueous layer was extracted with CH_2Cl_2 (25 ml) and the combined organic layer was dried with anhydrous Na_2SO_4 and evaporated under reduced pressure. The mixture was

purified by column chromatography (70% hexane: 30% ethyl acetate) to give a semi-solid (0.35g) with 96% yield.

^{1}H NMR (400Mz, $CDCl_3$ δ ppm) 1.49 (s, 3H), 3.69 (s, 3H), 6.27 (s, 1H), 6.38 (s, 1H), 6.92 (d, J = 8.45, 1H), 7.01 (d, J = 8.31 Hz, 1H), 7.09 (d, J = 8.03 Hz, 1H), 7.61 (d, J = 8.06 Hz, 1H). ^{13}C NMR (400Mz, $CDCl_3$ δ ppm) 161, 154.3, 137.8, 131.6, 129.9, 127.4, 122.5, 115. 8, 107.4, 96.9, 78.3, 55.2, 23.8.

3.3.21 Synthesis of 4-(3-(4-Iodo-phenyl)-1, 2, 3, 4-tetrahydro-7-methoxy-2,2-dimethylnaphthalen-4-yl) phenol

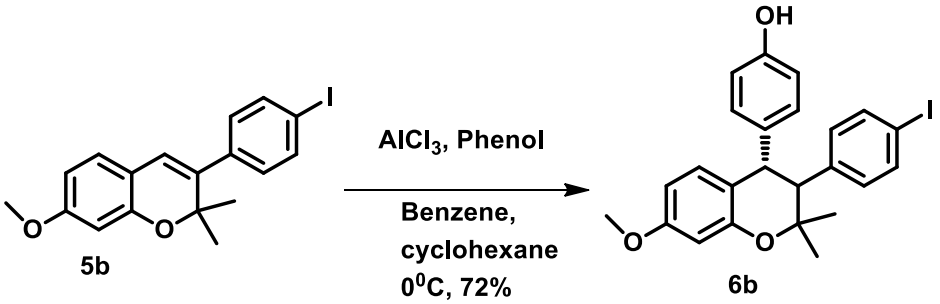

To a stirred solution of 3-(4-fluorophenyl)-7-methoxy-2, 2-dimethyl-2H-chromene (0.35g, 0.89 mmol) and phenol (0.24 g, 2.25 mmol) in benzene-cyclohexane mixture (1:1 ratio, 15 ml) at 0°C was added anhydrous aluminum chloride (0.22 g, 1.8 mmol) in portions. A solution of phenol (0.2 g, 2.13 mmol) in benzene- cyclohexane mixture (1:1 Ratio, 20 ml) was added after 30 min, and the mixture further stirred for 8 hrs. The reaction mixture was

quenched by adding a mixture of ice and cone. Hydrochloric acid (0.5 ml) and the organic layer was separated. The aqueous layer was re-extracted three times with dichloromethane (15 ml). The combined extract was washed with $NaHCO_3$ (10 %, 8ml), dried over anhydrous Na_2SO_4, filtered and concentrated under reduced pressure. The semi-solid obtained was purified by column chromatography (70% hexane: 30% ethyl acetate) to obtain the title compound (0.31g) with 72% yield.

^{1}H NMR (400Mz, $CDCl_3$, δ ppm) 1.27 (s, 3H) 1.39 (s, 3H), 3.80 (s, 3H), 4.41 (d, J = 12.34 Hz, 1H), 4.91 (s, 1H), 6.22 (dd, J = 8.06, 2.52 Hz, 1H), 6.49 (d, J = 2.5 Hz, 1H), 6.67 (d, J = 8.3 Hz, 2H), 6.88 (dd, J = 7.30, 1.05 Hz, 1H), 6.96 (d, J = 8.56 Hz, 2H), 7.48 (d, J = 8.31 Hz, 2H). ^{13}C NMR (400Mz, $CDCl_3$ δ ppm) 160.9, 158.2, 154.6, 140.3, 136.6, 131.1, 131.1, 129.7, 128.3, 121.8, 120.2, 115.6, 94.5, 78.4, 60.7, 55.5, 33.6, 23.9.

3.3.22 1-(2-(4-(3-(4-Iodo-phenyl)-1,2,3,4-tetrahydro-7-methoxy-2,2-dimethylnaphthalen-4-yl)phenoxy)ethyl)pyrrolidine

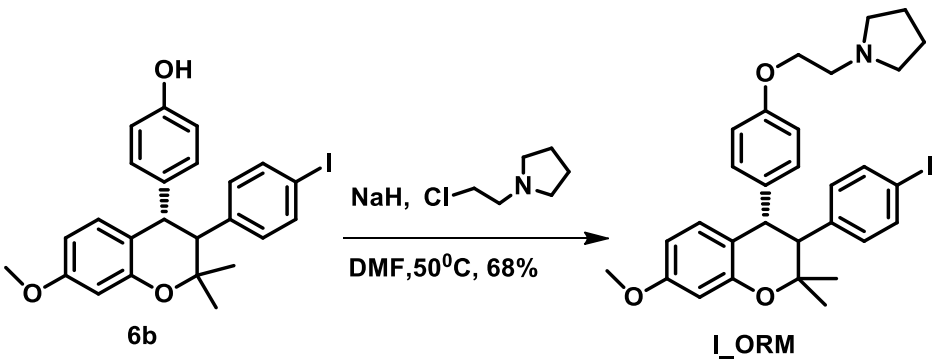

To a stirred solution of 4-(3-(4-fluorophenyl)-1, 2, 3, 4-tetrahydro-7-methoxy-2,2-dimethylnaphthalen-4-yl)phenol (0.48 g, 0.99 mmol) and DMF (13.0 ml) was added NaH (0.19 g, 8.0 mmol) under nitrogen atmosphere. The reaction mixture was vented with a needle for 20 min to allow the evolution of H_2 gas and then quenched with methanol (0.6 ml). After the evolution of all H_2 gas, 1-(2-chloroethyl) pyrrolidine hydrochloride (0.49 g, 2.66 mmo1) was added sequentially, and the reaction mixture was heated at 50°C overnight. After completion as indicated by TLC, the reaction mixture was quenched at 0°C by dropwise addition of $NaHCO_3$ over 20 min. It was then extracted with ethyl acetate (3x 10 ml) and the organic layer washed with water (3 x 5 ml). The organic layer was washed with brine, dried over $MgSO_4$, evaporated and purified by column chromatography (30% ethyl acetate: 70% hexane) to afford a semi-solid (0.039g) with 68% yield.

^{1}H NMR (400 MHz, Chloroform-*d*) δ 0.73 – 0.84 (m, 4H), 0.84 – 0.98 (m, 11H), 1.08 (d, *J* = 6.6 Hz, 3H), 1.18 – 1.34 (m, 26H), 1.38 (s, 2H), 1.68 (d, *J* = 5.7 Hz, 2H), 1.74 – 1.80 (m, 3H), 1.82 (dt, *J* = 7.2, 3.4 Hz, 5H), 2.74 (q, *J* = 6.7 Hz, 5H), 2.88 (dd, *J* = 17.8, 9.4 Hz, 1H), 2.96 (t, *J* = 5.7 Hz, 2H), 3.59 – 3.83 (m, 4H), 4.10 (t, *J* = 5.9 Hz, 2H), 6.33 – 6.47 (m, 2H), 6.57 (dt, *J* = 15.7, 8.2 Hz, 2H), 6.80 (d, *J* = 7.7 Hz, 9H), 6.82 – 6.93 (m, 4H), 6.97 (dt, *J* = 12.2, 6.7 Hz, 1H), 7.14 (t, *J* = 7.8 Hz, 4H), 7.21 (t, *J* = 7.9 Hz, 2H), 7.43 – 7.56 (m, 1H), 7.96 – 8.02 (m, 1H).^{13}C NMR (400Mz, $CDCl_3$ δ ppm) 160.3, 158.6, 155.7, 140.5, 136.6, 130.9, 129.9, 129.4, 120.5, 118.1, 114.7, 107.8, 95.3, 77.9, 71.2, 66.5, 60.9, 55.6, 51.4, 28.7, 24.4, 23.1. **HR-FT-MS calcd for $C_{30}H_{34}INO_3$ 583.50 found 583.51**

3.3.23 Synthesis of 3-(4-Chloro-phenyl)-2-oxo-2H-chromen-7-yl acetate

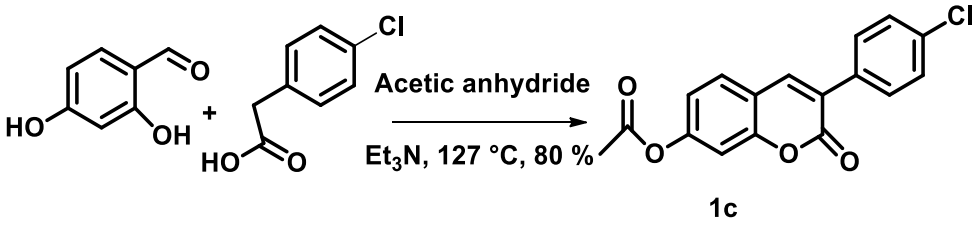

1c

To a round bottom flask with a stir bar under nitrogen was added 2, 4-dihydroxybenzaldehyde (1.06g, 7.84 mmol) followed by 4-Chloro-phenylacetic acid (1.24g, 7.27 mmol) and acetic anhydride (2.80 ml). Triethylamine (1.40 ml, 13.85 mmol) was slowly added, and the mixture was refluxed at 127°C for 7 hours. The reaction was monitored by TLC till completion and quenched with distilled water (30 ml) to give a white solid. The solid was crushed and recrystallized using methanol (70 ml) to afford (1.85g) 80 % of the desired product as white solid.

^{1}H NMR (400Mz, $CDCl_3$, δ ppm) 2.19 (s, 3H), 6.99 (s, 1H), 7.02 (d, J = 2.27, 1H), 7.05 (d, J = 2.27), 7.19 (s, 1H), 7.56 (d, J = 8.56), 7.85 (s, 1H). ^{13}C NMR (400Mz, $CDCl_3$ δ ppm) 168, 160, 154.1, 153.3, 139.5, 133.4, 131.8, 132.9, 128.9, 126.3, 123.3, 118.5, 117.3, 109.9, 18.9.

3.3.24 Synthesis of 3-(4-Chloro-phenyl)-7-hydroxy-chromen-2-one

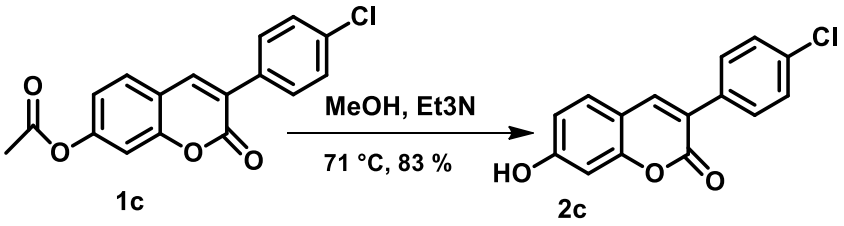

1c 2c

To a stirred solution of methanol (15.0 ml) and triethylamine (1.43g. 14.1mmol) in a round bottom flask under nitrogen atmosphere was added 3-(4-Chloro-phenyl)-2-oxo-2H-chromen-7-yl acetate (1.85g, 5.90 mmol). The reaction mixture was refluxed at 80ºC for 24 hours. After the reaction was completed as shown by TLC it was quenched by adding 1M HCl until the pH became acidic. The mixture was extracted using ethyl acetate (20 x 3 ml) and water (15 ml) and recrystallized with methanol (60 ml) to give (1.13 g) 71 % expected compound.

^{1}H NMR (400Mz, $CDCl_3$) 5.10 (s, 1H) 6.68 (s, 1H), 6.71 (d, J = 2.52 Hz, 1H), 7.19 (s, 1H), 7.24 (d, J = 8.31 Hz, 1H), 7.35 (d, J = 4.03 Hz, 1H), 7.90 (s, 1H).) ^{13}C NMR (400Mz, $CDCl_3$ δ ppm) 161.3, 159.8, 155.4, 139.6, 133.2, 129.4, 128.4, 127. 3, 123.1, 117. 4, 107.4, 107.5

3.3.25 Synthesis of 3-(4-Cloro-phenyl)-7-methoxy-chromen-2-one

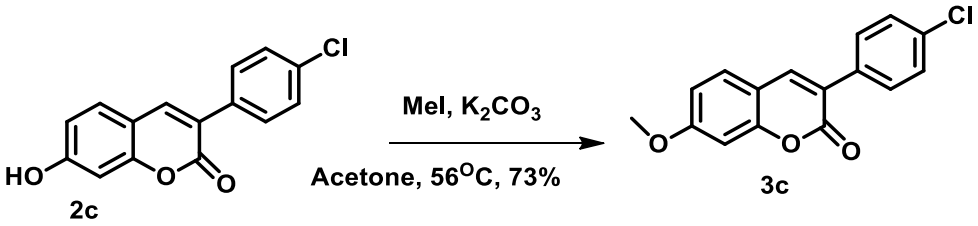

To a stirred solution of acetone (6.74 ml) was added 3-(4-Cloro-phenyl)-7-hydroxy-2H-chromen-2-one (0.49g, 2.60 mmol) under nitrogen atmosphere. K_2CO_3 (0.57 g, 4.13 mmol) was added while stirring followed by careful addition of MeI (0.25 ml, 1.82 mmol) and the mixture was refluxed overnight at 56ºC. Excess acetone was evaporated under vacuum after completion of the reaction and the mixture dissolved in CH_2Cl_2, washed with water (5.0 ml x 3), dried over $MgSO_4$ and evaporated under reduced pressure to give a white solid (0.54) of 73% yield.

^{1}H NMR (400Mz, $CDCl_3$, δ ppm) 3.71 (s, 3H), 6.71 (s, 1H), 6.77 (d, J = 2.52 Hz, 1H), 7.20 (s, 1H), 7.36 (d, J = 8.31 Hz, 1H), 7.53 (d, J = 4.03 Hz, 1H), 7.96 (s, 1H).) ^{13}C NMR (400Mz, $CDCl_3$ δ ppm) 161.9, 159.8, 155.4, 139.6, 132.7, 129.4, 128.4, 127. 5, 123.5, 117. 1, 107.8, 102.9, 56.1.

3.3.26 Synthesis of 2-((Z)-2-(4-Clorophenyl)-3-hydroxy-3-methylbut-1-enyl)-5-methoxyphenol

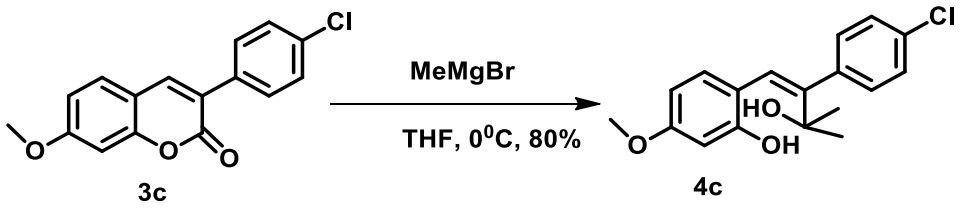

To a stirred solution of 3-(4-Cloro-phenyl)-7-methoxy-2H-chromen-2-one (0.32 g, 1.00 mmol) in THF (6.40 ml) under nitrogen atmosphere at -20°C was added MeMgBr (in 3M diethyl ether, 0.55 ml, 4.83 mmol) and stirred for 45 min. The reaction mixture was warmed to -10°C and monitored by TLC for 7 hours. After completion, the reaction mixture was quenched with saturated aqueous NH_4Cl solution (30 ml) and extracted with ethyl acetate (55 ml). The organic layer was separated, and the aqueous layer was again extracted with ethyl acetate (20 ml). The combined organic layer was dried over anhydrous $MgSO_4$ concentrated under reduced pressure and purified by column chromatography (20% ethyl acetate: 80% hexane) to give a semi-solid (0.27g) with 85% yield.

^{1}H NMR (400Mz, $CDCl_3$) 1.35 (s, 3H), 1.98 (s, 1H), 3.71 (s, 3H), 5.00 (s, 1H), 6.23 (s, 1H), 6.42 (s, 1H), 6.56 (d, J = 8.45, 1H), 6.97 (d, J = 8.31 Hz, 1H), 7.21 (d, J = 8.03 Hz, 1H), 7.38 (d, J = 8.06 Hz, 1H). ^{13}C NMR (400Mz, $CDCl_3$ δ ppm) 161.9, 156.4, 138.5, 131.6, 129.9, 127.4, 122.5, 114. 6, 107.4, 102.9, 73.6, 55.2, 27.3

3.3.27 Synthesis of 3-(4-Cloro-phenyl)-7-methoxy-2,2-dimethyl-2H-chromene

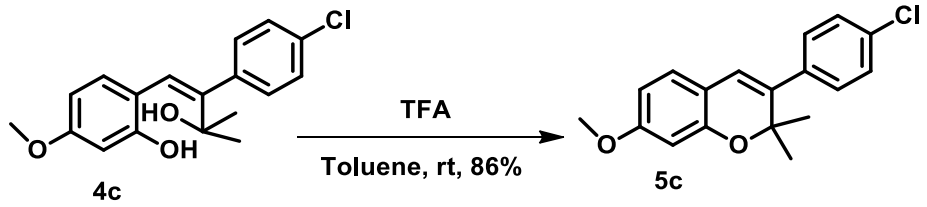

To a solution of 2-((Z)-2-(4-Cloro-phenyl)-3-hydroxy-3-methylbut-1-enyl)-5-methoxyphenol (0.36g, 1.13 mmol) in $CHCl_3$ (12.00 ml) was added para-toluene sulfonic acid (0.077 ml, 0.32 mmol) stirred overnight at 0°C. The reaction mixture was diluted with ethyl acetate (20.0 ml) followed by saturated aqueous $NaHCO_3$ (10.0 ml) and stirred vigorously until the reaction was completed (TLC). The organic layer was separated, and the aqueous layer was extracted with CH_2Cl_2 (23 ml), and the combined organic layer was dried with anhydrous Na_2SO_4 and evaporated under reduced pressure. The mixture was purified by column chromatography (70% hexane: 30% ethyl acetate) to give a semi-solid (0.29 g) with 86% yield.

^{1}H NMR (400Mz, $CDCl_3$ δ ppm) 1.57 (s, 3H), 3.69 (s, 3H), 6.30 (s, 1H), 6.32 (s, 1H), 6.99 (d, J = 8.45, 1H), 7.23 (d, J = 8.31 Hz, 1H), 7.28 (d, J = 8.03 Hz, 1H), 7.35 (d, J = 8.06 Hz, 1H). ^{13}C NMR (400Mz, $CDCl_3$ δ ppm) 161.6, 156.3, 142.8, 131.6, 129.9, 127.4, 122.0, 115. 8, 107.4, 99.9, 78.7, 56.2, 23.3.

3.3.28 Synthesis of 4-(3-(4-Cloro-phenyl)-1, 2, 3, 4-tetrahydro-7-methoxy-2,2-dimethylnaphthalen-4-yl) phenol

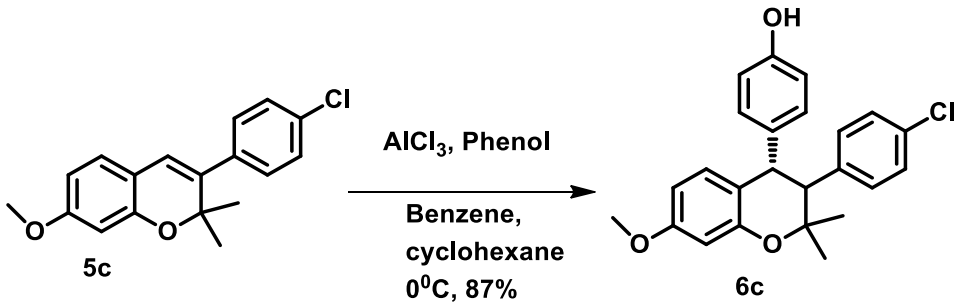

To a stirred solution of 3-(4-Chloro-phenyl)-7-methoxy-2, 2-dimethyl-2H-chromene (0.29 g, 0.96 mmol) and phenol (0.17 g, 1.6 mmol) in benzene-cyclohexane mixture (1:1 ratio, 15 ml) at 0°C was added anhydrous aluminum chloride (0.22 g, 1.8 mmol) in portions. A solution of phenol (0.18 g, 1.92 mmol) in benzene- cyclohexane mixture (1:1 Ratio, 15ml) was added after 30 min, and the mixture further stirred for 8 hrs. The reaction mixture was quenched by adding a mixture of ice and cone. Hydrochloric acid (0.4 ml) and the organic layer was separated. The aqueous layer was re-extracted three times with dichloromethane (15 ml). The combined extract was washed with $NaHCO_3$ (10 %, 8ml), dried over anhydrous Na_2SO_4, filtered and concentrated under reduced pressure. The semi-solid obtained was purified by column chromatography (70% hexane: 30% ethyl acetate) to obtain the title compound (0.33g) with 87 % yield.

^{1}H NMR (400Mz, $CDCl_3$, δ ppm) 1.32 (s, 3H) 1.29 (s, 3H), 3.84 (s, 3H), 4.27 (d, J = 12.34 Hz, 1H), 4.81 (s, 1H), 6.24 (dd, J = 8.06, 2.52 Hz, 1H), 6.72 (d, J = 2.5 Hz, 1H), 6.92 (d, J = 8.3 Hz, 2H), 6.98 (dd, J = 7.30, 1.05 Hz, 1H), 7.01 (d, J = 8.56 Hz, 2H), 7.22 (d, J = 8.31 Hz, 2H). ^{13}C NMR (400Mz, $CDCl_3$ δ ppm) 158.9, 155.2, 153.7, 139.3, 135.6, 131.1, 131.1, 129.7, 128.3, 120.9, 120.2, 115.6, 103.2, 78.4, 60.7, 55.5, 33.0, 23.1

3.3.29 1-(2-(4-(3-(4-Cloro-phenyl)-1,2,3,4-tetrahydro-7-methoxy-2,2-dimethylnaphthalen-4-yl)phenoxy)ethyl)pyrrolidine

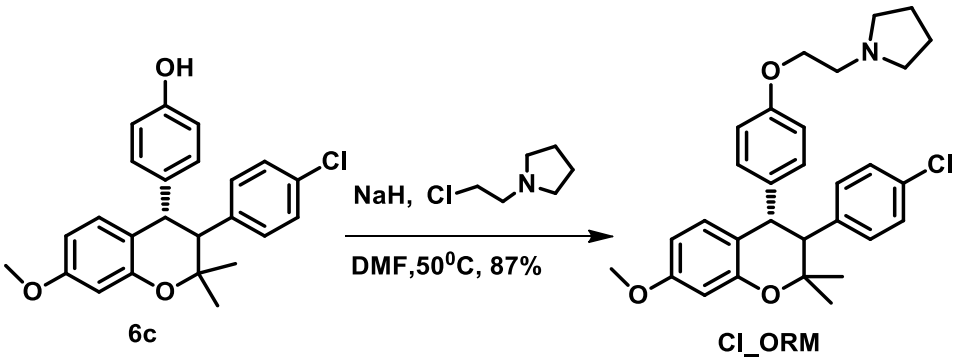

To a stirred solution of 4-(3-(4-Chlorophenyl)-1, 2, 3, 4-tetrahydro-7-methoxy-2,2-dimethylnaphthalen-4-yl)phenol (0.33 g, 0.84 mmol) and DMF (8.90 ml) was added NaH

(0.13 g, 5.47 mmol) under nitrogen atmosphere. The reaction mixture was vented with a needle for 20 min to allow the evolution of H_2 gas and then quenched with methanol (0.5 ml). After the evolution of all H_2 gas, 1-(2-chloroethyl) pyrrolidine hydrochloride (0.34 g, 1.83 mmo1) was added sequentially, and the reaction mixture was heated at 50°C overnight. After completion as indicated by TLC, the reaction mixture was quenched at 0°C by dropwise addition of $NaHCO_3$ over 20 min. It was then extracted with ethyl acetate (3x 10 ml) and the organic layer washed with water (3 x 5 ml). The organic layer was washed with brine, dried over $MgSO_4$, evaporated and purified by column chromatography (30% ethyl acetate: 70% hexane) to afford a semi-solid (0.36g) with 87% yield.

^{1}H NMR (400Mz, $CDCl_3$, δ ppm) 1.17 (s, 3H) 1.29 (s, 3H), 1.70 (s, 4H,), 2.57 (s, 4H), 2.77 (t, J = 6.0Hz, 2H), 3.08 (d, J = 12.09Hz, 1H), 3.61 (s, 3H), 3.91 (t, J = 5.62Hz, 2H), 4.22 (d, J = 12.09 Hz, 1H), 6.28 (dd, J = 2.52, 2.52 Hz 1H), 6.72 (d, J = 2.52 Hz, 1H), 6.80 (d, J = 6.55 Hz, 1H), 6.98 (d, J =6.80 Hz, 2H), 7.03 (d, J =8.56 Hz, 2H), 7.21 (d, J = 7.30 Hz, 2H); ^{13}C NMR (400Mz, $CDCl_3$ δ ppm) 159.3, 156.9, 153.9, 139.2, 136.5, 130.9, 129.9, 129.4, 120.5, 119.2, 114.7, 107.8, 101.3, 77.9, 71.2, 66.5, 56.9, 54.6, 44.4, 28.7, 24.6, 22.8.

HR-FT-MS calcd for $C_{30}H_{34}ClNO_3$ 492.04 found 492.09

3.3.30 Synthesis of 2-oxo-3-p-tolyl-2H-chromen-7-yl acetate

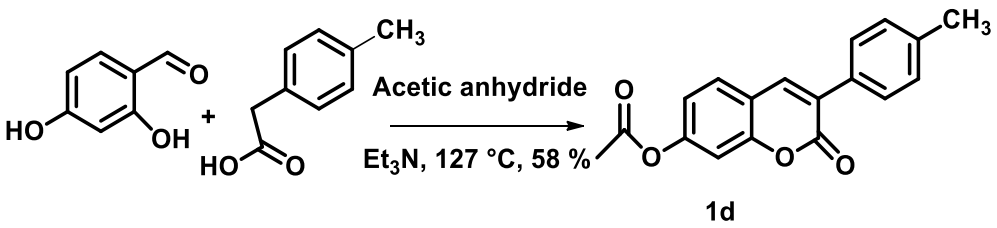

1d

To a round bottom flask with a stir bar under nitrogen was added 2, 4-dihydroxybenzaldehyde (2g, 14.40 mmol) followed by P-toluic acid (2.24g, 14.92 mmol) and acetic anhydride (4.52ml). Triethylamine (2.64 ml, 32.42 mmol) was slowly added, and the mixture was refluxed at 127°C for 7 hours. The reaction was monitored by TLC till completion and quenched with distilled water (65 ml) to give a gray solid. The solid was crushed and recrystallized using methanol (100 ml) to afford (2.475g) 58% of the desired product as white solid.

^{1}H NMR (400 MHz, Chloroform-d) δ 7.80 (s, 2H), 7.60 (s, 1H), 7.57 (s, 5H), 7.55 (d, J = 8.2 Hz, 3H), 7.15 (d, J = 2.2 Hz, 2H), 7.08 (dd, J = 8.5, 2.2 Hz, 2H), 2.39 (d, J = 7.9 Hz, 1H), 2.35 (s, 5H). 13C NMR (400 MHz, CDCl3) δ 168.73, 159.94, 154.07, 153.06, 139.35, 133.37, 131.70, 130.09, 128.72, 126.56, 123.28, 118.69, 117.30, 110.08, 23.24, 21.18.

3.3.31 Synthesis of 7-hydroxy-3-p-tolyl-2H-chromen-2-one

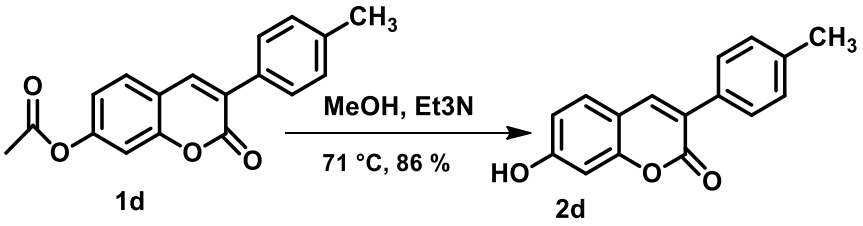

To a stirred solution of methanol (25.0 ml) and triethylamine (2.34 ml, 16.82 mmol) in a round bottom flask under nitrogen atmosphere was added 2-oxo-3-p-tolyl-2H-chromen-7-yl acetate (2.475, 8.41 mmol). The reaction mixture was refluxed at 80ºC for 24 hours. After the reaction was completed as shown by TLC, it was quenched by adding 1M HCl until the pH became acidic. The mixture was extracted using ethyl acetate (20 x 3 ml) and water (18 ml) and recrystallized using methanol (60 ml) to give (1.91) 86% expected compound.

^{1}H NMR (400 MHz, DMSO-d6) δ 10.67 (s, 1H), 8.15 (s, 2H), 7.69 – 7.54 (m, 10H), 6.83 (dd, J = 8.5, 2.3 Hz, 2H), 6.75 (d, J = 2.3 Hz, 2H), 3.20 (s, 1H), 2.28 (s, 3H). 13C NMR (400 MHz, DMSO) δ 161.44, 159.79, 154.95, 141.27, 134.23, 131.02, 130.20, 130.03, 121.24, 120.77, 113.44, 111.83, 101.70, 21.32.

3.3.32 Synthesis of 7-methoxy-3-p-tolyl-2H-chromen-2-one

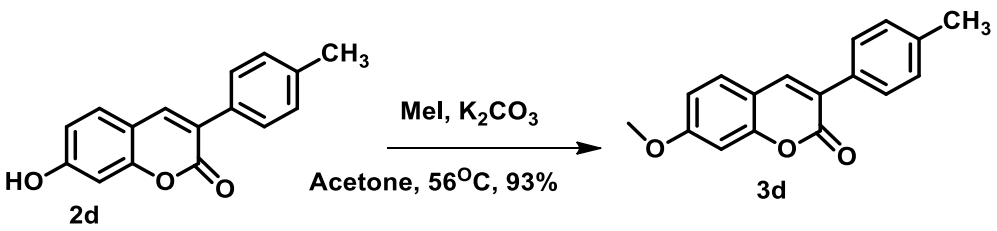

To a stirred solution of acetone (16.5 ml) was added 7-hydroxy-3-p-tolyl-2H-chromen-2-one (1.905g, 7.55 mmol) under nitrogen atmosphere. K_2CO_3 (2.10g, 15.10 mmol) was added while stirring followed by careful addition of MeI (2.14 ml, 15.1 mmol) and the mixture was refluxed overnight at 56°C. Excess acetone was evaporated under vacuum after completion of the reaction and the mixture dissolved in CH_2Cl_2, washed with water (15 ml x 3), dried over $MgSO_4$ and evaporated under reduced pressure to give a pale gray solid (1.85g) of 93% yield.

^{1}H NMR (400 MHz, Chloroform-d) δ 7.67 (s, 1H), 7.53 – 7.43 (m, 4H), 7.35 (dd, J = 8.9, 2.5 Hz, 1H), 6.84 – 6.72 (m, 2H), 3.80 (d, J = 1.8 Hz, 4H) 2.28 (s, 3H). 13C NMR (400 MHz, CDCl3) δ 162.88, 160.60, 155.38, 140.14, 133.89, 131.58, 129.98, 129.00, 123.51, 122.66, 113.15, 112.99, 100.44, 55.86, 21.28.

3.3.33 Synthesis of 2-((Z)-3-hydroxy-3-methyl-2-p-tolylbut-1-enyl)-5-methoxyphenol

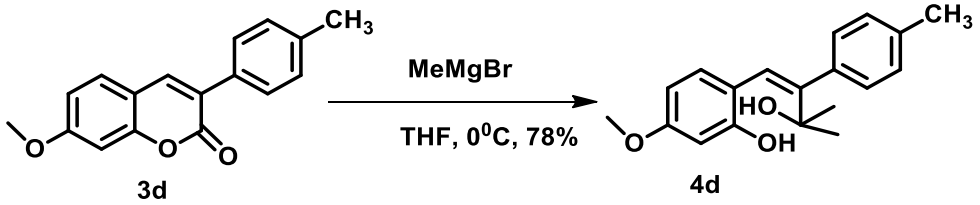

To a stirred solution of Synthesis of 7-methoxy-3-p-tolyl-2H-chromen-2-one (5.27g, 19.80 mmol) in THF (198 ml) under nitrogen atmosphere at 0°C was added MeMgBr (in 3M diethyl ether, 14 ml, 118.80 mmol) and stirred for 45 min. The reaction mixture was warmed to 22°C and monitored by TLC for 6 hours. After completion, the reaction mixture was quenched with saturated aqueous NH4Cl solution (80 ml) and extracted with ethyl acetate (75 ml). The organic layer was separated, and the aqueous layer was again extracted with ethyl acetate (3 x 50 ml). The combined organic layer was dried over anhydrous $MgSO_4$ concentrated under reduced pressure and purified by column chromatography (10% ethyl acetate: 90% hexane) to give a semi-solid (4.58g) with 78% yield.

^{1}H NMR (400 MHz, Chloroform-d) δ 7.70 (s, 3H), 7.54 – 7.47 (m, 12H), 7.41 (s, 1H), 7.40 – 7.36 (m, 4H), 7.19 (s, 4H), 7.13 (d, J = 8.5 Hz, 2H), 6.95 (dt, J = 7.7, 1.1 Hz, 1H), 6.82 (d, J = 2.4 Hz, 2H), 6.80 (q, J = 2.4 Hz, 4H), 6.45 (s, 1H), 6.15 (d, J = 1.0 Hz, 1H), 3.83 (s, 10H), 3.72 (s, 5H), 2.28 (s, 3H), 1.98 (s, 1H), 1.44 (s, 2H), 1.27 (s, 6H). (400Mz, CDCl3 δ ppm) 161, 156.4, 138.8, 131.6, 129.9, 127.4, 122.5, 115. 8, 107.4, 102.9, 73.6, 55.2, 26.8, 21.32

3.3.34 Synthesis of 7-methoxy-2,2-dimethyl-3-p-tolyl-2H-chromene

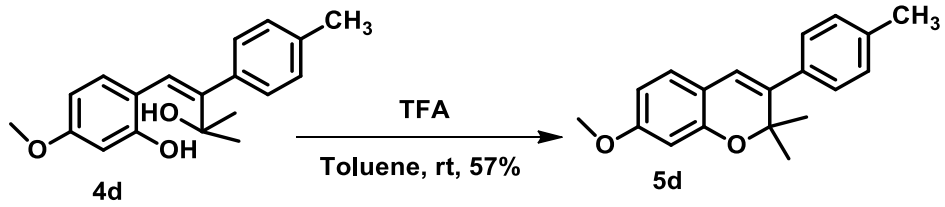

To a solution of 2-((Z)-3-hydroxy-3-methyl-2-p-tolylbut-1-enyl)-5-methoxyphenol (5.27g, 17.67 mmol) in CH_2Cl_2 (176.0 ml) was added p-TSOH (0.91 ml, 5.30 mmol) and stirred for 12 hours. The reaction mixture was diluted with ethyl acetate (25. ml) followed by 5% aqueous $NaHCO_3$ (45 ml) and stirred vigorously until the reaction was completed (TLC). The organic layer was separated, and the aqueous layer was extracted with ethyl acetate (3 x 50 ml) and the combined organic layer was dried with anhydrous Na_2SO_4 and evaporated under reduced pressure. The mixture was purified by column chromatography (70% hexane: 30% ethyl acetate) to give a semi-solid (2.81g) with 57% yield.

1H NMR (600 MHz, Chloroform-d) δ 7.42 (d, J = 8.3 Hz, 2H), 7.34 (d, J = 8.3 Hz, 2H), 7.14 (d, J = 8.3 Hz, 1H), 6.73 (d, J = 2.9 Hz, 1H), 6.67 (dd, J = 8.3, 2.6 Hz, 1H), 6.49 (s, 1H), 3.92 (s, 4H), 2.55 (d, J = 2.2 Hz, 4H), 1.78 (s, 7H). 13C NMR (600 MHz, $CDCl_3$) δ 160.92, 154.03, 139.30, 137.02, 129.10, 128.29, 127.38, 121.91, 116.56, 107.24, 102.31, 79.09, 77.71, 77.50, 77.29, 55.27, 27.34, 21.35.

3.3.35 Synthesis of 4-(3, 4-dihydro-7-methoxy-2, 2-dimethyl-3-p-tolyl-2H-chromen-4-yl) phenol

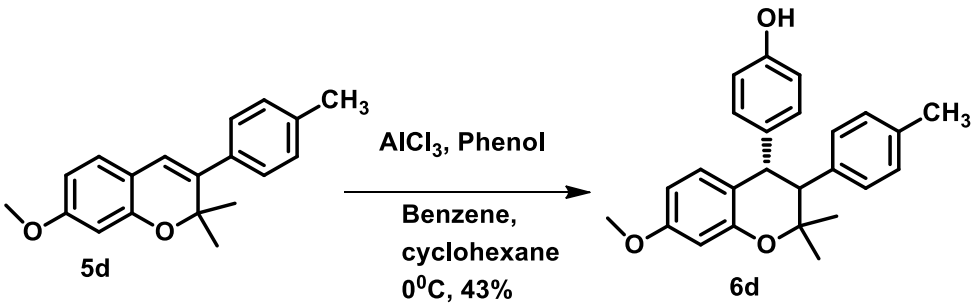

To a stirred solution of 7-methoxy-2,2-dimethyl-3-p-tolyl-2H-chromene (1.03, 3.67 mmol) and phenol (0.52 g, 5.50 mmol) in benzene-cyclohexane mixture (1:1 ratio, 37 ml) at 0°C was added anhydrous aluminum chloride (0.59g, 4.40 mmol) in portions. A solution of phenol (0.21 g, 2.20 mmol) in benzene- cyclohexane mixture (1:1 Ratio, 24 ml) was added after 30 min, and the mixture further stirred for 8 hrs. The reaction mixture was quenched by adding a mixture of ice and conc. Hydrochloric acid (1:1, 2.0 ml) and stirred for 30 minutes, the organic layer was separated, and the aqueous layer was re-extracted three times with dichloromethane (25 ml). The combined extract was washed with $NaHCO_3$ (10 %, 15 ml), dried over anhydrous Na_2SO_4, filtered and concentrated under reduced pressure. The solid obtained was purified by column chromatography (20 hexane: 80 % ethyl acetate) to obtain the titled compound (0.58 g) with 43 % yield.

1H NMR (600 MHz, DMSO-d6) δ 9.24 (d, J = 150.4 Hz, 2H), 7.17 (t, J = 7.8 Hz, 3H), 7.01 (d, J = 7.7 Hz, 2H), 6.87 (d, J = 8.2 Hz, 2H), 6.78 (d, J = 7.8 Hz, 3H), 6.52 (d, J = 8.0 Hz, 2H), 6.48 (d, J = 8.7 Hz, 1H), 6.38 (s, 1H), 6.34 (d, J = 9.0 Hz, 1H), 4.39 (d, J = 12.4 Hz, 1H), 4.16 (d, J = 6.4 Hz, 2H), 3.68 (d, J = 6.9 Hz, 3H), 3.45 (s, 4H), 3.20 (d, J = 4.3 Hz, 8H), 2.51 (s, 2H), 2.21 (s, 4H), 1.26 (s, 3H), 1.17 (s, 3H). 13C NMR (600 MHz, DMSO) δ 158.57, 157.30, 155.31, 153.44, 136.27, 135.36, 133.88, 130.51, 129.87, 129.33, 128.37, 118.94, 118.76, 115.19, 114.86, 106.80, 101.05, 77.91, 54.98, 54.90, 48.58, 42.13, 39.84, 39.70, 39.56, 39.43, 39.29, 39.15, 39.01, 28.55, 20.50, 19.84.

3.3.36 Synthesis of 1-(2-(4-(3,4-dihydro-7-methoxy-2,2-dimethyl-3-p-tolyl-2H-chromen-4-yl)phenoxy)ethyl)pyrrolidine

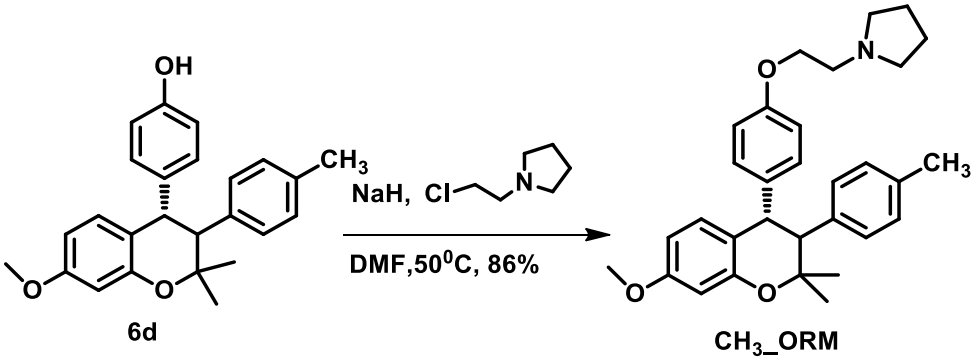

To a stirred solution4-(3, 4-dihydro-7-methoxy-2, 2-dimethyl-3-p-tolyl-2H-chromen-4-yl) phenol (0.18 g, 0.49 mmol) and DMF (4.88 ml) was added NaH (0.04 g, 1.46 mmol) under nitrogen atmosphere. The reaction mixture was vented with a needle for 20 min to allow evolution of H_2 gas and then quenched with methanol (1.5 ml). After evolution of all H_2

gas, 1-(2-chloroethyl) pyrrolidine hydrochloride (0.13 g, 0.98 mmol) was added sequentially and stirred for 15 minutes. The reaction mixture was heated at 50°C overnight. After completion as indicated by TLC, the reaction mixture was quenched at 0°C by drop wise addition of $NaHCO_3$ over 20 min. It was then extracted with ethyl acetate (3x 10 ml) and the organic layer washed with water (3 x 25 ml) , dried over $MgSO_4$, evaporated and purified by column chromatography (30% ethyl acetate: 70% hexane) to afford a semi-solid (0.19 g) with 86% yield. 1H NMR (600 MHz, Chloroform-d) δ 7.10 – 7.07 (m, 1H), 7.03 (d, J = 7.5 Hz, 2H), 6.98 – 6.96 (m, 2H), 6.93 (d, J = 8.7 Hz, 2H), 6.70 (d, J = 8.7 Hz, 2H), 6.66 (dd, J = 8.6, 0.9 Hz, 1H), 6.49 (d, J = 2.7 Hz, 1H), 6.41 (dd, J = 8.6, 2.6 Hz, 1H), 4.49 – 3.65 (m, 10H), 3.20 (d, J = 12.2 Hz, 1H), 2.94 (t, J = 6.0 Hz, 1H), 2.86 (t, J = 6.1 Hz, 2H), 2.67 (td, J = 6.8, 5.4, 2.8 Hz, 3H), 2.61 (td, J = 4.8, 4.3, 2.0 Hz, 3H), 2.28 (s, 3H), 1.41 (s, 3H), 1.34 (d, J = 15.1 Hz, 4H), 1.29 (s, 3H). 13C NMR (600 MHz, CDCl3) δ 159.22, 158.90, 157.13, 154.23, 136.33, 136.19, 136.07, 130.98, 130.04, 129.44, 128.72, 120.73, 118.72, 114.61, 114.10, 107.45, 101.43, 78.27, 66.99, 66.82, 57.05, 55.20, 55.17, 55.15, 54.77, 54.76, 43.96, 32.01, 29.79, 28.91, 23.57, 23.54, 22.78, 21.05, 20.21. **HR-FT-MS calcd for $C_{31}H_{37}NO_3$ 471.63 found 471.28**

3.4 Molecular Docking Studies

To screen for analogs of ormeloxifene with specific inhibition activity on EGFR pathway, binding affinities of several designed analogs to essential protein kinases were predicted using molecular docking study. Molecular modeling was conducted with OpenEye® Scientific Software: Fast Rigid exhaustive docking (FRED), Omega2, and VIDA. Molecular docking calculations were performed by FRED (OpenEye Scientific Software

®) to obtain a consensus score of calculated binding affinity of the virtual analogs toward target proteins[11]. Detailed information on OpenEye® Scientific Software can be found at **Software, Santa Fe, NM (USA). http://www.eyesopen.com.** The results were visualized by VIDA (OpenEye Scientific Software ®)

A virtual library of 800 analogs including ormeloxifene and a standard drug were designed using ChemDraw. Energy minimization, employing MMFF94 in ChemOffice, calculated the most stable conformation for each analog. Each analog was saved in .pdb format and compiled into a library of ligands. The compiled .pdb files were processed and used as input for Omega2, an OpenEye Scientific Software ® program that generates multi-conformer structures for each ligand in the library to enhance ligand flexibility in an otherwise ridged model. The processed files were compiled into a .oeb.gz file.

Protein kinase targets (EGFR, GSK3B, CDK2, mTOR, Akt, β-catenin, etc.) were downloaded from Protein Data Bank website in.pdb.gz format and were processed using Make Receptor, and the resulting protein receptor file was saved in.oeb.gz format. Docking was conducted using Open Eye Scientific Software ® including fast exhaustive docking (FRED), Omega and VIDA.

3.5 MTT Assay

Cell proliferation was determined by 3-(4,5-dimethylthiazol-2-yl)-2,5-diphenyltetrazolium bromide (MTT) assay[21]. Briefly, 5 X 10^6 cells of (A2780) were plated in 96 well plates and incubated for 24 hours at 37°C containing 5% of CO_2. Cells were treated with various analogs of ormeloxifene for 24 hours. 20µL of 50 mg/mL MTT was added in each well containing 100 mL of cell media. The cells were incubated for a further 6 hours, and the

media was replaced with 150 mL of DMSO. Plates vigorously shaken for 15 minutes and absorbance was taken at 570 nm on a microplate reader.

3.6 Western blot analysis

Western blot analysis was conducted to investigate the effect of ORM-Br on protein levels on cervical cancer cell lines. (CaSki and SiHa) Cells were treated with ORM-Br (5-20µM) concentration for 24 hours using DMSO (0.1%) as control. Cytoplasmic and nuclear lysates were prepared using a nuclear extract kit (Active Motif). 40µg of protein lysates were subjected to western blot analysis using 4-20% SDS-PAGE gels, blotted onto PVDF membrane and blocked with 10% bovine serum albumin (BSA) 1hr at room temperature[22]. The membrane was later incubated with the indicated primary antibodies followed by horseradish peroxidase secondary antibody and developed using enhanced chemiluminescence reagent (Roche) using a gel documentation system.

3.7 Cell Cycle analysis

Cells were plated in a 100mm dish and allowed to attach overnight. Cells were later exposed to ORM-Br (9.0 and 17.2µM) for 48 hrs. Cells were collected after ORM-Br treatment, fixed with 70% Telford Reagent containing ethanol, stained with propidium iodide, incubated overnight at 4 °C, and analyzed with an Accuri C6 flow cytometer. Cells with hypodiploid DNA were deemed apoptotic (G0/G1)[23].

3.8 Clonogenic assay

In the clonogenic assay, cells were seeded at 500 cells per 100 mm culture dish and allowed to attach overnight. The cells were treated with ORM-Br and maintained under standard cell culture conditions at 37 °C and 50% CO_2 in a humid environment. 10 days later, the

dishes were washed twice in PBS, fixed with methanol, stained with hematoxylin, washed with water and air dried. Visible colonies (approx. 50 cells) were counted, and % colonies were calculated using the number of colonies formed in treatment divided by several colonies established in the vehicle control (ethanol) as describe previously[24].

3.9 Confocal Microscopy

Cells were plated in four chamber slides at 5 x 104 cells per chamber and were allowed to attach at 60% confluence for 24 hours before being treated with 10µM ORM-Br for 18 hours. Cells were later processed for confocal microscopy[24]. Treated cells were rinsed with 1x HEPES/Hank buffer, fixed and permeabilized with cold methanol, washed with 1 x PBS and blocked with 10% normal goat serum in PBS. Cells were incubated with primary antibody followed by a species-specific Alexa Fluor® 488 secondary antibodies (Invitrogen). After washing, cells were stained with DAPI and coverslip were mounted in FluoroCare Anti-Fade mounting medium (Biocare Medical). Confocal microscopy was performed with Olympus Fluoview FV 1000 confocal microscope (Olympus cooperation)[25].

3.10 Cell Migration

Cell migration assay was performed using Boyden's Chambers assay, as per manufacturer's protocol (BD Biosciences). After 48 hr incubation, the migratory cells were fixed with methanol and stained with crystal violet and photographed under a light microscope. Migratory cells in ORM-Br treated group was compared with control[21].

3.11 Cell proliferation by xCELLigence assay

Cervical cancer cells (10,000 cells) were seeded in E-plate (Roche) following the xCELLigence. Real-Time Cell Analyzer (RTCA) DP instrument manual as provided by the manufacturer (Roche)[26]. ORM-Br (5-15µM) or vehicle control (0.1% DMSO) were added after 24 hrs, and the experiment was allowed to run for 100 hrs. Average baseline index for ORM-Br treated cells compared to control cells was calculated for at least two measurements for replicated experiments[27].

3.12 References

1. Siegel, R. L.; Miller, K. D.; Jemal, A., Cancer statistics, 2016. *CA: a cancer journal for clinicians* **2016,** *66* (1), 7-30.

2. Vehmanen, L.; Elomaa, I.; Blomqvist, C.; Saarto, T., Tamoxifen treatment after adjuvant chemotherapy has opposite effects on bone mineral density in premenopausal patients depending on menstrual status. *Journal of Clinical Oncology* **2006,** *24* (4), 675-680.

3. Lal, J., Clinical pharmacokinetics and interaction of centchroman—a mini review. *Contraception* **2010,** *81* (4), 275-280.

4. Misra, N.; Nigam, P.; Gupta, R.; Agarwal, A.; Kamboj, V., Centchroman—a non-steroidal anti-cancer agent for advanced breast cancer: Phase-II study. *International journal of cancer* **1989,** *43* (5), 781-783.

5. Maher, D. M.; Khan, S.; Nordquist, J. L.; Ebeling, M. C.; Bauer, N. A.; Kopel, L.; Singh, M. M.; Halaweish, F.; Bell, M. C.; Jaggi, M., Ormeloxifene efficiently inhibits ovarian cancer growth. *Cancer letters* **2015,** *356* (2), 606-612.

6. Weinberg, R., *The biology of cancer*. Garland science: 2013.

7. Chabner, B. A.; Roberts Jr, T. G., Chemotherapy and the war on cancer. *Nature Reviews Cancer* **2005,** *5* (1), 65.

8. Dressman, H. K.; Berchuck, A.; Chan, G.; Zhai, J.; Bild, A.; Sayer, R.; Cragun, J.; Clarke, J.; Whitaker, R. S.; Li, L., An integrated genomic-based approach to individualized treatment of patients with advanced-stage ovarian cancer. *Journal of Clinical Oncology* **2007,** *25* (5), 517-525.

9. Srivastava, V. K.; Gara, R. K.; Bhatt, M.; Sahu, D.; Mishra, D. P., Centchroman inhibits proliferation of head and neck cancer cells through the modulation of PI3K/mTOR pathway. *Biochemical and biophysical research communications* **2011,** *404* (1), 40-45.

10. Kumar Gara, R.; Sundram, V.; C Chauhan, S.; Jaggi, M., Anti-cancer potential of a novel SERM ormeloxifene. *Current medicinal chemistry* **2013,** *20* (33), 4177-4184.

11. Kitchen, D. B.; Decornez, H.; Furr, J. R.; Bajorath, J., Docking and scoring in virtual screening for drug discovery: methods and applications. *Nature reviews Drug discovery* **2004,** *3* (11), 935.

12. Kroemer, R. T., Structure-based drug design: docking and scoring. *Current protein and peptide science* **2007,** *8* (4), 312-328.

13. Singh, M., Centchroman, a selective estrogen receptor modulator, as a contraceptive and for the management of hormone-related clinical disorders. *Medicinal research reviews* **2001,** *21* (4), 302-347.

14. RAY, S.; GRovER, P.; ANAND, N., THE current interest in 3, 4-diphenylchromans. *Indian Journal of Chemistry* **1971,** *9*, 727.

15. Carney, R. W.; Bencze, W. L.; Wojtkunski, J.; Renzi, A. A.; Dorfman, L.; DeStevens, G., Derivatives of 3, 4-diphenylchromanes as estrogens and implantation inhibitors. *Journal of medicinal chemistry* **1966,** *9* (4), 516-520.

16. Ray, s.; grover, p.; anand, n., synth. Von cis-und trans-3, 4-diphenyl-dihydrocumarinen und threo-und erythro-2, 3-diphenyl-3-o-hydroxyphenyl-propionsaeuren. *Chemischer Informationsdienst. Organische Chemie* **1971,** *2* (42), no-no.

17. Ray, S.; Grover, P. K.; Kamboj, V. P.; Setty, B.; Kar, A. B.; Anand, N., Antifertility agents. 12. Structure-activity relation of 3, 4-diphenylchromenes and-chromans. *Journal of medicinal chemistry* **1976,** *19* (2), 276-279.

18. Ji, X.-S.; Miao, Y.; Liu, Y.; Jin, T.; Song, P., Improvement for the synthesis of Centchroman. *Journal of Chinese Pharmaceutical Sciences* **1998,** *7*, 69-71.

19. Ji, X.; Yan, J.; Wang, X., The total synthesis of centchroman. *CHINESE JOURNAL OF MEDICINAL CHEMISTRY* **1998,** *8*, 28-30.

20. Srivastava, A.; Lal, J.; Gupta, R.; Grover, P., A Facile Synthesis of a 3, 4-trans-7-Hydroxy-2, 2-dimethyl-3-phenyl-4-(p-pyrrolidinoethoxyphenyl) chroman. *ChemInform* **1994,** *25* (52), no-no.

21. Hafeez, B. B.; Ganju, A.; Sikander, M.; Kashyap, V. K.; Hafeez, Z. B.; Chauhan, N.; Malik, S.; Massey, A. E.; Tripathi, M. K.; Halaweish, F. T., Ormeloxifene suppresses prostate tumor growth and metastatic phenotypes via inhibition of oncogenic β-catenin signaling and EMT progression. *Molecular cancer therapeutics* **2017,** *16* (10), 2267-2280.

22. Sikander, M.; Hafeez, B. B.; Malik, S.; Alsayari, A.; Halaweish, F. T.; Yallapu, M. M.; Chauhan, S. C.; Jaggi, M., Cucurbitacin D exhibits potent anti-cancer activity in cervical cancer. *Scientific reports* **2016,** *6*, 36594.

23. Pozarowski, P.; Darzynkiewicz, Z., Analysis of cell cycle by flow cytometry. In *Checkpoint Controls and Cancer*, Springer: 2004; pp 301-311.

24. Chauhan, S. C.; Ebeling, M. C.; Maher, D. M.; Koch, M. D.; Watanabe, A.; Aburatani, H.; Lio, Y.; Jaggi, M., MUC13 mucin augments pancreatic tumorigenesis. *Molecular cancer therapeutics* **2012,** *11* (1), 24-33.

25. Webb, R. H., Confocal optical microscopy. *Reports on Progress in Physics* **1996,** *59* (3), 427.

26. Limame, R.; Wouters, A.; Pauwels, B.; Fransen, E.; Peeters, M.; Lardon, F.; De Wever, O.; Pauwels, P., Comparative analysis of dynamic cell viability, migration and invasion assessments by novel real-time technology and classic endpoint assays. *PloS one* **2012,** *7* (10), e46536.

27. Khan, S.; Ebeling, M. C.; Chauhan, N.; Thompson, P. A.; Gara, R. K.; Ganju, A.; Yallapu, M. M.; Behrman, S. W.; Zhao, H.; Zafar, N., Ormeloxifene suppresses desmoplasia and enhances sensitivity of gemcitabine in pancreatic cancer. *Cancer research* **2015**, canres. 2397.2014.

Chapter four

Design, Synthesis and Biological Evaluation of Ormeloxifene Analogs with pyrrolidine Moiety at C-7 targeting Epidermal Growth Factor towards the Treatment of Ovarian Cancer

4 Introduction

4.1 Ovarian cancer

In 2017, the incident of ovarian cancer rose to about 22,440 and caused over 14,080 death worldwide[1]. The occurrence of ovarian cancer rate is higher in Europe and North America, and it is known to be the 5th highest leading cause of deaths worldwide.[2] The five-year survival rate of ovarian cancer is between 30 – 92% depending on the stage at which the disease was diagnosed.[3] The risk factor includes null parity, age, late menopause and hereditary factors such as BRCA1 and BRCA2 mutation.[4] Advanced chemotherapy and the improved understanding of genetic risk factors as well as molecular pathogenesis have paved the way for new treatment options (**Fig 4.1**).

Different types of ovarian cancer have been identified according to the nature of cells from which they start. These include ovarian epithelial carcinoma, germ cell carcinoma tumor, stromal carcinoma, and small cell carcinoma[5].

Epithelial ovarian carcinogenesis makes up about 90% of all ovarian cancer cases and is rampant generally in postmenopausal women. According to ***Bryan T et al.,*** during postovulatory re-epithelial lisation, ovarian surface epithelial cells (OSE) (**blue**) divide and migrate to cover the ovulatory lesion (**black arrow**). Hyperplasia and transformation of OSE to adenocarcinoma can occur as a result of many factors including surges of pituitary

gonadotropins (**red arrow, top left**). The preovulatory surge of luteinizing hormone induces increased expression of cytokines and invasion of macrophages and monocytes (**orange cells**), leading to differentiation of follicle cells into luteal cells. Ovulation also stimulates the formation of invaginations and inclusion cysts. Cysts cells can differentiate between taking on Mullerian characteristics and proliferate under the effect of hormonal and cytokine stimulation and become ciliated (**yellow cells**) or secretory (**tan cells**). Eventually, these cells accumulate genetic aberrations. Rete ovarii tubules at the hilus of the ovary, close to the mesothelium to OSE (M-E) transition, also contain ciliated and secretory cells and can dilate to form a cyst. Whether cells in both cysts types can become cancerous is unknown. The role of any proposed ovarian stem or progenitor cells (purple cells) in epithelial ovarian carcinogenesis remains to be elucidated (**Fig 4.1**)[4].

Ormeloxifene has demonstrated excellent anti-cancer activity in different cancer cell lines including ovarian cancer. Currently, Ormeloxifene is being investigated to target the EGFR, and it is downstream, and studies have shown the ability of ormeloxifene to inhibit Akt phosphorylation in Head and neck squamous cell carcinomas (HNSCC)[6]. Ormeloxifene has shown to activates mTOR induces phosphorylation of effector molecule P70S6K and S6 ribosomal proteins, which effectively results in mTOR dependent gene transcription that control cell proliferation, metabolism, and protein synthesis [7]. The knowledge of varying inhibitory activity of ormeloxifene on multiple pathways is a possible lead towards the discovery of potential anticancer agent; we propose that ormeloxifene framework can be altered to generate possible drug candidates, which can help in the treatment of ovarian cancer.

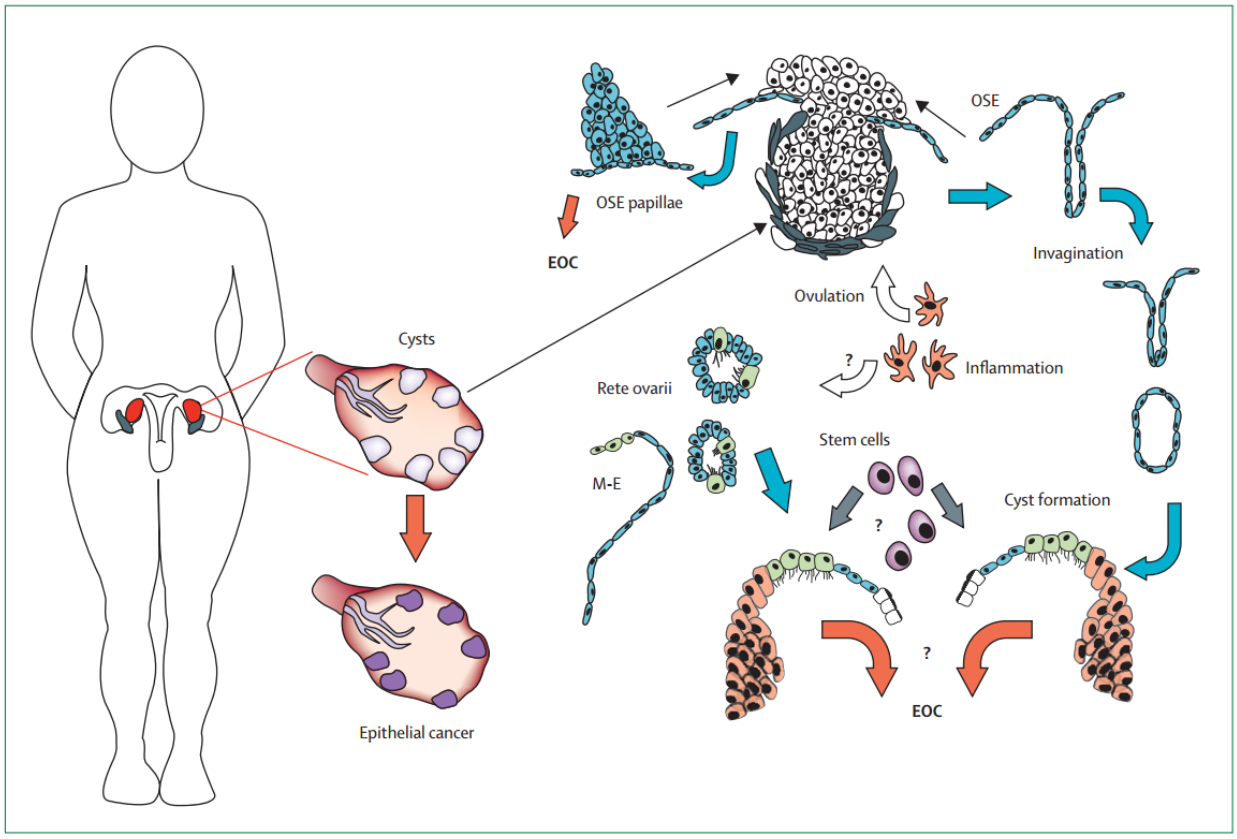

Figure 4.1 Epithelial ovarian carcinogenesis. Reproduced from Bryan T Hennessy, Robert l Coleman, Maurie Markman, Ovarian cancer The Lancet 2009, 374 (9698), 1371-1382. Main source[8]**.**

4.1.1 Diagnosis and treatment of ovarian cancer

The use of magnetic resonance imaging or computed tomography has been used in the diagnosis of different types of cancers including ovarian cancer[9]. However, these two procedures tend to underestimate the peritoneal and mesenteric tumors which are common in advanced ovarian carcinoma. There is a higher probability of survival rate when the disease is diagnosed at the early stages[10]. In advanced ovarian cancer, cisplatin and paclitaxel combinations are the most commonly used combination therapy, with

approximately 80 percent responds rate[11]. However, most patients suffer deterioration after about eight months of improvement. A significant disadvantage of the current treatment of ovarian carcinoma is the ability of the current therapies to fail at the diagnosis stage and resistance to combination therapy. Recently, cytotoxic drugs such as trabectedin and canfosfamide are used as a single efficient therapy to overcome drug resistance in ovarian cancer[12] compared to combination therapy.

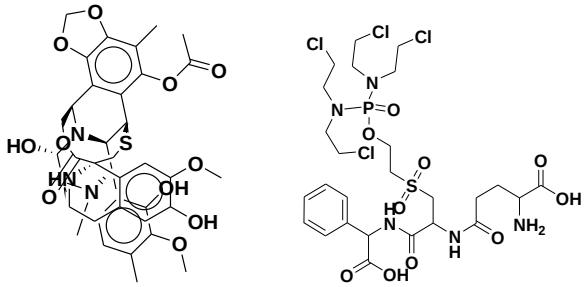

Figure 4.2. Trabectedin and canfosfamide, a drug resistance therapy

Currently, several therapeutic agents have been developed to target various stages of cell developments such as cell cycle regulation, protein translation angiogenesis, metastasis, apoptosis induction, and signal transduction[13]. However, no specific gene amplification or gene mutation responsible for progression or initiation of the disease has yet been identified. The nonexistence of a single pathogenic mutation is a challenge for target therapy[14]. Therefore the need for novel molecular targeted agents with potent and specific cytotoxic regiments would be a significant benefit towards the treatment of ovarian cancer.

Ormeloxifene, a selective estrogen receptor modulator, has demonstrated excellent anti-cancer activity in different cancer cell lines including ovarian carcinoma[15], breast cancer[16],

and head and neck squamous carcinoma[6]. Recent investigation has revealed the potential therapeutic index of ormeloxifene in pancreatic carcinoma via inhibiting sonic hedgehog (SHH) signaling pathway as well as modulating tumor microenvironment[17]. ***Bilal Bin Hafeez et al., 2017*** recently reported the ability of ormeloxifene to effectively inhibit molecular signatures of epithelial-mesenchymal transducers (EMT), β-catenin/TCF-4 transcriptional activity, induces phosphorylation of GSK3B and β-catenin degradation resulting in suppression of prostate tumor growth in xenograft mouse model[18].

The safe human use and excellent therapeutic index of ormeloxifene have as discussed in the previous chapter[19] have made it a potential drug candidate towards the treatment of ovarian cancer. In this study, we report the structural design, synthesis of novel ormeloxifene analogs with pyrrolidine moiety installed at the C-7 position of benzopyran skeleton to enhance its antiproliferation activities as well as the pharmacokinetic properties.

4.2 Results and discussion

4.2.1 Molecular docking

Molecular docking was conducted to know whether ormeloxifene and its analogs bind to various receptor proteins such as EGFR, GSK3B, and CDK2. Virtual library of 600 structurally modified C-4, C-7, and C-3 ormeloxifene analogs containing pyrrolidine, trifluoromethoxy benzene side chain, standard ormeloxifene and known EGFR inhibitors were prepared, and their energies minimized using Chem Office, with PM3 minimization along with standard drug of choice for the treatment of ovarian cancer. These files were converted into *pdb files maintaining all heavy atoms and concentrated into single

continuous *pdb file to be used as an input for Omega. Omega uses the MMF94 force field to generate multiple conformers for each input ligand to induce ligand flexibility in a rigid model. Modifications were applied to the default settings of OMEGA[20]. Receptor files (PDB files) were downloaded from protein data bank (PDB) website (GSK3B, EGFR, CDK2, mTOR) were prepared using OpenEye,s Fred Receptor program[21]. This program defines the space in which the search algorithm performs and define the shape potential for calculation (shape fitting step)[22]. Multiple scoring functions such as shapegsuss, chemguass3, Oechemscore, Screen score, and PLP were employed to obtain a consensus structure and scores in the final output.

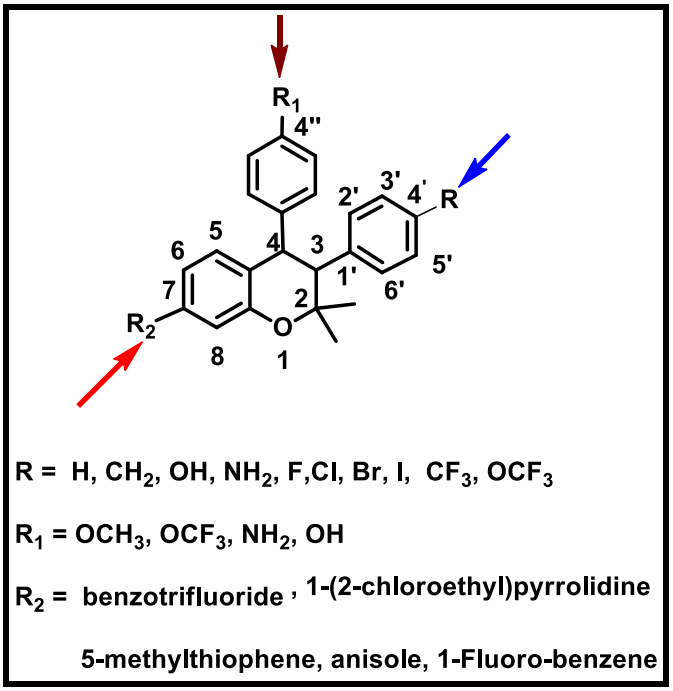

Figure 4.3 Proposed structure of ormeloxifene analogs with arrows showing various positions for structural modification

4.2.2 Results of molecular Docking

Molecular modeling studies of ormeloxifene analogs showed quite several analogs with a significant calculated binding affinity towards EGFR and it downstream (**Table 4.1**). Analogs with (ethyl)pyrrolidine at **C-7** and anisole at C-4 such as **JA_20** showed higher binding mode in EGFR binding site by forming two hydrogen bonds with **ASP:200: A** and **GLY:65: B** the same amino acid that bond to ormeloxifene in EGFR binding site (**Fig.4.5**). However, a stronger hydrogen bonding of **JA_15** and **JA_17** with **GLU: 234: A** in the crystal structure of EGFR, did not improve the binding affinities of these analogs in EGFR binding pocket.

In GSK3B binding pocket, analogs with (ethyl)pyrrolidine side chain at C-7 of Ormeloxifene scaffolds such as **JA_20, JA_25 JA_15, JA_18, JA_19,** and **JA_17** showed both hydrophilic and hydrophobic interactions. Most analogs with anisole and aniline at C-4 of ormeloxifene skeleton revealed higher binding affinity by forming two hydrogen bonds with **LYS:85: B** and **ASP:200: B** in GSK3B binding pocket **(Fig 4.4).** Ormeloxifene analogs with trifluoromethyl benzene at C-4 of ormeloxifene skeleton such as **JA_22,** and **JA_15** formed hydrogen bond with **LYS: 85: B** and **ASP: 200: B** in GSK3B binding pocket.

Molecular docking also showed a significant number of analogs bind to CDK2 binding pocket also showed a significant binding mode with ormeloxifene analogs compared to known estrogen receptor modulators. Substitution the (ethyl)pyrrolidine group at the phenoxy position with trifluoromethoxy moiety and replacing the methoxy group at C-7 with (ethyl)pyrrolidine moiety such as **JA_15, JA_16, JA_17,** and **JA_18** resulted in hydrogen bond with **HIS:84:A,** the same amino acid in CDK2 pocket that ormeloxifene

binds to induce its anticancer activity **(Fig 4.6, 4.7). JA_15**, an analog with hydrogen at C-4' demonstrated outstanding binding affinity towards CDK2 binding site relative to similar analogs such as JA**_16, JA_17, JA_18** with halogens substituted at C-4'(**Table 4.1**). All the designed analogs showing lower higher binding affinity will be chemically synthesized to be evaluated biologically as an anti-cancer candidate.

Table 4.1 Sample of consensus score of FRED docking in CDK2 receptor

VIDA Name	VIDA ID	PLP	Chemgauss3	OEChemscore	Screenscore	Consensus Score
JA_15_8	**2**	**-62.1912**	**-98.9223**	**-50.9355**	**-161.426**	**4**
JA_23_65	**3**	**-63.1604**	**-85.4124**	**-53.3115**	**-148.521**	**9**
JA_18_194	**4**	**-55.5819**	**-94.061**	**-49.7552**	**-156.399**	**15**
JA_31_197	**5**	**-58.7091**	**-78.7798**	**-50.6628**	**-138.252**	**31**
ORM_Me_70	**6**	**-58.9203**	**-88.0918**	**-48.9543**	**-130.846**	**31**
JA_17_124	**7**	**-60.2571**	**-82.0704**	**-46.9993**	**-151.993**	**33**
JA_30_136	**8**	**-54.9044**	**-82.1141**	**-49.7006**	**-133.778**	**34**
JA_20_91	**9**	**-55.1979**	**-82.9193**	**-52.6244**	**-128.111**	**34**
JA_29_196	**10**	**-56.4896**	**-74.7738**	**-51.4356**	**-136.43**	**37**
JA_22_18	**11**	**-57.7173**	**-76.0436**	**-49.6441**	**-141.795**	**38**
JA_24_136	**12**	**-54.9044**	**-82.1141**	**-49.7006**	**-133.778**	**38**
JA_16_118	**13**	**-50.2681**	**-89.5709**	**-47.0727**	**-145.829**	**41**

JA_19_43	**14**	**-51.9849**	**-86.1558**	**-49.8197**	**-128.74**	**41**
JA_33_173	**15**	**-52.6577**	**-80.5097**	**-48.3041**	**-139.799**	**43**
JA_35_136	**16**	**-49.7391**	**-81.7393**	**-46.085**	**-134.599**	**58**
JA_25_26	**17**	**-52.629**	**-76.5679**	**-47.4447**	**-128.804**	**63**
JA_28_130	**18**	**-52.1154**	**-73.6299**	**-49.4652**	**-122.123**	**65**
JA_26_58	**19**	**-50.8557**	**-75.0371**	**-48.8462**	**-128.441**	**65**
JA_32_166	**20**	**-49.3175**	**-79.5876**	**-48.1438**	**-121.453**	**68**
JA_34_4	**21**	**-48.3862**	**-71.7791**	**-48.2779**	**-130.937**	**69**
ORM_188	**22**	**-46.7276**	**-86.295**	**-45.0742**	**-110.072**	**69**
JA_27_4	**23**	**-48.3862**	**-71.7791**	**-48.2779**	**-130.937**	**73**
ORM_F_106	**24**	**-54.664**	**-70.7967**	**-42.5575**	**-119.368**	**79**
ORM_Cl_107	**25**	**-46.5579**	**-78.3947**	**-41.5806**	**-103.429**	**86**
ORM_Br_166	**26**	**-36.8834**	**-79.3884**	**-41.2741**	**-92.8488**	**87**
ORM_I_109	**27**	**-30.6345**	**-79.4347**	**-40.6518**	**-85.7905**	**89**

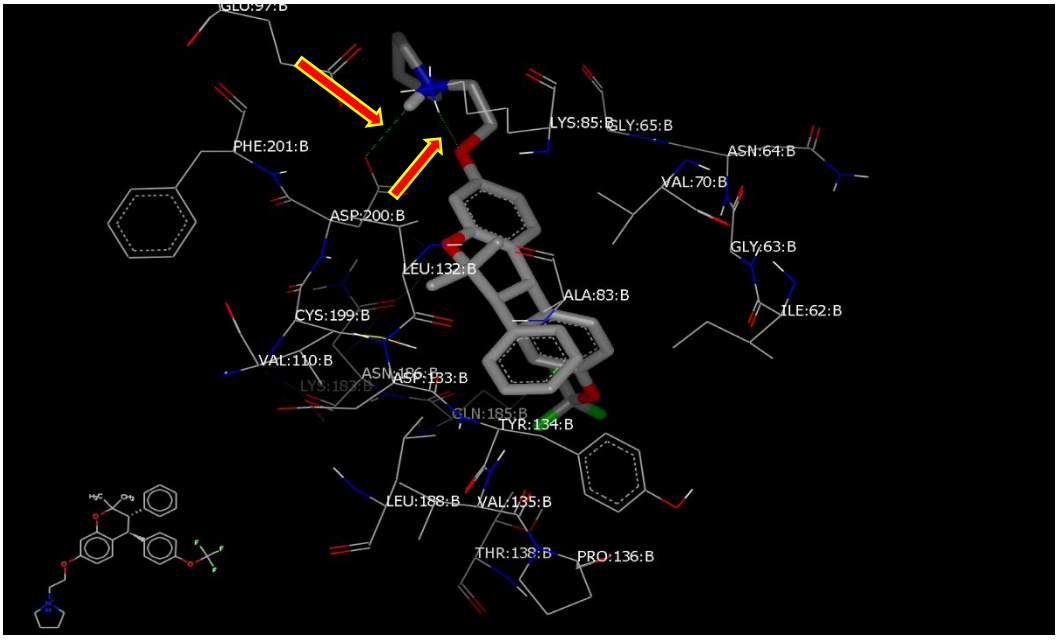

Figure 4.4. JA_15 is forming two hydrogen bonds in GSK3B binding pocket.

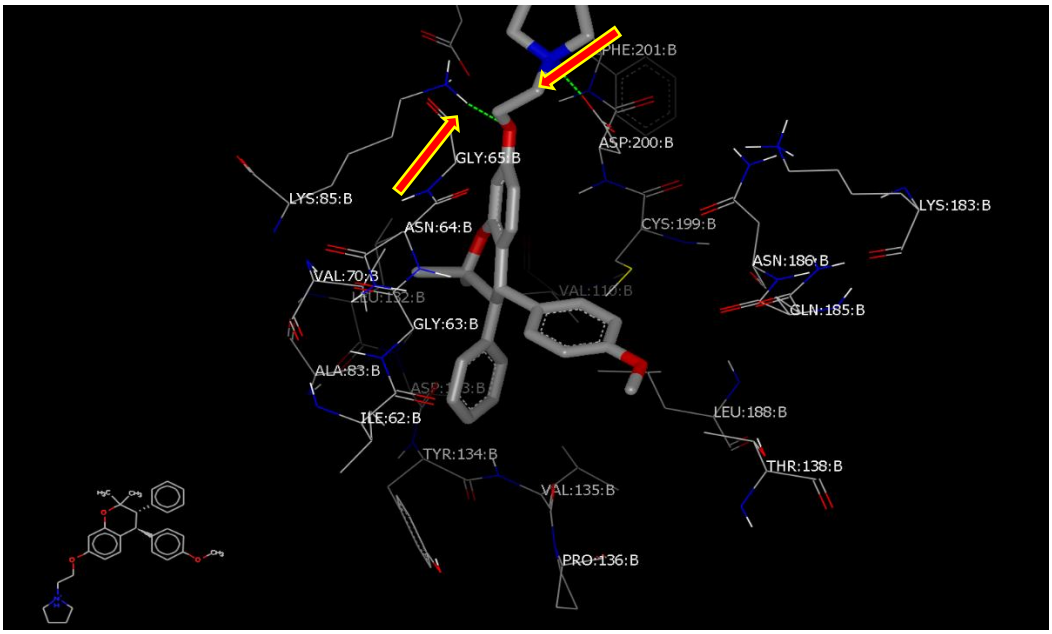

Figure 4.5 JA-20 in EGFR pocket showing hydrogen bonding with ASP:200B and GLY:65: B

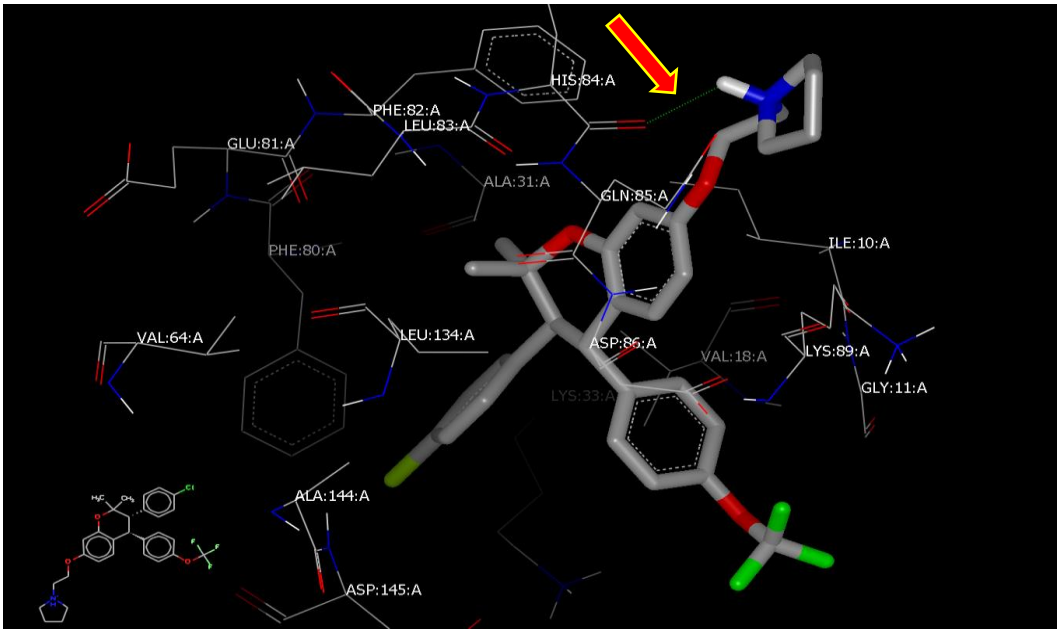

Figure 4.6 JA_17 forming hydrogen bonds with **His**:**84: A** in CDK2 binding pocket

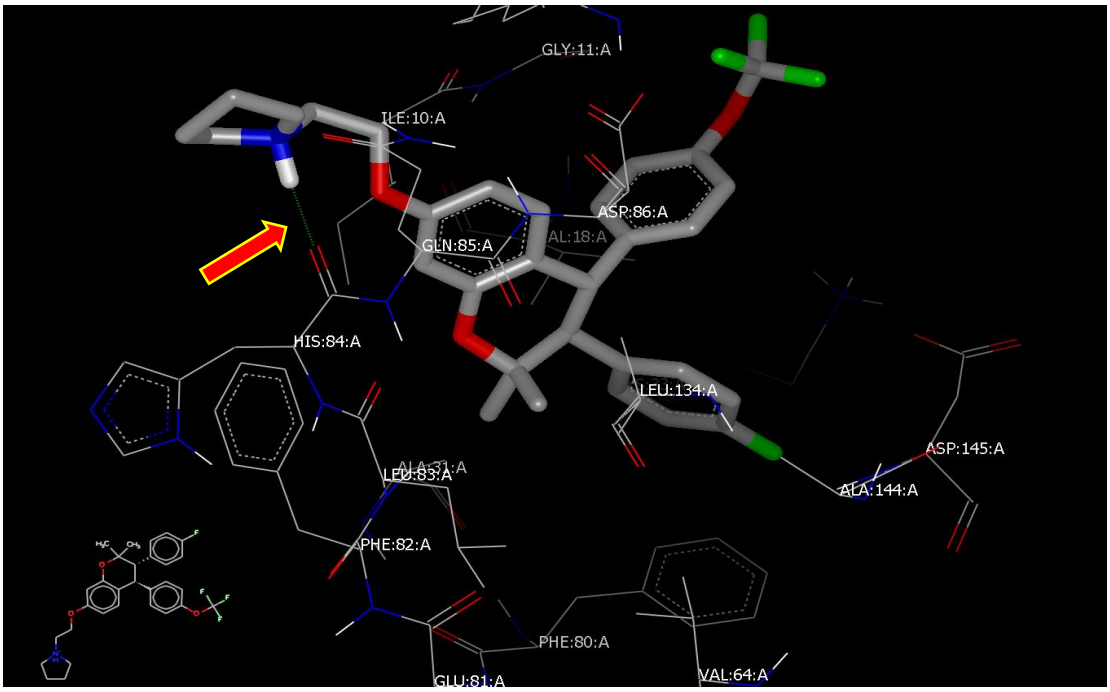

Figure 4.7 JA-18 form a hydrogen bond with HIS:84: A in the crystal structure of CDK2

4.2.3 Synthesis of ormeloxifene analogs

Synthetic schemes of the top analogs that showed higher binding affinities toward molecular targets such as EGFR, CDK2, Akt, and GSK3B were outlines. Several synthetic trials were conducted to optimize the synthetic routes. Successful synthetic routes were employed to install (ethyl) pyrrolidine, side chain at C-7 or halogens at C-4', and aniline, anisole, and trifluoromethyl benzene at C-4 of ormeloxifene skeleton (**Fig 4.3)**. It was painstaking to install various functionalities on ormeloxifene skeleton, especially the installation of (ethyl) pyrrolidine side at C-7 of ormeloxifene skeleton. Due to the higher polarity of (ethyl) pyrrolidine, several chemical reactions were initiated, and the concept of trial and error were employed to optimize the complete reaction schemes. The synthesis started by protecting the alcohol on intermediate compound **2** using TBSCl/Imidazole in the presence of DMF to give compound[23] **8.** Grignard reaction of **8** with methyl magnesium bromide (MeMgBr) in tetrahydrofuran (THF) produced compound **9**. Intramolecular dehydration of **9** with TFA in the presence of toluene gave compound **10**. Hydroarylation of **10** with phenol in benzene and cyclohexane afforded compound[24] **11**. Deprotection of compound **11** using tetrabuthyl ammonium fluoride (TBAF) in THF produced compound[25] **12**. Condensation of compound **12** with 1-(2-chloroethyl) pyrrolidine in the presence of potassium carbonate (K_2CO_3) in acetone at 60 °C produced **JA-15**. Other analogs **JA-16** to **JA-26** were synthesized using the same synthetic routes described in the scheme below **(Scheme 4.1).** The synthesized analogs are listed in **Table 4.1** below. The stereochemistry of the analogs was achieved by using aprotic solvent such as THF was used.

So far, a total of 8 compounds with pyrrolidine moiety at C-7 have been synthesized, and their antiproliferation studies will be conducted to identify their effects on ovarian cancer cells.

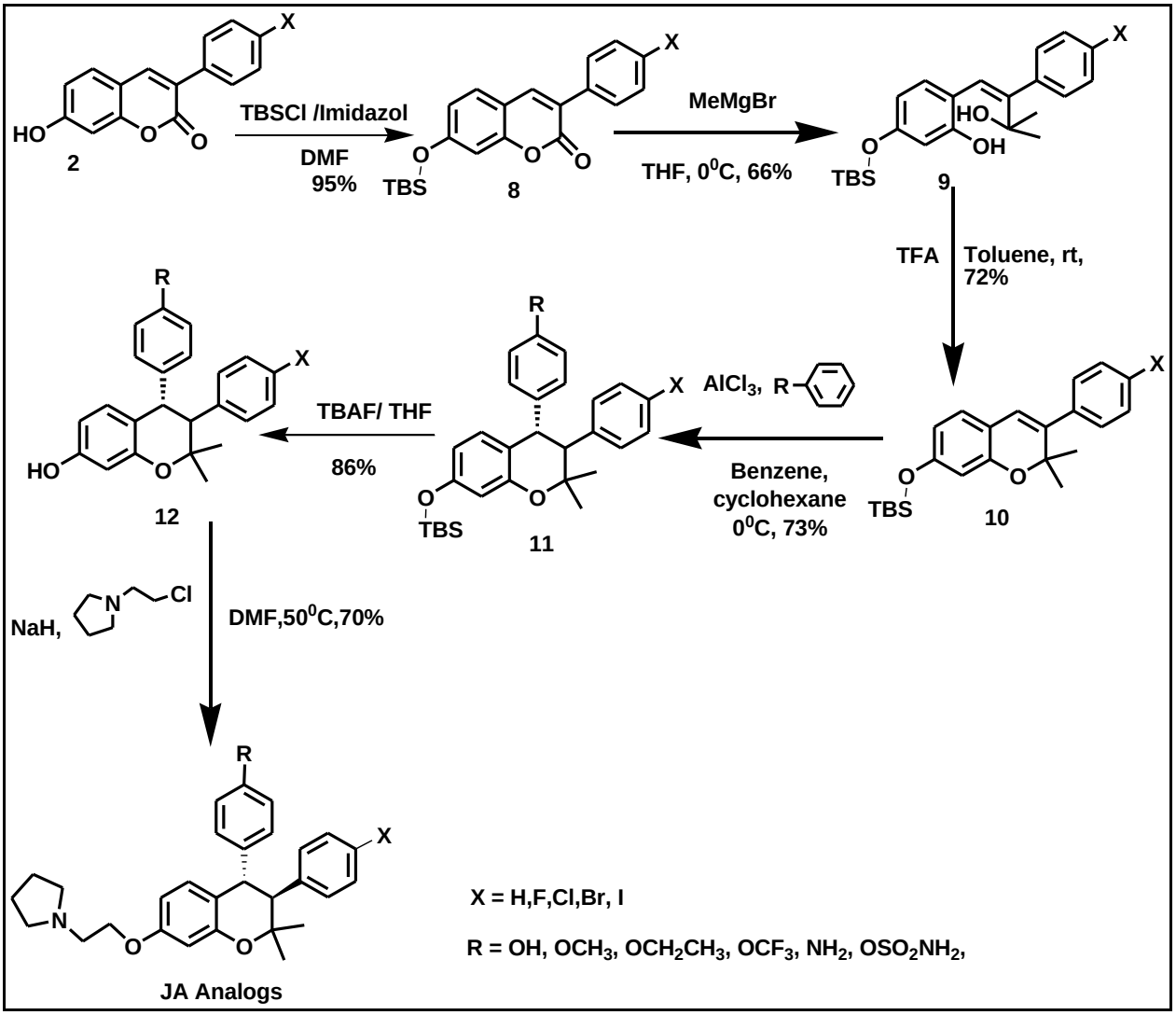

Scheme 4.1 Synthesis of ormeloxifene analogs with a pyrrolidine side chain at C-7

Table 4.2 Synthesized ormeloxifene analogs

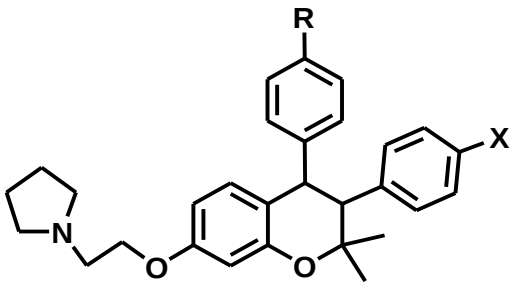

Compound	R	X
JA_15	OCF_3	H
JA_16	OCF_3	Br
JA_17	OCF_3	Cl
JA_18	OCF_3	F
JA_19	OH	H
JA_20	OCH_3	H
JA_25	NH_2	H
JA_26	CH_3	Br

4.2.4 Biological Evaluation of synthesized analogs

Treatment of ormeloxifene analogs such as **JA_15, JA_17, JA_16, JA_20, JA_18, JA_19, JA_25** and **JA_26** inhibits viability of **A2780** cells in a (10-40 mm) dose-dependent manner. The IC_{50} analogs including **JA_15, JA_17, JA_16, JA_20, JA_18, JA_19,** and **JA_26** were 9.0µM, 20.4µM, 37.6µM, 74.8µM, 74.9µM, 36.2µ, and 67.3µM respectively, after 48 hours treatment (**Table 4.3**), but **JA_25,** completely lost its inhibitory activity in (A2780) ovarian cancer cell lines. Compounds with (ethyl) pyrrolidine side chain at C-7 of Ormeloxifene scaffold such as **JA_15** showed higher inhibitory activity with IC_{50} of 9.0µM compared with ormeloxifene **(IC_{50} = 17.5µM).** However, the introduction of halogen at C-4' such as **JA_17, JA-16,** and **JA_18** (IC_{50} 20.4µM, 37.6µM, 79.7µM respectively) decreases the inhibitory activity relative to Ormeloxifene. The same compound but with phenol at C-4 such as **JA_19** (IC_{50} = 36.2µM) showed moderate inhibitory activity compared to ormeloxifene, but inhibitory activity reduced drastically when the phenol at C-4 was replaced with anisole as in **JA_20** (IC_{50} = 74.8). This an evidence that presence of anisole, at C-4 and halogens at C-4' reduces inhibitory activity in A2780 cells.

Table 4.3 MTT Cell viability results of ormeloxifene analogs on the A2780 Cell line

Compound	IC_{50} (µM)	Compound	IC_{50} (µM)
Ormeloxifene	17.5	JA_16	37.6
JA_15	9.0	JA_20	74.8
JA_17	20.4	JA_26	N/A
JA_18	79.7	JA_25	85.6

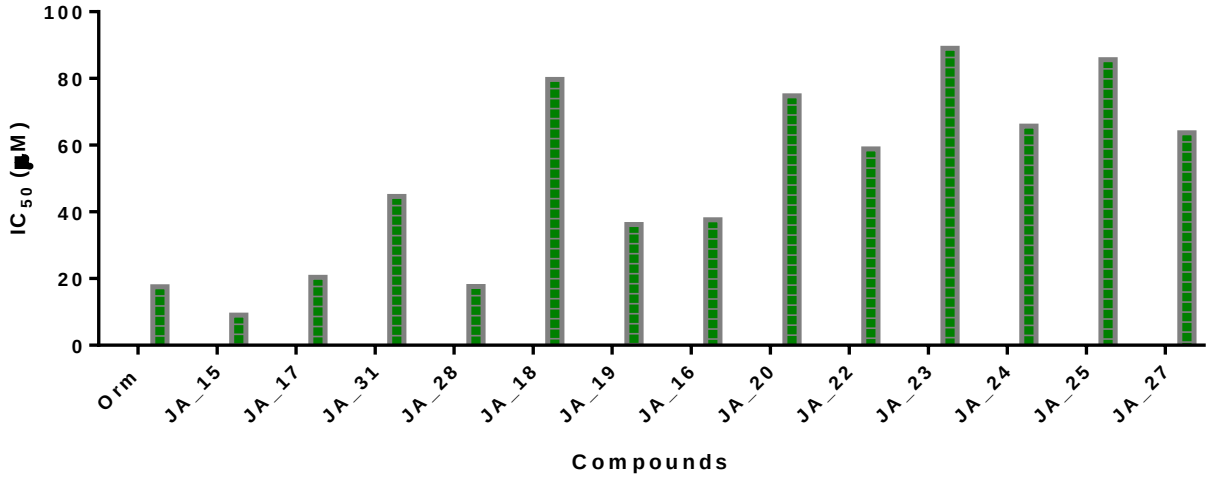

Figure 4.8 Ability of Ormeloxifene analogs to inhibit the growth of A2780 cell lines

4.2.5 Cell cycle via modulation of cell-cycle regulatory proteins

The effect of ormeloxifene analogs on ovarian cancer cell cycle distribution was determined using A2780 cells. The cells were synchronized and treated with the most active analogs **JA-15** for 24 hours, with vehicle-control as DMSO. The cell cycle analysis performed by flow cytometry revealed that **JA-15** arrest A2780 cells in the $G_0 - G_1$ phase (**Fig 4.10**), (**Table. 4.6). JA-15** showed an increase in the fraction of cells in the G_0-G_1 phase with 61.98% compared to the control with 53.42% (**Table. 4.6).** This result indicates that JA-15 has the potential to chemotherapeutic effects because it arrests (A2780) ovarian cell cycle in G0-G_1 phase[26,27]. The promising antiproliferation activity data of **JA_15** demonstrated the importance of transposition of pyrrolidine moiety to C-7 of ormeloxifene skeleton. Docking results showed that **JA-15** has a higher binding affinity than ormeloxifene. This observation coupled with biological effects can be attributed to several factors such as stereochemistry of the aromatic at C-4, type of pharmacophores at pyrrolidine side chain and the electron withdrawing functional groups at C-4''.

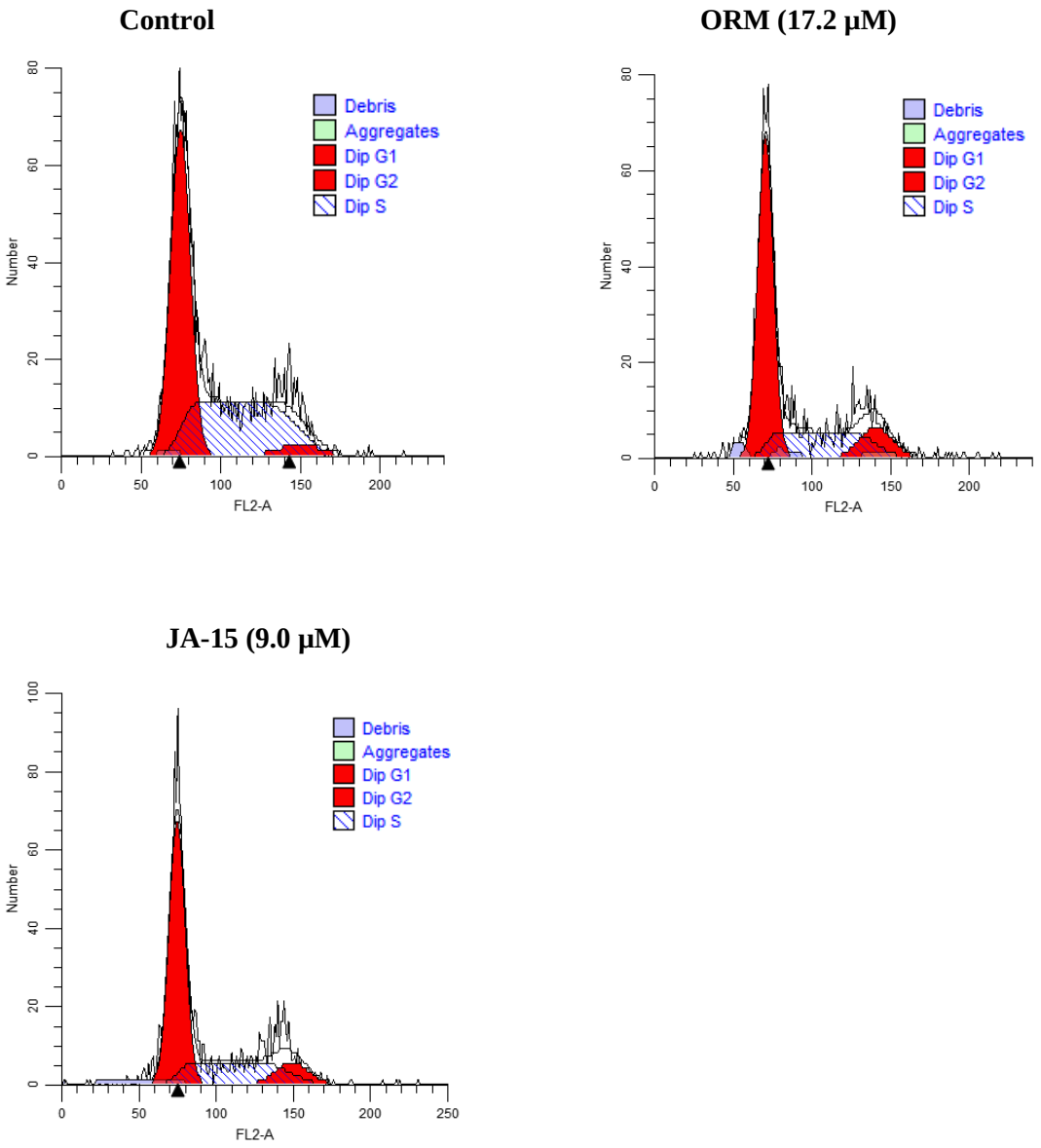

Figure 4.9. Effects of Ormeloxifene and JA-15 on cell cycle phase distribution of ovarian cancer cells

Table 4.4. Cell distribution in (A2780) ovarian cancer cells

Groups	$G_0 – G_1$	S	G_2 - M
Control	**53.42**	**43.06**	**3.52**
Orm (17.2 µM/L)	**60.69**	**27.93**	**11.38**
JA-15 (9.0 µM/L)	**61.98**	**28.07**	**9.94**

4.3 Conclusion

Ormeloxifene analogs were designed using structural based molecular modeling to installed biological important pharmacophores such as ethyl pyrrolidine at -7 and various aromatic and heterocyclic substituents at C-4 and C-7. All analogs were explored biologically to ascertain their potency towards ovarian cancer cell lines. **JA_15** performed better in cytotoxicity assays with IC_{50} of 9 µM higher than a known EGFR inhibitor Ormeloxifene. Installation of trifluromethoxybenze at the C-4 position of Ormeloxifene skeleton improved the cytotoxicity activities compared with similar compounds with anisole, aniline and phenol groups at C-4. **JA-15** caused cell cycle arrest in G_0-G_1 phase which indicates that JA-15 has the potential to chemotherapeutic effects.

4.4 Experimental section

4.4.1 General

All chemicals and solvents were purchased from Fisher Scientific, Across Chemical or Sigma Aldrich and used without further purification. All glassware used was washed, cleaned and oven dried overnight before conducting any chemical reaction. Any reaction that requires anhydrous condition were performed under argon or nitrogen environment. Pre-coated silica gel plates were used to analyze the progress and completion reaction. UV light at 254 or 365 or CAM stain was used to visualize the chemical reaction spot. All synthetic intermediates and final compounds were purified by column chromatography with 230 x 400 silica gel. Proton (^1H) and Carbon (^{13}C) NMR spectra were analyzed by Bruker Avance-400 MHz and 600 MHz NMR using D-acetone or $CDCl_3$. NMR chemical

shifts were presented in σ(PPM) using residual solvent peaks as standard ($CDCl_3$, 7.26 (H), 77.16 (C)). High-resolution mass spectrometer (HRMS) was gained using Thermo Finnigan MAT 95XL mass spectrometer at the University of Buffalo mass spectroscopy facility. All synthetic intermediate and final compounds were purified using column chromatography with 230ˣ400 mesh silica gel. ^{1}H and ^{13}C NMR spectra were using Bruker AVANCE-400 MHZ and 600 MHZ NMR spectrometer, in $CDCl_3$ and D-acetone. NMR chemical shifts were presented in σ(PPM) using residual solvent peaks as standards ($CDCl_3$, 7.26 (H), 77.16 (C)).

4.4.2 3-(4-bromophenyl)-3,4-dihydro-2,2-dimethyl-4-(4-(trifluoromethoxy)phenyl)-2H-chromen-7-ol

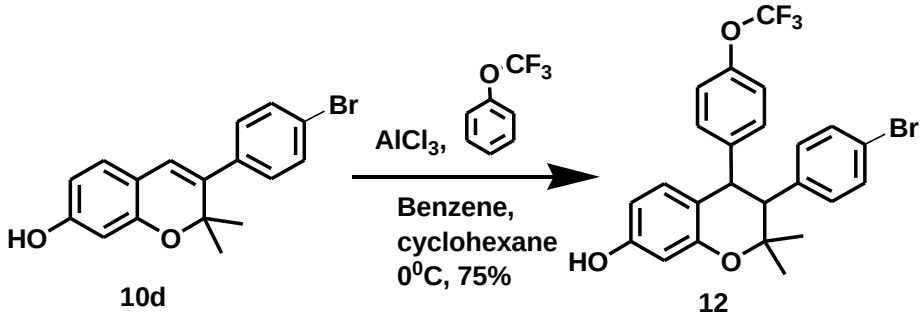

To a stirred solution of **10d** (3.30 g, 9.96 mmol) and trifluoromethyl benzene (2.80 g, 20.92 mmol) in benzene-cyclohexane mixture (1:1 ratio, 100 ml) at 0°C was added anhydrous aluminum chloride (1.6g, 11.95 mmol) in portions and stirred for 30 min. The mixture further stirred at room temperature for 8 hrs. The reaction mixture was quenched by adding a mixture of ice and conc. Hydrochloric acid (1:1 5.0 ml) and the organic layer was separated. The aqueous layer was re-extracted

three times with dichloromethane (35.0 ml). The combined extract was washed with $NaHCO_3$ (10 %, 20.0ml), dried over anhydrous Na_2SO_4, filtered and concentrated under reduced pressure. The semi-solid obtained was purified by column chromatography (70% hexane: 30% ethyl acetate) to obtain (3.69g, 75%) **12**.

^{1}H NMR (600 MHz, Chloroform-*d*) δ 8.31 – 8.25 (m, 4H), 7.87 (dd, *J* = 8.3, 1.4 Hz, 1H), 7.73 – 7.67 (m, 6H), 7.59 – 7.52 (m, 11H), 7.49 – 7.44 (m, 9H), 7.34 (ddd, *J* = 9.9, 5.7, 1.9 Hz, 10H), 7.30 – 7.24 (m, 10H), 7.20 (d, *J* = 8.5 Hz, 4H), 6.97 – 6.92 (m, 1H), 6.89 – 6.84 (m, 2H), 6.60 (s, 1H), 6.23 (s, 1H), 4.35 – 4.28 (m, 1H), 3.97 (s, 1H), 3.04 (s, 1H), 2.42 (d, *J* = 10.8 Hz, 1H), 1.61 (s, 7H). ^{13}C NMR (151 MHz, $CDCl_3$) δ 160.18, 156.03, 151.04, 151.00, 139.11, 138.25, 137.92, 133.72, 132.61, 131.93, 131.65, 131.55, 131.44, 131.38, 130.42, 130.25, 130.19, 129.88, 129.66, 129.61, 129.59, 129.57, 129.00, 128.88, 128.86, 128.67, 128.53, 128.44, 128.38, 126.40, 126.01, 121.83, 121.79, 121.66, 120.99, 120.39, 115.42, 114.83, 113.71, 104.91, 80.41, 78.87, 68.33, 47.13, 30.44, 29.79, 29.46, 27.62, 22.79.

4.4.3 1-{2-[3-(4-Bromo-phenyl)-2,2-dimethyl-4-(4-trifluoromethoxy-phenyl)-chroman-7-yloxy]-ethyl}-pyrrolidine

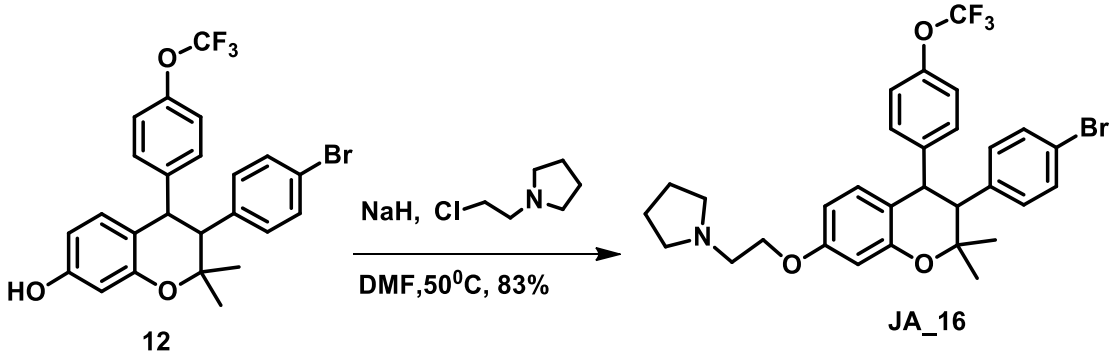

To a stirred solution of3-(4-bromophenyl)-2,2-dimethyl-4-(4-(trifluoromethoxy)phenyl)chroman-7-ol (0.20 g, 0.41 mmol) and DMF (5.0 ml) was added NaH (0.034 g, 1.43 mmol) under nitrogen atmosphere. The reaction mixture was vented with a needle for 20 min to allow the evolution of H_2 gas and then quenched with methanol (1.3 ml). After the evolution of all H_2 gas, 1-(2-chloroethyl) pyrrolidine hydrochloride (0.15g, 0.82 mmol) was added sequentially and stirred for 15 minutes. The reaction mixture was heated at 50°C overnight. After completion as indicated by TLC, the reaction mixture was quenched at 0°C by dropwise addition of $NaHCO_3$ over 20 min. It was then extracted with ethyl acetate (3x 10 ml) and the organic layer washed with water (3 x 25 ml), dried over $MgSO_4$, evaporated and purified by column chromatography (30% ethyl acetate: 70% hexane) to afford a semi-solid (0.20 g) with 83% yield**.**

1H NMR (600 MHz, Chloroform-d) δ 8.08 – 8.04 (m, 1H), 7.80 – 7.75 (m, 3H), 7.54 – 7.45 (m, 5H), 7.44 – 7.38 (m, 5H), 7.24 (s, 1H), 7.20 – 7.16 (m, 3H), 6.49 (s, 1H), 6.29 (s, 1H), 4.48 (t, J = 6.0 Hz, 1H), 4.01 (t, J = 5.8 Hz, 4H), 3.36 (s, 1H), 2.89 (t, J = 6.0 Hz, 2H), 2.64 (dq, J = 7.1, 3.7 Hz, 4H), 2.49 (t, J = 5.9 Hz, 3H), 2.32 (d, J = 6.1 Hz, 7H), 1.66 (t, J = 3.5 Hz, 10H), 1.56 (s, 7H). 13C NMR (600 MHz, CDCl3) δ 158.79, 156.60, 139.25, 138.64, 138.10, 132.89, 132.23, 131.68, 131.46, 131.37, 130.42, 129.87, 129.63, 129.48, 128.91, 128.33, 128.25, 127.99, 122.09, 121.81, 121.67, 115.53, 100.85, 79.62, 68.26, 64.24, 54.73, 54.56, 54.27, 54.18, 31.96, 29.74, 29.69, 29.40, 23.59, 23.44, 22.72, 14.17. **HR-FT-MS calcd for $C_{31}H_{31}BrF_3NO_3$ 590.47 found 590.15**

4.4.4 3,4-dihydro-2,2-dimethyl-3-phenyl-4-(4-(trifluoromethoxy)phenyl)-2H-chromen-7-ol

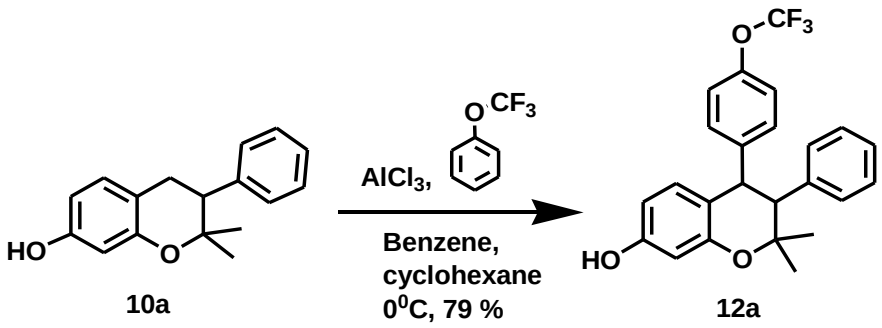

To a stirred solution of 2,2-dimethyl-3-phenyl-2H-chromen-7-ol (0.40g, 1.6mmol) and 1-(trifluoromethoxy) benzene (0.46ml, 3.40 mmol) in benzene-cyclohexane mixture (1:1 ratio, 16.0 ml) at 0°C was added anhydrous aluminum chloride (0.26g, 1.92 mmol) in portions and the mixture further stirred for 8 hrs. The reaction mixture was quenched by adding a mixture of ice and conc. Hydrochloric acid (1:1 4.0 ml) and the organic layer was separated. The aqueous layer was re-extracted three times with dichloromethane (15.0 ml). The combined extract was washed with $NaHCO_3$ (10 %, 5.0ml), dried over anhydrous Na_2SO_4, filtered and concentrated under reduced pressure. The semi-solid obtained was purified by column chromatography (70% hexane: 30% ethyl acetate) to obtain (0.52g, 79%) **12a**.

^{1}H NMR (400 MHz, Chloroform-*d*) δ 8.28 (dd, *J* = 8.3, 1.4 Hz, 1H), 7.73 – 7.67 (m, 3H), 7.62 – 7.51 (m, 5H), 7.51 – 7.44 (m, 2H), 7.36 (dd, *J* = 13.0, 2.4 Hz, 11H), 6.61 (s, 1H), 6.22 (s, 1H), 1.64 (s, 7H). ^{13}C NMR (400 MHz, $CDCl_3$) δ 160.23, 151.07, 140.38, 139.06, 138.39, 133.59, 131.66, 131.49, 130.22, 130.11, 129.50, 128.89, 128.60, 128.34, 128.31,

128.24, 128.20, 127.67, 125.89, 121.79, 121.17, 115.03, 113.60, 104.84, 80.64, 32.05, 29.84, 29.80, 29.50, 27.67, 22.82.

4.4.5 1-{2-[2,2-Dimethyl-3-phenyl-4-(4-trifluoromethoxy-phenyl)-chroman-7-yloxy]-ethyl}-pyrrolidine

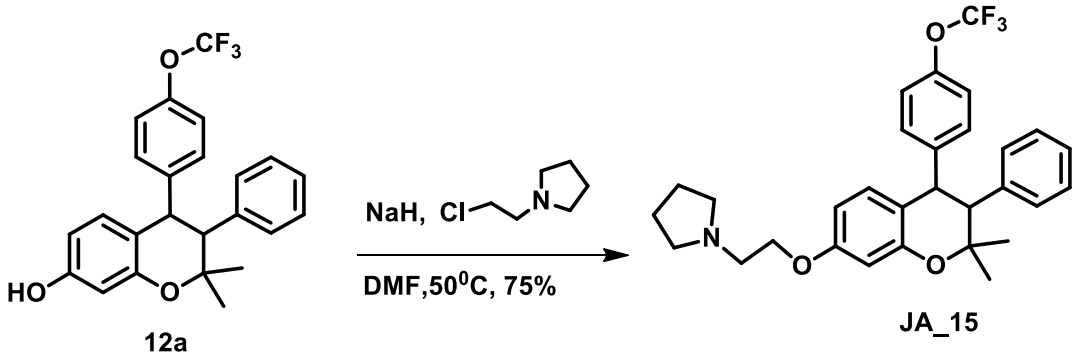

To a stirred solution of 2,2-dimethyl-3-phenyl-4-(4-(trifluoromethoxy)phenyl)chroman-7-ol (0.23 g, 0.55 mmol) and DMF (5.51 ml) was added NaH (0.046 g, 1.93 mmol) under nitrogen atmosphere. The reaction mixture was vented with a needle for 20 min to allow evolution of H_2 gas and then quenched with methanol (1.7 ml). After evolution of all H_2 gas, 1-(2-chloroethyl) pyrrolidine hydrochloride (0.147 g, 1.10 mmol) was added sequentially and stirred for 15 minutes. The reaction mixture was heated at 50°C overnight. After completion as indicated by TLC, the reaction mixture was quenched at 0°C by drop wise addition of $NaHCO_3$ over 20 min. It was then extracted with ethyl acetate (3x 15 ml) and the organic layer washed with water (3 x 35 ml) , dried over $MgSO_4$, evaporated and

purified by column chromatography (30% ethyl acetate: 70% hexane) to afford a semi-solid (0.21 g) with 75% yield**.**

1H NMR (600 MHz, Chloroform-d) δ 7.83 – 7.78 (m, 2H), 7.70 – 7.65 (m, 2H), 7.60 – 7.48 (m, 6H), 7.44 (t, J = 7.8 Hz, 3H), 7.39 – 7.33 (m, 10H), 7.32 – 7.28 (m, 6H), 7.26 (s, 2H), 6.95 (dt, J = 8.8, 1.5 Hz, 2H), 6.56 – 6.50 (m, 2H), 6.33 (s, 1H), 6.21 (s, 1H), 4.14 (t, J = 6.0 Hz, 2H), 4.03 (t, J = 5.9 Hz, 3H), 2.94 (t, J = 6.0 Hz, 2H), 2.66 (ddd, J = 6.8, 4.8, 2.7 Hz, 4H), 2.52 (t, J = 5.9 Hz, 3H), 2.37 – 2.33 (m, 5H), 2.19 (s, 1H), 1.86 – 1.81 (m, 5H), 1.69 (p, J = 3.2 Hz, 6H), 1.60 (d, J = 5.8 Hz, 15H), 1.30 (s, 9H). 13C NMR (600 MHz, CDCl3) δ 166.18, 160.19, 158.87, 158.67, 156.65, 140.38, 140.01, 139.34, 139.25, 139.01, 138.33, 132.22, 131.65, 131.49, 130.09, 129.51, 129.43, 128.83, 128.71, 128.34, 128.30, 128.25, 128.21, 128.17, 128.00, 127.78, 127.64, 127.55, 121.98, 121.31, 121.12, 120.71, 115.84, 115.02, 114.60, 113.58, 104.77, 100.86, 80.66, 79.98, 68.28, 66.95, 55.13, 54.74, 54.61, 54.23, 29.74, 27.65, 27.34, 23.52, 23.46. **HR-FT-MS calcd for $C_{30}H_{32}F_3NO_3$ 511.57 found 511.27**

4.4.6 3-(4-Fluoro-phenyl)-2,2-dimethyl-4-(4-trifluoromethoxy-phenyl)-chroman-7-ol

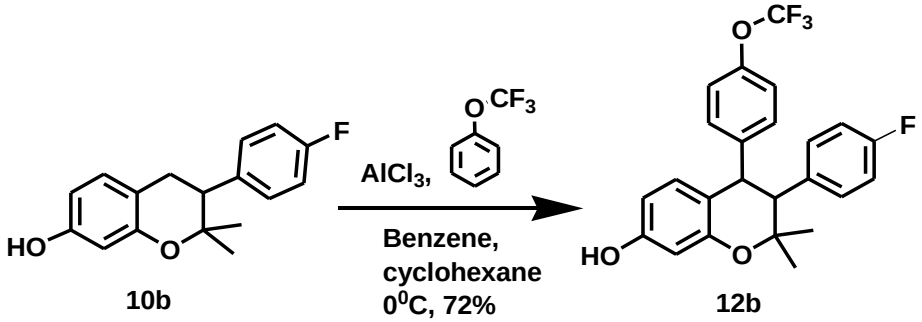

To a stirred solution of 3-(4-fluorophenyl)-3,4-dihydro-2,2-dimethyl-2H-chromen-7-ol (0.54g, 2.0 mmol) and 1-(trifluoromethoxy) benzene (0.68 g, 0.37 mmol) in benzene-cyclohexane mixture (1:1 ratio, 20.0 ml) at 0°C was added anhydrous aluminum chloride (0.32 g, 2.41 mmol) in portions and the mixture further stirred for 8 hrs. The reaction mixture was quenched by adding a mixture of ice and conc. Hydrochloric acid (1:1 3.0 ml) and the organic layer was separated. The aqueous layer was re-extracted three times with dichloromethane (8.0 ml). The combined extract was washed with $NaHCO_3$ (10 %, 5.0ml), dried over anhydrous Na_2SO_4, filtered and concentrated under reduced pressure. The semi-solid obtained was purified by column chromatography (70% hexane: 30% ethyl acetate) to obtain (0.87g, 69%) 12b.

1H NMR (600 MHz, Chloroform-d) δ 7.49 (dd, J = 26.9, 8.1 Hz, 1H), 7.34 – 7.19 (m, 4H), 7.09 – 6.98 (m, 1H), 6.97 – 6.87 (m, 2H), 4.18 (q, J = 7.2 Hz, 2H), 1.93 (d, J = 1.2 Hz, 2H), 1.59 (s, 1H), 1.40 – 1.18 (m, 6H). 13C NMR (600 MHz, CDCl3) δ 162.44, 160.81, 160.24, 156.43, 156.36, 139.34, 138.20, 135.26, 133.12, 131.08, 131.03, 130.21, 129.93, 129.55, 128.85, 128.65, 128.50, 128.40, 128.32, 128.24, 126.85, 125.81, 121.75, 121.44, 120.06, 115.48, 115.27, 115.20, 115.13, 115.10, 111.82, 111.63, 104.80, 102.96, 80.58, 60.74, 34.52, 27.53, 26.96, 26.21.

4.4.7 1-{2-[3-(4-Fluoro-phenyl)-2,2-dimethyl-4-(4-trifluoromethoxy-phenyl)-chroman-7-yloxy]-ethyl}-pyrrolidine

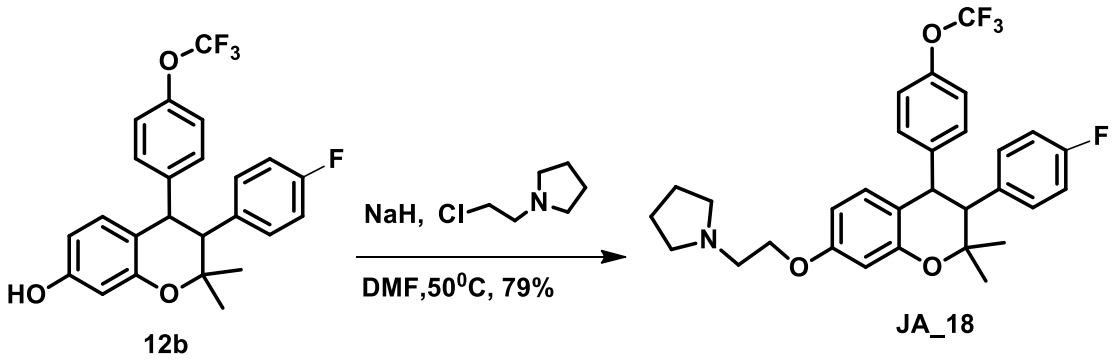

To a stirred solution of 3-(4-fluorophenyl)-2,2-dimethyl-4-(4-(trifluoromethoxy)phenyl)chroman-7-ol (0.61g, 1.41 mmol) and DMF (14.11 ml) was added NaH (0.12 g, 4.93 mmol) under nitrogen atmosphere. The reaction mixture was vented with a needle for 20 min to allow the evolution of H_2 gas and then quenched with methanol (1.1 ml). After the evolution of all H_2 gas, 1-(2-chloroethyl) pyrrolidine hydrochloride (0.38 g, 2.82 mmol) were added sequentially and stirred for 15 minutes. The reaction mixture was heated at 50°C overnight. After completion as indicated by TLC, the reaction mixture was quenched at 0°C by dropwise addition of $NaHCO_3$ over 20 min. It was then extracted with ethyl acetate (3x 20 ml) and the organic layer washed with water (3 x 40 ml), dried over $MgSO_4$, evaporated and purified by column chromatography (30% ethyl acetate: 70% hexane) to afford a semi-solid (0.59 g) with 79% yield**.**

1H NMR (600 MHz, Chloroform-d) δ 7.75 – 7.70 (m, 2H), 7.70 – 7.67 (m, 2H), 7.67 – 7.61 (m, 2H), 7.50 – 7.40 (m, 3H), 7.38 (t, J = 7.7 Hz, 2H), 7.36 – 7.26 (m, 5H),

7.21 – 7.15 (m, 4H), 7.07 (d, J = 8.1 Hz, 2H), 7.03 – 6.92 (m, 6H), 6.92 – 6.85 (m, 4H), 6.85 – 6.79 (m, 3H), 6.52 – 6.44 (m, 1H), 6.39 (s, 1H), 6.18 (s, 1H), 4.13 – 3.98 (m, 6H), 3.92 (t, J = 5.8 Hz, 2H), 3.27 (d, J = 3.3 Hz, 2H), 2.89 – 2.77 (m, 5H), 2.60 – 2.52 (m, 9H), 2.47 – 2.39 (m, 2H), 2.24 (d, J = 6.0 Hz, 3H), 1.96 (s, 2H), 1.86 – 1.78 (m, 2H), 1.73 (qd, J = 6.6, 2.7 Hz, 10H), 1.57 (p, J = 3.2 Hz, 4H), 1.46 (s, 4H), 1.22 – 1.12 (m, 9H), 0.78 (dq, J = 12.1, 6.5 Hz, 3H). 13C NMR (600 MHz, CDCl3) δ 162.53, 160.90, 155.92, 155.81, 151.34, 149.98, 148.15, 145.30, 135.21, 131.10, 131.05, 130.07, 129.67, 128.90, 128.51, 128.45, 128.37, 126.90, 125.86, 125.44, 120.53, 115.68, 115.49, 115.35, 115.21, 111.92, 111.57, 103.05, 80.66, 61.02, 46.69, 44.71, 39.50, 39.20, 37.24, 34.58, 32.07, 29.86, 29.81, 29.51, 27.03, 26.28, 22.83, 21.10. **HR-FT-MS calcd for $C_{30}H_{31}F_4NO_3$ 529.56 found 529.20**

4.4.8 3-(4-chlorophenyl)-3,4-dihydro-2,2-dimethyl-4-(4-(trifluoromethoxy)phenyl)-2H-chromen-7-ol

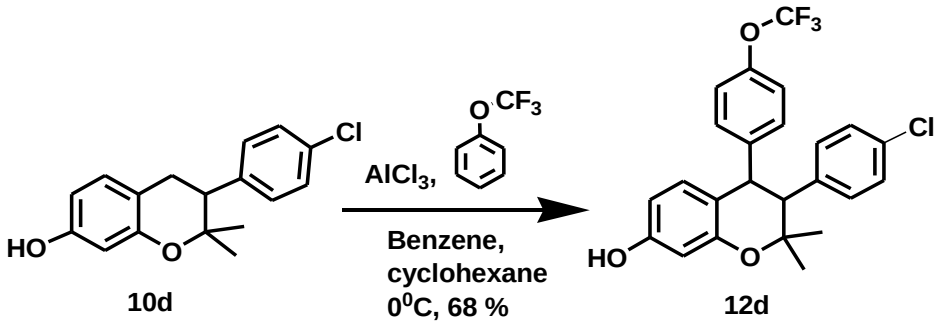

To a stirred solution of 3-(4-chlorophenyl)-3,4-dihydro-2,2-dimethyl-2H-chromen-7-ol (0.41g, 2.4 mmol) and 1-(trifluoromethoxy) benzene (0.39 g, 2.97 mmol) in benzene-cyclohexane mixture (1:1 ratio, 15.0 ml) at 0°C was added anhydrous aluminum chloride

(0.23 g, 1.69 mmol) in portions and the mixture further stirred for 8 hrs. The reaction mixture was quenched by adding a mixture of ice and conc. Hydrochloric acid (1:1 4.0 ml) and the organic layer was separated. The aqueous layer was re-extracted three times with dichloromethane (15.0 ml). The combined extract was washed with $NaHCO_3$ (10 %, 5.0ml), dried over anhydrous Na_2SO_4, filtered and concentrated under reduced pressure. The semi-solid obtained was purified by column chromatography (70% hexane: 30% ethyl acetate) to obtain (0.75g, 68%) 12d.

^{1}H NMR (600 MHz, Chloroform-*d*) δ 7.81 – 7.76 (m, 1H), 7.68 (dt, *J* = 7.0, 1.4 Hz, 1H), 7.51 (d, *J* = 7.8 Hz, 2H), 7.47 (d, *J* = 8.3 Hz, 3H), 7.35 – 7.28 (m, 5H), 7.23 (ddd, *J* = 10.7, 8.3, 4.9 Hz, 11H), 7.08 – 7.03 (m, 2H), 6.96 – 6.89 (m, 8H), 6.79 (d, *J* = 8.4 Hz, 1H), 6.66 (d, *J* = 2.5 Hz, 1H), 6.60 – 6.57 (m, 1H), 4.76 (s, 1H), 4.18 (q, *J* = 7.2 Hz, 9H), 2.09 (s, 14H). ^{13}C NMR (151 MHz, $CDCl_3$) δ 160.81, 160.24, 156.43, 156.36, 151.25, 150.07, 148.09, 145.28, 138.20, 135.26, 133.12, 131.08, 131.03, 130.21, 129.93, 129.55, 128.85, 128.65, 128.50, 128.40, 128.32, 128.24, 126.85, 125.81, 125.36, 121.75, 121.44, 120.06, 115.48, 115.27, 115.20, 115.13, 115.10, 111.82, 111.63, 104.80, 102.96, 80.58, 60.74, 46.62, 44.64, 34.52, 27.53, 26.96, 26.21, 21.03.

4.4.9 1-{2-[3-(4-Chloro-phenyl)-2,2-dimethyl-4-(4-trifluoromethoxy-phenyl)-chroman-7-yloxy]-ethyl}-pyrrolidine

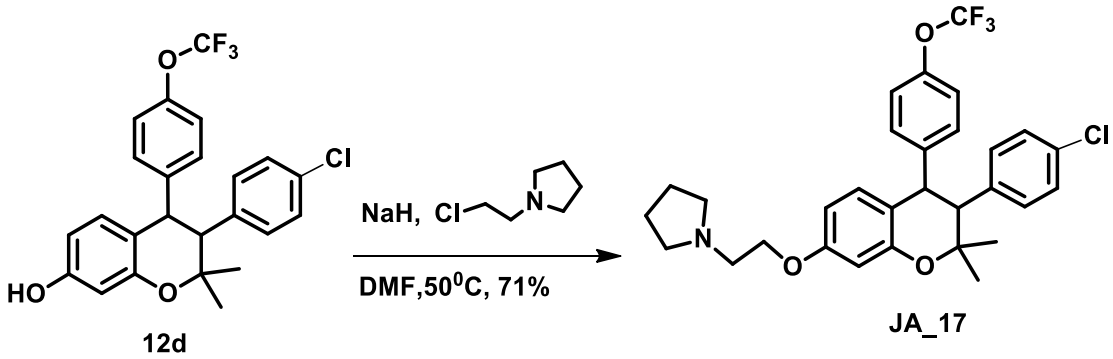

To a stirred solution of 3-(4-chlorophenyl)-2,2-dimethyl-4-(4-(trifluoromethoxy)phenyl)chroman-7-ol (0.16g, 0.35 mmol) and DMF (3.46ml) was added NaH (0.03 g, 1.21 mmol) under nitrogen atmosphere. The reaction mixture was vented with a needle for 20 min to allow evolution of H_2 gas and then quenched with methanol (1.00 ml). After evolution of all H_2 gas, 1-(2-chloroethyl) pyrrolidine hydrochloride (0.09 g, 0.69 mmol) was added sequentially and stirred for 15 minutes. The reaction mixture was heated at 50°C overnight. After completion as indicated by TLC, the reaction mixture was quenched at 0°C by drop wise addition of $NaHCO_3$ over 20 min. It was then extracted with ethyl acetate (3x 10 ml) and the organic layer washed with water (3 x 15 ml) , dried over $MgSO_4$, evaporated and purified by column chromatography (30% ethyl acetate: 70% hexane) to afford a semi-solid (0.13 g) with 71% yield**.**

1H NMR (600 MHz, Chloroform-d) δ 7.78 (dq, J = 6.9, 1.8 Hz, 2H), 7.56 – 7.50 (m, 1H), 7.45 – 7.39 (m, 3H), 7.36 – 7.31 (m, 3H), 7.27 – 7.22 (m, 3H), 6.49 (s, 1H), 6.30 (s, 1H), 4.02 (t, J = 5.9 Hz, 3H), 2.52 (t, J = 5.9 Hz, 3H), 2.42 – 2.28 (m, J = 3.9, 2.7 Hz, 5H), 1.68 (p, J = 3.2 Hz, 5H), 1.57 (s, 7H). 13C NMR (600 MHz, CDCl3) δ 158.77, 156.59,

139.24, 138.67, 137.65, 133.52, 132.27, 129.57, 129.49, 128.90, 128.42, 128.01, 122.05, 121.81, 115.55, 100.85, 79.72, 68.21, 54.55, 54.17, 27.25, 23.43. **HR-FT-MS calcd for $C_{30}H_{31}ClF_3NO_3$ 546.02 found 546.23**

4.4.10 1-[2-(2,2-Dimethyl-3-phenyl-2H-chromen-7-yloxy)-ethyl]-pyrrolidine

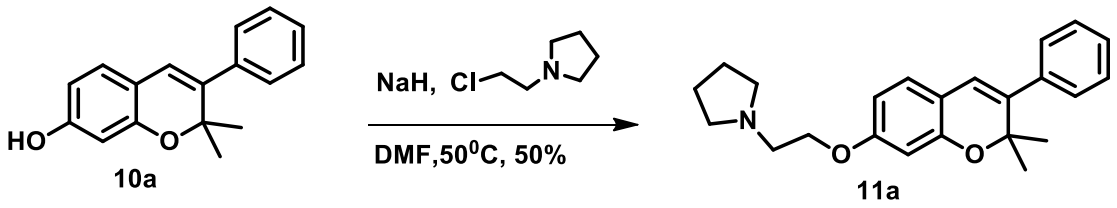

To a stirred solution of 2,2-dimethyl-3-phenyl-2H-chromen-7-ol (0.13 g, 0.35 mmol) and DMF (5.0 ml) was added NaH (0.04 g, 1.73 mmol) under nitrogen atmosphere. The reaction mixture was vented with a needle for 20 min to allow the evolution of H_2 gas and then quenched with methanol (0.50 ml). After the evolution of all H_2 gas, 1-(2-chloroethyl) pyrrolidine hydrochloride (0.13 g, 0.99 mmol)were added sequentially and stirred for 15 minutes. The reaction mixture was heated at 50°C overnight. After completion as indicated by TLC, the reaction mixture was quenched at 0°C by dropwise addition of $NaHCO_3$ over 20 min. The mixture was extracted with ethyl acetate (3x 15 ml) and the organic layer washed with water (3 x 10 ml), dried over $MgSO_4$, evaporated and purified by column chromatography (30% ethyl acetate: 70% hexane) to afford a semi-solid (0.17 g) with 50% yield.

1H NMR (600 MHz, Chloroform-d) δ 7.26 – 7.17 (m, 5H), 6.87 – 6.82 (m, 1H), 6.38 (d, J = 7.7 Hz, 2H), 6.18 (s, 1H), 4.00 (t, J = 6.0 Hz, 2H), 2.80 (t, J = 6.0 Hz, 2H), 2.55 – 2.50 (m, 4H), 1.74 – 1.69 (m, 5H), 1.43 (s, 6H). 13C NMR (600 MHz, CDCl3) δ 159.96, 153.68, 139.71, 139.19, 128.21, 128.11, 127.25, 127.11, 122.01, 116.27, 107.78, 102.69, 78.91, 67.18, 55.05, 54.72, 54.20, 53.91, 29.75, 29.71, 29.41, 27.07, 23.52, 23.50, 22.74.

4.4.11 1-{2-[4-(4-Methoxy-phenyl)-2,2-dimethyl-3-phenyl-chroman-7-yloxy]-ethyl}-pyrrolidine

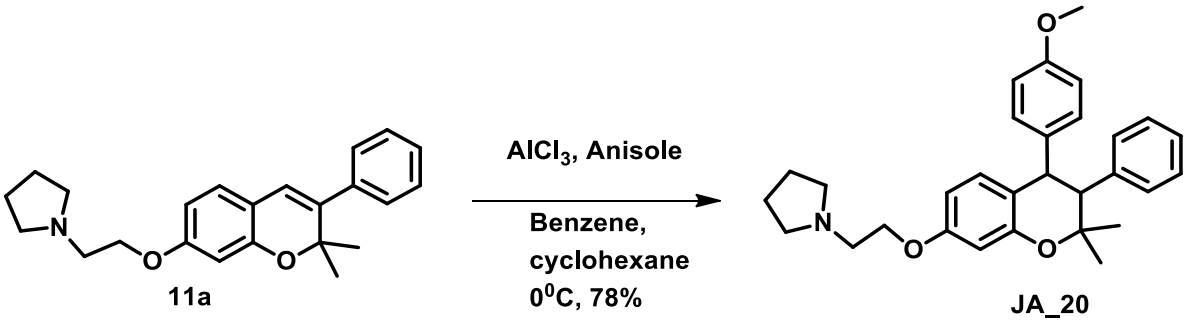

To a stirred solution of1-(2-((2,2-dimethyl-3-phenyl-2H-chromen-7-yl)oxy)ethyl)pyrrolidine (0.23 g, 0.69 mmol) and anisole (0.14 g, 1.25 mmol) in benzene-cyclohexane mixture (1:1 ratio, 4 ml) at 0°C was added anhydrous aluminum chloride (0.33 g, 2.46 mmol) in portions. A solution of anisole (0.34 g, 3.14 mmol) in benzene-cyclohexane mixture (1:1 Ratio, 6.00 ml) was added after 30 min, and the mixture further stirred for 8 hrs. The reaction mixture was quenched by adding a mixture of ice and conc. Hydrochloric acid (1:1 2.0 ml) and the organic layer was separated. The aqueous layer was re-extracted three times with dichloromethane (10 ml). The combined extract was washed with $NaHCO_3$ (10 %, 8ml), dried over anhydrous Na_2SO_4, filtered and concentrated under

reduced pressure. The semi-solid obtained was purified by column chromatography (70% hexane: 30% ethyl acetate) to obtain the titled compound.

1H NMR (400 MHz, Chloroform-d) δ 7.27 – 7.23 (m, 2H), 7.22 – 7.12 (m, 9H), 7.12 – 7.03 (m, 11H), 7.03 – 6.99 (m, 4H), 6.82 – 6.71 (m, 6H), 6.70 (d, J = 2.5 Hz, 2H), 6.57 – 6.47 (m, 3H), 6.30 (qd, J = 8.7, 4.3 Hz, 3H), 4.00 (q, J = 7.1 Hz, 4H), 3.65 (t, J = 1.8 Hz, 1H), 3.65 – 3.58 (m, 3H), 3.58 – 3.47 (m, 3H), 2.46 – 2.39 (m, 1H), 1.91 (s, 5H), 1.37 – 1.22 (m, 11H). 13C NMR (400 MHz, CDCl3) δ 163.06, 158.06, 153.75, 139.27, 137.39, 137.21, 130.10, 127.48, 122.69, 115.46, 108.62, 103.87, 92.73, 78.57, 36.83, 31.97, 31.79, 29.74, 29.70, 29.41, 27.00,23.68, 23.67, 22.73. **HR-FT-MS calcd for $C_{30}H_{35}NO_3$ 457.60 found 457.25**

4.4.12 4-[2,2-Dimethyl-3-phenyl-7-(2-pyrrolidin-1-yl-ethoxy)-chroman-4-yl]-phenol

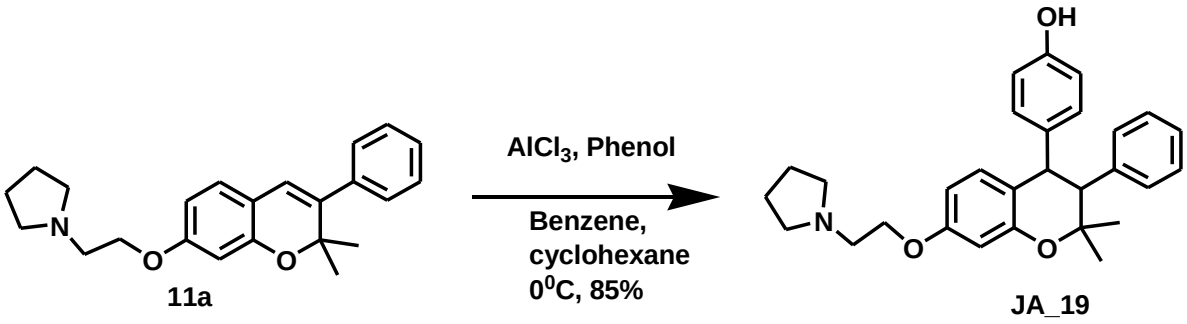

To a stirred solution of1-(2-((2,2-dimethyl-3-phenyl-2H-chromen-7-yl)oxy)ethyl)pyrrolidine (0.09 g, 0.25 mmol) and phenol (0.034 g, 0.37 mmol) in benzene-cyclohexane mixture (1:1 ratio, 3.0 ml) at 0°C was added anhydrous aluminum chloride (0.040 g, 0.29 mmol) in portions. A solution of phenol (0.004 g, 0.015 mmol) in benzene-cyclohexane mixture (1:1 Ratio, 2.0 ml) was added after 30 min and the mixture further

stirred for 8 hrs. The reaction mixture was quenched by adding a mixture of ice and conc. Hydrochloric acid (1:1 1.0 ml) and the organic layer was separated. The aqueous layer was re-extracted three times with dichloromethane (8.0 ml). The combined extract was washed with $NaHCO_3$ (10 %, 3.0ml), dried over anhydrous Na_2SO_4, filtered and concentrated under reduced pressure. The semi-solid obtained was purified by column chromatography (70% hexane: 30% ethyl acetate) to obtain (0.092g, 85%) the titled compound.

1H NMR (400 MHz, DMSO-d6) δ 9.08 (s, 1H), 7.35 – 7.25 (m, 2H), 7.20 (t, J = 7.5 Hz, 2H), 7.13 (dd, J = 7.3, 1.4 Hz, 1H), 6.91 – 6.81 (m, 2H), 6.54 – 6.43 (m, 3H), 6.41 – 6.30 (m, 2H), 4.42 (d, J = 12.4 Hz, 1H), 3.69 (s, 3H), 3.37 (s, 4H), 2.51 (p, J = 1.9 Hz, 4H), 1.26 (s, 3H), 1.16 (s, 3H). 13C NMR (400 MHz, CDCl3) δ 158.56, 155.31, 153.41, 139.39, 131.28133.78, 129.86, 122.58, 127.70, 118.86, 114.83, 101.06, 77.84, 55.42, 54.93, 28.54, 19.90. **HR-FT-MS calcd for $C_{29}H_{33}NO_3$ 443.57 found 443.35**

4.5 Molecular docking

A virtual library of 800 analogs including ormeloxifene and a standard drug were designed using ChemDraw. Energy minimization, employing MMFF94 in ChemOffice, calculated the most stable conformation for each analog. Each analog was saved in .pdb format and compiled into a library of ligands. The compiled .pdb files were processed and used as input for Omega2, an OpenEye Scientific Software ® program that generates multi-conformer structures for each ligand in the library to enhance ligand flexibility in an otherwise ridged model. The processed files were compiled into a .oeb.gz file. Protein

kinase targets (EGFR, GSK3B, CDK2, mTOR, Akt, β-catenin, etc.) were downloaded from Protein Data Bank website in.pdb.gz format and were processed using Make Receptor, and the resulting protein receptor file was saved in.oeb.gz format. Docking was conducted using Open Eye Scientific Software ® including fast exhaustive docking (FRED), Omega and VIDA.

4.6 MTT Assay

Cell proliferation was determined by MTT assay. Briefly, 5 X 10^6 cells of (A2780) were plated in 96 well plates and incubated for 24 hours at 37°C containing 5% of CO_2. Cells were treated with various analogs of ormeloxifene for 24 hours. 20µL of 50 mg/mL MTT was added in each well containing 100 mL of cell media. The cells were incubated for a further 6 hours, and the media was replaced with 150 mL of DMSO. Plates vigorously shaken for 15 minutes and absorbance was taken at 570 nm on a microplate reader.

4.7 Cell Cycle analysis

Cell distribution of ormeloxifene analogs on A2780 cell lines were determined by cell cycle analysis. The cells were seeded as $2.5x10^5$ cells/mL in a 6-well plate (2 mL/well) and allowed to adhere overnight at 37 °C and 5% CO_2. The cells were incubated with **JA-15** (9.0 µM) and DMSO (0.001%) as a control for 24 h. The cells were washed twice with ice-cold 1X PBS (Hyclone™ Laboratories, Inc) and collected after trypsinization[28]. The cell pellet was washed two times with ice-cold 1X PBS and fixed with ice-cold 70% ethanol overnight at -20 °C. After that, the cells were washed once with ice-cold PBS and the second wash with ice-cold PBS-2% FBS. The cell pellet was re-suspended in 500µL

propidium iodide (PI)/RNase staining solution (BD Biosciences) and 0.1% Triton x-100 for 30 min. at room temperature in the dark and analyzed within one h by flow cytometer (BD Accuri C6, Becton-Dickinson, Mountain View, CA). Data were analyzed by MFLT32 software, and 10,000 events with slow flow rate were recorded for each sample[29,30]

4.8 References

1. Parkin, D. M.; Bray, F.; Ferlay, J.; Pisani, P., Global cancer statistics, 2002. *CA: a cancer journal for clinicians* **2005,** *55* (2), 74-108.

2. Siegel, R.; Ma, J.; Zou, Z.; Jemal, A., Cancer statistics, 2014. *CA: a cancer journal for clinicians* **2014,** *64* (1), 9-29.

3. Jemal, A.; Siegel, R.; Ward, E.; Hao, Y.; Xu, J.; Murray, T.; Thun, M. J., Cancer statistics, 2008. *CA: a cancer journal for clinicians* **2008,** *58* (2), 71-96.

4. Hennessy, B. T.; Coleman, R. L.; Markman, M., Ovarian cancer. *The Lancet* **2009,** *374* (9698), 1371-1382.

5. Weiss, N. S.; Homonchuk, T.; Young, J. L., Incidence of the histologic types of ovarian cancer: the US Third National Cancer Survey, 1969–1971. *Gynecologic Oncology* **1977,** *5* (2), 161-167.

6. Srivastava, V. K.; Gara, R. K.; Bhatt, M.; Sahu, D.; Mishra, D. P., Centchroman inhibits proliferation of head and neck cancer cells through the modulation of PI3K/mTOR pathway. *Biochemical and biophysical research communications* **2011,** *404* (1), 40-45.

7. Huang, S.; Houghton, P. J., Targeting mTOR signaling for cancer therapy. *Current opinion in pharmacology* **2003,** *3* (4), 371-377.

8. Fleming, J. S.; Beaugié, C. R.; Haviv, I.; Chenevix-Trench, G.; Tan, O. L., Incessant ovulation, inflammation and epithelial ovarian carcinogenesis: revisiting old hypotheses. *Molecular and cellular endocrinology* **2006,** *247* (1), 4-21.

9. Kinkel, K.; Lu, Y.; Mehdizade, A.; Pelte, M.-F.; Hricak, H., Indeterminate ovarian mass at US: incremental value of second imaging test for characterization—meta-analysis and Bayesian analysis. *Radiology* **2005,** *236* (1), 85-94.

10. Burges, A.; Schmalfeldt, B., Ovarian cancer: diagnosis and treatment. *Deutsches Ärzteblatt International* **2011,** *108* (38), 635.

11. Agarwal, R.; Kaye, S. B., Ovarian cancer: strategies for overcoming resistance to chemotherapy. *Nature Reviews Cancer* **2003,** *3* (7), 502.

12. Monk, B., A randomized phase III study of trabectedin with pegylated liposomal doxorubicin (PLD) versus PLD in relapsed, recurrent ovarian cancer (OC). *CURRENT TREATMENT OPTIONS IN ONCOLOGY* **2008,** *9* (1), 30-30.

13. Dinh, P.; Harnett, P.; Piccart-Gebhart, M. J.; Awada, A., New therapies for ovarian cancer: cytotoxics and molecularly targeted agents. *Critical reviews in oncology/hematology* **2008,** *67* (2), 103-112.

14. Darcy, K. M.; Schilder, R. J., Relevant molecular markers and targets. *Gynecologic oncology* **2006,** *103* (2), 6-13.

15. Maher, D. M.; Khan, S.; Nordquist, J. L.; Ebeling, M. C.; Bauer, N. A.; Kopel, L.; Singh, M. M.; Halaweish, F.; Bell, M. C.; Jaggi, M., Ormeloxifene efficiently inhibits ovarian cancer growth. *Cancer letters* **2015,** *356* (2), 606-612.

16. Nigam, M.; Ranjan, V.; Srivastava, S.; Sharma, R.; Balapure, A. K., Centchroman induces G0/G1 arrest and caspase-dependent apoptosis involving mitochondrial membrane depolarization in MCF-7 and MDA MB-231 human breast cancer cells. *Life sciences* **2008,** *82* (11-12), 577-590.

17. Khan, S.; Ebeling, M. C.; Chauhan, N.; Thompson, P. A.; Gara, R. K.; Ganju, A.; Yallapu, M. M.; Behrman, S. W.; Zhao, H.; Zafar, N., Ormeloxifene suppresses desmoplasia and enhances sensitivity of gemcitabine in pancreatic cancer. *Cancer research* **2015**, canres. 2397.2014.

18. Hafeez, B. B.; Ganju, A.; Sikander, M.; Kashyap, V. K.; Hafeez, Z. B.; Chauhan, N.; Malik, S.; Massey, A. E.; Tripathi, M. K.; Halaweish, F. T., Ormeloxifene suppresses prostate tumor growth and metastatic phenotypes via inhibition of oncogenic β-catenin signaling and EMT progression. *Molecular cancer therapeutics* **2017**, molcanther. 0157.2017.

19. Ravibabu, K.; Palla, J.; Chintada, G. S., A study of efficacy of ormeloxifene in the pharmacological management of dysfunctional uterine bleeding. *Journal of clinical and diagnostic research: JCDR* **2013,** *7* (11), 2534.

20. Kellenberger, E.; Rodrigo, J.; Muller, P.; Rognan, D., Comparative evaluation of eight docking tools for docking and virtual screening accuracy. *Proteins: Structure, Function, and Bioinformatics* **2004,** *57* (2), 225-242.

21. McGann, M., FRED pose prediction and virtual screening accuracy. *Journal of chemical information and modeling* **2011,** *51* (3), 578-596.

22. Schulz-Gasch, T.; Stahl, M., Binding site characteristics in structure-based virtual screening: evaluation of current docking tools. *Journal of molecular modeling* **2003,** *9* (1), 47-57.

23. Zhao, Y.; Rodrigo, J.; Hoveyda, A. H.; Snapper, M. L., Enantioselective silyl protection of alcohols catalysed by an amino-acid-based small molecule. *Nature* **2006,** *443* (7107), 67.

24. Nevado, C.; Echavarren, A. M., Intramolecular hydroarylation of alkynes catalyzed by platinum or gold: Mechanism and endo selectivity. *Chemistry–A European Journal* **2005,** *11* (10), 3155-3164.

25. Bajwa, J. S.; Vivelo, J.; Slade, J.; Repič, O.; Blacklock, T., Selective deprotection of alkyl t-butyldimethylsilyl ethers in the presence of aryl t-butyldimethylsilyl ethers with bismuth bromide. *Tetrahedron Letters* **2000,** *41* (32), 6021-6024.

26. Gupta, S.; Hussain, T.; Mukhtar, H., Molecular pathway for (−)-epigallocatechin-3-gallate-induced cell cycle arrest and apoptosis of human prostate carcinoma cells. *Archives of biochemistry and biophysics* **2003,** *410* (1), 177-185.

27. Johnson, J. J.; Petiwala, S. M.; Syed, D. N.; Rasmussen, J. T.; Adhami, V. M.; Siddiqui, I. A.; Kohl, A. M.; Mukhtar, H., α-Mangostin, a xanthone from mangosteen fruit, promotes cell cycle arrest in prostate cancer and decreases xenograft tumor growth. *Carcinogenesis* **2011,** *33* (2), 413-419.

28. Rasmussen, J. G.; Frøbert, O.; Pilgaard, L.; Kastrup, J.; Simonsen, U.; Zachar, V.; Fink, T., Prolonged hypoxic culture and trypsinization increase the pro-angiogenic potential of human adipose tissue-derived stem cells. *Cytotherapy* **2011,** *13* (3), 318-328.

29. Gerdes, J.; Lemke, H.; Baisch, H.; Wacker, H.-H.; Schwab, U.; Stein, H., Cell cycle analysis of a cell proliferation-associated human nuclear antigen defined by the monoclonal antibody Ki-67. *The journal of immunology* **1984,** *133* (4), 1710-1715.

30. Nunez, R., DNA measurement and cell cycle analysis by flow cytometry. *Current issues in molecular biology* **2001,** *3*, 67-70.

Chapter 5

Design, synthesis and biological evaluations of selective estrogen receptor modulators analogs with 4-(3-hydroxypropyl) phenol and (E)-4-(3-hydroxyprop-1-en-1-yl) phenol at C-7 targeting EGFR pathway towards the treatment of ovarian cancer.

5 Introduction

5.1 Estrogen

Estrogens are class of naturally occurring sex hormones that are synthesized from cholesterol and are secreted by the ovaries. One of the most predominant intracellular estrogens is known to be 17β-estradiol (**Fig 5.1**). They are critical to the function of the female reproductive system as well as healthy breast epithelium[1]. Estrogen has other essential effects on the heart[2] and bones[3]. There is evidence that estrogen influence the part of the brain that regulates body temperature and enables the vaginal linings to stay thick and lubricated[4]. Loss of estrogen especially at the onset of menopause in women results in hot flashes and night sweats, a rise in low-density lipoprotein (LDL) cholesterol and other cardiovascular changes which usually leads to progressively increased in coronary diseases and heart attacks as well as an increase in bone loss. At this stage, most women compensate for the loss of estrogen by taking hormone replacement therapy (HRT), which effectively reduces the osteoporotic fractures and suppresses severe menopausal symptoms[5].

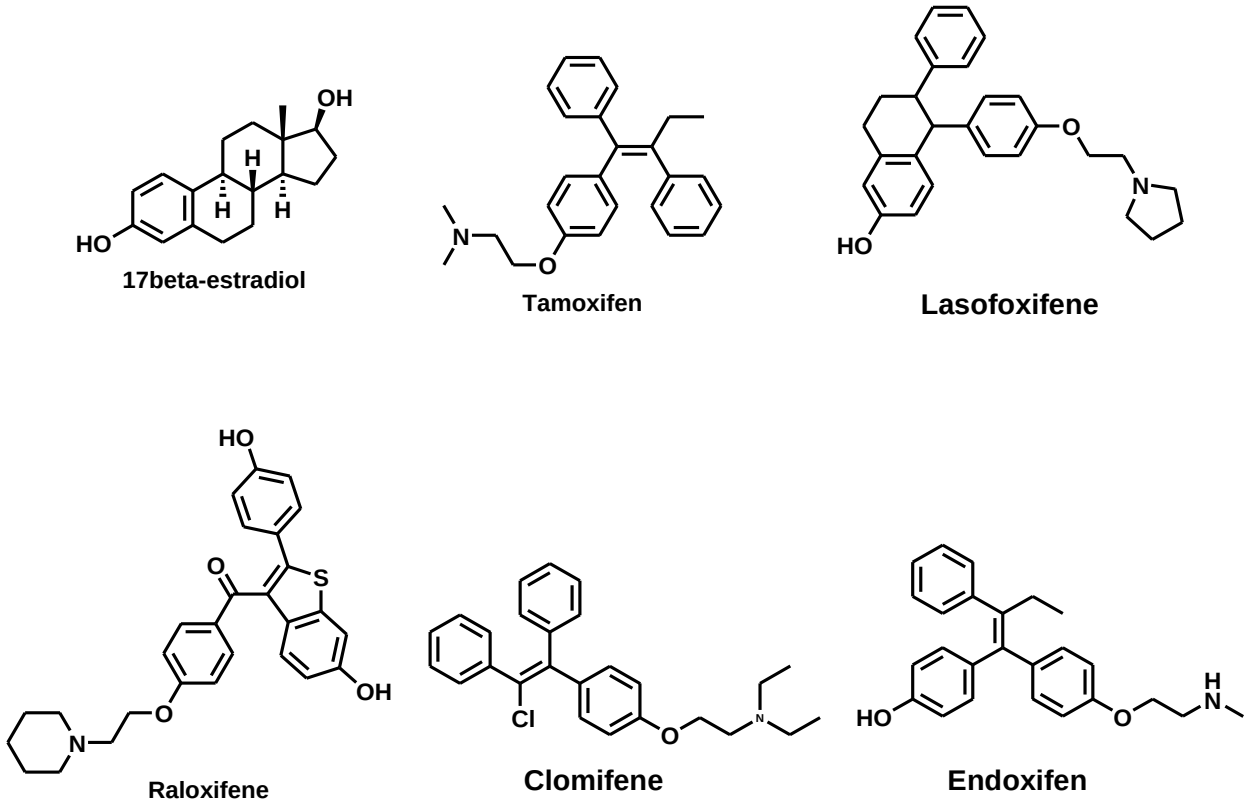

Figure 5.1 Chemical structure of 17β-estradiol and the SERM'S

The two major isoforms of the estrogen receptor (ER) (**Fig 5-2**) are ERα and ERβ. They are involved in a wide range of physiological processes such as the development of the female reproductive system, protection of cardiovascular tissue and the central nervous system[6]. Deregulation of ER signaling within breast, ovarian and the uterine tissue has been associated with the onset of cancerous tumors in these organs and has led to the investigation and development of antiestrogenic therapies[7]. ERα and ERβ are encoded by two essential genes that are located on distinct chromosomes, and each is responsible for the regulation of specific tissue effects[8]. The ER isoforms consist of different domains such as activated function (AF) domains, AF-1 (A/B domain) and AF-2 (E/F domain), which

facilitates transcriptional activation of the receptor. It has a DNA binding domain (C domain) that influence ER binding to DNA and a hinge region (D domain) which contains the nuclear delocalization signal (**Fig 5.3**). The role of ERα in breast cancer initiation and progression has been well established. However, little is known about its role in ovarian and endometrial cancers[9]. The role of ERβ on all cancers, on the other hand, remain unclear, but studies have shown that they are associated with elevated cell proliferation markers, Ki67, and cyclin A, in human breast cancer [10,11].

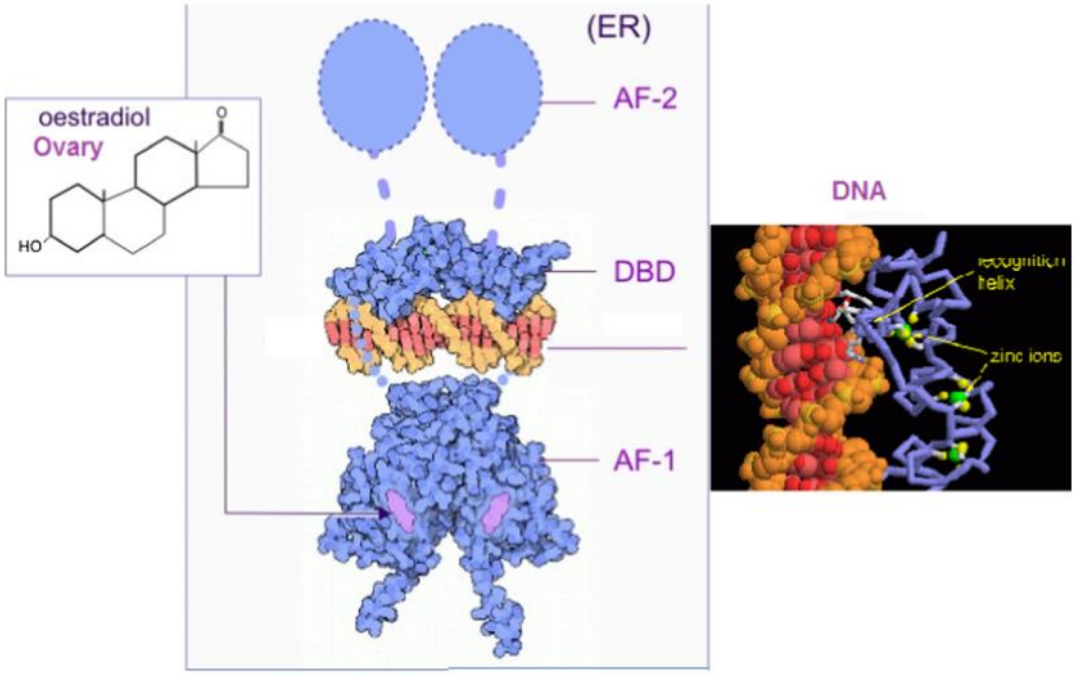

AF-1: Activation Factor 1, AF-2: Activation Factor 2, DBD: Drug Binding Domain

Begam, A. J.; Jubie, S.; Nanjan, M., Estrogen receptor agonists/antagonists in breast cancer therapy: A critical review. Bioorganic chemistry 2017, 71, 257-274.

Figure 5.2 Structure of estrogen receptor (ER) showing various structural domains at both N and C terminals.

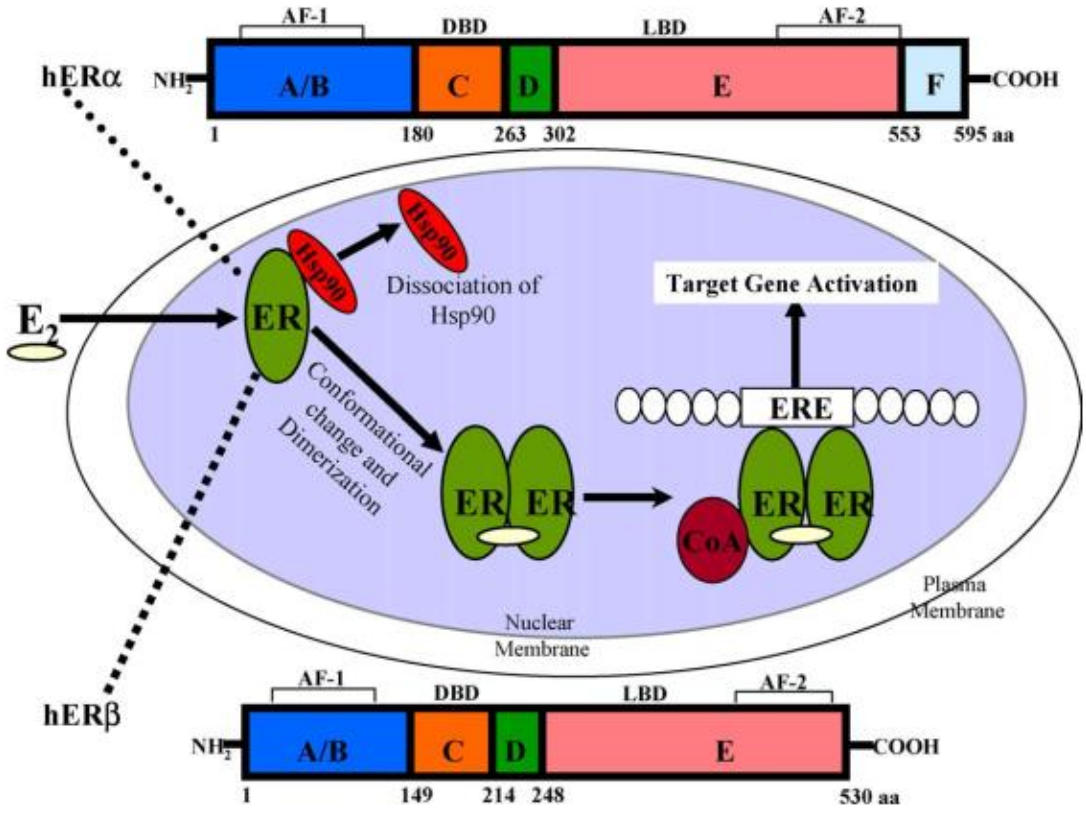

Lewis, J. S.; Jordan, V. C., Selective estrogen receptor modulators (SERMs): mechanisms of anticarcinogenesis and drug resistance. Mutation Research/Fundamental and Molecular Mechanisms of Mutagenesis 2005, 591 (1-2), 247-263.

Figure 5.3 Functional domains and mechanism of action of ERα and ERβ in target cells

Selective estrogen receptor modulators are a class of agents available for the treatment of breast cancer and other diseases such as bone loss[12]. These class of compounds (e.g., Tamoxifen, ormeloxifene, raloxifene) (**Fig.5.1**) displays unusual tissue-selective pharmacology; they sometimes act as estrogen agonistic in tissues such as bone, liver and cardiovascular system and acts as estrogen antagonistic in other tissues such as brain and breast, and both in the uterus. Their therapeutic effects and lesser side effects have made them the best hormonal treatment for various carcinomas[13].

Though the antiestrogenic and estrogenic action of SERM is not well understood, it is believed that most of its unique pharmacology can be explained in three mechanisms: (1) Differential ER conformation upon ligand binding; (2) differential expression and binding to the ER of coregulator protein: and (3) differential ER expression and gene activation via none ERE interaction (tethered pathway) (**Fig 5.4**)[14].

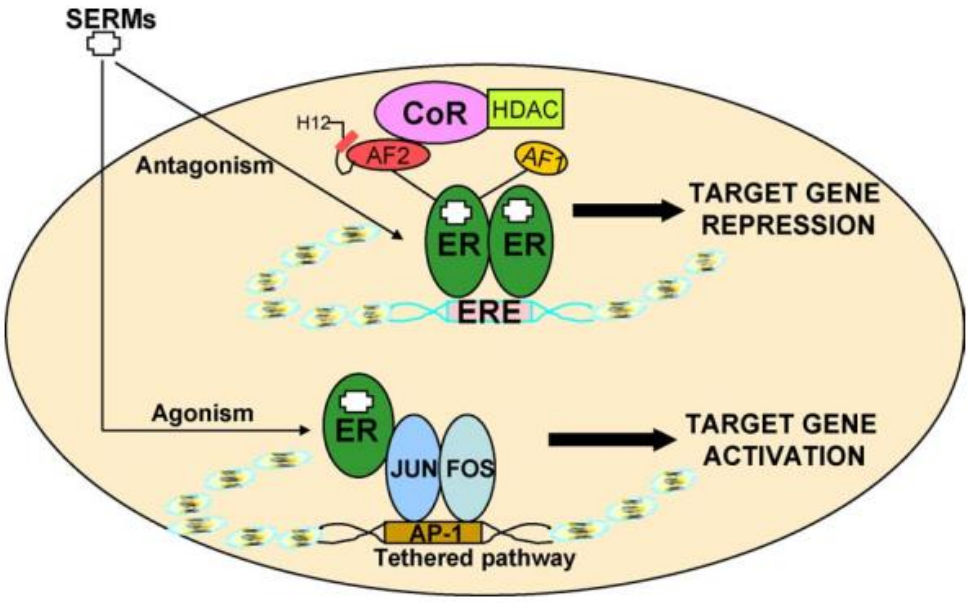

J.S. Lewis, V.C. Jordan / Mutation Research 591 (2005) 247–263

Figure 5.4 A model for the action of SERMs via estrogen response element (ERE)-dependent and none-ERE-dependent (AP1-tethered) pathway in target tissues.

The biological evaluation and structural activity relationships (SAR) of SERMs have revealed that analogs with ring closure through proximal phenyl ring have a better affinity with estrogen receptors (ER) and more selectivity for ERα[15] (e.g., Lasofoxifene in **Fig. 5.1**). Also, the 2,2-dimethylbenzopyran scaffold is an important pharmacophore that needs to be incorporated in the designing of ER ligands as evident by many non-steroidal estrogen receptor modulators including ormeloxifene[16,17,18,19,20]. We envisage that incorporation of these moieties in these ligands will enhance the overall efficacy and reduce the issue of drug resistance.

The emergence of drug resistance as a major issue in the treatment of ovarian cancer, coupled with the problem of low tumor selectivity and toxicity, has made it an urgent need for discovery of less toxic and potent Selective estrogen receptor modulators with

protective effect as well as anti-cancer effect for the treatment of ovarian cancer. In this communication, we report the structural design, synthesis of novel selective estrogen receptor modulators using 2, 2-dimethylbenzopyran base and their biological efficacy for ER-mediated anti-ovarian cancer activity.

To find the hit analogs and to identify the lead compounds (LDs) targeting EGFR, bioisosterism process was employed to design the ormeloxifene analogs (**Fig 5.5**). Several structural modifications were made at a various position such as C-7, C-4, C-4' and C-4'' of ormeloxifene skeleton to change the pharmacokinetics of the analogs as well as improve their biological activities (**Fig 5.5**). Molecular docking was conducted to investigate whether ormeloxifene and its analogs bind to various receptor proteins such as EGFR, GSK3B, mTOR, STAT3, and CDK2. In our previous studies (Chapter 3 and 4), analogs showed higher binding affinity towards these receptors (EGFR, GSK3B, mTOR, STAT3, and CDK2). Therefore there is a need to investigate the effects of other structural modifications (analogs) on these proteins. Preliminary docking results revealed that most analogs with 4-(3-hydroxypropyl) phenol at C-7 has better binding affinity to various receptor proteins compared to other analogs with functionalities such as ethyl alcohol, ethylamine, methylbenzene, etc. These studies and results proved that analogs with 4-(3-hydroxypropyl) phenol at C-7 would enhance the anticancer activities as well as pharmacokinetic properties of ormeloxifene analogs. Based on this modified structure (**Fig 5.5**), a virtual library of analogs was prepared, and molecular docking was conducted using OpenEye® scientific software utilizing fast executive docking (FRED), ONEGA and VIDA.

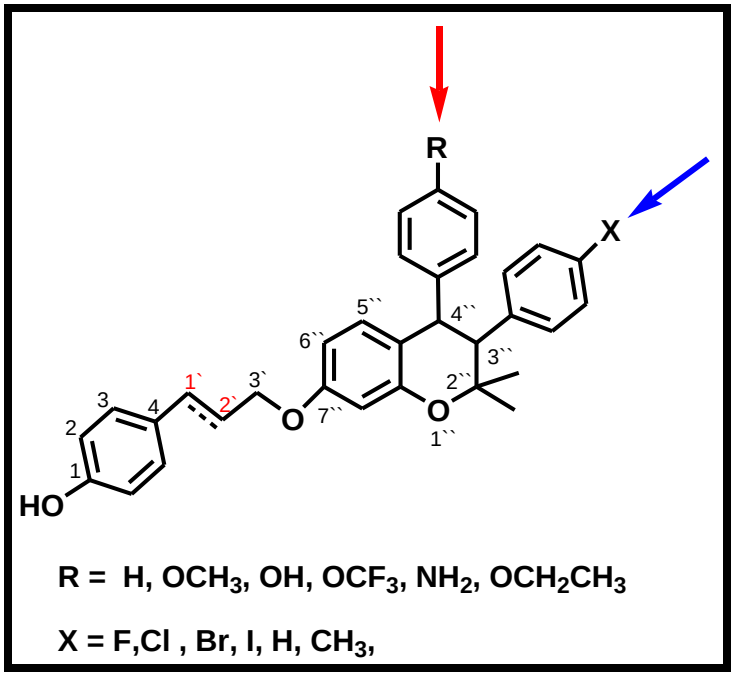

Figure 5.5 Proposed structure of ormeloxifene analogs with arrows showing various positions for structural modification

5.2 Results and discussion

5.2.1 Results of molecular Docking

Molecular docking studies of ormeloxifene analogs with 4-(3-hydroxypropyl) phenol and (E)-4-(3-hydroxyprop-1-en-1-yl) phenol at C-7 revealed significant binding affinity toward

the crystal structure of EGFR. Analogs with 4-(3-hydroxypropyl) phenol and (E)-4-(3-hydroxyprop-1-en-1-yl) phenol at **C-7** and phenol at C-4 such as **JA_31, JA_29, JA_30, JA_33, and JA_24** showed higher binding mode in EGFR binding site by forming hydrogen bond with **HIS:84:A** the same amino acid that bond to ormeloxifene in EGFR binding site (**Fig 5.6**).

In GSK3B binding pocket, analogs with 4-(3-hydroxypropyl) phenol at C-7phenol side chain at C-4 of Ormeloxifene scaffolds such as **JA_31, JA_28, JA_29,** and **JA_24** showed hydrogen bond as well as hydrophilic and hydrophobic interactions. Most analogs with anisole and aniline at C-4 of ormeloxifene skeleton revealed higher binding affinity by forming two hydrogen bonds with **LYS:85: B** and **ASP:200: B** in GSK3B binding pocket **(Fig 5.7).** Ormeloxifene analogs with trifluoromethyl benzene at C-4 of ormeloxifene skeleton such as **JA_22,** and **JA_33** formed hydrogen bond with **LYS: 85: B** and **ASP: 200: B** in GSK3B binding pocket. Analogs with 4-(3-hydroxypropyl) phenol at C-7 demonstrated higher binding affinity and formed a hydrogen bond with **LYS:85: B** and **LYS:183: B** in the crystal structure of GSK3B (**Fig 5.8**). Substitution of phenol at C-4 and introduction of 4-(3-hydroxypropyl) phenol at the **C-7** position of ormeloxifene skeleton improved the binding affinity with the crystal structure of GSK3B. The hydroxyl-OH on 4-(3-hydroxypropyl) phenol such as **JA-24** formed two hydrogen bonds with **GLU: 97: B** and **PHE: 201: B** in the crystal structure of GSK3B **(Fig 5.8).**

Molecular docking results in CDK2 binding pocket also showed a significant binding mode with ormeloxifene analogs compared to known estrogen receptor modulators. Substitution the 4-(3-hydroxypropyl) phenol with (E)-4-(3-hydroxyprop-1-en-1-yl) phenol moiety at **C-7** position such as **JA_31** resulted in higher binding affinity in the CDK2 binding pocket

(**Fig 5.9**). Unsubstituted analog demonstrated outstanding binding affinity towards CDK2 binding site relative to similar analogs such as JA**_16, JA_17, JA_18** with halogens substituted para to aromatic ring at C-3.

Analogs such as JA_31, JA_29, JA_30, JA_33, JA-23, JA-35, 34, 22 and JA_24 showed higher binding affinity in several receptors (GSK3B, STAT3, mTOR, EGFR, etc.), an example is shown in **Table 5.1** below. These most promising analogs from molecular docking studies will be synthesized and biologically investigated to identify the lead compounds.

Table 5.1 Consensus score of FRED docking in GSK3B receptor

VIDA Name	VIDA ID	PLP	Chemgauss 3	OEChemscore	Screenscore	Consensus Score
JA_33_195	2	-69.7706	-86.6225	-51.6373	-172.291	2
JA_27_195	3	-65.5174	-85.0519	-48.1456	-169.37	9
JA_34_195	4	-65.5174	-85.0519	-48.1456	-169.37	13

JA_22_109	5	-63.4487	-75.2457	-49.0157	-151.454	23
ORM_Br_31	6	-60.4673	-78.4293	-44.6155	-151.325	31
JA_32_15	7	-60.212	-76.9438	-46.7599	-152.291	33
JA_35_48	8	-62.6458	-68.1517	-49.4359	-147.485	37
JA_17_175	9	-60.5379	-76.6181	-43.6912	-152.825	38
JA_28_40	10	-63.7486	-74.9482	-47.6724	-143.316	41
JA_24_48	11	-60.2165	-68.1734	-48.4074	-143.858	47

JA_29_4	12	-60.1552	-77.0875	-43.1687	-148.647	49
ORM_30_48	13	-60.2165	-68.1734	-48.4074	-143.858	51
ORM _158	14	-59.3852	-75.1556	-48.1866	-136.677	52

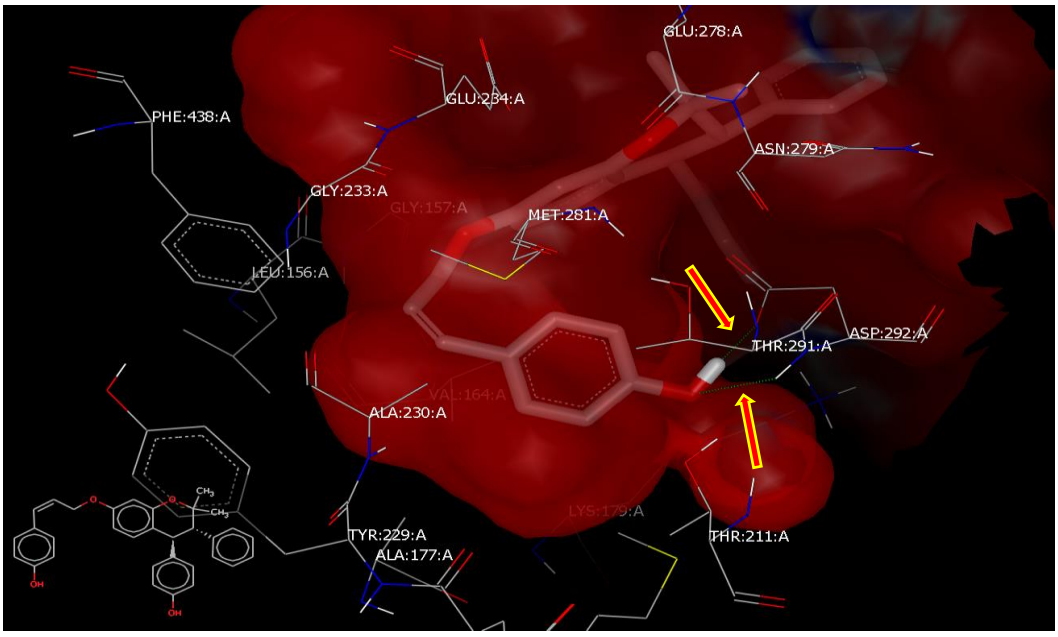

Figure 5.6 JA_31 forming two hydrogen bonds with THR:291: A and THR:211: A in EGFR binding pocket

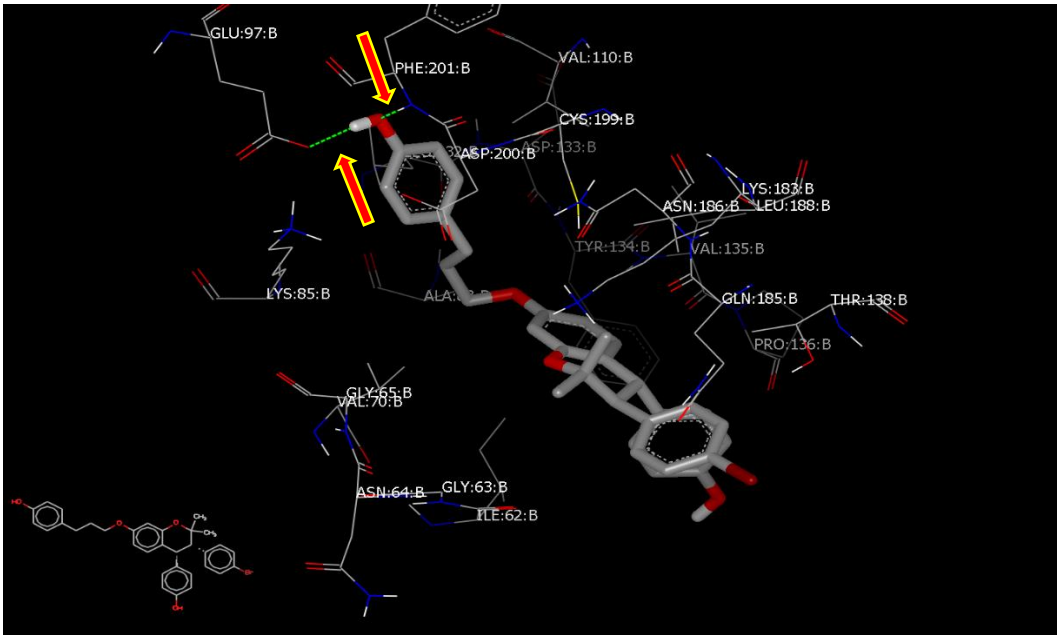

Figure 5.7 JA_28 forming two hydrogen bonds with GLU:97: B and ASP: 200: B in GSK3B binding pocket

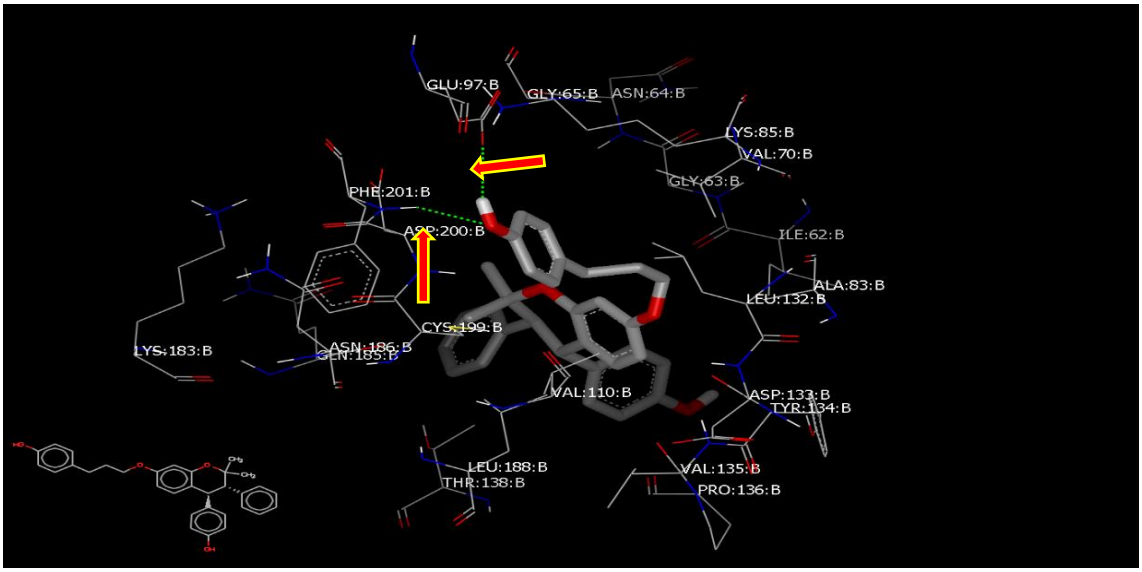

Figure 5.8 JA-24 with nitrogen forming two hydrogen bonding with GLU

:97: B and PHE:201: B in GSK3B pocket

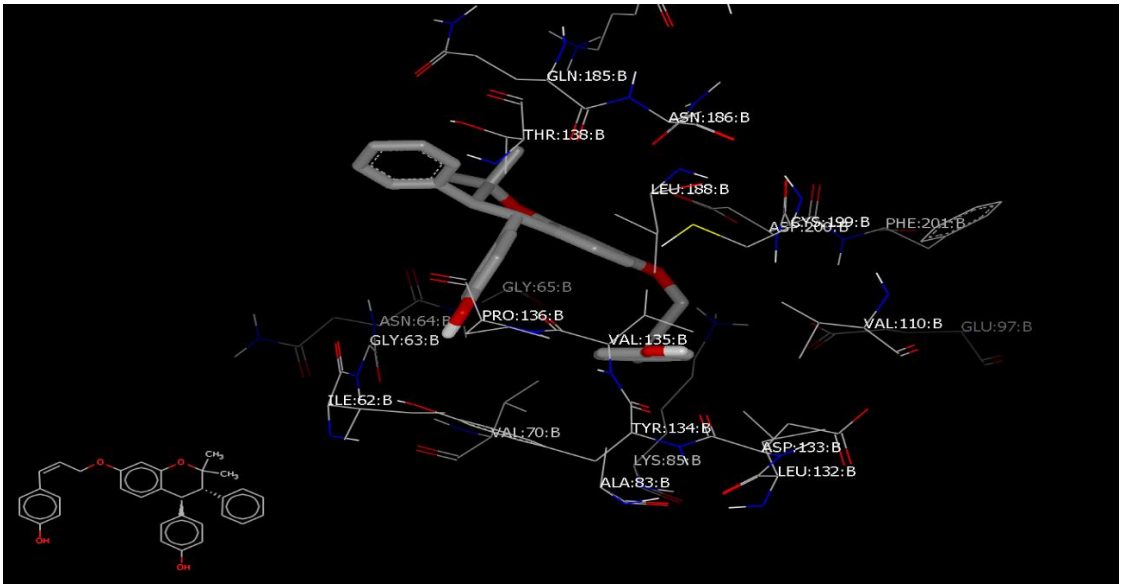

Figure 5.9 JA-31 in GSK3B binding pocket with no hydrogen bonding, the higher binding affinity is as a result of hydrophobic interactions with the receptor.

5.2.2 Synthesis of ormeloxifene analogs

Following the previous procedure to prepare compound **12** (**Scheme 4.1**), the second set of ormeloxifene analogs (with 4-(3-hydroxypropyl) phenol and (E)-4-(3-hydroxyprop-1-en-1-yl) phenol at C-7) were synthesized as shown below **(Scheme 5.1).** P-coumaric acid was protected with tetrabuthyl dimethyl silyl chloride (TBSCl) in the presence of imidazole and DMF to produce compound **13** (**Fig 5.10**). Esterification[21] of **13** using H_2SO_4/MeOH produced **14.** Reduction[22] of compound **14** by reducing agent diisobythylaluminum hydride (DIBAL-H) to give compound **16a**. Compound **16a** compound **18a** undergo mitsunobu reaction using triphenylphosphine (PPh_3) and DIAD (diethyl azodicarboxylate) in THF to produce compound[23] **19**. Deprotection of **19** with TBAF/THF gave JA_36-50. **(Scheme 5.1).** Various synthetic analogs are listed in **Table 5.1**.

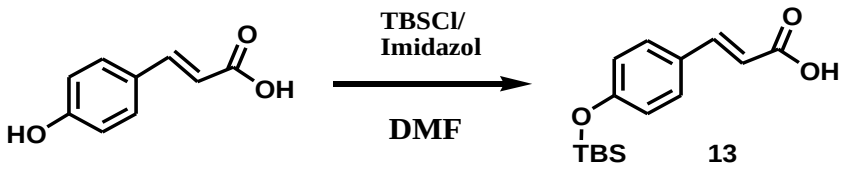

Figure 5.10 TBS Protection of P-coumaric acid

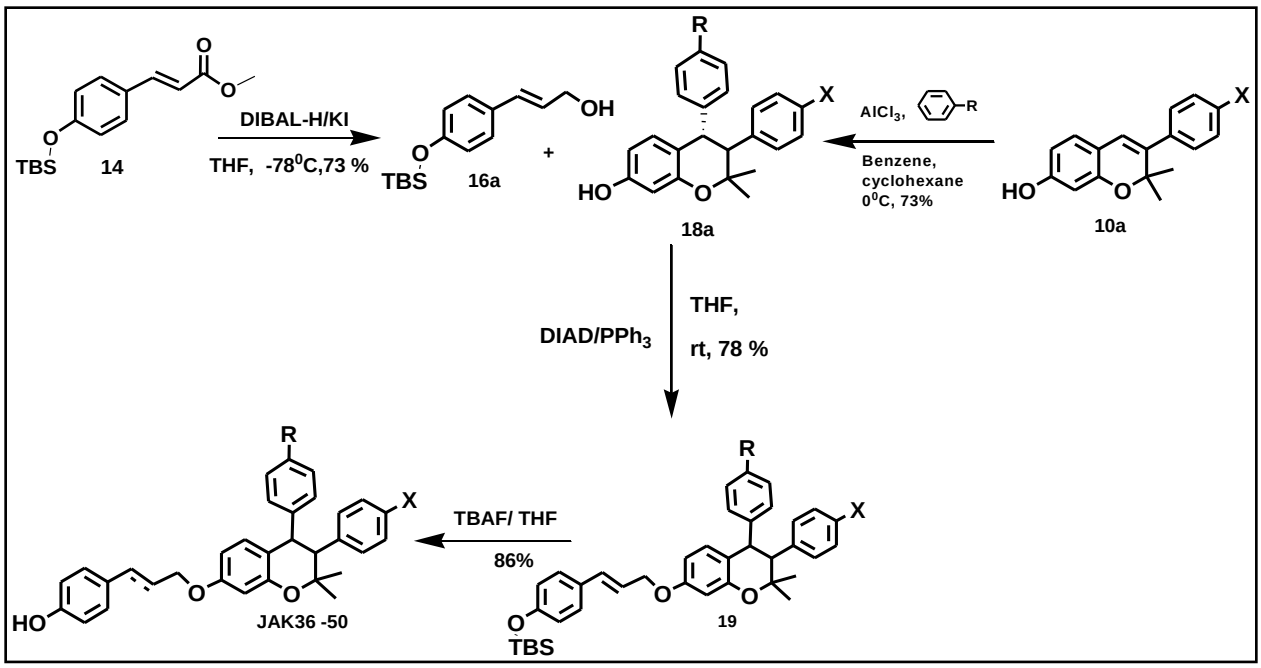

Scheme 5.1 Synthesis of ormeloxifene analogs series 2

Table 5.2 Synthesized analogs of ormeloxifene series 2

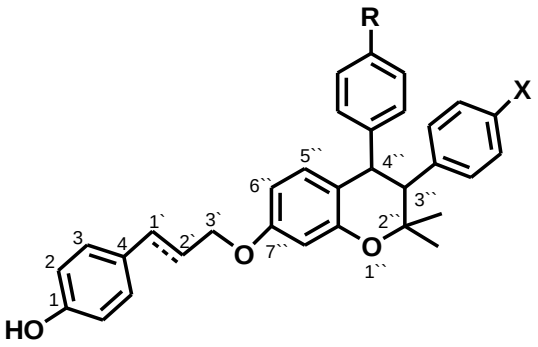

Compound	$\Delta^{1`}$	R	(X)
JA_22	-	OCF_3	H
JA_23	-	OCH_3	H
JA_24	-	OH	H
JA_27	-	CF_3	Br
JA_28	-	OH	Br
JA_29	+	OH	Br
JA_31	+	OH	H
JA_32	-	OCH_3	I
JA_33	-	OCF_3	I
JA_34	-	OCH_3	Br
JA_35	-	NH_2	H

5.2.3 Biological Evaluation of synthesized analogs

Studying the cytotoxic activities of ormeloxifene analogs **JA_31, JA_28, JA_22, JA_23, JA_24,** and **JA_27** inhibits the viability of **A2780** cells in a (10-40 mm) dose-dependent manner. The IC_{50} of analogs **JA_31, JA_28, JA_22, JA_23, JA_24**, and **JA_27** showed antiproliferation range of cytotoxicity 44.6µM, 17.6µM, 58.9µM, 89.0µM, 65.7µM, and 63.7µM after 48 hours treatment respectively (**Table 5.2**), but analogs such as **JA_29, JA_32, JA_33, JA_34,** and **JA_35** completely lost their inhibitory cytotoxicity activity to (A2780) ovarian cancer cell lines.

On the other hand, compounds with 4-(3-hydroxypropyl) phenol and (E)-4-(3-hydroxyprop-1-en-1-yl) phenol at **C-7** and phenol, trifluoromethyl benzene at C-4'' such as **JA-31, JA_28,** and **JA_24** exhibited moderate inhibitory activity (IC50 = 44.6, 17.6 and 65.7 respectively) in ovarian cancer cell lines. Presence of double bonds also played a significant inhibitory effect on ovarian cancer cell lines, for instance, the introduction of double bound at C-7 position as in **JA_31** showed IC_{50} = 44.6 a higher the inhibitory on **A2780** cells compared to the similar compound without double bond **JA_24** (IC_{50} = 65.7µM). Similar analogs with halogens at the para position of the aromatic ring at C-3'' and aniline, anisole and trifluoromethyl benzene at C-4'' position such as **JA_35, JA_34, JA-33, JA_32,** and **JA_29** exhibited no inhibitory activity on ovarian cancer cell lines.

Table 5.3 MTT Cell viability results of ormeloxifene analogs on the A2780 Cell line

Compound	IC_{50} (µM)	Compound	IC_{50} (µM)
Ormeloxifene	17.5	JA_31	44.6
JA_28	17.6	JA_22	58.9
JA_35	NA	JA_23	89.0
JA_33	NA	JA_24	65.7
JA_29	NA	JA_32	NA
JA_34	NA	JA_27	63.7

5.2.4 Cell cycle via modulation of cell-cycle regulatory proteins

The biological studies for the synthesized compounds started with studying the in vitro cytotoxic activities to identify their ability to inhibit EGFR and its downstream. The effect of ormeloxifene analogs with 4-(3-hydroxypropyl) phenol and (E)-4-(3-hydroxyprop-1-en-1-yl) phenol at **C-7** on ovarian cancer cell cycle distribution was determined using A2780

cells. The cells were synchronized and treated with the most active analogs **JA-28** for 24 hours, with vehicle-control as DMSO. The cell cycle analysis performed by flow cytometry revealed that **JA-28** arrest A2780 cells in G_2-M phase (**Fig 5.11**), (**Table. 5.4).** **JA-28** showed an increase in the fraction of cells in the G_2-M phase with 8.74% compared to the control (Ormeloxifene) with 3.52% (**Table. 5.4).** This result indicates that **JA-28** has the potential to chemotherapeutic effects because it arrests (A2780) ovarian cell cycle in G_2-M phase[24,25]. The promising antiproliferation activity data of **JA_28** demonstrated the importance of transposition of 4-(3-hydroxypropyl) phenol and (E)-4-(3-hydroxyprop-1-en-1-yl) phenol at **C-7** of ormeloxifene skeleton.

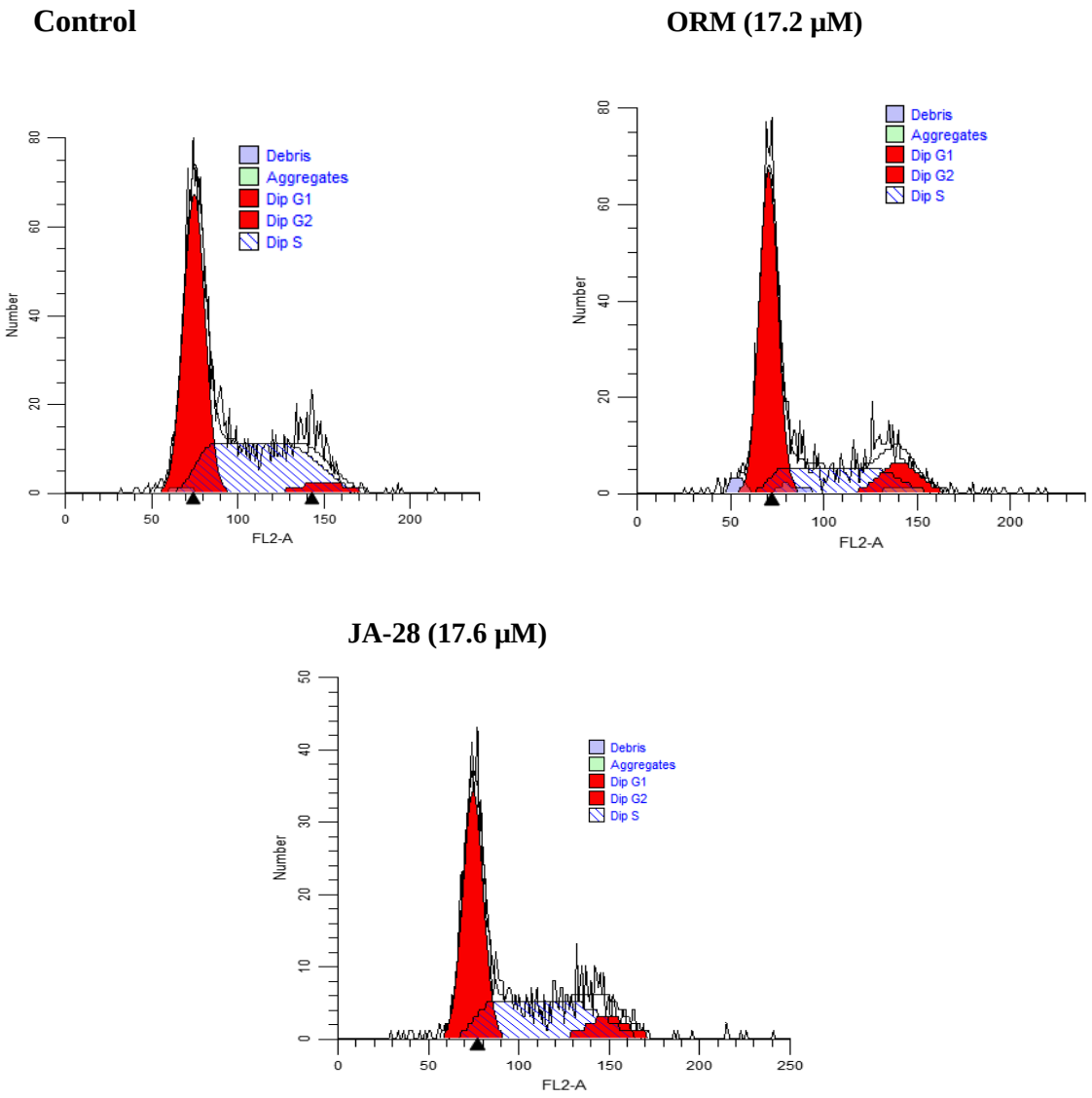

Figure 5.11 Effects of Ormeloxifene and JA-28 on cell cycle phase distribution of ovarian cancer cells

Table 5.4 Cell distribution in (A2780) ovarian cancer cells

Groups	$G_0 – G_1$	S	G_2 - M
Control	**53.42**	**43.06**	**3.52**
Orm (17.2 µM/L)	**60.69**	**27.93**	**11.38**
JA-28 (17.6 µM/L)	**50.95**	**40.31**	**8.74**

5.3 Conclusion

In conclusion series of ormeloxifene analogs with 4-(3-hydroxypropyl) phenol at C-7 were designed, synthesized and evaluated for their antiproliferation activity against ovarian cancer (A2780) cell line. Ormeloxifene analogs **JA-28, JA-35, JA-33, JA-29, JA-34, JA-31, JA-22, JA-23, JA-24, JA-32,** and **JA-27,** were generated using in-silico drug design strategies to installing pharmacophores of various aromatic and heterocyclic substituents at C-4 and C-7. Analogs such as **JA-33, JA-24, JA-27,** and **JA-22** showed higher binding affinity in several receptors. Biological studies showed that JA**_28** has better cytotoxicity (IC_{50} of 17.6 µM) than a known EGFR inhibitor Ormeloxifene. Other analogs such as **JA-31, JA-22,** and **JA-24** showed moderate cytotoxic activity in A2780 human ovarian cancer cell line with IC_{50} values of 44.6µM, 58.9µM, and 65.7µM respectively. However, **JA-34, JA-35, JA-32,** and **JA-29** completely lost their activity in human ovarian cancer cell lines. Installation of trifluromethoxybenze at the C-4 position and 4-(3-hydroxypropyl) phenol at C-7 of Ormeloxifene skeleton improved the cytotoxicity activities compared with similar compounds with anisole, aniline and phenol groups at C-4.**JA-28** arrests cells in the S phase with 8.74% compared to 3.52% for control (Ormeloxifene) which indicates that it has the potential to chemotherapeutic effects.

5.4 Experimental section

5.4.1 General

All chemicals and solvents were purchased from Fisher Scientific, Across Chemical or Sigma Aldrich and used without further purification. All glassware used was washed, cleaned and oven dried overnight before conducting any chemical reaction. Any reaction that requires anhydrous condition were performed under argon or nitrogen environment.

Pre-coated silica gel plates were used to analyze the progress and completion reaction. UV light at 254 or 365 or CAM stain was used to visualize the chemical reaction spot. All synthetic intermediates and final compounds were purified by column chromatography with 230 x 400 silica gel. Proton (^{1}H) and Carbon (^{13}C) NMR spectra were analyzed by Bruker Avance-400 MHz and 600 MHz NMR using D-acetone or $CDCl_3$. NMR chemical shifts were presented in σ(PPM) using residual solvent peaks as standard ($CDCl_3$, 7.26 (H), 77.16 (C)). High-resolution mass spectrometer (HRMS) was gained using Thermo Finnigan MAT 95XL mass spectrometer at the University of Buffalo mass spectroscopy facility. All synthetic intermediate and final compounds were purified using column chromatography with 230ˣ400 mesh silica gel. ^{1}H and ^{13}C NMR spectra were using Bruker AVANCE-400 MHZ and 600 MHZ NMR spectrometer, in $CDCl_3$ and D-acetone. NMR chemical shifts were presented in σ(PPM) using residual solvent peaks as standards ($CDCl_3$, 7.26 (H), 77.16 (C)).

5.4.2 3-[4-(tert-Butyl-dimethyl-silanyloxy)-phenyl]-acrylic acid

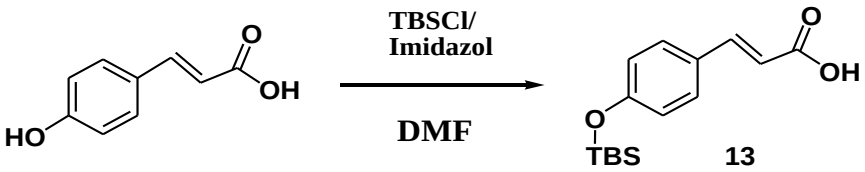

To a solution of (E)-3-(4-hydroxyphenyl) acrylic acid (8.2g, 49.9mmol) in dimethyl formamide (DMF) (120 ml), tert-buthylsilylchloride (TBSCl) (11.29g, 74.95mmol) and imidazole (9.18g, 134.89mmol) were added sequentially. The reaction was stirred for 24h and quenched with saturated $NaHCO_3$ (50ml). The aqueous layer was extracted with ethyl acetate (3 x 60ml), dried over anhydrous sodium sulfate (Na2SO4), filtered and the organic

layer evaporated under reduced pressure. The crude product was purified by column chromatography (10% ethyl acetate: hexane) to give ester 13 (12.7g, 97%).

^{1}H NMR (400 MHz, Chloroform-*d*) δ 10.98 (s, 1H), 7.85 (s, 1H), 7.46 (d, *J* = 15.9 Hz, 1H), 7.27 (d, *J* = 8.6 Hz, 1H), 6.73 (d, *J* = 8.5 Hz, 1H), 6.23 (d, *J* = 15.8 Hz, 1H), 3.81 (s, 7H), 2.99 (d, *J* = 7.3 Hz, 1H), 2.86 – 2.71 (m, 7H), 1.20 – 1.07 (m, 9H), 1.03 – 0.87 (m, 6H). ^{13}C NMR (400 MHz, $CDCl_3$) δ 162.81, 129.40, 120.06, 77.44, 36.42, 31.40, 25.73, 17.73, 17.67, 17.62, 12.58, 12.47, 12.33, 8.35.

5.4.3 3-(4-triisopropylsilanyloxy-phenyl)-acrylic acid methyl ester

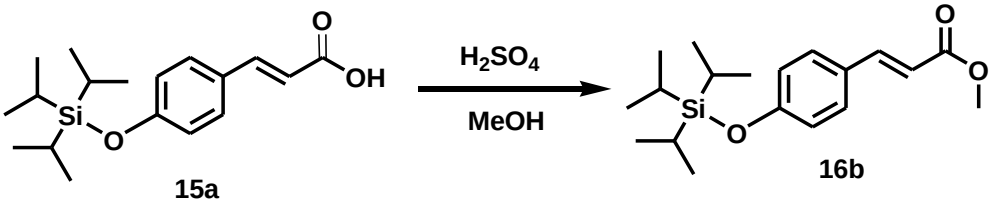

15a 16b

Compound **15a** (5.0g, 16.2mmol) was dissolved in MeOH (33 ml) and concentrated hydrochloric acid (HCl) (0.83ml) was added. The reaction mixture was refluxed for 16h, cooled to room temperature and the solvent was evaporated under reduced pressure. The resulting residue was dissolved in ethyl acetate (25ml) and washed successively with 1M $NaHCO_3$ (2 X 17 ml) and water (18ml). The organic phase was dried with over anhydrous Na_2SO_4, filtered and the solvent was removed under reduced pressure to give a colorless crystal (5.35g, 97%).

1H NMR (400 MHz, Chloroform-d) δ 7.55 (d, J = 16.0 Hz, 1H), 7.33 – 7.27 (m, 2H), 6.81 – 6.75 (m, 2H), 6.19 (d, J = 16.0 Hz, 1H), 3.70 (s, 3H), 1.96 (s, 4H), 0.98 (s, 21H). 13C

NMR (400 MHz, CDCl3) δ 171.78, 168.43, 159.02, 145.29, 129.97, 126.23, 115.96, 114.26, 60.66, 51.67, 20.99, 17.65, 14.08, 12.30.

5.4.4 3-[4-(tert-Butyl-dimethyl-silanyloxy)-phenyl]-prop-2-en-1-ol

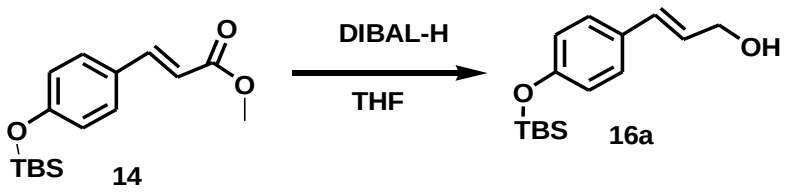

To a solution of ester (9.0g, 30.1mmol) in toluene (75.0ml), Diisobutylaluminium hydride (DIBAL-H) (75ml, 90.1mmol) was added at -78°C dropwise and the reaction was stirred for half an hour at 0°C. The temperature was reduced to room temperature after 20min. and the reaction cooled back at -78°C before an addition of solution of potassium sodium titrate (50ml). The reaction was stirred overnight, and the aqueous layer extracted with ethyl acetate (3 x 70ml), dried over anhydrous sodium sulfate (Na_2SO_4) and the volume reduced under vacuum. The extract was purified using column chromatography (20% ethyl acetate: hexane) to afford a colorless liquid (6.85g, 86%).

1H NMR (400 MHz, Chloroform-d) δ 7.21 – 7.10 (m, 3H), 6.75 – 6.65 (m, 3H), 4.15 (dd, J = 5.9, 1.5 Hz, 3H), 3.77 (s, 1H), 0.92 (s, 17H), 0.89 – 0.75 (m, 17H), 0.12 (s, 12H). 13C NMR (400 MHz, CDCl3) δ 155.30, 130.67, 130.22, 127.62, 126.56, 120.19, 69.34, 63.33, 31.64, 30.69, 25.74, 25.71, 22.69, 18.98, 18.22, 18.03, -3.56, -4.41.

5.4.5 3-(4-((tert-butyldimethylsilyl)oxy)phenyl)propan-1-ol

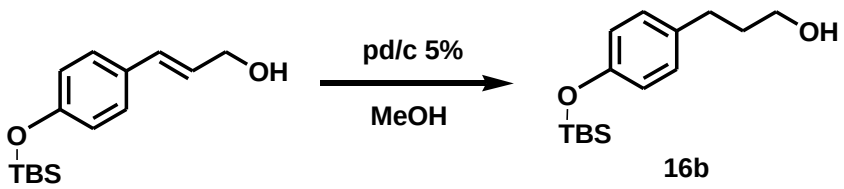

16a **16b**

To an oven dry round 25ml round bottom flask under H_2 gas, was added a solution of unsaturated alcohol **16a** (5.4g, 20.4 mmol) in methanol (90 ml) and stirred until the solution is completely dissolved. (4.21g, 6.67 mmol) 5% pd/c was added to the mixture and the compound was hydrogenated at room temperature for 4 hours. The reaction was quenched and concentrated under reduced pressure after completion and purified by column chromatography (30% ethyl acetate: hexane) to obtain the desired product alcohol (4.2g, 96 %)

1H NMR (400 MHz, Chloroform-d) δ 6.94 – 6.87 (m, 1H), 6.71 – 6.63 (m, 1H), 3.55 (s, 2H), 2.75 (t, J = 7.8 Hz, 1H), 2.48 (dd, J = 8.4, 7.1 Hz, 1H), 0.92 (s, 17H), 0.89 – 0.75 (m, 17H), 0.12 (s, 12H). 13C NMR (400 MHz, CDCl3) δ 155.30, 130.67, 130.22, 127.62, 126.56, 120.19, 69.34, 63.33, 31.64, 30.69, 25.74, 25.71, 22.69, 18.98, 18.22, 18.03, -3.56, -4.41.

5.4.6 (4-(4-(3-(4-fluorophenyl)-2,2-dimethyl-2H-chromen-7 yloxy)butyl)phenoxy) (tert-butyl) dimethylsilane

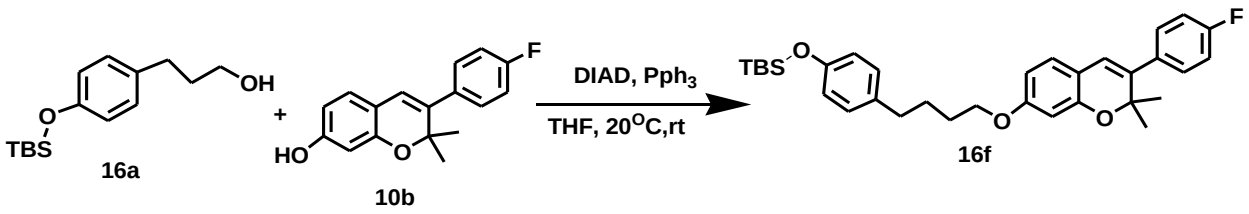

To a solution of 3-(4-((tert-butyldimethylsilyl)oxy)phenyl)propan-1-ol (**16b**) (0.35g, 1.35 mmol), **10b** (0.37g, 1.35 mmol) in Tetrahydrofuran (THF) (10 ml) was cooled to 0°C. Triphenylphosphine (Pph_3) (0.35g, 2.83 mmol) was added followed by addition of (DIAD (0.270ml, 1.20 mmol) in dropwise for 30 min. The mixture was stirred overnight at room temperature and quenched with 1N NaOH (85ml) after completion. The aqueous layer was extracted with ethyl acetate (3 x 50ml), washed with brine (45ml), dried over anhydrous Na_2SO_4 and concentrated under reduced pressure to give a yellow oil (0.60g, 84%).

1H NMR (600 MHz, Chloroform-d) δ 7.51 (s, 1H), 7.32 – 7.26 (m, 2H), 7.05 (tdd, J = 8.7, 5.8, 2.4 Hz, 4H), 6.92 (d, J = 8.1 Hz, 1H), 6.85 (dd, J = 8.3, 5.4 Hz, 2H), 6.53 – 6.48 (m, 2H), 6.28 (s, 1H), 5.03 (ddt, J = 20.7, 14.4, 7.3 Hz, 1H), 3.65 – 3.54 (m, 1H), 2.61 (t, J = 7.7 Hz, 1H), 1.93 (p, J = 7.4 Hz, 1H), 1.44 – 1.41 (m, 6H), 1.38 (s, 3H), 1.18 – 1.13 (m, 11H), 0.95 (s, 9H), 0.20 (s, 6H) 13C NMR (600 MHz, CDCl3) δ 162.93, 161.30, 157.76, 153.71, 150.29, 137.63, 135.83, 135.81, 129.91, 129.85, 129.20, 127.39, 122.49, 119.77, 115.67, 115.44, 115.07, 114.93, 108.58, 103.89, 78.73, 72.73, 32.00, 29.78, 29.74, 29.44, 22.76, 22.04, 21.95, 21.62, 18.08, 17.93, 17.90, 17.83, 17.76, 14.21, -3.41, -4.36

5.4.7 (4-(4-(3-(4-fluorophenyl)-3,4-dihydro-2,2-dimethyl-4-(4-(trifluoromethoxy) phenyl) -2H-chromen-7-yloxy)butyl)phenoxy)(tert-butyl)dimethylsilane

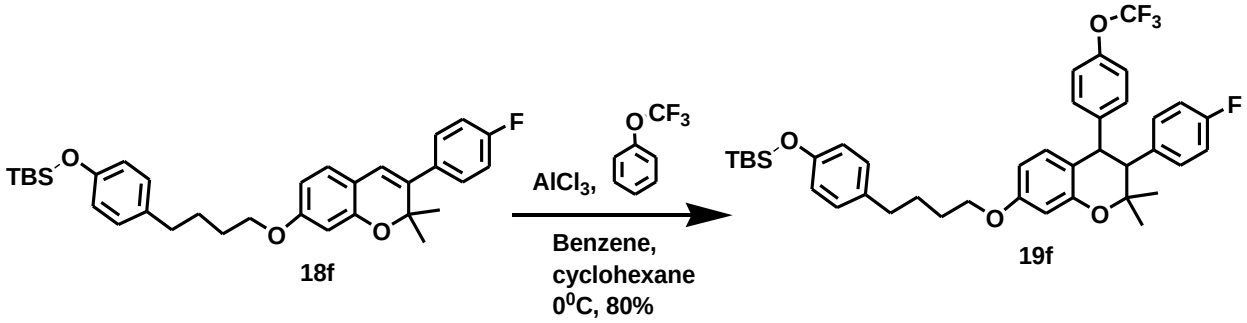

To a stirred solution of **18f** (0.28 g, 0.53 mmol) and phenol (0.18 g, 1.10 mmol) in benzene-cyclohexane mixture (1:1 ratio, 8.0 ml) at 0°C was added anhydrous aluminum chloride (0.09g, 0.64 mmol) in portions. A solution of phenol (0.06 g, 0.37 mmol) in benzene-cyclohexane mixture (1:1 Ratio, 8.0 ml) was added after 30 min, and the mixture further stirred for 8 hrs. The reaction mixture was quenched by adding a mixture of ice and conc. Hydrochloric acid (1:1 2.0 ml) and the organic layer was separated. The aqueous layer was re-extracted three times with dichloromethane (16.0 ml). The combined extract was washed with $NaHCO_3$ (10 %, 10.0ml), dried over anhydrous Na_2SO_4, filtered and concentrated under reduced pressure. The semi-solid obtained was purified by column chromatography (70% hexane: 30% ethyl acetate) to obtain (0.29g, 80%) **19f**.

1H NMR (600 MHz, Chloroform-d) δ 8.09 (dd, J = 8.3, 1.4 Hz, 1H), 7.72 – 7.68 (m, 1H), 7.65 – 7.61 (m, 1H), 7.37 (d, J = 7.8 Hz, 1H), 7.29 (dd, J = 8.5, 7.4 Hz, 2H), 7.17 – 7.11

(m, 4H), 7.11 – 7.05 (m, 3H), 6.93 – 6.87 (m, 3H), 6.80 – 6.74 (m, 2H), 6.71 (dt, J = 7.6, 1.1 Hz, 2H), 6.34 (d, J = 7.4 Hz, 1H), 6.15 – 6.11 (m, 1H), 1.92 (s, 1H), 1.44 – 1.41 (m, 6H), 1.38 (s, 3H), 1.18 – 1.13 (m, 11H), 0.95 (s, 9H), 0.20 (s, 6H) 13C NMR (600 MHz, CDCl3) δ 157.23, 156.16, 153.51, 151.01, 138.31, 135.77, 133.69, 133.03, 130.25, 130.01, 129.92, 129.86, 129.84, 129.57, 129.41, 129.28, 128.64, 128.36, 128.24, 128.15, 127.03, 122.46, 121.77, 121.08, 120.96, 120.28, 119.99, 119.73, 116.64, 115.45, 115.38, 115.26, 115.12, 114.98, 113.12, 108.39, 100.57, 78.69, 67.38, 60.66, 34.74, 32.02, 31.68, 29.80, 29.46, 27.31, 27.15, 26.89, 25.35, 22.79, 22.74, 18.01, 17.99, 17.89, 17.81, 17.76, 14.20, -3.44, -4.31.

5.4.8 4-{4-[3-(4-Fluoro-phenyl)-2,2-dimethyl-4-(4-trifluoromethoxy-phenyl)-chroman-7-yloxy]-butyl}-phenol

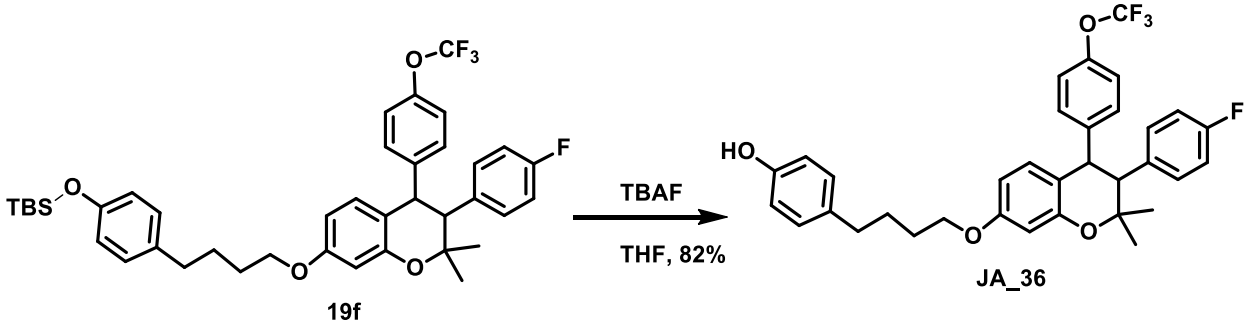

Tetrabutyl ammonium fluoride (TBAF) (0.90 ml, 3.5mmol) was added to a stirred solution of (4-(3-(3-(4-fluorophenyl)-3,4-dihydro-2,2-dimethyl-2H-chromen-7-yloxy)propyl)phenoxy)(tert-butyl)dimethylsilane (0.48g, 0.69 mmol) and stirred for 6h . The reaction was quenched with ammonium chloride (NH_4Cl) solution and extracted with

ethyl acetate (3 x 40ml), dried over anhydrous sodium sulfate (Na_2SO_4). The solution was filtered, and the volume reduced under vacuum. Purification was done by column chromatography (10% ethyl acetate: hexane) to give the titled compound. (0.33g, 82%).

1H NMR (600 MHz, Chloroform-d) δ 8.09 (dd, J = 8.3, 1.4 Hz, 1H), 7.72 – 7.68 (m, 1H), 7.65 – 7.61 (m, 1H), 7.37 (d, J = 7.8 Hz, 1H), 7.29 (dd, J = 8.5, 7.4 Hz, 2H), 7.17 – 7.11 (m, 4H), 7.11 – 7.05 (m, 3H), 6.93 – 6.87 (m, 3H), 6.80 – 6.74 (m, 2H), 6.71 (dt, J = 7.6, 1.1 Hz, 2H), 6.34 (d, J = 7.4 Hz, 1H), 6.15 – 6.11 (m, 1H), 1.92 (s, 1H), 1.44 – 1.41 (m, 3H), 1.38 (s, 3H), 1.18 – 1.13 (m, 11H), 1.00 (dq, J = 7.9, 4.3, 3.4 Hz, 26H), 0.95 (s, 6H). 13C NMR (600 MHz, CDCl3) δ 157.23, 156.16, 153.51, 151.01, 138.31, 135.77, 133.69, 133.03, 130.25, 130.01, 129.92, 129.86, 129.84, 129.57, 129.41, 129.28, 128.64, 128.36, 128.24, 128.15, 127.03, 122.46, 121.77, 121.08, 120.96, 120.28, 119.99, 119.73, 116.64, 115.45, 115.38, 115.26, 115.12, 114.98, 113.12, 108.39, 100.57, 78.69, 67.38, 60.66, 34.74, 32.02, 31.68, 29.80, 29.46, 27.31, 27.15, 26.89, 25.35, 22.79, 22.74, 18.01, 17.99, 17.89, 17.81, 17.76, 14.20, 12.95, 12.73, 12.72, 12.69, 12.37, 11.51. **HR-FT-MS calcd for $C_{34}H_{32}F_4O_4$ 580.60 found 580.28**

5.4.9 Tert-butyl(4-(4-((3-(4-iodophenyl)-2,2-dimethyl-2H-chromen-7-yl)oxy)butyl) phenoxy)dimethylsilane

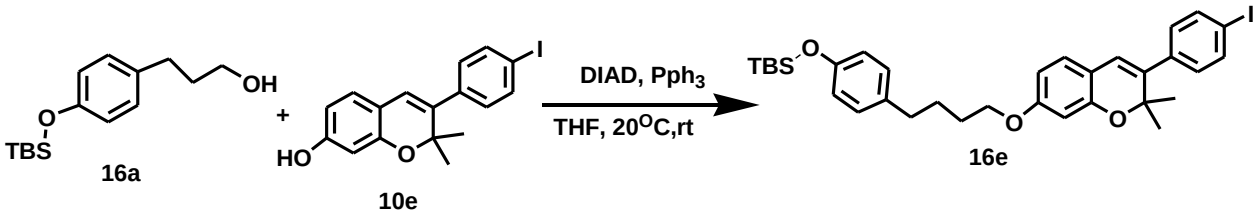

To a solution of 3-(4-((tert-butyldimethylsilyl)oxy)phenyl)propan-1-ol (**16a**) (0.23g, 1.0 mmol), **10e** (0.33g, 1.0 mmol) in Tetrahydrofuran (THF) (15 ml) was cooled to 0°C. Triphenyphospine (Pph_3) (0.35g, 2.66 mmol) was added followed by addition of (DIAD (0.20ml, 1.0 mmol) in dropwise for 30 min. The mixture was stirred overnight at room temperature and quenched with 1N NaOH (85ml) after completion. The aqueous layer was extracted with ethyl acetate (3 x 45ml), washed with brine (20ml), dried over anhydrous Na_2SO_4 and concentrated under reduced pressure to give yellow oil (0.60g, 95%).

^{1}H NMR (400 MHz, Chloroform-*d*) δ 8.14 (s, 2H), 7.61 (t, *J* = 9.7 Hz, 14H), 4.84 (qt, *J* = 12.1, 8.4, 6.1 Hz, 4H), 3.99 (dd, *J* = 10.7, 6.5 Hz, 1H), 3.49 (d, *J* = 3.3 Hz, 1H), 2.76 (qd, *J* = 15.7, 15.1, 7.5 Hz, 1H), 2.45 (td, *J* = 15.4, 13.8, 7.5 Hz, 1H), 1.88 (d, *J* = 3.3 Hz, 1H), 1.05 (q, *J* = 14.5 Hz, 51H). ^{13}C NMR (400 MHz, $CDCl_3$) δ 156.69, 153.36, 139.28, 136.99, 136.88, 133.49, 133.29, 132.50, 131.87, 131.83, 131.73, 131.46, 128.70, 128.54, 128.39, 128.31, 128.27, 127.93, 127.83, 121.76, 119.55, 116.58, 115.53, 107.97, 78.42, 68.61, 60.03, 51.11, 21.69, 20.59, 17.73, 17.71, 13.91, 12.40, 12.34, -3.11.

5.4.10 4-{3-[3-(4-Iodo-phenyl)-2,2-dimethyl-4-(4-trifluoromethoxy-phenyl)-chroman-7-yloxy]-propyl}-phenol

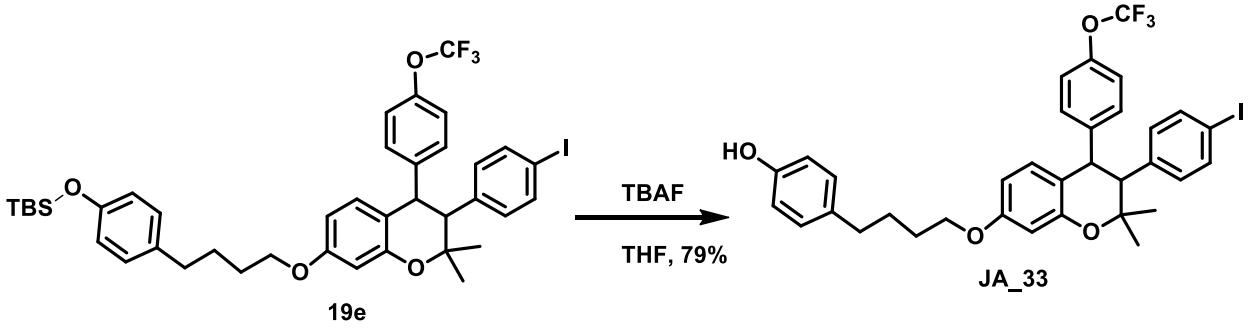

Following the procedure for the preparation of **JA_23**, (4-(4-(3,4-dihydro-3-(4-iodophenyl)-2,2-dimethyl-4-(4-(trifluoromethoxy)phenyl)-2H-chromen-7-yloxy)butyl)phenoxy)(tert-butyl)dimethylsilane (0.39, 0.49 mmol) was reacted with tetrabutylammonium fluoride (0.64g, 2.45mmol) to give JA_33 (0.27g, 79%).

1H NMR (600 MHz, Chloroform-d) δ 7.59 (ddt, J = 12.1, 6.9, 1.4 Hz, 5H), 7.50 – 7.42 (m, 2H), 7.37 (tdd, J = 7.5, 3.1, 1.9 Hz, 5H), 7.20 – 7.11 (m, 1H), 6.98 – 6.86 (m, 1H), 6.85 – 6.62 (m, 1H), 4.92 – 4.84 (m, 1H), 1.95 (s, 1H), 1.46 – 1.38 (m, 2H), 1.24 – 1.13 (m, 15H), 1.01 (dd, J = 7.4, 2.0 Hz, 3H), 0.96 (s, 1H), 0.83 – 0.75 (m, 6H). 13C NMR (600 MHz, CDCl3) δ 157.41, 156.51, 137.32, 137.22, 133.60, 132.64, 132.15, 132.08, 132.04, 132.03, 131.95, 130.18, 130.08, 129.49, 129.26, 128.59, 128.51, 121.73, 119.18, 115.64, 69.87, 60.41, 34.68, 31.94, 31.60, 29.72, 29.68, 29.38, 29.07, 22.71, 22.67, 21.96, 21.72, 17.94, 14.14. **HR-FT-MS calcd for $C_{34}H_{32}F_3IO_4$ 580.60 found 580.28**

5.4.11 4-(4-((tert-butyldimethylsilyl)oxy)phenyl)-2,2-dimethyl-3-phenylchroman-7-ol

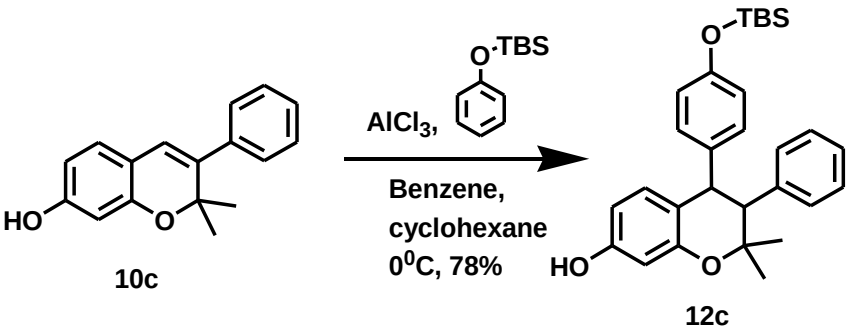

Following the procedure in the preparation of **JA_20**, **10c** (0.73g, 3.48mmol) reacted with tert-butyldimethyl(phenoxy)silane (0.35ml, 1.69 mmol) in the presence of $AlCl_3$ (0.52g, 3.90 mmol) to afford **12c** (1.09g, 78%).

1H NMR (400 MHz, Chloroform-d) δ 7.21 (s, 2H), 7.08 – 7.04 (m, 15H), 6.73 (tt, J = 7.3, 1.1 Hz, 9H), 6.75 – 6.61 (m, 14H), 6.61 (d, J = 8.5 Hz, 1H), 6.46 – 6.39 (m, 1H), 6.32 (d, J = 2.5 Hz, 1H), 6.22 – 6.13 (m, 8H), 2.34 (d, J = 10.9 Hz, 1H), 1.2 – 1.10 (m, 10H), 0.81 – 0.70 (m, 7H), 0.21 (s, 1H), 0.08 (s, 6H). 13C NMR (400 MHz, CDCl3) δ 158.83, 155.10, 153.71, 153.49, 138.20, 135.36, 131.01, 130.19, 129.60, 128.22, 120.73, 118.54, 115.47, 107.79, 101.61, 78.36, 55.34, 43.70, 37.60, 28.50, 26.84,25.8, 24.72 ,17.7, 14.17, 14.02, 10.87, -6.1

5.4.12 (E)-tert-butyl(4-(4-((4-(4-((tert-butyldimethylsilyl)oxy)phenyl)-2,2-dimethyl-3-phenylchroman-7-yl)oxy)but-1-en-1-yl)phenoxy)dimethylsilane

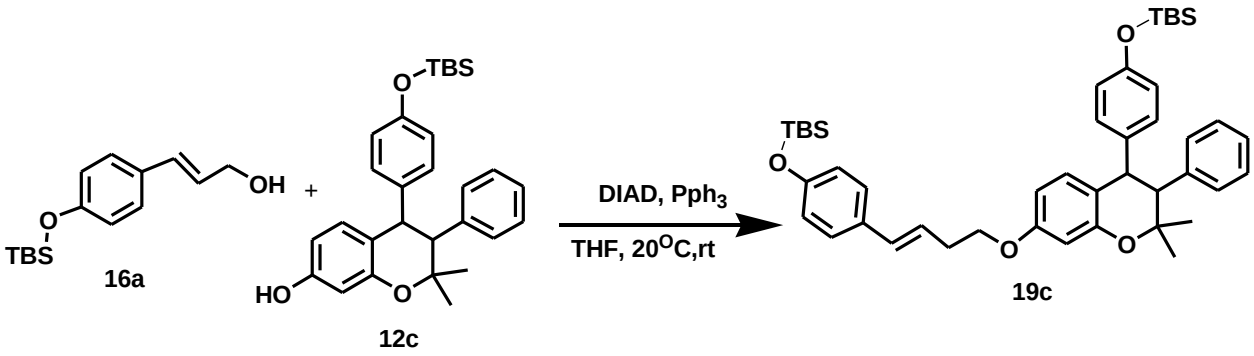

To a solution of unsaturated alcohol (**16a**) (0.38g, 1.43 mmol), **12c** (0.68g, 1.43 mmol) in Tetrahydrofuran (THF) (20 ml) was cooled to 0°C. Triphenylphosphine (Pph_3) (0.75g, 2.87 mmol) was added followed by addition of (DIAD (0.29 ml, 1.43 mmol) in dropwise for 30 min. The mixture was stirred overnight at room temperature and quenched with 1N NaOH (35.0ml) after completion. The aqueous layer was extracted with ethyl acetate (3 x 45ml), washed with brine (20.0 ml), dried over anhydrous Na_2SO_4 and concentrated under reduced pressure to give yellow oil (0.37g, 35%).

1H NMR (400 MHz, Chloroform-d) δ 7.47 (dd, J = 12.2, 7.5 Hz, 9H), 7.23 (dt, J = 33.0, 7.4 Hz, 13H), 7.14 – 6.95 (m, 8H), 6.72 – 6.51 (m, 4H), 4.71 (p, J = 6.2 Hz, 3H), 3.81 (q, J = 7.1 Hz, 1H), 1.76 (s, 1H), 0.94 (d, J = 6.3 Hz, 17H), 0.81 (s, 10H), 0.03 (s, 6H). 13C NMR (400 MHz, CDCl3) δ 157.60, 156.81, 155.51, 137.20, 137.43, 13315, 133.45, 132.44, 132.15, 132.13, 132.08, 131.97, 131.39, 129.41, 129.19, 128.73, 128.65, 128.57,

128.53, 128.46, 121.37, 120.01, 115.67, 77.88, 69.36, 60.32, 25.86, 25.72, 21.93, 20.90, 18.15, 14.17, -3.45, -4.39.

5.4.13 (E)-4-(4-((4-(4-hydroxyphenyl)-2,2-dimethyl-3-phenylchroman-7-yl)oxy)but-1-en-1-yl)phenol

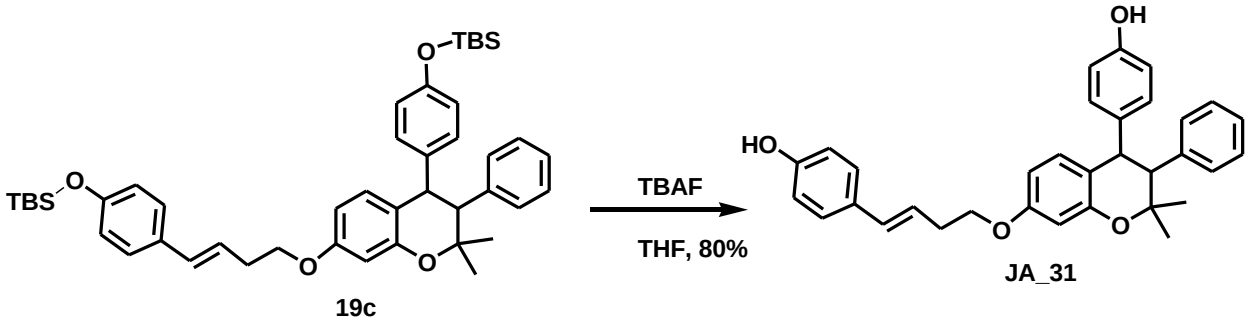

Tetrabutyl ammonium fluoride (TBAF) (0.63ml, 2.4mmol) was added to a stirred solution of **19C** (0.35g, 0.48 mmol) and stirred for 6h. The reaction was quenched with ammonium chloride (NH_4Cl) solution and extracted with ethyl acetate (3 x 30ml), dried over anhydrous sodium sulfate (Na_2SO_4). The solution was filtered, and the volume reduced under vacuum. Purification was done by column chromatography (10% ethyl acetate: hexane) to give JA_31 (0.19g, 80%).

1H NMR (400 MHz, Chloroform-d) δ 7.88 (s, 1H), 7.44 (dd, J = 12.0, 7.5 Hz, 6H), 7.26 – 7.20 (m, 3H), 7.15 (td, J = 7.6, 2.7 Hz, 6H), 7.02 (t, J = 4.7 Hz, 3H), 4.74 – 4.60 (m, 2H), 3.82 (d, J = 7.1 Hz, 1H), 3.03 (t, J = 8.1 Hz, 1H), 2.50 – 2.16 (m, 1H), 0.90 (d, J = 6.3 Hz, 6H). 13C NMR (400 MHz, CDCl3) δ 156.67, 137.02, 136.91, 133.53, 133.34, 132.61, 131.88, 131.86, 131.77, 131.57, 128.57, 128.42, 128.35, 128.29, 128.28, 115.62, 114.33,

77.99, 68.70, 60.08, 54.19, 53.34, 21.75, 20.69, 13.97, 13.92, 13.49. **HR-FT-MS calcd for $C_{33}H_{32}O_4$ 492.60 found 492.24**

5.4.14 Tert-butyl(4-(4-((2,2-dimethyl-3-phenyl-2H-chromen-7yl)oxy)butyl)phenoxy) dimethylsilane

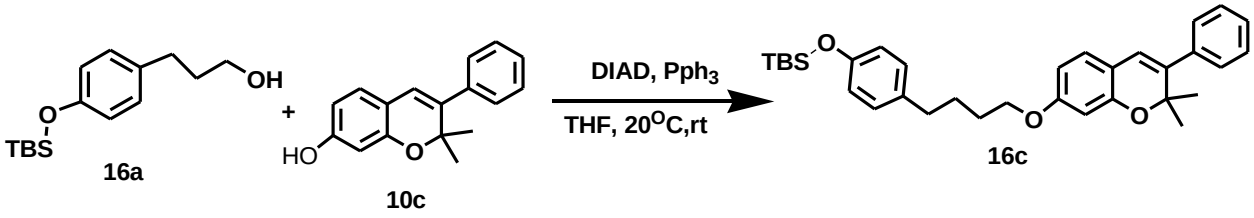

To a solution of 3-(4-((tert-butyldimethylsilyl)oxy)phenyl)propan-1-ol (**16a**) (0.25g, 0.96 mmol), **10c** (0.21g, 0.83 mmol) in Tetrahydrofuran (THF) (6.30 ml) was cooled to 0°C. Triphenylphosphine (Pph_3) (0.54g, 2.1 mmol) was added followed by addition of (DIAD (0.16ml, 079 mmol) in dropwise for 30 min. The mixture was stirred overnight at room temperature and quenched with 1N NaOH (45ml) after completion. The aqueous layer was extracted with ethyl acetate (3 x 40ml), washed with brine (40ml), dried over anhydrous Na_2SO_4 and concentrated under reduced pressure to give yellow oil (0.38g, 92%).

1H NMR (600 MHz, Chloroform-d) δ 7.51 (s, 1H), 7.32 – 7.26 (m, 2H), 7.05 (tdd, J = 8.7, 5.8, 2.4 Hz, 4H), 6.91 (d, J = 8.1 Hz, 1H), 6.85 (dd, J = 8.3, 5.4 Hz, 2H), 6.53 – 6.48 (m, 2H), 6.28 (s, 1H), 5.03 (ddt, J = 20.7, 14.4, 7.3 Hz, 1H), 3.64 – 3.55 (m, 1H), 2.21 (t, J = 7.7 Hz, 1H), 1.93 (p, J = 7.4 Hz, 1H), 1.51 – 1.41 (m, 6H), 1.38 (s, 3H), 1.18 – 1.13 (m, 11H), 0.98 (s, 9H), 0.21 (s, 6H) 13C NMR (600 MHz, CDCl3) δ 162.91, 161.10, 157.72, 153.81, 150.19, 137.33, 135.73, 135.84, 129.90, 129.81, 129.20, 127.29, 122.59, 119.72, 115.66, 115.1, 115.01, 114.94, 108.48, 103.80, 78.73, 72.71, 32.08, 29.88, 29.77, 29.34, 22.71, 22.04, 21.85, 21.60, 18.07, 17.92, 17.93, 17.80, 17.76, -0.91.

5.4.15 Tert-butyl(4-(4-((4-(4-((tert-butyldimethylsilyl)oxy)phenyl)-2,2-dimethyl-3-phenylchroman-7-yl)oxy)butyl)phenoxy)dimethylsilane

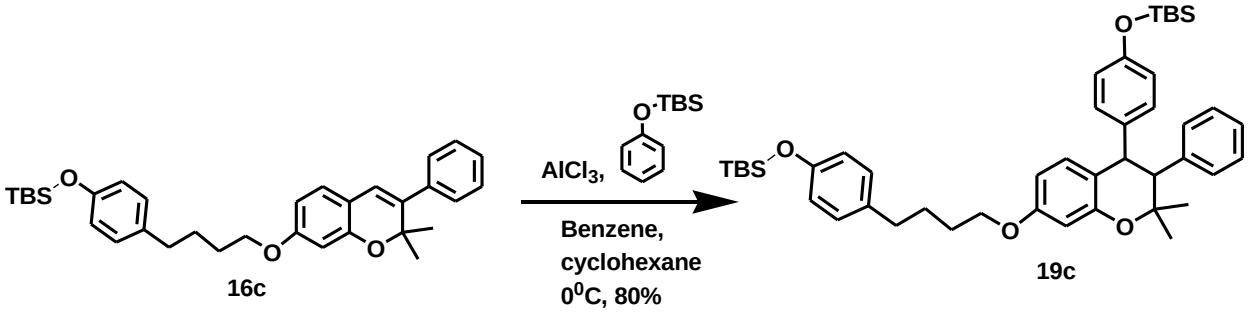

To a stirred solution of **16c** (0.36 g, 0.71 mmol) and tert-buthyldimethyl(phenoxy)silane (0.31 g, 1.49 mmol) in benzene-cyclohexane mixture (1:1 ratio, 10 ml) at 0°C was added anhydrous aluminum chloride (0.13g, 0.85 mmol) in portions and stirred for 30 min and the mixture was further stirred for 8 hrs. at room temperature. The reaction mixture was quenched by adding a mixture of ice and conc. Hydrochloric acid (1:1 3.0 ml) and the

organic layer was separated. The aqueous layer was re-extracted three times with dichloromethane (18.0 ml). The combined extract was washed with $NaHCO_3$ (10 %, 11.0ml), dried over anhydrous Na_2SO_4, filtered and concentrated under reduced pressure. The semi-solid obtained was purified by column chromatography (70% hexane: 30% ethyl acetate) to obtain (0.40g, 80%) **19c**.

1H NMR (600 MHz, Chloroform-d) δ 8.10 (dd, J = 8.3, 1.4 Hz, 1H), 7.71 – 7.67 (m, 1H), 7.65 – 7.59 (m, 1H), 7.35 (d, J = 7.8 Hz, 1H), 7.20 (dd, J = 8.5, 7.4 Hz, 2H), 7.18 – 7.13 (m, 4H), 7.11 – 7.05 (m, 3H), 6.92 – 6.88 (m, 3H), 6.81 – 6.74 (m, 2H), 6.71 (dt, J = 7.6, 1.1 Hz, 2H), 6.32 (d, J = 7.4 Hz, 1H), 6.15 – 6.10 (m, 1H), 2.02 (s, 1H), 1.43 – 1.42 (m, 6H), 1.37 (s, 3H), 0.95 (s, 9H), 0.22 (s, 6H) 13C NMR (600 MHz, CDCl3) δ 157.13, 156.15, 153.41, 151.78, 138.34, 135.75, 133.62, 133.03, 130.35, 130.00, 129.91, 129.86, 129.83, 129.55, 129.42, 129.78, 128.62, 128.33, 128.23, 128.14, 127.01, 122.43, 121.77, 121.09, 120.96, 120.29, 119.98, 119.69, 116.61, 115.45, 115.37, 115.24, 115.10, 114.96, 113.11, 108.39, 100.51, 78.67, 67.35, 60.69, 34.71, 32.00, 31.68, 29.82, 29.45, 27.32, 27.14, 26.88, 25.35, 22.77, 22.71, 18.01, 17.98, 17.87, 17.81, 17.73, 14.20, -3.40, -4.32.

5.4.16 4-(7-(4-(4-((tert-butyldimethylsilyl)oxy)phenyl)butoxy)-2,2-dimethyl-3-phenylchroman-4-yl)phenol

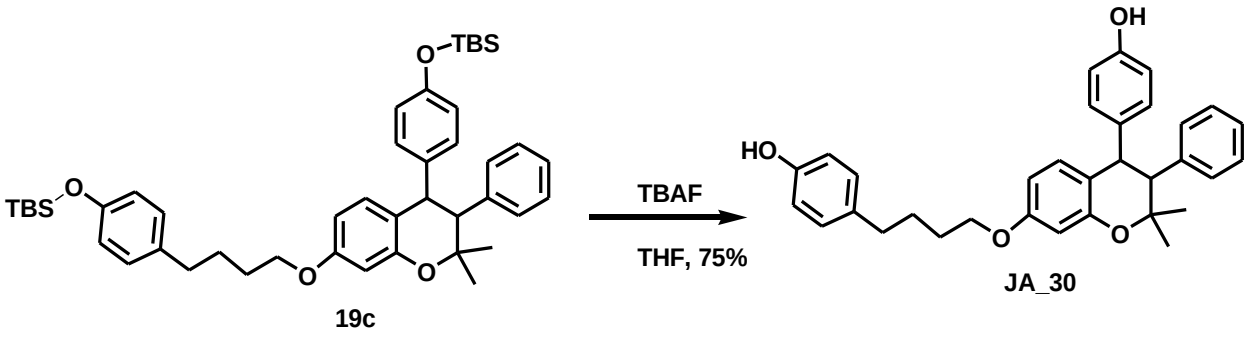

Tertbutyl ammonium fluoride (TBAF) (0.63ml, 1.94mmol) was added to a stirred solution of **19b** (0.28g, 0.39 mmol) and stirred for 6h. The reaction was quenched with ammonium chloride (NH_4Cl) solution and extracted with ethyl acetate (3 x 25ml), dried over anhydrous sodium sulfate (Na_2SO_4). The solution was filtered, and the volume reduced under vacuum. Purification was done by column chromatography (10% ethyl acetate: hexane) to give JA_30 (0.15g, 75%).

1H NMR (400 MHz, Chloroform-d) δ 7.87 – 7.78 (m, 10H), 7.62 (td, J = 7.4, 1.5 Hz, 6H), 7.52 (dt, J = 7.6, 3.9 Hz, 12H), 7.47 (d, J = 2.1 Hz, 3H), 7.34 – 7.27 (m, 15H), 7.22 – 7.18 (m, 2H), 7.11 (dd, J = 7.6, 1.5 Hz, 13H), 7.00 (t, J = 7.3 Hz, 9H), 5.17 – 5.06 (m, 3H), 4.27 (q, J = 7.1 Hz, 1H), 3.71 (s, 1H), 2.71 (t, J = 7.9 Hz, 1H), 2.10 – 2.00 (m, 1H), 1.33 (s, 3H), 1.32 (s, 3H). 13C NMR (400 MHz, CDCl3) δ 157.58, 156.53, 156.19, 154.11, 142.85, 134.03, 133.84, 132.80, 132.78, 132.31, 132.26, 132.20, 131.51, 130.46, 129.72, 129.66, 129.44, 129.09, 128.96, 128.85, 128.00, 120.27, 120.18, 115.82, 115.19, 77.89, 70.83, 61.23, 41.71, 31.33, 29.95, 22.11, 21.96, 21.18, 18.20, 18.18, 17.97. **HR-FT-MS calcd for $C_{33}H_{34}O_4$ 494.62 found 494.36**

5.4.17 4-(7-(4-(4-((tert-butyldimethylsilyl)oxy)phenyl)butoxy)-2,2-dimethyl-3-phenylchroman-4-yl)aniline

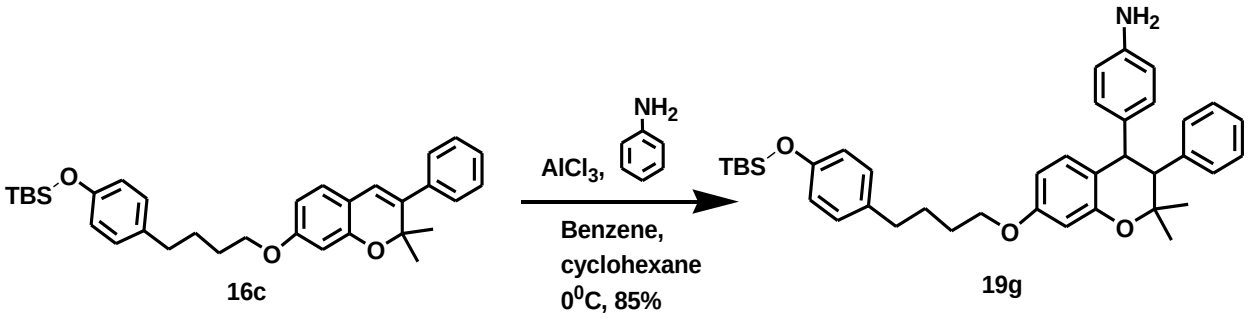

To a stirred solution of 16c (0.40 g, 0.79 mmol) and aniline (0.07 g, 0.75 mmol) in benzene-cyclohexane mixture (1:1 ratio, 13.0 ml) at 0°C was added anhydrous aluminum chloride (0.18g, 1.35 mmol) in portions. A solution of aniline (0.18 g, 1.94 mmol) in benzene-cyclohexane mixture (1:1 Ratio, 21.0 ml) was added after 30 min and the mixture further stirred for 8 hrs. The reaction mixture was quenched by adding a mixture of ice and conc. Hydrochloric acid (1:1 4.0 ml) and the organic layer was separated. The aqueous layer was re-extracted three times with dichloromethane (25.0 ml). The combined extract was washed with $NaHCO_3$ (10 %, 15.0ml), dried over anhydrous Na_2SO_4, filtered and concentrated under reduced pressure. The semi-solid obtained was purified by column chromatography (70% hexane: 30% ethyl acetate) to obtain (0.39g, 85%) 19g.

^{1}H NMR (400 MHz, Chloroform-d) δ 7.72 (s, 2H), 7.53 (dd, J = 12.1, 7.4 Hz, 11H), 7.32 (t, J = 7.4 Hz, 6H), 7.20 (td, J = 7.6, 2.8 Hz, 11H), 7.04 (d, J = 4.3 Hz, 4H), 6.85 (t, J = 7.6 Hz, 1H), 6.79 – 6.70 (m, 1H), 6.43 (d, J = 7.8 Hz, 1H), 4.81 – 4.69 (m, 4H), 3.43 (d, J = 14.1 Hz, 2H), 2.71 – 2.57 (m, 1H), 2.37 (q, J = 7.8, 6.7 Hz, 1H), 0.98 (d, J = 6.3 Hz, 22H), 0.28 (d, J = 3.1 Hz, 8H), 0.95 (s,9H), 0.21 (s, 6H). 13C NMR (400 MHz, CDCl3) δ 157.10,

156.81, 156.04, 153.51, 146.66, 137.03, 136.91, 133.56, 133.57, 132.49, 132.07, 132.03, 132.00, 131.91, 131.42, 130.54, 129.11, 128.96, 128.91, 128.68, 128.55, 128.48, 128.44, 128.41, 128.01, 117.81, 115.62, 115.06, 78.41, 69.09, 51.35, 43.80, 36.08, 30.87, 26.91, 21.85, 17.87, -3.52, 0-.91.

5.4.18 4-{3-[4-(4-Amino-phenyl)-2,2-dimethyl-3-phenyl-chroman-7-yloxy]-propyl}-phenol

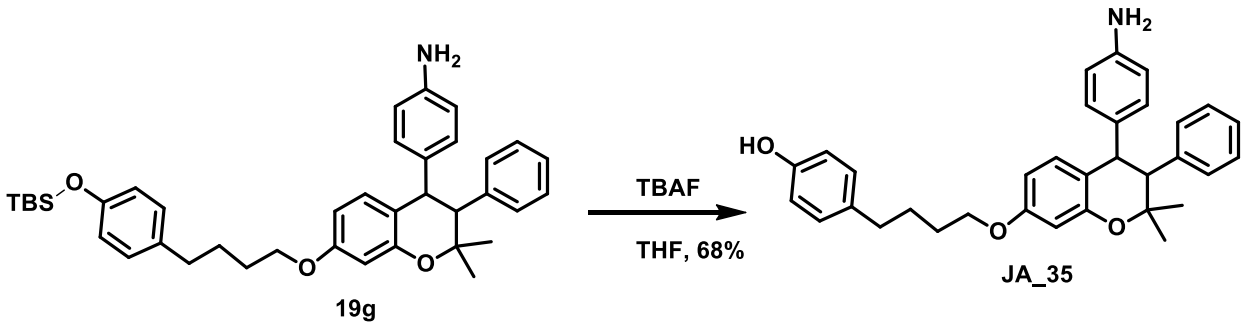

Tertbutyl ammonium fluoride (TBAF) (1.63ml, 4.12mmol) was added to a stirred solution of **19g** (0.52g, 0.86 mmol) and stirred for 6h. The reaction was quenched with ammonium chloride (NH_4Cl) solution and extracted with ethyl acetate (3 x 38ml), dried over anhydrous sodium sulfate (Na_2SO_4). The solution was filtered, and the volume reduced under vacuum. Purification was done by column chromatography (10% ethyl acetate: hexane) to give JA_35 (0.29g, 68%).

1H NMR (400 MHz, Chloroform-d) δ 7.71 (s, 2H), 7.50 (dd, J = 12.1, 7.4 Hz, 11H), 7.30 (t, J = 7.4 Hz, 6H), 7.22 (td, J = 7.6, 2.8 Hz, 11H), 7.10 (d, J = 4.3 Hz, 4H), 6.86 (t, J = 7.6 Hz, 1H), 6.79 – 6.71 (m, 1H), 6.45 (d, J = 7.8 Hz, 1H), 4.83 – 4.67 (m, 4H), 3.42 (d,

J = 14.1 Hz, 2H), 2.72 – 2.58 (m, 1H), 2.36 (q, J = 7.8, 6.7 Hz, 1H), 0.98 (d, J = 6.3 Hz, 22H), 0.89 (d, J = 3.1 Hz, 8H). 13C NMR (400 MHz, CDCl3) δ 159.10, 156.80, 156.06, 153.58, 146.76, 137.09, 136.99, 133.66, 133.47, 132.49, 132.07, 132.04, 132.00, 131.90, 131.45, 130.56, 129.10, 128.96, 128.90, 128.69, 128.56, 128.47, 128.44, 128.40, 128.01, 117.85, 115.62, 115.08, 78.40, 69.09, 51.36, 43.82, 36.08, 30.09, 26.92, 21.85, 17.87, 17.83, 12.55, 12.42. . **HR-FT-MS calcd for $C_{33}H_{35}NO_3$ 493.63 found 493.58**

5.4.19 Tert-butyl(4-(4-((4-(4-methoxyphenyl)-2,2-dimethyl-3-phenylchroman-7-yl)oxy)butyl)) dimethylsilane

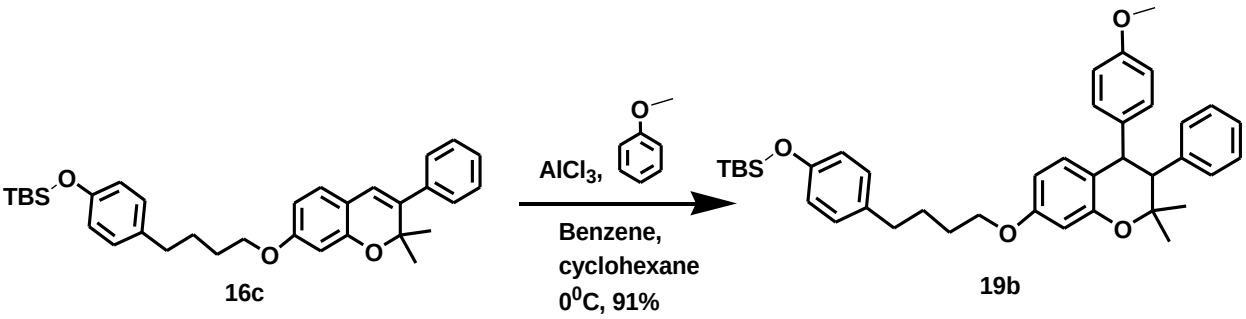

To a stirred solution of 18c (0.42 g, 0.83 mmol) and anisole (0.136 g, 1.25 mmol) in benzene-cyclohexane mixture (1:1 ratio, 15.0 ml) at 0°C was added anhydrous aluminum chloride (0.13g, 0.97 mmol) in portions. A solution of anisole (0.005 g, 0.049 mmol) in benzene- cyclohexane mixture (1:1 Ratio, 10.0 ml) was added after 30 min, and the mixture further stirred for 8 hrs. The reaction mixture was quenched by adding a mixture of ice and conc. Hydrochloric acid (1:1 2.0 ml) and the organic layer was separated. The aqueous layer was re-extracted three times with dichloromethane (20.0 ml). The combined extract was washed with $NaHCO_3$ (10 %, 5.0ml), dried over anhydrous Na_2SO_4, filtered and

concentrated under reduced pressure. The semi-solid obtained was purified by column chromatography (70% hexane: 30% ethyl acetate) to obtain (0.45g, 91%) 19c.

1H NMR (600 MHz, Chloroform-d) δ 7.73 – 7.68 (m, 1H), 7.65 – 7.60 (m, 1H), 7.35 (d, J = 7.8 Hz, 1H), 7.28 (dd, J = 8.5, 7.4 Hz, 2H), 7.17 – 7.11 (m, 4H), 7.11 – 7.04 (m, 3H), 6.91 – 6.86 (m, 3H), 6.80 – 6.74 (m, 2H), 6.72 (dt, J = 7.6, 1.1 Hz, 2H), 6.31 (d, J = 7.4 Hz, 1H), 6.15 – 6.12 (m, 1H), 1.99 (s, 1H), 1.45 – 1.40 (m, 6H), 1.37 (s, 3H), 1.18 – 1.12 (m, 11H), 0.98 (s, 9H), 0.23 (s, 6H) 13C NMR (600 MHz, CDCl3) δ 157.22, 156.17, 153.56, 151.06, 137.91, 135.67, 133.67, 132.73, 130.35, 130.01, 129.91, 129.86, 129.82, 129.59, 129.43, 129.24, 128.67, 128.36, 128.20, 128.15, 127.1, 122.56, 121.78, 121.05, 120.98, 120.21, 119.99, 119.72, 116.54, 115.48, 115.35, 115.26, 115.18, 114.97, 113.19, 108.37, 100.52, 78.63, 67.38, 60.56, 34.84, 32.00, 31.69, 29.81, 29.3, 27.33, 27.15, 26.88, 25.32, 22.79, 22.75, 18.00, 17.95, 17.88, 17.82, 17.76, 14.24, -0.93.

5.4.20 4-{3-[4-(4-Methoxy-phenyl)-2,2-dimethyl-3-phenyl-chroman-7-yloxy]-propyl}-phenol

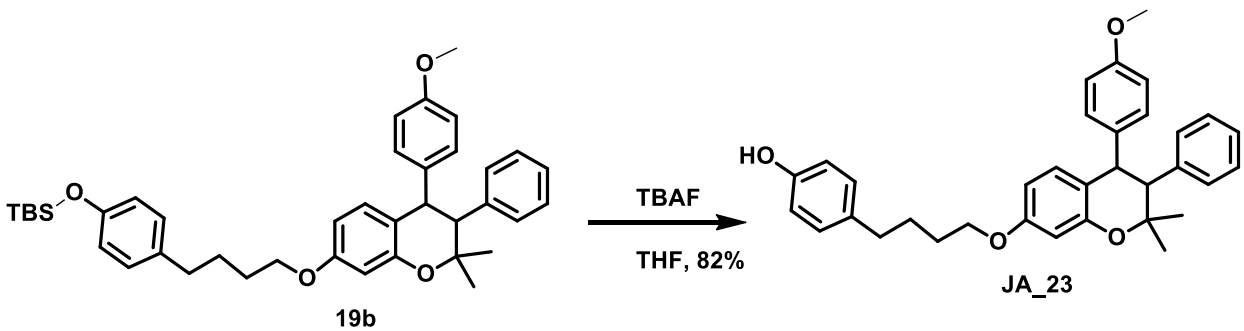

Tetrabutyl ammonium fluoride (TBAF) (0.72ml, 2.73mmol) was added to a stirred solution of **19b** (0.34g, 0.55 mmol) and stirred for 6h. The reaction was quenched with ammonium chloride (NH_4Cl) solution and extracted with ethyl acetate (3 x 45ml), dried over anhydrous sodium sulfate (Na_2SO_4). The solution was filtered and the volume reduced under vacuum. Purification was done by column chromatography (10% ethyl acetate: hexane) to give JA_23 (0.23g, 82%).

1H NMR (600 MHz, Chloroform-d) δ 7.37 – 7.32 (m, 2H), 7.01 (tt, J = 7.3, 1.2 Hz, 4H), 6.99 – 6.95 (m, 2H), 5.04 (p, J = 6.2 Hz, 1H), 3.83 (s, 3H), 1.32 (d, J = 6.8 Hz, 6H). 13C NMR (400 MHz, CDCl3) δ 159.59, 156.89, 156.82, 129.49, 129.47, 128.39, 120.72, 119.82, 115.50, 113.95, 77.53, 69.98, 55.06, 37.32, 26.98, 21.97, 17.98, 17.80. . **HR-FT-MS calcd for $C_{34}H_{36}O_4$ 508.64 found 508.01**

5.4.21 4-[3-(4-Bromo-phenyl)-7-(tert-butyl-dimethyl-silanyloxy)-2,2-dimethyl-chroman-4-yl]-phenol

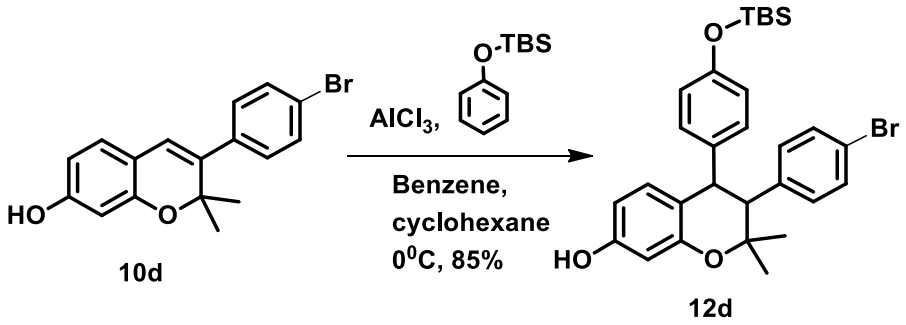

Following the procedure in the preparation of **JA_20**, **10d** (3.3g, 9.96mmol) reacted with tert-butyldimethyl(phenoxy)silane (2.8ml, 20.9mmol) in the presence of AlCl (1.6g, 11.95mmol) to afford 12d (4.8g, 90%).

1H NMR (400 MHz, Chloroform-d) δ 7.24 (s, 2H), 7.12 – 7.04 (m, 15H), 6.79 (tt, J = 7.3, 1.1 Hz, 9H), 6.75 – 6.68 (m, 14H), 6.65 (d, J = 8.5 Hz, 1H), 6.47 – 6.41 (m, 1H), 6.32 (d, J = 2.5 Hz, 1H), 6.24 – 6.12 (m, 8H), 2.36 (d, J = 10.9 Hz, 1H), 1.25 – 1.12 (m, 10H), 0.82 – 0.72 (m, 7H), 0.20 (s, 1H), -0.00 (s, 1H). 13C NMR (400 MHz, CDCl3) δ 158.86, 155.20, 153.78, 153.56, 138.26, 135.66, 131.11, 130.20, 129.70, 128.32, 120.83, 118.74, 115.43, 107.81, 101.67, 78.32, 55.24, 43.76, 30.71, 28.54, 26.87, 22.91, 19.96, 14.15, 14.02, 10.87, 0.00.

5.4.22 3-(4-Bromo-phenyl)-4-[4-(tert-butyl-dimethyl-silanyloxy)-phenyl]-7-{3-[4-(tert-butyl-dimethyl-silanyloxy)-phenyl]-allyloxy}-2,2-dimethyl-chroman

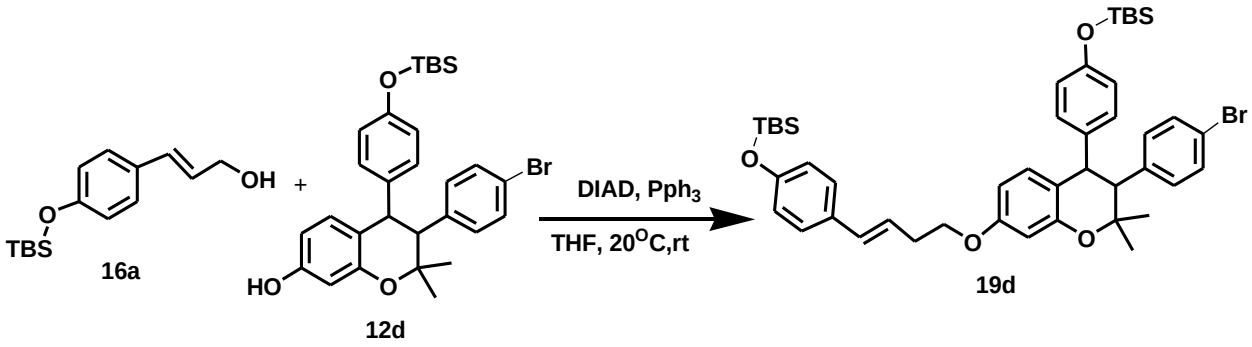

To a solution of unsaturated alcohol (**16a**) (0.26g, 1.0 mmol), **12d** (0.33, 1.0 mmol) in Tetrahydrofuran (THF) (10 ml) was cooled to 0°C. Triphenyphospine (Pph_3) (0.35g, 2.66 mmol) was added followed by addition of (DIAD (0.20ml, 1.0 mmol) in dropwise for 30 min. The mixture was stirred overnight at room temperature and quenched with 1N NaOH (100ml) after completion. The aqueous layer was extracted with ethyl acetate (3 x 50ml), washed with brine (50ml), dried over anhydrous Na_2SO_4 and concentrated under reduced pressure to give yellow oil (0.75g, 94%).

1H NMR (400 MHz, Chloroform-d) δ 7.47 (dd, J = 12.2, 7.5 Hz, 9H), 7.23 (dt, J = 33.0, 7.4 Hz, 13H), 7.14 – 6.97 (m, 8H), 6.79 – 6.53 (m, 4H), 4.73 (p, J = 6.2 Hz, 3H), 3.88 (q, J = 7.1 Hz, 1H), 1.78 (s, 1H), 0.97 (d, J = 6.3 Hz, 17H), 0.80 (s, 10H), 0.00 (s, 6H). 13C NMR (400 MHz, CDCl3) δ 157.61, 156.85, 155.54, 137.23, 137.12, 133.75, 133.56, 132.47, 132.15, 132.13, 132.08, 131.98, 131.43, 129.40, 129.19, 128.73, 128.65, 128.57, 128.53, 128.46, 121.37, 120.06, 115.67, 77.87, 69.30, 60.33, 25.86, 25.72, 21.93, 20.90, 18.15, 14.17, -3.45, -4.39.

5.4.23 4-(4-((3-(4-bromophenyl)-4-(4-hydroxyphenyl)-2,2-dimethylchroman-7-yl)oxy)butyl)phenol

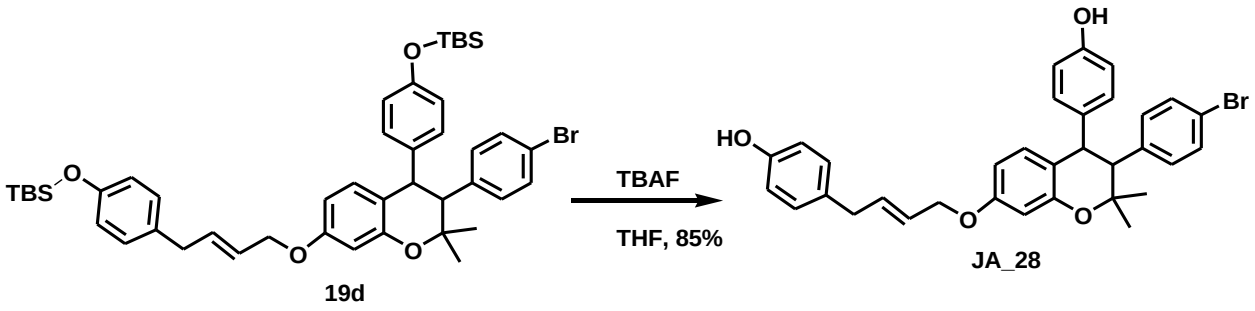

Tetrabutyl ammonium fluoride (TBAF) (0.99 ml, 3.8mmol) was added to a stirred solution of 19d (0.61g, 0.76 mmol) and stirred for 6h. The reaction was quenched with ammonium chloride (NH_4Cl) solution and extracted with ethyl acetate (3 x 50ml), dried over anhydrous sodium sulfate (Na_2SO_4). The solution was filtered, and the volume reduced under vacuum. Purification was done by column chromatography (10% ethyl acetate: hexane) to give JA_28 (0.37g, 85%).

1H NMR (400 MHz, Chloroform-d) δ 7.63 (ddt, J = 12.1, 6.8, 1.4 Hz, 5H), 7.49 (ddt, J = 8.8, 3.0, 1.5 Hz, 3H), 7.41 (ddd, J = 8.5, 6.8, 3.1 Hz, 5H), 7.26 – 7.19 (m, 1H), 7.12 (d, J = 8.1 Hz, 1H), 6.80 (d, J = 8.5 Hz, 1H), 4.91 (p, J = 6.2 Hz, 2H), 1.18 (s, 3H), 1.17 (s, 3H). 13C NMR (400 MHz, CDCl3) δ 156.76, 132.31, 132.20, 132.17, 132.11, 132.01, 131.27, 128.67, 128.55, 127.60, 115.71, 78.52, 69.71, 60.46, 29.66, 22.05, 21.92. . **HR-FT-MS calcd for $C_{33}H_{33}BrO_4$ 571.03 found 571.32**

5.4.24 (4-(4-((3-(4-bromophenyl)-4-(4-((tert-butyldimethylsilyl)oxy)phenyl)-2,2-dimethylchroman-7-yl)oxy)butyl)phenoxy)(tert-butyl)dimethylsilane

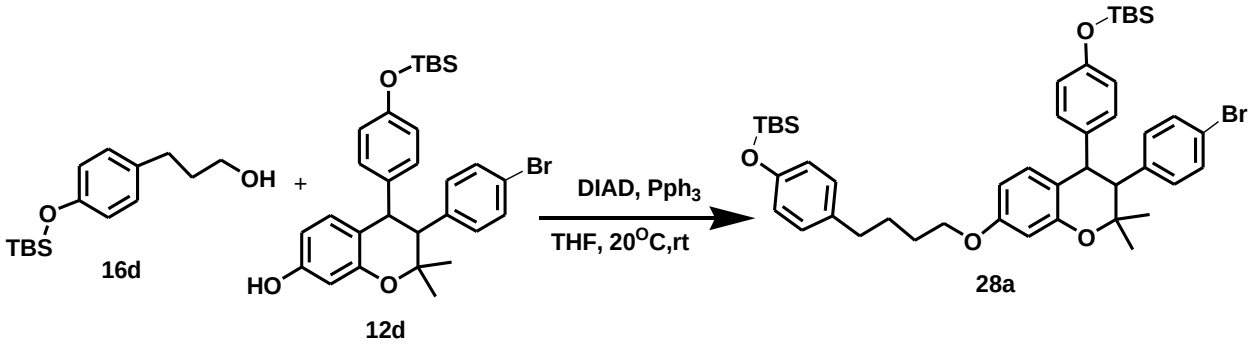

To a solution of saturated alcohol (**16d**) (0.23g, 1.0 mmol), **12d** (0.33, 1.0 mmol) in Tetrahydrofuran (THF) (10 ml) was cooled to 0°C. Triphenyphospine (Pph_3) (0.35g, 2.66 mmol) was added followed by addition of (DIAD (0.20ml, 1.0 mmol) in dropwise for 30 min. The mixture was stirred overnight at room temperature and quenched with 1N NaOH (100ml) after completion. The aqueous layer was extracted with ethyl acetate (3 x 50ml), washed with brine (50ml), dried over anhydrous Na_2SO_4 and concentrated under reduced pressure to give yellow oil (0.71g, 92%).

1H NMR (400 MHz, Chloroform-d) δ 7.47 (dd, J = 12.2, 7.5 Hz, 9H), 7.23 (dt, J = 33.0, 7.4 Hz, 13H), 7.14 – 6.97 (m, 8H), 6.79 – 6.53 (m, 4H), 4.73 (p, J = 6.2 Hz, 3H), 3.88 (q, J = 7.1 Hz, 1H), 1.78 (s, 1H), 0.97 (d, J = 6.3 Hz, 17H), 0.80 (s, 10H), 0.00 (s, 6H). 13C NMR (400 MHz, CDCl3) δ 157.61, 156.85, 155.54, 137.23, 137.12, 133.75, 133.56, 132.47, 132.15, 132.13, 132.08, 131.98, 131.43, 129.40, 129.19, 128.73, 128.65, 128.57, 128.53, 128.46, 121.37, 120.06, 115.67, 77.87, 69.30, 60.33, 25.86, 25.88, 21.91, 20.96, 18.19, 14.11, -3.47, -4.33.

5.4.25 4-(4-((3-(4-bromophenyl)-4-(4-hydroxyphenyl)-2,2-dimethylchroman-7-yl)oxy)butyl)phenol

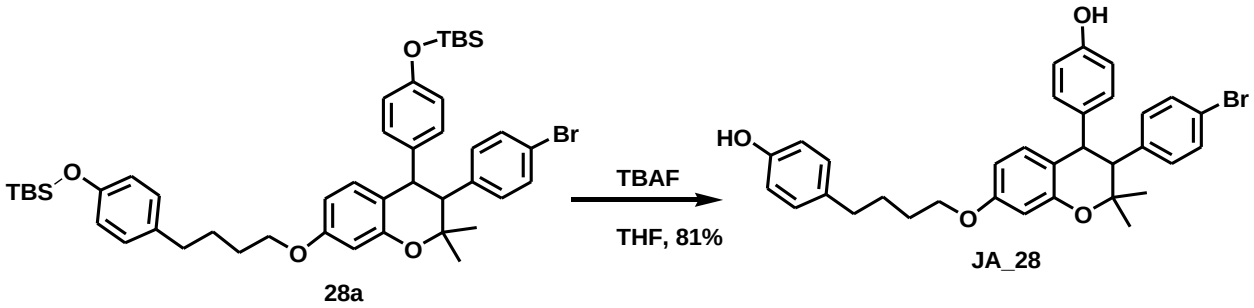

Tetrabutyl ammonium fluoride (TBAF) (0.97 ml, 3.8mmol) was added to a stirred solution of **28a** (0.63g, 0.76 mmol) and stirred for 6h. The reaction was quenched with ammonium chloride (NH_4Cl) solution and extracted with ethyl acetate (3 x 50ml), dried over anhydrous sodium sulfate (Na_2SO_4). The solution was filtered, and the volume reduced under vacuum. Purification was done by column chromatography (10% ethyl acetate: hexane) to give JA_28 (0.35g, 81%).

1H NMR (400 MHz, Chloroform-d) δ 7.63 (ddt, J = 12.1, 6.8, 1.4 Hz, 5H), 7.49 (ddt, J = 8.8, 3.0, 1.5 Hz, 3H), 7.41 (ddd, J = 8.5, 6.8, 3.1 Hz, 5H), 7.26 – 7.19 (m, 1H), 7.12 (d, J = 8.1 Hz, 1H), 6.80 (d, J = 8.5 Hz, 1H), 4.91 (p, J = 6.2 Hz, 2H), 1.18 (s, 3H), 1.17 (s, 3H). 13C NMR (400 MHz, CDCl3) δ 156.76, 132.31, 132.20, 132.17, 132.11, 132.01, 131.27, 128.67, 128.55, 127.60, 115.71, 78.52, 69.71, 60.46, 29.66, 22.05, 21.92. . **HR-FT-MS calcd for $C_{33}H_{33}BrO_4$ 573.51 found 573.20**

5.4.26 3-(4-Bromo-phenyl)-2,2-dimethyl-chroman-7-yloxy]-tert-butyl-dimethyl-silane

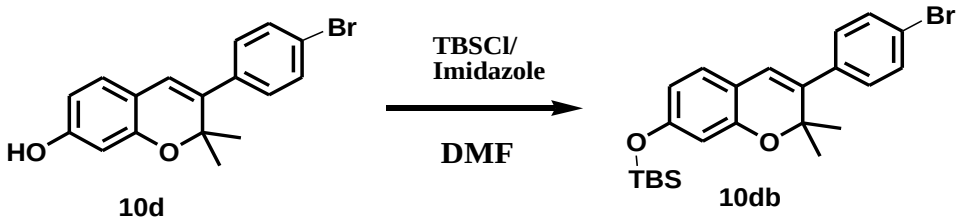

10d **10db**

To a solution of **10d** (6.43g, 26.9mmol) in dimethyl formamide (DMF) (99.88ml), tert-buthylsilylchloride (TBSCl) (6.38g, 40.45mmol) and imidazole (5.1g, 74.2mmol) were added sequentially. The reaction was stirred for 24h and quenched with saturated $NaHCO_3$ (30ml). The aqueous layer was extracted with ethyl acetate (3 x 40ml), dried over anhydrous sodium sulfate (Na_2SO_4), filtered and the organic layer evaporated under reduced pressure. The crude product was purified by column chromatography (10% ethyl acetate: hexane) to give ester **10db** (7.31g, 74%).

1H NMR (400 MHz, Chloroform-d) δ 7.22 (d, J = 8.3 Hz, 2H), 7.08 – 6.98 (m, 2H), 6.86 – 6.75 (m, 1H), 6.27 (d, J = 2.3 Hz, 1H), 6.22 (dd, J = 8.3, 2.4 Hz, 1H), 6.05 (s, 1H), 3.91 (q, J = 7.1 Hz, 1H), 3.57 – 3.48 (m, 2H), 1.83 (s, 2H), 1.72 – 1.61 (m, 2H), 1.10 (d, J = 5.7 Hz, 11H), 0.79 (s, 11H), 0.00 (s, 6H). 13C NMR (400 MHz, CDCl3) δ 156.01, 153.93, 149.72, 143.06, 130.70, 130.63, 130.45, 126.46, 120.64, 119.01, 112.07, 108.43, 77.50, 75.38, 73.19, 67.79, 67.54, 60.47, 33.03, 31.96, 25.79, 25.62, 25.54, 14.10, -4.50.

5.4.27 3-(4-triisopropylsilanyloxy-phenyl)-acrylic acid methyl ester

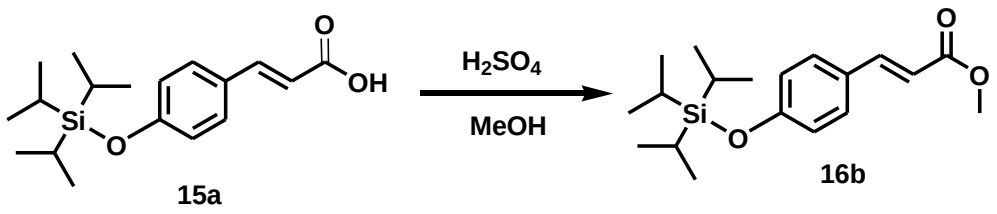

15a 16b

Compound **15a** (5.0g, 16.2mmol) was dissolved in MeOH (33 ml) and concentrated hydrochloric acid (HCl) (0.83ml) was added. The reaction mixture was refluxed for 16h, cooled to room temperature and the solvent was evaporated under reduced pressure. The resulting residue was dissolved in ethyl acetate (25ml) and washed successively with 1M $NaHCO_3$ (2 X 17 ml) and water (18ml). The organic phase was dried with over anhydrous Na_2SO_4, filtered and the solvent was removed under reduced pressure to give a colorless crystal (5.35g, 97%).

1H NMR (400 MHz, Chloroform-d) δ 7.55 (d, J = 16.0 Hz, 1H), 7.33 – 7.27 (m, 2H), 6.81 – 6.75 (m, 2H), 6.19 (d, J = 16.0 Hz, 1H), 3.70 (s, 3H), 1.96 (s, 4H), 0.98 (s, 21H). 13C NMR (400 MHz, CDCl3) δ 171.78, 168.43, 159.02, 145.29, 129.97, 126.23, 115.96, 114.26, 60.66, 51.67, 20.99, 17.65, 14.08, 12.30.

5.4.28 3-(4-Triisopropylsilanyloxy-phenyl)-propionic acid methyl ester

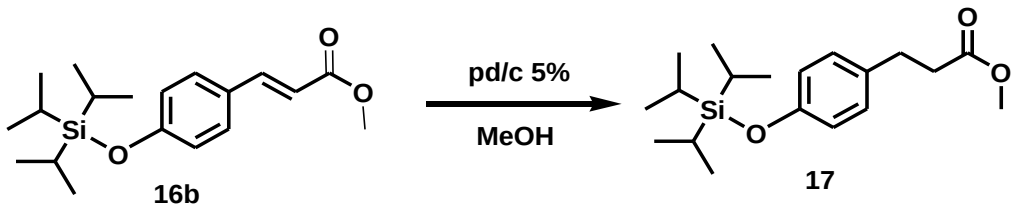

Following the procedure for the preparation of (**16**), unsaturated alcohol (3.12g, 9.33mmol) in methanol (50ml) was reacted with 5% pd/c (1.60g, 1.55mmol) to give the alcohol (2.60g, 90%).

1H NMR (400 MHz, Chloroform-d) δ 7.00 – 6.83 (m, 2H), 6.74 – 6.61 (m, 2H), 3.54 (s, 3H), 2.74 (t, J = 7.8 Hz, 2H), 2.47 (dd, J = 8.4, 7.1 Hz, 2H), 0.96 (s, 18H). 13C NMR (400 MHz, CDCl3) δ 174.34, 154.69, 131.73, 129.23, 115.51, 51.78, 36.13, 30.10, 17.92, 17.68, 17.31, 12.91, 12.35, 11.82.

5.4.29 3-(4-Triisopropylsilanyloxy-phenyl)-propan-1-ol

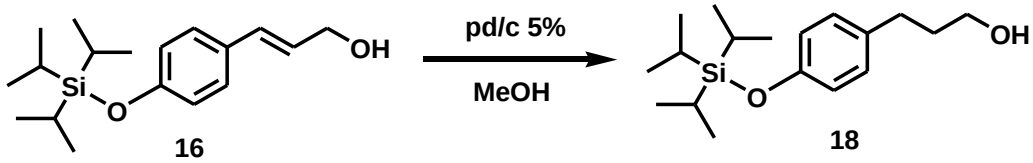

To an oven dry round 25ml round bottom flask under H_2 gas, was added a solution of unsaturated alcohol (6.1g, 34mmol) in methanol (100ml) and stirred until the solution is completely dissolved. (3.64g, 5.7mmol) 5% pd/c was added to the mixture and the compound was hydrogenated at room temperature for 4 hours. The reaction was quenched and concentrated under reduced pressure after completion and purified by column

chromatography (30% ethyl acetate: hexane) to obtain the desired product alcohol (5.91g, 97 %)

1H NMR (400 MHz, Chloroform-d) δ 6.94 – 6.87 (m, 1H), 6.71 – 6.63 (m, 1H), 3.55 (s, 2H), 2.75 (t, J = 7.8 Hz, 1H), 2.48 (dd, J = 8.4, 7.1 Hz, 1H), 1.04 – 0.97 (m, 3H), 0.96 (s, 11H), 0.94 – 0.83 (m, 2H). 13C NMR (101 MHz, CDCl3) δ 174.25, 154.67, 131.77, 129.23, 115.51, 51.77, 36.13, 30.11, 17.93, 17.68, 17.31, 12.91, 12.34.

5.4.30 3-(4-((tert-butyldimethylsilyl)oxy)phenyl)propan-1-ol

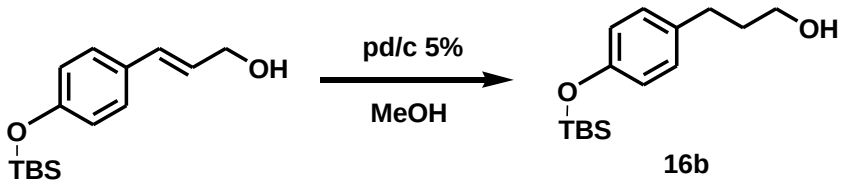

16a 16b

To an oven dry round 25ml round bottom flask under H_2 gas, was added a solution of unsaturated alcohol (5.4g, 20.4 mmol) in methanol (90 ml) and stirred until the solution is completely dissolved. (4.21g, 6.67 mmol) 5% pd/c was added to the mixture and the compound was hydrogenated at room temperature for 4 hours. The reaction was quenched and concentrated under reduced pressure after completion and purified by column chromatography (30% ethyl acetate: hexane) to obtain the desired product alcohol (4.2g, 96 %)

^{1}H NMR (400 MHz, Chloroform-d) δ 6.94 – 6.87 (m, 1H), 6.71 – 6.63 (m, 1H), 3.55 (s, 2H), 2.75 (t, J = 7.8 Hz, 1H), 2.48 (dd, J = 8.4, 7.1 Hz, 1H), 0.92 (s, 17H), 0.89 – 0.75 (m, 17H), 0.12 (s, 12H). 13C NMR (400 MHz, CDCl3) δ 155.30, 130.67, 130.22, 127.62,

126.56, 120.19, 69.34, 63.33, 31.64, 30.69, 25.74, 25.71, 22.69, 18.98, 18.22, 18.03, -3.56, -4.41.

5.5 Alternative synthetic routes for other analogs

5.5.1 3-(4-Triisopropylsilanyloxy-phenyl)-propan-1-ol

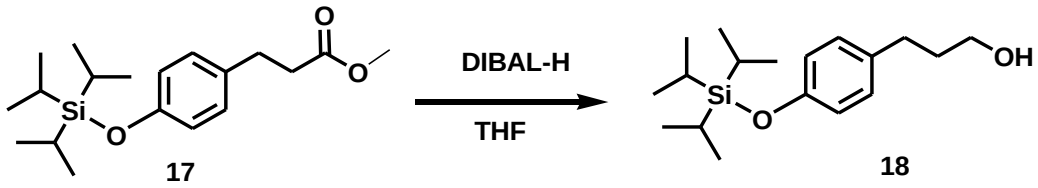

17 18

To a solution of ester (3.86g, 11.59mmol) in toluene (23.0ml), Diisobutylaluminium hydride (DIBAL-H) (20ml, 24.2mmol) was added at -78°C dropwise and the reaction was stirred for half an hour at 0°C. The temperature was reduced to room temperature after 20min. and the reaction cooled back at -78°C before the addition of a solution of potassium sodium titrate (30ml). The reaction was stirred overnight, and the aqueous layer extracted with ethyl acetate (3 x 40ml), dried over anhydrous sodium sulfate (Na_2SO_4) and the volume reduced under vacuum. The extract was purified using column chromatography (20% ethyl acetate: hexane) to afford a colorless liquid (3.48, 97%).

1H NMR (400 MHz, Chloroform-d) δ 7.13 – 7.02 (m, 2H), 6.89 – 6.80 (m, 2H), 3.65 (t, J = 6.5 Hz, 2H), 3.35 (s, 1H), 2.65 (dd, J = 8.5, 6.8 Hz, 2H), 1.94 – 1.82 (m, 2H), 1.39 – 1.28 (m, 4H), 1.28 – 1.11 (m, 25H), 1.11 (d, J = 2.8 Hz, 6H). 13C NMR (400 MHz, CDCl3) δ 154.07, 134.28, 129.21, 119.74, 77.50, 61.89, 34.33, 31.27, 17.96, 17.77, 12.71, 12.44.

5.5.2 3-(4-Fluoro-phenyl)-2,2-dimethyl-4-(4-trifluoromethoxy-phenyl)-chroman-7-ol

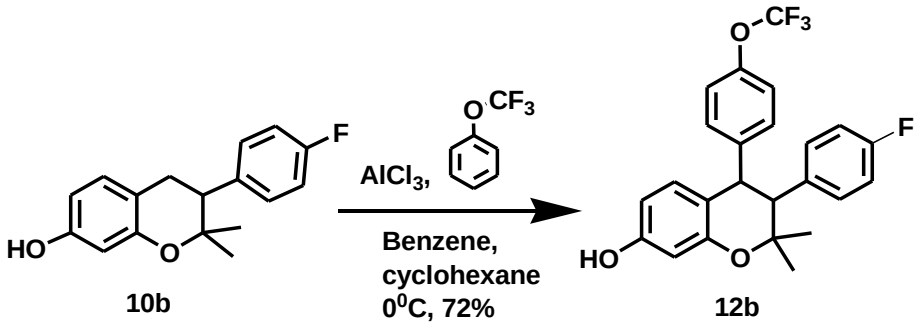

To a stirred solution of 3-(4-fluorophenyl)-3,4-dihydro-2,2-dimethyl-2H-chromen-7-ol (0.54g, 2.0 mmol) and 1-(trifluoromethoxy) benzene (0.68 g, 0.37 mmol) in benzene-cyclohexane mixture (1:1 ratio, 20.0 ml) at 0°C was added anhydrous aluminum chloride (0.32 g, 2.41 mmol) in portions and the mixture further stirred for 8 hrs. The reaction mixture was quenched by adding a mixture of ice and conc. Hydrochloric acid (1:1 3.0 ml) and the organic layer was separated. The aqueous layer was re-extracted three times with dichloromethane (8.0 ml). The combined extract was washed with $NaHCO_3$ (10 %, 5.0ml), dried over anhydrous Na_2SO_4, filtered and concentrated under reduced pressure. The semi-solid obtained was purified by column chromatography (70% hexane: 30% ethyl acetate) to obtain (0.87g, 69%) 12b**.**

1H NMR (600 MHz, Chloroform-d) δ 7.49 (dd, J = 26.9, 8.1 Hz, 1H), 7.34 – 7.19 (m, 4H), 7.09 – 6.98 (m, 1H), 6.97 – 6.87 (m, 2H), 4.18 (q, J = 7.2 Hz, 2H), 1.93 (d, J = 1.2 Hz, 2H), 1.59 (s, 1H), 1.40 – 1.18 (m, 6H). 13C NMR (600 MHz, CDCl3) δ 162.44, 160.81, 160.24, 156.43, 156.36, 139.34, 138.20, 135.26, 133.12, 131.08, 131.03, 130.21, 129.93, 129.55,

128.85, 128.65, 128.50, 128.40, 128.32, 128.24, 126.85, 125.81, 121.75, 121.44, 120.06, 115.48, 115.27, 115.20, 115.13, 115.10, 111.82, 111.63, 104.80, 102.96, 80.58, 60.74, 34.52, 27.53, 26.96, 26.21.

5.5.3 4-{3-[3-(4-Fluoro-phenyl)-2,2-dimethyl-2H-chromen-7-yloxy]-propyl}-phenol

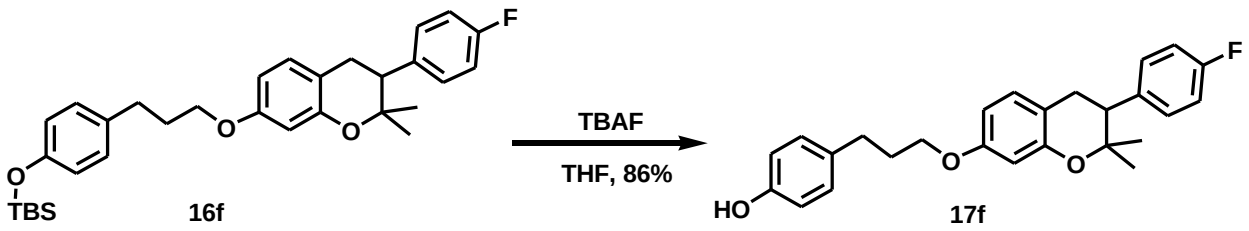

Tetrabutyl ammonium fluoride (TBAF) (.15 ml, 5.2mmol) was added to a stirred solution of (4-(3-(3-(4-fluorophenyl)-3,4-dihydro-2,2-dimethyl-2H-chromen-7-yloxy)propyl)phenoxy)(tert-butyl)dimethylsilane (0.54g, 1.0mmol) and stirred for 6h . The reaction was quenched with ammonium chloride (NH_4Cl) solution and extracted with ethyl acetate (3 x 30ml), dried over anhydrous sodium sulfate (Na_2SO_4). The solution was filtered and the volume reduced under vacuum. Purification was done by column chromatography (10% ethyl acetate: hexane) to give the titled compound. (0.39g, 95%).

1H NMR (600 MHz, Chloroform-d) δ 7.51 (s, 1H), 7.32 – 7.26 (m, 2H), 7.05 (tdd, J = 8.7, 5.8, 2.4 Hz, 4H), 6.92 (d, J = 8.1 Hz, 1H), 6.85 (dd, J = 8.3, 5.4 Hz, 2H), 6.53 – 6.48 (m, 2H), 6.28 (s, 1H), 5.03 (ddt, J = 20.7, 14.4, 7.3 Hz, 1H), 3.65 – 3.54 (m, 1H), 2.61 (t, J = 7.7 Hz, 1H), 1.93 (p, J = 7.4 Hz, 1H), 1.55 (d, J = 8.7 Hz, 7H). 13C NMR (151 MHz, CDCl3) δ 162.93, 161.30, 157.76, 153.71, 150.29, 137.63, 135.83, 135.81, 129.91, 129.85,

129.20, 127.39, 122.49, 119.77, 115.67, 115.44, 115.07, 114.93, 108.58, 103.89, 78.73, 72.73, 32.00, 29.78, 29.74, 29.44, 22.76, 22.04, 21.95, 21.62.

5.6 Molecular docking

Molecular docking was conducted to know whether ormeloxifene and its analogs bind to various receptor proteins such as EGFR, GSK3B, and CDK2. A virtual library of 800 ormeloxifene analogs was prepared and structurally modified at C-4, C-7 and C-3 based on ormeloxifene scaffold with 4-(3-hydroxypropyl) phenol, trifluoromethoxy benzene side chain, including ormeloxifene and known EGFR inhibitors. Energy minimization using Chem Office, with MMF94 minimization was performed along with standard drug of choice for the treatment of ovarian cancer. These files were converted into *pdb files maintaining all heavy atoms and concentrated into single continuous *pdb file to be used as an input for Omega. Omega uses the MMF94 force field to generate multiple conformers for each input ligand to induce ligand flexibility in a rigid model. Modifications were applied to the default settings of OMEGA[26]. Receptor files (PDB files) were downloaded from protein data bank (PDB) website (GSK3B, EGFR, CDK2) were prepared using OpenEye,s Fred Receptor program[27]. This program defines the space in which the search algorithm performs and define the shape potential for calculation[28]. Multiple scoring functions such as shapegsuss, chemguass3, Oechemscore, Screen score, and PLP were employed to obtain a consensus structure and scores in the final output.

5.7 MTT Assay

Cell proliferation was determined by MTT assay. Briefly, 5 X 10^6 cells of (A2780) were plated in 96 well plates and incubated for 24 hours at 37°C containing 5% of CO_2. Cells were treated with various analogs of ormeloxifene for 24 hours. 20µL of 50 mg/mL MTT was added in each well containing 100 mL of cell media. The cells were incubated for a further 6 hours, and the media was replaced with 150 mL of DMSO. Plates vigorously shaken for 15 minutes and absorbance was taken at 570 nm on a microplate reader.

5.8 Cell Cycle analysis

Cell cycle analysis was conducted using ormeloxifene analogs and A2780 cell lines; the cells were seeded as 2.5x10^5 cells/mL in a 6-well plate (2 mL/well) and allowed to adhere overnight at 37 °C and 5% CO_2. The cells were incubated with **JA-28** (17.6 µM) and DMSO (0.001%) as a control for 24 h. The cells were washed twice with ice-cold 1X PBS (Hyclone™ Laboratories, Inc) and collected after trypsinization[29]. The cell pellet was washed two times with ice-cold 1X PBS and fixed with ice-cold 70% ethanol overnight at -20 °C. After that, the cells were washed once with ice-cold PBS and the second wash with ice-cold PBS-2% FBS. The cell pellet was re-suspended in 500µL propidium iodide (PI)/RNase staining solution (BD Biosciences) and 0.1% Triton x-100 for 30 min. at room temperature in the dark and analyzed within 1 h by flow cytometer (BD Accuri C6, Becton-Dickinson, Mountain View, CA). Data were analyzed by MFLT32 software, and 10,000 events with slow flow rate were recorded for each sample[30,31]. The cells were synchronized and treated with the most active analogs **JA-28** for 24 hours, with vehicle-control as DMSO

5.9 References

1. Russo, I. H.; Russo, J., Role of hormones in mammary cancer initiation and progression. *Journal of mammary gland biology and neoplasia* **1998,** *3* (1), 49-61.

2. Huang, A.; Kaley, G., Gender-specific regulation of cardiovascular function: estrogen as key player. *Microcirculation* **2004,** *11* (1), 9-38.

3. Riggs, B. L.; Khosla, S.; Melton III, L. J., Sex steroids and the construction and conservation of the adult skeleton. *Endocrine reviews* **2002,** *23* (3), 279-302.

4. Maggi, A.; Ciana, P.; Belcredito, S.; Vegeto, E., Estrogens in the nervous system: mechanisms and nonreproductive functions. *Annu. Rev. Physiol.* **2004,** *66*, 291-313.

5. Investigators, W. G. f. t. W. s. H. I., Risks and benefits of estrogen plus progestin in healthy postmenopausal women: principal results from the Women's Health Initiative randomized controlled trial. *Jama* **2002,** *288* (3), 321-333.

6. Sotoca, A. M.; Vervoort, J.; Rietjens, I. M.; Gustafsson, J.-Å., Human ERα and ERβ splice variants: understanding their domain structure in relation to their biological roles in breast cancer cell proliferation. In *Biochemistry*, InTech: 2012.

7. Manavathi, B.; Samanthapudi, V. S.; Gajulapalli, V. N. R., Estrogen receptor coregulators and pioneer factors: the orchestrators of mammary gland cell fate and development. *Frontiers in cell and developmental biology* **2014,** *2*, 34.

8. Bai, Z.; Gust, R., Breast cancer, estrogen receptor and ligands. *Archiv der Pharmazie: An International Journal Pharmaceutical and Medicinal Chemistry* **2009,** *342* (3), 133-149.

9. Jia, M.; Dahlman-Wright, K.; Gustafsson, J.-Å., Estrogen receptor alpha and beta in health and disease. *Best practice & research Clinical endocrinology & metabolism* **2015,** *29* (4), 557-568.

10. Speirs, V.; Parkes, A. T.; Kerin, M. J.; Walton, D. S.; Carleton, P. J.; Fox, J. N.; Atkin, S. L., Coexpression of estrogen receptor α and β: poor prognostic factors in human breast cancer? *Cancer research* **1999,** *59* (3), 525-528.

11. Jensen, E. V.; Cheng, G.; Palmieri, C.; Saji, S.; Mäkelä, S.; Van Noorden, S.; Wahlström, T.; Warner, M.; Coombes, R. C.; Gustafsson, J.-Å., Estrogen receptors and proliferation markers in primary and recurrent breast cancer. *Proceedings of the National Academy of Sciences* **2001,** *98* (26), 15197-15202.

12. Jordan, V. C., Selective estrogen receptor modulation: concept and consequences in cancer. *Cancer cell* **2004,** *5* (3), 207-213.

13. Lewis, J. S.; Jordan, V. C., Selective estrogen receptor modulators (SERMs): mechanisms of anticarcinogenesis and drug resistance. *Mutation Research/Fundamental and Molecular Mechanisms of Mutagenesis* **2005,** *591* (1-2), 247-263.

14. Lewis, J. S.; Jordan, V. C., Selective estrogen receptor modulators (SERMs): mechanisms of anticarcinogenesis and drug resistance. *Mutation Research/Fundamental and Molecular Mechanisms of Mutagenesis* **2005,** *591* (1), 247-263.

15. Kim, S.-H.; Katzenellenbogen, J. A., Triarylethylene bisphenols with a novel cycle are ligands for the estrogen receptor. *Bioorganic & medicinal chemistry* **2000,** *8* (4), 785-793.

16. Wani, M. C.; Rector, D. H.; Christensen, H. D.; Kimmel, G. L.; Cook, C. E., Flavonoids. 8. Synthesis and antifertility and estrogen receptor binding activities of

coumarins and. DELTA. 3-isoflavenes. *Journal of medicinal chemistry* **1975,** *18* (10), 982-985.

17. Ray, S.; Grover, P. K.; Kamboj, V. P.; Setty, B.; Kar, A. B.; Anand, N., Antifertility agents. 12. Structure-activity relation of 3, 4-diphenylchromenes and-chromans. *Journal of medicinal chemistry* **1976,** *19* (2), 276-279.

18. Gupta, A.; Purkayastha, S.; Bodhey, N.; Kapilamoorthy, T.; Kesavadas, C., Preoperative embolization of hypervascular head and neck tumours. *Australasian radiology* **2007,** *51* (5), 446-452.

19. Gupta, A.; Mandal, S. K.; Leblanc, V.; Descôteaux, C.; Asselin, É.; Bérubé, G., Synthesis and cytotoxic activity of benzopyran-based platinum (II) complexes. *Bioorganic & medicinal chemistry letters* **2008,** *18* (14), 3982-3987.

20. Hussain, M. K.; Ansari, M. I.; Yadav, N.; Gupta, P. K.; Gupta, A. K.; Saxena, R.; Fatima, I.; Manohar, M.; Kushwaha, P.; Khedgikar, V., Design and synthesis of ERα/ERβ selective coumarin and chromene derivatives as potential anti-breast cancer and anti-osteoporotic agents. *RSC Advances* **2014,** *4* (17), 8828-8845.

21. Neises, B.; Steglich, W., Simple method for the esterification of carboxylic acids. *Angewandte Chemie International Edition in English* **1978,** *17* (7), 522-524.

22. Dickson, H. D.; Smith, S. C.; Hinkle, K. W., A convenient scalable one-pot conversion of esters and Weinreb amides to terminal alkynes. *Tetrahedron letters* **2004,** *45* (29), 5597-5599.

23. Grochowski, E.; Hilton, B. D.; Kupper, R. J.; Michejda, C. J., Mechanism of the triphenylphosphine and diethyl azodicarboxylate induced dehydration reactions

(Mitsunobu reaction). The central role of pentavalent phosphorus intermediates. *Journal of the American Chemical Society* **1982,** *104* (24), 6876-6877.

24. Gupta, S.; Hussain, T.; Mukhtar, H., Molecular pathway for (−)-epigallocatechin-3-gallate-induced cell cycle arrest and apoptosis of human prostate carcinoma cells. *Archives of biochemistry and biophysics* **2003,** *410* (1), 177-185.

25. Johnson, J. J.; Petiwala, S. M.; Syed, D. N.; Rasmussen, J. T.; Adhami, V. M.; Siddiqui, I. A.; Kohl, A. M.; Mukhtar, H., α-Mangostin, a xanthone from mangosteen fruit, promotes cell cycle arrest in prostate cancer and decreases xenograft tumor growth. *Carcinogenesis* **2011,** *33* (2), 413-419.

26. Kellenberger, E.; Rodrigo, J.; Muller, P.; Rognan, D., Comparative evaluation of eight docking tools for docking and virtual screening accuracy. *Proteins: Structure, Function, and Bioinformatics* **2004,** *57* (2), 225-242.

27. McGann, M., FRED pose prediction and virtual screening accuracy. *Journal of chemical information and modeling* **2011,** *51* (3), 578-596.

28. Schulz-Gasch, T.; Stahl, M., Binding site characteristics in structure-based virtual screening: evaluation of current docking tools. *Journal of molecular modeling* **2003,** *9* (1), 47-57.

29. Rasmussen, J. G.; Frøbert, O.; Pilgaard, L.; Kastrup, J.; Simonsen, U.; Zachar, V.; Fink, T., Prolonged hypoxic culture and trypsinization increase the pro-angiogenic potential of human adipose tissue-derived stem cells. *Cytotherapy* **2011,** *13* (3), 318-328.

30. Gerdes, J.; Lemke, H.; Baisch, H.; Wacker, H.-H.; Schwab, U.; Stein, H., Cell cycle analysis of a cell proliferation-associated human nuclear antigen defined by the monoclonal antibody Ki-67. *The journal of immunology* **1984,** *133* (4), 1710-1715.

31. Nunez, R., DNA measurement and cell cycle analysis by flow cytometry. *Current issues in molecular biology* **2001,** *3*, 67-70.

Chapter 6

6 General conclusion

The goals and objectives of this study were achieved based on the drug discovery cycle. Various ormeloxifene analogs were studied and reviewed to determine their essential pharmacophores responsible for their anticancer activities. Studies have confirmed the significant pharmacophores of ormeloxifene including the phenolic group at C-7 of ormeloxifene skeleton which is responsible for active binding to estrogen receptors, and the pyrrolidine moiety at C-4 of ormeloxifene framework responsible for anti-estrogenic activities. The project started using structure base molecular design to assemble the ormeloxifene pharmacophores. The concept of bioisosterism was utilized to install various functionalities at C-3, C-4, C-7 and para position of the aromatic ring at C-3.

The first set of analogs were prepared by incorporating moieties such as halogens, electron donating and electron withdrawing groups para to 3-phenyl-2H-chromen position without altering the rest of ormeloxifene framework. Molecular modeling results revealed that the presence of electron donating group at the para position of the aromatic ring at C-3 elevated the binding affinity in the crystal structure of EGFR. **ORM-CH_3** exhibited stronger hydrophobic interaction in the **EGFR** binding pocket. Electron withdrawal moieties at the same para position also resulted in significant hydrophobic interaction inside EGFR binding pocket. Compounds that exhibited that binding affinity are **ORM-F, ORM-Cl, ORM-Br**, **ORM-I,** and **ORM-CH_3** and were identified as most effective EGFR inhibitors. Para substituted analogs were predicted to have higher binding affinity in EGFR binding site relative to meta and ortho-substituted analogs.

Meanwhile, **ORM-Br** and **ORM-F** exhibited significant hydrogen bond with Glu-234: A in Akt kinase binding pocket via the nitrogen on the pyrrolidine moiety. Analogs such as **ORM-Br, ORM-F,** and **ORM-I** formed higher binding affinity in the hydrophobic pocket of Akt binding pocket. In the GSK3B structure, **ORM-Br** and **ORM-I** formed hydrogen bonding with ASP:200: B as well as the formation of hydrophobic interactions compared to ormeloxifene.

Biological assays including, western blot analysis, MTT cell cytotoxicity assay were conducted on the analogs to study the mechanism of action of these compounds towards ovarian cancer cell lines. It is interesting to note that, ORM-Br showed stronger cytotoxicity on ovarian cancer cell line with an IC_{50} value of 11.2 µM towards ovarian cancer cell line (A2780), a value lower than that of ormeloxifene. But ORM-F and ORM-CH_3 lost their cytotoxicity on ovarian cancer cell lines. There was a complete loss of cytotoxicity in analogs such as **ORM-Cl, ORM-I,** and **ORM-OH.** These results showed that **ORM-Br** has significant cytotoxic activity on ovarian cancer cell lines. Anti-proliferation mechanism by western blot analysis on cervical cancer cell lines showed a significant decrease in protein levels of β-catenin in CaSki and SiHa cells compared to cycloheximide. ORM-Br also suppressed the clonogenic potential, inhibits the migration and suppresses the invasion of cervical cancer cell lines. This compound also decreases the expression of nuclear β-catenin in the cytoplasm of cervical cancer cell lines after subjecting to western blot analysis to determine the protein levels of β-catenin. Further investigation revealed that ORM-Br inhibits the EMT associated markers in both CaSki and SiHa cell lines.

The second set of analogs were designed by switching the pyrrolidine side chain to C-7 of ormeloxifene skeleton and substitute electron donating, withdrawing and other functional substituents at phenoxy position. The third set of analogs were prepared by introducing moieties such as 4-(3-hydroxypropyl) phenol and (E)-4-(3-hydroxyprop-1-en-1-yl) phenol at **C-7** and phenol, methoxy, aniline, anisole, and trifluoromethoxy benzene at C-4.

Docking results revealed such as **JA_31, JA_29, JA_30, JA_33, and JA_24** exhibited higher binding affinity in EGFR pocket by forming a hydrogen bond with **HIS:84: A** the same amino acid that bond to ormeloxifene in EGFR binding site. Also, analogs with (ethyl)pyrrolidine side chain at C-7 of Ormeloxifene scaffold such demonstrated an outstanding binding affinity by forming hydrogen bonding with **ASP:292: A and THR:291: A** in EGFR pocket. Analogs with (ethyl) pyrrolidine side chain at C-7 of Ormeloxifene skeleton such (**JA_20, JA_25 JA_15, JA_18, JA_19,** and **JA_17**) showed both hydrophilic and hydrophobic interactions in GSK3B binding site. In GSK3B binding pocket, analogs with (ethyl) pyrrolidine side chain at C-7 of Ormeloxifene frameworks such as **JA_20, JA_25 JA_15, JA_18, JA_19,** and **JA_17** showed both hydrophilic and hydrophobic interactions. Meanwhile, the introduction of trifluoromethoxy benzene at C-4 of ormeloxifene skeleton showed higher binding affinity by forming hydrogen bonds with **LYS:85: B** and **ASP:200: B** in GSK3B binding pocket. The higher binding affinity of these analogs is attributed to the direct interaction of fluorine with protein or indirectly by influencing the polarity of other moieties that interacts with the protein. Molecular modeling results in the CDK2 binding site revealed higher binding mode in analogs with trifluoromethoxy moiety C-4 and (ethyl) pyrrolidine groups at C-7. **JA_15, JA_16, JA_17,** and **JA_18** exhibited hydrogen bond with **HIS:84: A,** the same amino acid in CDK2 pocket

that ormeloxifene binds to induce its anticancer activity. Considering the overall binding affinity in CDK2 binding site, JA_15, an unsubstituted analog showed an outstanding binding affinity towards CDK2 binding site compares to similar analogs with halogens substituted at the para position of the aromatic ring at C-3.

Biological evaluation of these analogs was conducted using MTT cell viability assay revealed that **JA_15, JA_17, JA_31, JA_28, JA_16, JA_20, JA_22, JA_23, JA_24, JA_18, JA_19, JA_25,** and **JA_27** inhibits the viability of **A2780** cells in a dose-dependent manner. The IC_{50} of **JA_15, JA_17, JA_31, JA_28, JA_16, JA_20, JA_22, JA_23, JA_24**, **JA_18, JA_19, JA_25** and **JA_27** were 9.0μM, 20.4μM, 44.6μM, 17.6μM, 37.6μM, 74.8μM, 58.9μM, 89.0μM, 65.7μM, 74.9μM, 36.2μ, 85.6μM and 63.7μM respectively. However, analogs such as **JA_29, JA_32, JA_33, JA_34,** and **JA_35** completely lost their activities towards (A2780) ovarian cancer cell lines. Among all the synthesized analogs, **JA_15** exhibited higher inhibitory activity with IC_{50} of 9.0μM, a value twice lower than the reference compound, however, the substitution of halogen at the para position of the aromatic ring at C-3 negatively affected the overall inhibitory activity of the compound. Introduction of double bonds at the C-7 position of ormeloxifene resulted in higher inhibitory activity on ovarian cancer cell lines relative to similar analogs with no double bonds. Cell cycle analysis by flow cytometry showed that **JA-15** and **JA-28** arrest A2780 cells in the $G_0 – G_1$ phase. **JA-15** exhibited an increased in the fraction of cells in the G_0-G_1 phase with 61.98% compared to the control with 53.42%. **JA-28, however,** exhibited an increase in the fractions of cells in the G_2-M phase with 8.74% relative to 3.52% for control. The results confirmed that **JA-15** has the potential to chemotherapeutic effects because it arrests (A2780) ovarian cell cycle in G0-G_1 phase

This project offered potential analogs of ormeloxifene as a promising drug candidate for the treatment of ovarian cancer, however further studies are needed to elucidate the effects of these class of compounds in an animal model.

Appendix

Molecular docking protocol

7 Design of virtual library

The first step of creating a virtual library was done by drawing all the analogs with ChemDraw software, followed by copying all the compounds and paste in the Chem 3-D software and minimize their energies using MOPAC application, MMF94 to obtain relative crystal structure for each compound. Each file is named saved in pdb format and later combined into a single pdb file. Command prompt was used to execute this process by selecting start menu > accessories > command prompt then the folder where the pdb file of the ligands was copied to be used into single pdb file by writing the following: copy *pdb input_ligands_file.pdb (enter). The created pdb file can be opened using notepad as shown in fig A-1.

7.1 Generating different conformers for each ligand

Omega Application is a command that uses interface to create fast rigid exhaustive docking process. Omega uses the MMF94 force field to create different conformers for each ligand. The resultant file now in pdb.gz format was generated using the following inputs:

1. Copy the combined pdb ligands
2. Paste in OMEGA application. Application license is located at this place.

3. Use the following command to generate the conformers: omega2.2.1 –in name.pdb-out newname.gz.pdb –includeinput –wartz (Enter). This created file is used in FRED calculation.

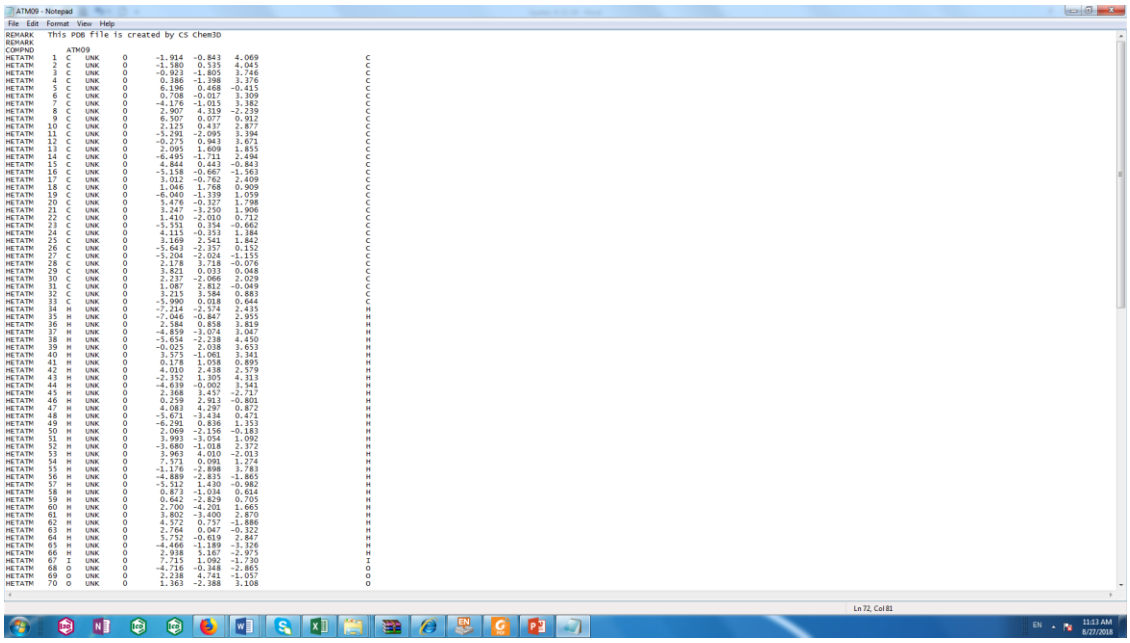

Fig AP-1. Pdb file using the command prompt.

7.2 Preparation of target receptor/protein

To prepare a target receptor, Fred make receptor was utilized. Click on the file for the program to import the pdb file of the receptor downloaded from the protein data bank to show chains of proteins, water molecules any endogenous ligands and co-factors that may be present. Selection the ligands and proteins are important as it helps to create the grid box for docking calculations. The box size should be adjusted to 50,000 – 60,000 Armstrong. The site shape is generated by choosing the shape mode to create the shape of the active site of the receptor that will be used for molecular docking. There are two types of active sites, the inner contours, and the outer contours. The receptor file is finally saved as oeb.gz (**Fig AP-2**).

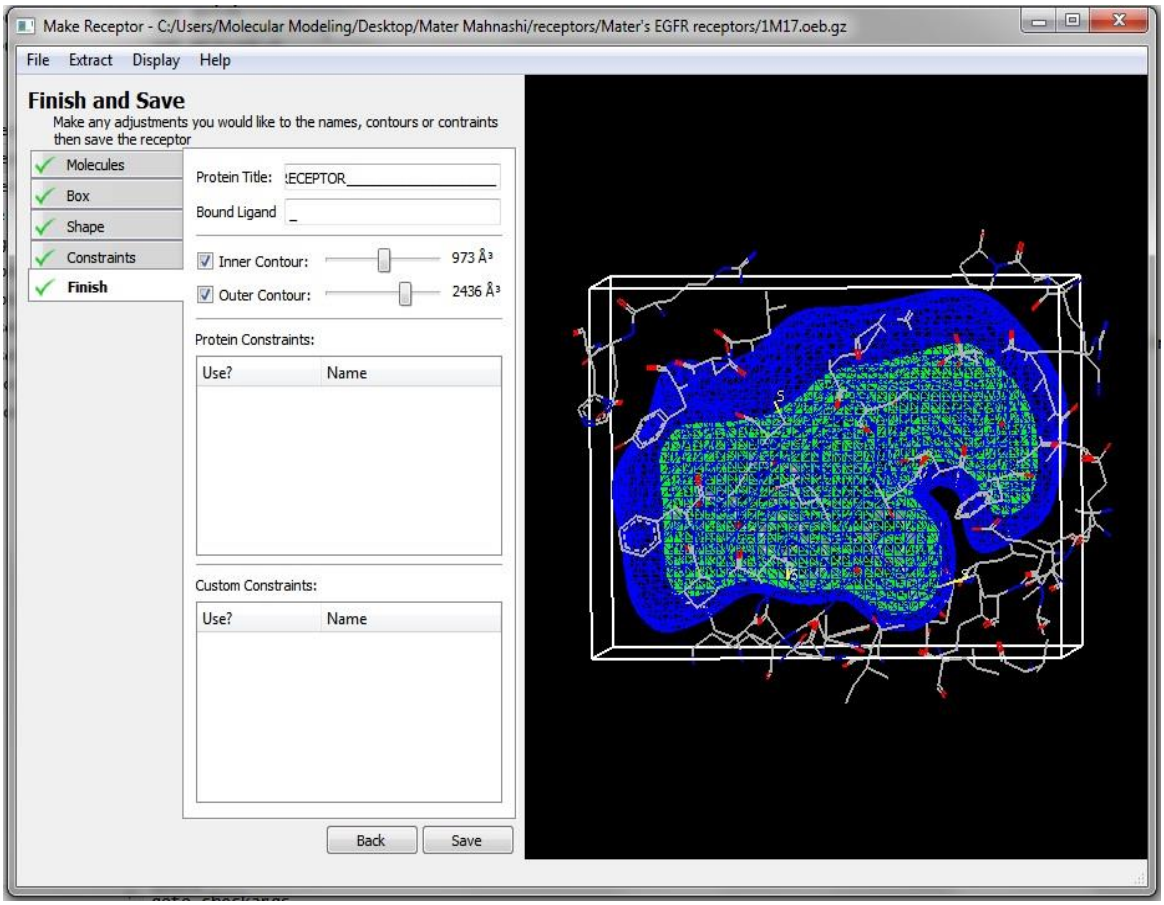

Fig AP-2. Sample of the prepared grid box

7.3 Fred docking calculations

Fred calculation was performed by navigating through the files where Fred files and licensed are located. The following command lines were used to run the program: Fred.exe-rec receptor.oeb.gz –dbase name.gz.pdb –prefix newname shapegauss –chemguass3 –oechemscore –screenscore –plp –hitlist_size 5000 (enter). This command results in creating a consensus score, which calculates the binding affinity between the ligand and

the target receptors. Lower consensus score is an indication of higher binding affinity and vice versa **(Table AP-3).**

Table AP-3. Sample of consensus score of FRED docking

VIDA Name	VIDA ID	PLP	Chemgauss3	OEChemscore	Screenscore	Consensus Score
JA_15_8	2	-62.1912	-98.9223	-50.9355	-161.426	4
JA_23_65	3	-63.1604	-85.4124	-53.3115	-148.521	9
JA_18_194	4	-55.5819	-94.061	-49.7552	-156.399	15
JA_31_197	5	-58.7091	-78.7798	-50.6628	-138.252	31
ORM_Me_70	6	-58.9203	-88.0918	-48.9543	-130.846	31
JA_17_124	7	-60.2571	-82.0704	-46.9993	-151.993	33
JA_30_136	8	-54.9044	-82.1141	-49.7006	-133.778	34
JA_20_91	9	-55.1979	-82.9193	-52.6244	-128.111	34
JA_29_196	10	-56.4896	-74.7738	-51.4356	-136.43	37
JA_22_18	11	-57.7173	-76.0436	-49.6441	-141.795	38
JA_24_136	12	-54.9044	-82.1141	-49.7006	-133.778	38
JA_16_118	13	-50.2681	-89.5709	-47.0727	-145.829	41
JA_19_43	14	-51.9849	-86.1558	-49.8197	-128.74	41
JA_33_173	15	-52.6577	-80.5097	-48.3041	-139.799	43
JA_35_136	16	-49.7391	-81.7393	-46.085	-134.599	58
JA_25_26	17	-52.629	-76.5679	-47.4447	-128.804	63
JA_28_130	18	-52.1154	-73.6299	-49.4652	-122.123	65
JA_26_58	19	-50.8557	-75.0371	-48.8462	-128.441	65
JA_32_166	20	-49.3175	-79.5876	-48.1438	-121.453	68

JA_34_4	21	-48.3862	-71.7791	-48.2779	-130.937	69
ORM_188	22	-46.7276	-86.295	-45.0742	-110.072	69
JA_27_4	23	-48.3862	-71.7791	-48.2779	-130.937	73
ORM_F_106	24	-54.664	-70.7967	-42.5575	-119.368	79
ORM_Cl_107	25	-46.5579	-78.3947	-41.5806	-103.429	86
ORM_Br_166	26	-36.8834	-79.3884	-41.2741	-92.8488	87
ORM_I_109	27	-30.6345	-79.4347	-40.6518	-85.7905	89

7.4 Visualization of docking results using VIDA

The final stage of molecular docking is where VIDA application is utilized to visualize the 3D structure of all docked analogs and potential binding interactions inside the target receptor.

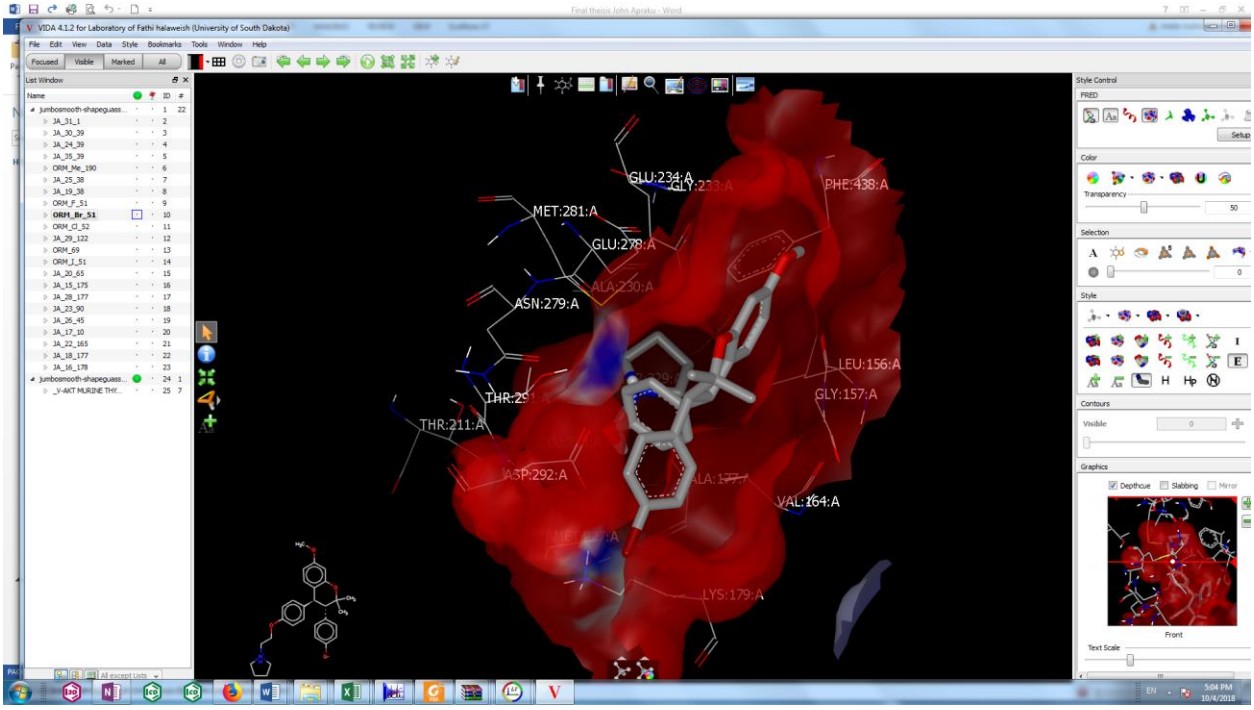

Fig AP-3. VIDA Visualization in 3D